



Fakultät für Mathematik und Wirtschaftswissenschaften
Institut für Numerische Mathematik

Dissertation

**On High-Order NURBS-Based Boundary Element
Methods in Two Dimensions**

Numerical Integration and Implementation

zur Erlangung des Doktorgrades Dr. rer. nat.
der Fakultät für Mathematik und Wirtschaftswissenschaften
der Universität Ulm

vorgelegt von
Andreas Bantle
aus Ulm

Amtierender Dekan: Prof. Dr. Werner Smolny

1. Gutachter: Prof. Dr. Stefan A. Funken (Universität Ulm)

2. Gutachter: Prof. Dr. Dirk Praetorius (Technische Universität Wien)

Tag der Promotion: 3. Juli 2015

Abstract

In this thesis we address the implementation of collocation and Galerkin boundary element methods (BEM) in two dimensions and the numerical evaluation of the arising nearly singular and singular integrals. The focus is on methods that are based on a NURBS (non-uniform rational b-splines) parametrization of the boundary, which we refer to as NURBS-based methods. The advantage of NURBS-based methods is that a geometric error is avoided, which is induced by the boundary approximation in standard methods and diminishes the convergence of BEM.

The first part of this thesis is devoted to the derivation of new, stable algorithms for the accurate and efficient numerical evaluation of the arising integrals. By exploiting the special structure of the NURBS parametrization and by interpolating parts of the kernel functions by Legendre polynomials, we are able to evaluate the boundary integral operators in a stable way. Apart from weakly singular boundary integral operators, our algorithm can also be applied to singular and hypersingular boundary integral operators.

The singular integrals arising in the assembly of the Galerkin matrices are regularized with coordinate transformations and evaluated with adapted quadrature rules. For all arising integrals, an exponential convergence of the error is proven and rigorous error bounds are derived. We use these bounds for the estimation of the consistency errors and the a priori computation of the quadrature orders for Galerkin methods.

The algorithms for the numerical integration are used for the implementation of NURBS-based methods in the second part of this dissertation. Our implementation is the first, which is known to us, that can be used for solving boundary integral equations arising from Laplace, Lamé, and Helmholtz problems with collocation and Galerkin methods on exact boundary parametrizations. Furthermore, it allows the use of different basis functions. The final numerical experiments show that even for high degrees ($p \leq 128$) of the polynomial basis functions accurate results are obtained and practice-relevant problem can be efficiently solved.

Kurzzusammenfassung

Diese Arbeit beschäftigt sich mit der Implementierung der Kollokations- und Galerkin-Randelementmethode (BEM) in zwei Dimensionen sowie der numerischen Berechnung der auftretenden fast-singulären und singulären Integrale. Der Fokus liegt dabei auf Methoden, die auf einer NURBS (nicht-uniforme, rationale B-Splines) Parametrisierung des Randes basieren, kurz NURBS-basierte Methoden. Der Vorteil von NURBS-basierten Methoden liegt in der Vermeidung des geometrischen Fehlers, der bei Standardmethoden durch die Randapproximation verursacht wird und die hohe Genauigkeit der BEM beeinträchtigt.

Im ersten Teil der Arbeit werden neue, stabile Algorithmen für die genaue und effiziente numerische Auswertung der auftretenden Integrale entwickelt. Indem wir die spezielle Struktur der NURBS Parametrisierung ausnutzen und Teile der Kernfunktion mit Legendre Polynomen interpolieren, ermöglichen wir die stabile Auswertung der Randintegraloperatoren mit hoher Genauigkeit für alle Auswertungspunkte. Neben schwachsingulären Randintegraloperatoren können diese Algorithmen auch für die Auswertung von singulären und hypersingulären Randintegraloperatoren verwendet werden.

Die singulären Integrale, die bei der Berechnung der Galerkinmatrizen auftreten, werden durch Koordinatentransformation regularisiert und mit angepassten Quadraturformeln ausgewertet. Für alle auftretenden Integrale wird eine exponentielle Konvergenz des Fehlers bewiesen und es werden rigorose Fehlerschranken hergeleitet. Wir verwenden diese Fehlerschranken für die Abschätzung des Konsistenzfehlers und die a-priori Berechnung der Quadraturordnungen bei Galerkin-Methoden.

Die Algorithmen zur numerischen Integration werden im zweiten Teil der Arbeit für die Implementierung NURBS-basierter Methoden verwendet. Unsere Implementierung ist die erste uns bekannte, die für das Lösen von Laplace, Lamé und Helmholtz Problemen mit Kollokations- und Galerkin-Verfahren auf exakten Randparametrisierungen verwendet werden kann und verschiedene Basisfunktionen unterstützt. Die numerischen Experimente zeigen schließlich, dass auch für hohe Polynomgrade ($p \leq 128$) der polynomialen Basisfunktionen akkurate Ergebnisse erzielt und praxisrelevante Probleme effizient gelöst werden können.

Acknowledgements

Dedicated to my farther.

Though my name is listed as the sole author, there were many people whose efforts and consideration were essential to make this work possible.

First and foremost, I owe my deepest gratitude to my advisor, teacher, and - above all - mentor Prof. Dr. Stefan Funken. I thank him for his friendliness and patience, his steadfast collaboration whenever I had questions or needed to discuss problems, and his tireless support reaching back to the beginning of my studies at University of Ulm.

I would also like to thank Prof. Dr. Dirk Praetorius for the collaboration and inspiring discussions during the last years. I am honored to have him as the second reviewer for this dissertation. Thank you to all my colleagues and friends at the Institute for Numerical Mathematics and the Scientific Computing Centre Ulm for the wonderful time. You have made it a pleasure to be a member of this community.

To Markus Bantle, I would like to offer my gratitude for always being available for discussions, answering numerous questions, supporting me during my whole studies of mathematics, and editing this thesis. Furthermore, I thank Natalie Selinski, Pascal Heiter, and Benjamin Wenger for proofreading this work so carefully.

Last but not least, thank you to my entire family, Gisela, Gerhard, Markus, Daniela Bantle, and Franziska Merkle for always supporting and encouraging me. I have been extremely fortunate in my life to have you as a family. Without your love, advice and continuous support, this dissertation would not exist.

Contents

Introduction	iii
1. Analytical Basics and Notation	1
1.1. Function spaces	1
1.2. Boundary Integral Equations	5
1.3. BIEs for Elliptic Partial Differential Operators	11
1.4. Triangulation and Discrete Spaces	16
1.5. Collocation Methods	18
1.5.1. Discrete Collocation BEM	18
1.5.2. A Priori Error Analysis	21
1.6. Galerkin Methods	23
1.6.1. Discrete Galerkin BEM	23
1.6.2. A Priori Error Analysis	26
2. Orthogonal Polynomials and Gauss Quadrature Rules	29
2.1. Orthogonal Polynomials	31
2.2. Gauss Quadrature Rules	34
2.2.1. Computation of Gauss Quadrature Rules	35
2.2.2. Error Bounds for Gauss Quadrature Rules	39
3. High-Order NURBS-Based Boundary Element Methods	49
3.1. Non-Uniform Rational B-Splines	51
3.2. Discrete Ansatz Spaces	55
3.3. Boundary Meshes and Refinement	63
4. Numerical Integration for High-Order NURBS-Based BEM	69
4.1. Existing Approaches for the Numerical Integration in BEM	70
4.2. Evaluation of Boundary Integral Operators	74
4.2.1. Far-field Case	78
4.2.2. Near-Field Case	83
4.2.3. Identical Case	89

Contents

4.3. Computation of Galerkin Entries	91
4.3.1. Far-field Elements	92
4.3.2. Neighboring elements	96
4.3.3. Identical Elements	106
4.3.4. Consistency Error Analysis	111
5. Implementation and Numerical Results	125
5.1. Overview on Existing Software Packages	125
5.2. Implementation	127
5.2.1. General Aspects of Implementation	129
5.2.2. Collocation Methods	135
5.2.3. Galerkin Methods	155
Conclusions	175
A. Explicit Representation of the Integral Operators	179
Bibliography	191
List of Symbols	201
Curriculum Vitae	205
Erklärung	207

Introduction

The boundary element method (BEM) is a modern numerical method for the solution of boundary integral equations (BIEs) arising in various fields of engineering, such as potential theory, solid mechanics, acoustics, and electromagnetics. As compared to other methods for the solution of these problems, it has several advantages, particularly the natural treatment of unbounded domains. However, the implementation of BEM is very challenging, because singular and nearly singular integrals have to be evaluated up to a high accuracy. Therefore, in order to exploit the full potential of BEM, efficient algorithms for the accurate numerical integration are required.

Boundary integral equations can be solved with different approaches. In Galerkin BEM, the variational formulation of the BIE is solved in a discrete ansatz space. For collocation BEM, the BIE is evaluated at a given number of collocation points. Both approaches give rise to a system of linear equations, which is solved numerically.

There are several versions of BEM. In h -versions, the unknown solution is approximated by piecewise low-order polynomials, typically polynomials of order $p = 0$ or $p = 1$, on fine boundary meshes. In p -versions, high-order polynomials are used for the approximation of the solution on coarse meshes. A combination of h - and p -versions is called hp -BEM. While uniform h -methods yield an algebraic convergence with respect to the degrees of freedom, uniform p -methods have twice the convergence rate as compared to uniform h -methods ([StSu91]) and even show an exponential decay for smooth solutions. For certain types of hp -methods, an exponential decay of the error can also be observed for non-smooth solutions [Heu96].

In most existing BEM implementations, the exact boundary is approximated by piecewise polynomials, typically of order $q = 1$ (polygonal boundaries) or order $q = 2$, which induces a geometric error. However, on complicated geometries arising in industrial applications a significant loss of accuracy of the numerical solution is observed. In order to eliminate the geometric error, non-uniform rational b-spline (NURBS) parametrizations of the boundary are used for the computation, generally based on models developed using computer-aided design (CAD) software. To see the impact of the geometric error on high-order BEM and the importance of NURBS-based methods, we consider the following simple example of a BIE on a circle.

Model Problem

We consider the BIE arising from the Laplace problem

$$\begin{aligned} -\Delta u(x) &= 0, & x \in \Omega &:= \left\{ z \in \mathbb{R}^2 : \|z\|_2 < \frac{1}{4} \right\}, \\ u(x) &= x_1^3 x_2^2, & x \in \Gamma &:= \left\{ z \in \mathbb{R}^2 : \|z\|_2 = \frac{1}{4} \right\}. \end{aligned}$$

The BIE is solved numerically with a Galerkin method by a uniform h -refinement with polynomial degrees $p = 1$ or $p = 2$. The boundary is discretized by polynomial approximations of orders $q = 1, 2$ and by an exact NURBS parametrization, respectively. Figure 1 shows the point-wise absolute error of the solution $|u(x^*) - u_h(x^*)|$ for the arbitrarily chosen point $x^* = (0.135, -0.143) \in \Omega$ over the degrees of freedom \mathcal{N} as well as the convergence rates indicated by the numbers in the triangles.

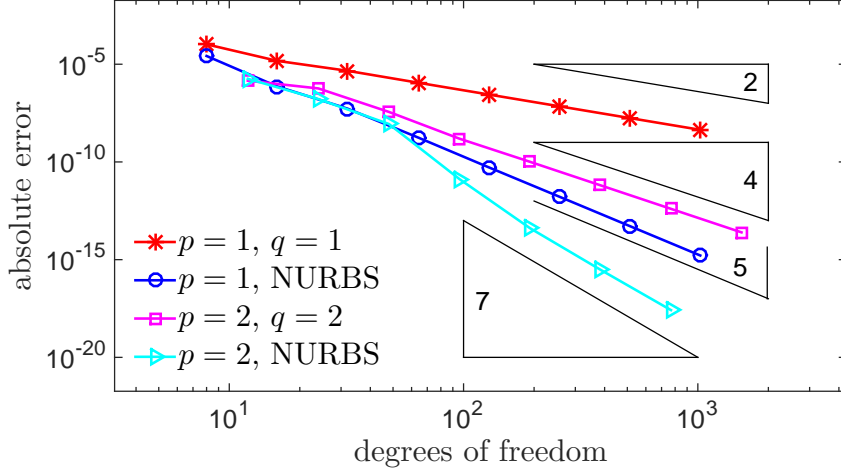


Figure 1: Absolute error $|u(x^*) - u_h(x^*)|$ with $x^* = (0.135, -0.143)$ over the degrees of freedom \mathcal{N} for uniform h -methods with linear, quadratic, and exact boundary parametrizations.

It can be seen that the convergence rates obtained with the exact boundary representation are diminished by the geometric error resulting from the polynomial boundary approximations. Particularly, high-order boundary approximations with degree $q = p + 1$ are required to obtain the full convergence rates of the Galerkin error.

While standard BEM is well understood from a theoretical and practical point of view, there are still several open questions for NURBS-based BEM. In this work, we discuss some of these challenges including:

- Accurate and efficient numerical evaluation of integrals arising in high-order NURBS-based BEM

- Efficient and stable implementation of NURBS-based collocation and Galerkin BEM

In the course of this dissertation, we discuss both aspects in more detail and elaborate on the progress made in these areas of NURBS-based BEM.

Numerical Integration for NURBS-Based BEM

The solution of the boundary integral equations with NURBS-based methods requires the evaluation of nearly singular and singular integrals, which exist as Cauchy principle values or in the sense of Hadamard finite parts. As the Galerkin error decays exponentially with respect to the degrees of freedom on geometrically graded hp -meshes [Heu96], an exponential decay of the evaluation error is needed in order to preserve the convergence of the Galerkin method. Hence, the evaluation of the integrals arising in NURBS-based BEM is numerically challenging.

Common techniques for the evaluation of these integrals are analytic approaches, semi-analytic approaches, and quadrature formulae. For polygonal boundary representations, approaches for the analytic integration of the nearly singular and singular integrals are presented in e.g. [RS07, Ban13, Mai96, Mai97, ST99]. While these analytic methods avoid the introduction of a consistency error and provide the possibility of an accurate evaluation of the nearly singular and singular integrals, their field of application is limited to simple boundary representations. Furthermore, the analytic integration leads to cancellation effects for small integration domains and high-order basis functions. This problem is addressed in [Ban13], where algorithms for the stable analytic integration for high-order basis functions via three-term-recurrence relations are developed.

Semi-analytic approaches split the integrand into regular and singular parts using kernel expansions, see e.g. [Sau92, HS93, SISI98, NWW⁺05] and the references therein. While the regular parts are evaluated with quadrature rules, the singular and nearly singular integrals are evaluated analytically. For the numerical integration with quadrature rules, composite rules [Sch94], adapted quadrature rules, and coordinate transformations [SISI98, Tel86, TM74, Duf82, SaSch97] are used for the evaluation of the nearly singular and singular integrals. Although an exponential decay of the quadrature error is achieved, all three approaches have limitations in the case of nearly singular integrals. Composite rules require the exact knowledge regarding the location of the nearly singular point, adapted quadrature rules cannot be pre-computed and are inefficient, and coordinate transformations do not eliminate the dependence of the quadrature error on the near singularity which still results in a slow exponential convergence of the quadrature error.

Introduction

In this work, we develop algorithms for the accurate and efficient numerical integration for all integrals arising in high-order NURBS-based BEM including a priori estimates for the absolute error.

The accurate evaluation of the boundary integral operators is based on the classification of the evaluation points in far-field, near-field, and singular points. In implementing NURBS-enhanced methods, we use the Legendre polynomials as basis functions of the polynomial ansatz space, allowing us to evaluate all far-field integrals for high-order basis functions. With a Legendre expansion of the kernel function and the orthogonality of the Legendre polynomials, we prove that the error and the complexity are independent of the polynomial degree p . For the near-field and singular integrals, we use the knowledge of the (near) singularity for splitting the kernel function into regular and (nearly) singular parts. With Legendre expansions of the regular parts, the evaluation of the potentials can be reduced to the evaluation of the basic integrals defined in [Ban13]. As compared to the existing semi-analytic approaches, our method is stable even for high-order Legendre expansions, since efficient and stable algorithms for the analytic evaluation of these basic integrals are presented in [Ban13]. Furthermore, we prove that the convergence rate only depends on the boundary parametrization but is independent of the evaluation point.

As an example, we consider the evaluation of the integral

$$I(x) := -\frac{1}{2\pi} \int_{\Gamma} \log |x - y| ds_y \quad (1)$$

for $\Gamma = \{x \in \mathbb{R}^2 : x = (r \cos(\theta), r \sin(\theta)), r = 0.25, \theta \in (0, \pi/2)\}$ and two near-field points $x(D) = \frac{1+4D}{4\sqrt{2}} \cdot (1, 1)$ with different distances D to the boundary. We compare our algorithm with the evaluation with the cubic Telles transformation, which is introduced in [Tel86] and proposed for evaluation of the boundary integral equations in [SBT⁺12].

Figure 2 shows the absolute error over the evaluation order n . A significant improvement can be observed. Particularly, the integral is evaluated up to double machine precision with order $n \approx 20$ for both points using our algorithm.

For the evaluation of the double integrals arising in Galerkin methods, we regularize the singular integrals with a coordinate transformation introduced in [Duf82] and proposed for the use of three-dimensional BEM in [SaSch97]. In contrast to the approach of Sauter and Schwab [SaSch97], which is used in many software packages such as BEM++ and HyENA, we regularize the remaining weakly singular integrals with an adapted quadrature rule instead of using composite rules. Our approach has the advantage that the convergence of the quadrature error depends only on the boundary parametrization, while the convergence of composite rules depends significantly on the grading parameters [Sch94]. For all arising integrals, we are able to prove an exponential decay of the quadrature error and provide a complete consistency error analysis. Using the consistency error estimates, the quadrature orders are computed a priori such that the convergence rates of the Galerkin method are not diminished by the consistency errors.

This is the foundation for an efficient implementation of Galerkin methods.

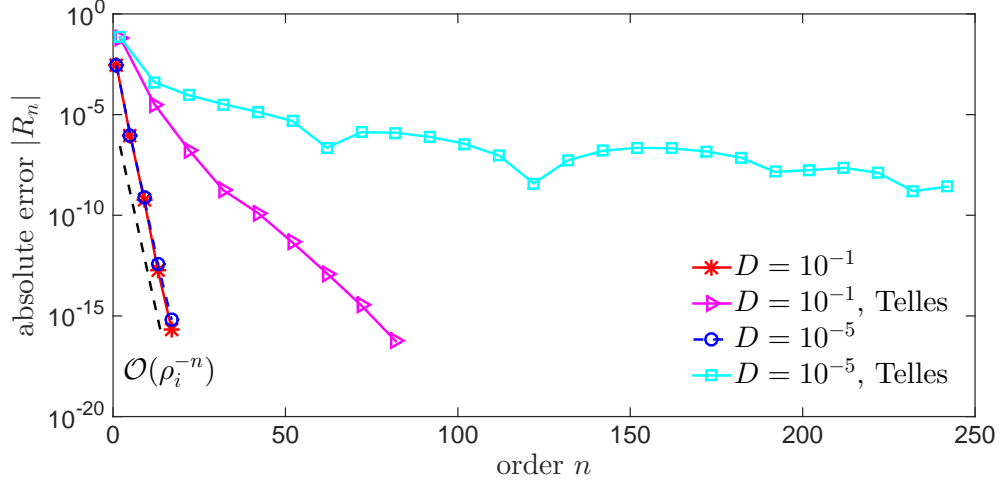


Figure 2: Absolute error plotted against the order n for the evaluation of (1) with two evaluation points with different distances D to the boundary. Comparison of our near-field algorithm based on Legendre expansions and the Telles transformation [Tel86].

Implementation of NURBS-Based BEM

There are a variety of software packages implementing collocation and Galerkin boundary element methods, such as BEMLIB [Poz02], BEM++ [ŠBA⁺15], HILBERT [AEF⁺14], epsBEM [BBF13, Ban13], and HyENA [MMR⁺14] to mention a few but not all. All software packages feature the solution of specific BIEs, boundary representations, and basis functions. Except for the implementation of isogeometric collocation BEM [Sim12], these software packages implement polynomial boundary approximations of orders $q \in \{1, 2, 3\}$ and polynomial basis functions. While most software packages focus on low-order BEM, high-order methods are considered in epsBEM [BBF13] and by Maischak [Mai96] for Laplace, Lamé, and Helmholtz equations on polygonal boundaries.

Thus far, there has been no software package able to implement the full spectrum of NURBS-based BEM including isogeometric and NURBS-enhanced methods, and collocation and Galerkin approaches for various partial differential equations. This is the second issue addressed in this work. With the algorithms for the efficient and accurate evaluation of the integrals arising in NURBS-based collocation and Galerkin methods, we develop a black box software package that implements NURBS-based BEM for two-dimensional Laplace, Lamé, and Helmholtz equations. By considering fundamental solutions of a general type we are able to incorporate other

Introduction

PDEs such as the Stokes equation. With the variability of our implementation, particularly the use of different types of basis functions, we use the implementation to investigate several open issues of collocation and Galerkin BEM. Specifically, we present numerical results concerning the choice of the collocation points for high-order methods and the effect of the high inter-element regularity of the ansatz functions used in isogeometric methods.

A NURBS parametrization of the boundary serves as the basis for the efficient solution of PDEs on complicated domains, allowing us to represent these domains with few degrees of freedoms. The stability of our implementation of high-order NURBS-enhanced methods for polynomial degrees $p \leq 128$ is achieved by using the Legendre polynomials and their antiderivatives as basis functions. Hence, our implementation permits us to compute highly accurate solutions of practice-relevant problems in potential theory, linear elasticity, and acoustic scattering. As an example we consider two problems in linear elasticity (Figure 3) and acoustic scattering (Figure 4), respectively.

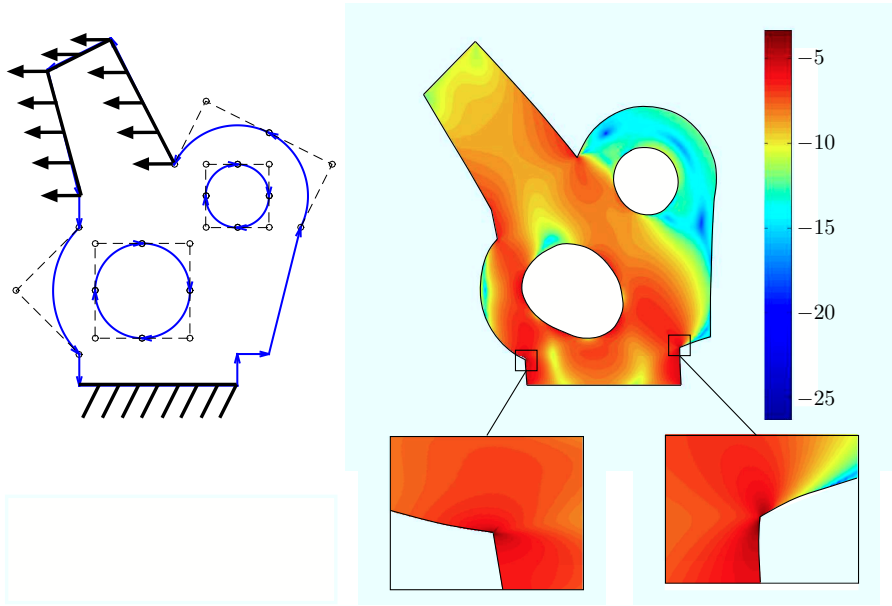


Figure 3: NURBS parametrization of the boundary with control polygon and boundary conditions (left) and shear energy density on displaced domain (right). The material coefficients correspond to plexiglass ($E = 2900$, $\nu = 0.4$) and the displacement is scaled by a factor of 500.

Figure 3 shows the solution of the mixed traction and displacement problem in linear elasticity, which is computed by solving the Lamé equation with mixed boundary conditions. The workpiece is fixed at the bottom side and the arrows indicate the applied traction. The right picture shows the shear energy density on the displaced workpiece, which is computed with 21 elements and polynomial degree $p = 16$.

Figure 4 shows the scattering of an acoustic plane wave with wave number $\kappa = 10$, which corresponds to the solution of the Helmholtz equation. The direction of the incoming plane wave as well as the geometry of the obstacle are depicted in the left picture. The right picture shows the total acoustic wave comprised of the incoming and the scattered wave. The solution is computed with 12 elements and polynomial degree $p = 32$.

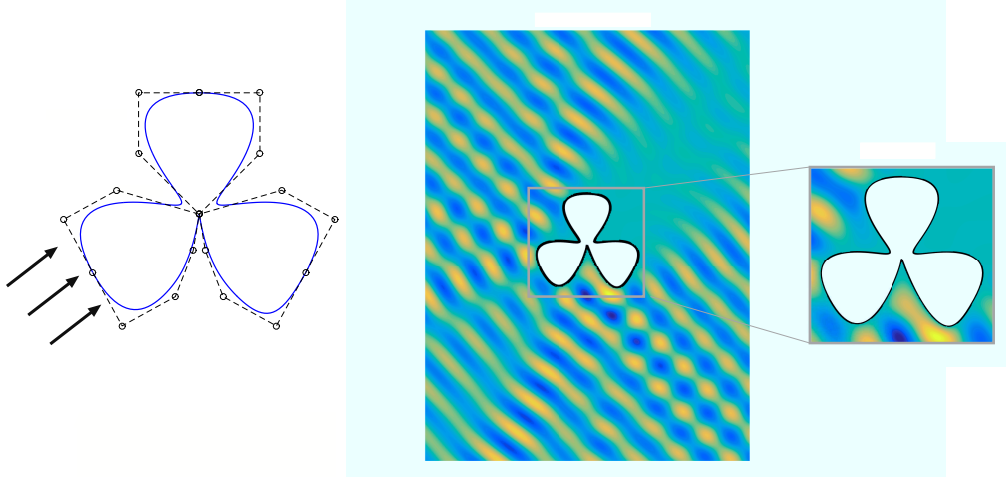


Figure 4: NURBS parametrization with control polygon and direction of incoming wave (left) and total acoustic wave consisting of incoming and scattered wave with wave number $\kappa = 10$ (right).

Outline

In the first chapter we introduce the function spaces, boundary integral operators, and boundary integral equations for Laplace, Lamé, and Helmholtz equations. We also summarize the main existing results for collocation and Galerkin methods, introduce the geometrically graded hp -meshes, and present standard a priori estimates for collocation and Galerkin methods.

The second chapter serves as foundation for the efficient implementation of NURBS-based boundary element methods. After introducing orthogonal polynomials and reviewing their main properties, we introduce quadrature rules for the numerical integration. The traditional method for computing Gauss quadrature nodes and weights is the Golub-Welsh algorithm, which exploits the three term-recurrence relation satisfied by all real orthogonal polynomials. The relation gives rise to a symmetric tridiagonal matrix, whose eigenvalues are the nodes of the quadrature rule. The weights can be easily computed by the corresponding eigenvectors [GW69]. Besides the Gauss-Legendre quadrature we also consider a Gauss quadrature with respect to a logarithm-

Introduction

mic weight function, which we refer to as Gauss-Log quadrature. For the stable computation of the nodes and weights of the Gauss-Log quadrature we use the modified Chebyshev algorithm [Gau10] and modified moments, for which we derive explicit formulae [BF14]. Furthermore, we derive error estimates for the Gauss quadrature rules, which are based on the remainder theory of analytic functions [DR75]. While we present the standard error estimate for the Gauss-Legendre quadrature, we also propose a new error bound for the Gauss-Log quadrature based on numerical experiments.

The ansatz spaces for NURBS-based boundary element methods are presented in Chapter 3. After defining NURBS curves and summarizing their basic properties, we introduce the basis functions used for isogeometric and NURBS-enhanced methods. Furthermore, we discuss algorithms used for different mesh refinement strategies including uniform h -, p -, and geometric hp -refinements as well as the uniform k -refinement [HCB05]. At the end of this chapter, the regularity of NURBS curves is analyzed. Particularly, we explicitly compute the size of the largest ellipse in which the NURBS parametrizations can be analytically extended. As the semi-axis sums of these ellipses occur in the error estimates for Gauss quadrature rules, this information is the foundation for an a priori error analysis in NURBS-based BEM.

Chapter 4 is concerned with the derivation of algorithms for the efficient and accurate numerical integration in NURBS-based BEM. We discuss the accurate evaluation of the boundary integral operators for all evaluation points $x \in \mathbb{R}^2$. Based on Legendre expansions of the kernel and parts of the kernel, an exponential decay of the error with optimal rate is proven for regular, nearly singular, and singular integrals. We also explore the assembly of the Galerkin matrices. For the singular integrals, we combine the coordinate transformations introduced by Sauter and Schwab [SaSch97] with the Gauss-Log quadrature and prove an exponential decay of the quadrature error for all integrals. For NURBS-enhanced BEM, where Legendre polynomials are chosen as ansatz functions, we derive h - and p -asymptotic error estimates, which we use in the subsequent consistency error analysis. Finally, we present formulae for the a priori computation of the quadrature orders, which is the key for the efficient implementation of Galerkin methods.

Lastly, we present a black box software package implementing of NURBS-based BEM in Chapter 5. For NURBS-enhanced collocation methods, we present numerical experiments for the appropriate choice of the collocation points based on optimization problems. The effect of the high inter-element regularity of the isogeometric ansatz functions is investigated for Galerkin methods, particularly we present new results concerning uniform k -methods. The final numerical experiments show the stability of our implementation for high-order NURBS-enhanced methods with $p \leq 128$. While also for low-order isogeometric methods accurate results are ob-

tained, the implementation is restricted to moderate polynomial degrees due to the exponential growth of the condition number of the system matrix with respect to the polynomial degree. On geometrically graded hp -meshes an exponential decay of the error can be observed for collocation and Galerkin methods.

As a visual guide to the discussion that follows, Figure 5 shows an overview on the chapters in this work and their relationships.

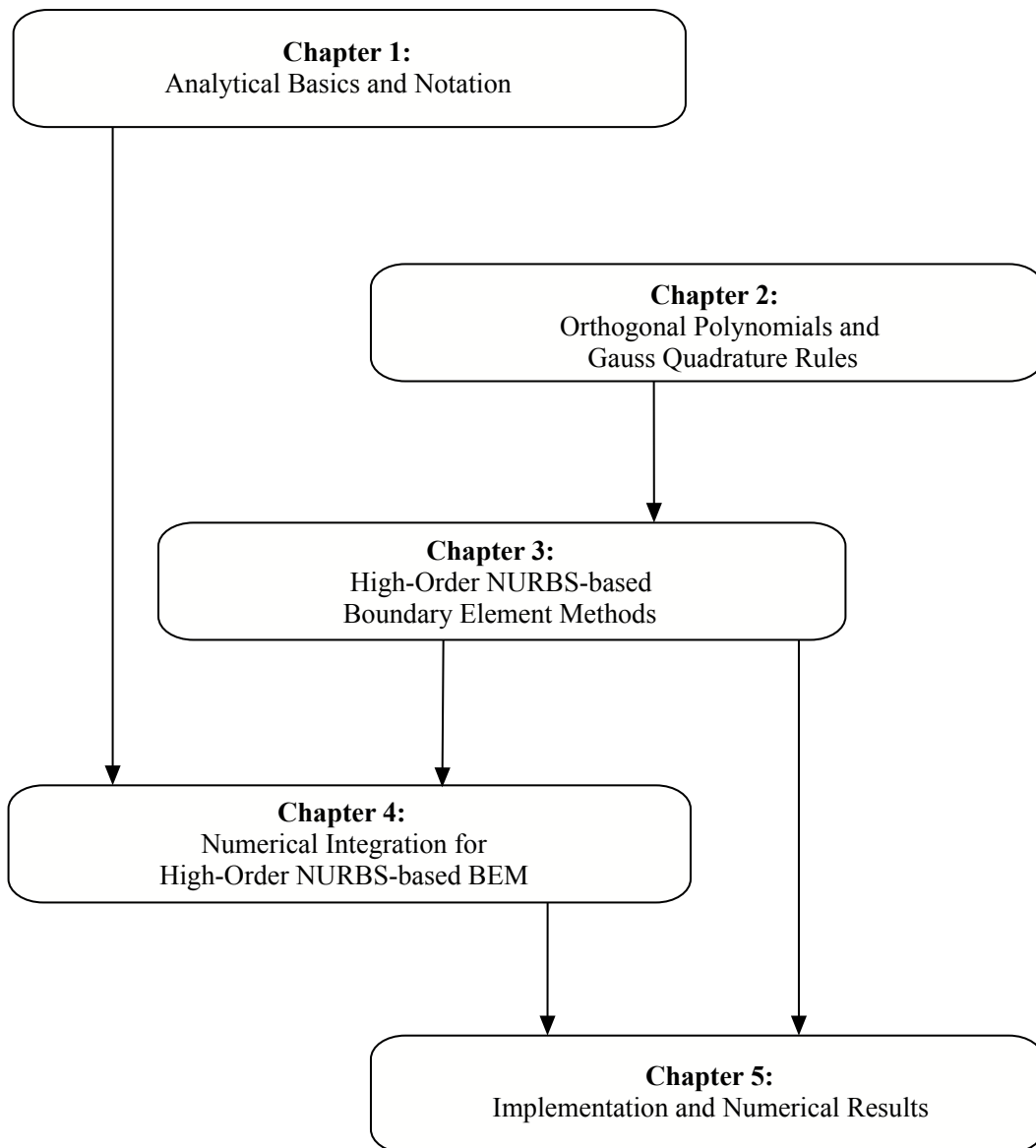


Figure 5: Overview on the chapters in this work and the relationships between the chapters.

1. Analytical Basics and Notation

The notation and basic theoretical results used in this work are introduced in this chapter. The first section is devoted to the definition of function spaces. In the second section we give a short introduction to boundary integral equations before we apply the general results to the boundary integral equations (BIE) arising from three partial differential equations (PDE), that we consider throughout this work, namely the Laplace, the Lamé, and the Helmholtz equation. In the third section, we introduce different boundary meshes and ansatz spaces. Finally, we discuss the numerical solution of boundary integral equations using collocation and Galerkin methods.

1.1. Function spaces

For the definition of Lebesgue and Sobolev spaces for domains and boundaries of domains, we only state the main results and refer to [AF03] for a detailed discussion of Sobolev spaces.

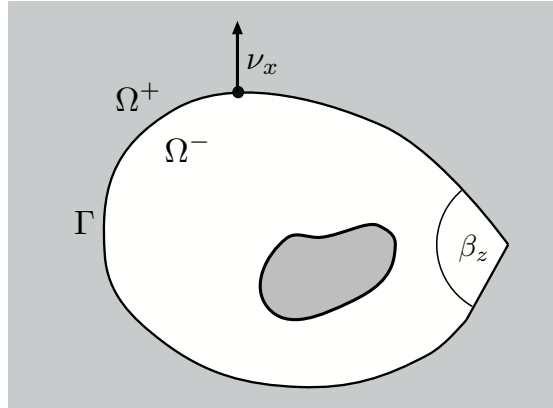


Figure 1.1.: Lipschitz domain Ω^- and its complement Ω^+ . The unit normal vector at $x \in \Gamma$ pointing from Ω^- to Ω^+ is denoted by ν_x , the interior angle at each corner z by β_z .

Throughout this section we denote by $\Omega^- \subset \mathbb{R}^2$ a bounded Lipschitz domain and by $\Gamma \subseteq \partial\Omega^-$ the boundary of Ω^- or a connected subset of the boundary $\partial\Omega^-$. Furthermore, we introduce the complement of Ω^- by $\Omega^+ := \mathbb{R}^2 \setminus \overline{\Omega^-}$. The boundary of a Lipschitz domain can locally be represented by a Lipschitz continuous function and Ω^- is locally only on one side of Γ . This implies that Ω^+ is an unbounded Lipschitz domain if it is connected. For a detailed definition

1. Analytical Basics and Notation

we refer to [SaSch04, McL00].

Let $k \in \mathbb{N}_0$, $m \in \mathbb{N}$, $\Omega \in \{\Omega^-, \Omega^+\}$ be connected, and $u : \Omega \rightarrow \mathbb{C}^m$. We write $u \in \mathcal{C}^k(\Omega)^m$ if each component of u is k times continuously differentiable. Furthermore, we introduce the space $\mathcal{C}^\infty(\Omega)^m$ of all infinitely differentiable functions by

$$\mathcal{C}^\infty(\Omega)^m := \bigcap_{k \in \mathbb{N}_0} \mathcal{C}^k(\Omega)^m.$$

The space of all $\mathcal{C}^k(\Omega)^m$ ($k \in \mathbb{N}_0 \cup \{\infty\}$) functions with compact support is denoted by $\mathcal{C}_0^k(\Omega)^m$. We define the Lebesgue space $L^1(\Omega)^m$ of all measurable and integrable functions, i.e.

$$\int_{\Omega} |u_i(x)| dx < \infty \quad \forall i = 1, \dots, m.$$

The space of all locally integrable functions is denoted by $L_{loc}^1(\Omega)^m$. We define the Lebesgue space $L^2(\Omega)^m$ of all measurable functions, which satisfy

$$\int_{\Omega} |u_i(x)|^2 dx < \infty \quad \forall i = 1, \dots, m.$$

The Lebesgue space $L^2(\Omega)^m$ equipped with the L^2 scalar product

$$(u, v)_{L^2(\Omega)^m} := \int_{\Omega} \overline{u(x)}^T v(x) dx \quad \forall u, v \in L^2(\Omega)^m$$

is a Hilbert space. Furthermore, the L^2 scalar product induces a norm on L^2 as follows

$$\|u\|_{L^2(\Omega)^m}^2 := (u, u)_{L^2(\Omega)^m}.$$

The space of all locally integrable L^2 functions is given by

$$L_{loc}^2(\Omega)^m := \{u : \Omega \rightarrow \mathbb{C}^m \text{ measurable} : u|_K \in L^2(K)^m, \forall K \subseteq \Omega \text{ compact}\}.$$

We denote the space of all essentially bounded functions by $L^\infty(\Omega)^m$.

For singular functions, we introduce the Cauchy principle value and the Hadamard finite part.

Let $a_j \in \mathbb{C}$ with $\operatorname{Re} a_j \geq 0$ and $a_j \neq a_k$ for $j \neq k$. If a function g satisfies

$$g(\varepsilon) = \sum_{j=1}^n \frac{b_j}{\varepsilon^{a_j}} + b_{n+1} \log \varepsilon + b_{n+2} + o(1) \quad \text{for } \varepsilon \rightarrow 0,$$

then the term b_{n+2} is called the **finite part** of $g(\varepsilon)$ as $\varepsilon \rightarrow 0$, i.e. $f.p. \lim_{\varepsilon \rightarrow 0} g(\varepsilon) = b_{n+2}$. If no singular terms are present, $b_1 = \dots = b_{n+1} = 0$, and g exists as a limit, we call the limit the **Cauchy principle value**, i.e. $p.v. \lim_{\varepsilon \rightarrow 0} g(\varepsilon) = b_{n+2}$.

Sobolev spaces on domains. For notational convenience, we restrict to scalar functions for the introduction of Sobolev spaces. For vector valued functions we refer to [McL00, Chapter 3] and add the superscript index m to all function spaces. In order to define Sobolev spaces we first introduce weak partial derivatives.

Definition 1.1.1. We call $u \in L^1_{loc}(\Omega)$ weakly differentiable if there exists a function $\partial_i u \in L^1_{loc}(\Omega)$ ($i = 1, 2$) such that

$$(u, \partial_i v)_{L^2(\Omega)} = -(\partial_i u, v)_{L^2(\Omega)} \quad \forall v \in C_0^\infty(\Omega).$$

Remark 1.1.2. If $u \in L^2(\Omega)$ has a weak derivative and if u is differentiable on a subset of Ω in the classical sense, then the weak and the classical derivative coincide almost everywhere on the subset. In the following we write D^k for the k -th (weak) derivative, $\nabla u := (\partial_1 u, \partial_2 u)$ for the weak gradient, and $(\nabla u, \nabla v)_{L^2(\Omega)} = (\partial_1 u, \partial_1 v)_{L^2(\Omega)} + (\partial_2 u, \partial_2 v)_{L^2(\Omega)}$.

Definition 1.1.3. (i) We identify the Sobolev space $H^0(\Omega)$ with the Lebesgue space $L^2(\Omega)$.

Furthermore, we define

$$H^1(\Omega) := \{u \in L^2(\Omega) : u \text{ is weakly differentiable with } \nabla u \in L^2(\Omega)^2\},$$

which is equipped with the scalar product

$$(u, v)_{H^1(\Omega)} := (u, v)_{L^2(\Omega)} + (\nabla u, \nabla v)_{L^2(\Omega)}.$$

The scalar product induces a norm on $H^1(\Omega)$ which is given by

$$\|u\|_{H^1(\Omega)}^2 = (u, u)_{H^1(\Omega)} = \|u\|_{L^2(\Omega)}^2 + \|\nabla u\|_{L^2(\Omega)}^2.$$

Higher order Sobolev spaces are defined recursively for $k \in \mathbb{N}$ by

$$H^k(\Omega) = \{u \in L^2(\Omega) : u \text{ is weakly differentiable with } \nabla u \in H^{k-1}(\Omega)^2\}$$

and are associated with the scalar product and norm

$$\begin{aligned} (u, v)_{H^k(\Omega)} &= (u, v)_{L^2(\Omega)} + (\nabla u, \nabla v)_{H^{k-1}(\Omega)}, \\ \|u\|_{H^k(\Omega)}^2 &= (u, u)_{H^k(\Omega)} = \|u\|_{L^2(\Omega)}^2 + \|\nabla u\|_{H^{k-1}(\Omega)}^2. \end{aligned}$$

(ii) The space of all local H^k functions is defined by

$$H^k_{loc}(\Omega) := \{u : \Omega \rightarrow \mathbb{R} \text{ measurable} : u|_K \in H^k(K), \forall K \subseteq \Omega \text{ compact}\}.$$

Theorem 1.1.4 ([BS08, Theorem 1.3.4]). *For $k \in \mathbb{N}_0$, the spaces $C^\infty(\Omega) \cap H^k(\Omega)$ and $C^\infty(\overline{\Omega})$ are dense subspaces of $H^k(\Omega)$.*

We define fractional order Sobolev spaces using the Sobolev-Slobodeckij semi-norm as follows.

Definition 1.1.5. (i) Let $s \in (0, 1)$ and $k \in \mathbb{N}_0$. We define the scalar product

$$(u, v)_{H^s(\Omega)} := \int_{\Omega} \int_{\Omega} \frac{\overline{(u(x) - u(y))(v(x) - v(y))}}{|x - y|^{2+2s}} dx dy,$$

1. Analytical Basics and Notation

which induces the Sobolev-Slobodeckij semi-norm

$$|u|_{H^s(\Omega)}^2 = (u, u)_{H^s(\Omega)}.$$

The fractional order Sobolev space $H^{k+s}(\Omega)$ is defined by

$$H^{k+s}(\Omega) := \{u \in H^k(\Omega) : |D^k u|_{H^s(\Omega)} < \infty\}.$$

A norm on $H^{k+s}(\Omega)$ is induced by the scalar product

$$(u, v)_{H^{k+s}(\Omega)} := (u, v)_{H^k(\Omega)} + (D^k u, D^k v)_{H^s(\Omega)}.$$

(ii) We define the space $\tilde{H}^{k+s}(\Omega)$ as the closure of $C_0^\infty(\Omega)$ in $H^{k+s}(\mathbb{R}^n)$.

Theorem 1.1.6 ([AF03, Theorem 3.5]). *For $k \geq 0$, $H^k(\Omega)$ equipped with the scalar product $(\cdot, \cdot)_{H^k(\Omega)}$ is a Hilbert space.*

Sobolev spaces with negative orders are defined as the dual spaces of the Sobolev spaces with positive orders. The Riesz representation theorem leads to the following definition of dual spaces with the extended L^2 scalar product.

Definition 1.1.7. For $k \geq 0$, we denote by $\tilde{H}^{-k}(\Omega)$ the dual space of $H^k(\Omega)$ with respect to the extended L^2 scalar product $\langle \cdot, \cdot \rangle_{\tilde{H}^{-k}(\Omega) \times H^k(\Omega)}$. The norm on $\tilde{H}^{-k}(\Omega)$ is given by the dual norm

$$\|u\|_{\tilde{H}^{-k}(\Omega)} := \sup_{0 \neq v \in H^k(\Omega)} \frac{|\langle u, v \rangle_{\tilde{H}^{-k}(\Omega) \times H^k(\Omega)}|}{\|v\|_{H^k(\Omega)}}.$$

Similarly the space $H^{-k}(\Omega)$ can be defined as the dual space of $\tilde{H}^k(\Omega)$

Whenever it is clear which spaces are involved we write $\langle \cdot, \cdot \rangle$ for the extended L^2 scalar product.

Sobolev spaces on boundaries. Sobolev spaces on the boundary or a subset of the boundary are defined through a local parametrization. The idea is to define these spaces by Sobolev spaces on the parameter domain and lifting up. We only state the main facts and refer to [SaSch04, Chapter 2.4] for a detailed discussion.

For a Lipschitz domain Ω , the boundary Γ can be locally parametrized by a Lipschitz-continuous function, which allows the construction of Sobolev spaces $H^k(\Gamma)$ for $k \leq 1$. For the construction of higher order Sobolev spaces smoother boundaries are needed. For Lipschitz domains Ω with a boundary that can be locally parametrized by a Hölder continuous function of order $(k-1, 1)$, short C^k domains, the Sobolev spaces $H^k(\Gamma)$ can be defined. Here, we are only interested in the space $H^s(\Gamma)$, $s \in [0, 1]$.

For the definition of the dual space of the Sobolev space we again use the Riesz representation

theorem. For $s \in (0, 1)$, the space $H^{-s}(\Gamma)$ is defined as the dual space of $\tilde{H}^s(\Gamma)$ and the norm on $H^{-s}(\Gamma)$ as the dual norm

$$\|u\|_{H^{-s}(\Gamma)} := \sup_{0 \neq v \in \tilde{H}^s(\Gamma)} \frac{|\langle u, v \rangle_{H^{-s}(\Gamma) \times \tilde{H}^s(\Gamma)}|}{\|v\|_{\tilde{H}^s(\Gamma)}}.$$

Here, $\langle \cdot, \cdot \rangle_{H^{-s}(\Gamma) \times \tilde{H}^s(\Gamma)}$ denotes the extended L^2 scalar product.

Trace operators. For Lipschitz domains Ω , we can define trace operators on Sobolev spaces $H^k(\Omega)$ in order to obtain an analytic representation of Sobolev functions on the boundary.

Theorem 1.1.8 ([McL00, Theorems 3.37, 3.38]). *Let Ω be a Lipschitz domain with boundary Γ and $s \in (1/2, 3/2)$. There exists a linear bounded operator $\gamma_0 : H^s(\Omega) \rightarrow H^{s-1/2}(\Gamma)$ with*

$$\gamma_0 u = u|_{\Gamma} \quad \forall u \in C^\infty(\overline{\Omega}).$$

Furthermore, we can define the one-sided trace operators by $\gamma_0^- : H^s(\Omega^-) \rightarrow H^{s-1/2}(\Gamma)$ and $\gamma_0^+ : H^s(\Omega^+) \rightarrow H^{s-1/2}(\Gamma)$.

Remark 1.1.9. With the previous theorem, the space $H^{1/2}(\Gamma)$ is characterized as the trace space of $H^1(\Omega)$, i.e. $H^{1/2}(\Gamma) = \{\gamma_0 u : u \in H^1(\Omega)\}$.

We further introduce the co-normal derivative for a linear, second-order, and self-adjoint partial differential operator L with associated sesquilinear form $b(\cdot, \cdot) : H^1(\Omega) \times H^1(\Omega) \rightarrow \mathbb{C}$. Let $H_L^k(\Omega) := \{v \in H_{loc}^k : Lv \in L_{loc}^2(\Omega) \text{ in a weak sense}\}$. The co-normal derivative can be defined using Green's first identity as follows.

Lemma 1.1.10 ([SaSch04, Theorem 2.2.7]). *Let $\Omega \in \{\Omega^-, \Omega^+\}$ be a Lipschitz domain with boundary Γ . Then, the co-normal derivative $\gamma_1 : H_L^1(\Omega) \rightarrow H^{-1/2}(\Gamma)$ with*

$$\langle \gamma_1 u, \gamma_0 v \rangle = \sigma_\Omega \left(b(u, v) - \langle Lu, v \rangle_{\tilde{H}^{-1}(\Omega) \times H^1(\Omega)} \right) \quad \forall v \in H_{loc}^1(\Omega)$$

is continuous. Here, we set $\sigma_\Omega = 1$ for interior domains $\Omega = \Omega^-$ and $\sigma_\Omega = -1$ for exterior domains $\Omega = \Omega^+$.

For the one sided co-normal derivatives we write γ_1^+ and γ_1^- depending on the domain Ω^+ and Ω^- , respectively.

1.2. Boundary Integral Equations

In order to apply the boundary element method to an elliptic partial differential equation (PDE), the PDE has to be transformed into an equivalent boundary integral equation. This can be done for all partial differential operators for which a fundamental solution can be calculated. While

1. Analytical Basics and Notation

Ehrenpreis [Ehr54] proved the existence of a fundamental solution for all partial differential operators with constant coefficients, they are not known explicitly for all PDEs. In this work we are interested in the two-dimensional Laplace, Lamé, and Helmholtz operators, for which the fundamental solutions are known explicitly and hence the boundary element method can be applied.

In the remainder of this section, we denote by L an elliptic, linear, second-order, self-adjoint partial differential operator and a fundamental solution of L by $G(x, y) = G(x - y)$. Further, we assume that the domain $\Omega \in \{\Omega^-, \Omega^+\}$, in which the partial differential equation is solved, is a connected Lipschitz domain, but may contain holes. The boundary Γ is divided into the Dirichlet boundary Γ_D and the Neumann boundary Γ_N with $\Gamma = \Gamma_D \cup \overline{\Gamma_N}$. We are interested in solving the homogenous interior or exterior mixed problem

$$\begin{aligned} Lu &= 0 \quad \text{in } \Omega^\pm, \\ \gamma_0^\pm u &= \psi_D \quad \text{on } \Gamma_D, \\ \gamma_1^\pm u &= \varphi_N \quad \text{on } \Gamma_N. \end{aligned} \tag{1.1}$$

We also consider the Dirichlet problem, i.e. $\Gamma = \Gamma_D$ and the Neumann problem, i.e. $\Gamma = \Gamma_N$. For exterior problems, the solution has to satisfy an appropriate radiation condition.

The main theorem is the representation theorem for the interior and exterior problems, which states that the solution of (1.1) is uniquely determined by its Cauchy data, specifically the trace and the co-normal derivative of u .

Theorem 1.2.1 (Interior representation formula, [SaSch04, Theorem 3.1.6]). *For $u \in H^1(\Omega^-)$ with $Lu = 0$ there holds almost everywhere in Ω^-*

$$u(x) = \int_{\Gamma} G(x - y) \gamma_1^- u(y) ds_y - \int_{\Gamma} \gamma_{1,y}^- G(x - y) \gamma_0^- u(y) ds_y. \tag{1.2}$$

A similar result can be stated for exterior Laplace and Helmholtz problems with an appropriate condition at infinity, which is called the Sommerfeld radiation condition in the case of the Helmholtz equation.

Theorem 1.2.2 (Exterior representation formula, [CS85b, Lemma 3.5]). *Let $\kappa \in \mathbb{C}$ and $u \in H^1(\Omega^+)$ with $-\Delta u - \kappa^2 u = 0$ and*

$$\begin{cases} u(x) = \mathcal{O}(|x|^{-1/2}), \quad \frac{\partial u(x)}{\partial |x|} - i\kappa u = o(|x|^{-1/2}), \quad |x| \rightarrow \infty, & \kappa \neq 0 \\ u(x) = a_\infty + \frac{b_\infty}{2\pi} \log |x|, \quad |x| \rightarrow \infty, \quad a_\infty, b_\infty \in \mathbb{C}, & \kappa = 0. \end{cases} \tag{1.3}$$

Then, there holds almost everywhere in Ω^+ for $\kappa \neq 0$

$$u(x) = - \int_{\Gamma} G(x - y) \gamma_1^+ u(y) ds_y + \int_{\Gamma} \gamma_{1,y}^+ G(x - y) \gamma_0^+ u(y) ds_y \tag{1.4}$$

and for $\kappa = 0$

$$u(x) = - \int_{\Gamma} G(x - y) \gamma_1^+ u(y) ds_y + \int_{\Gamma} \gamma_{1,y}^+ G(x - y) \gamma_0^+ u(y) ds_y + a_\infty. \tag{1.5}$$

The two integral operators arising in the representation theorems are called the **single layer potential**

$$(\tilde{\mathcal{V}}\varphi)(x) := \int_{\Gamma} G(x-y) \varphi(y) ds_y \quad x \in \mathbb{R}^2 \setminus \Gamma,$$

which is well defined for $\varphi : \Gamma \rightarrow \mathbb{C}^m$, and the **double layer potential**

$$(\tilde{\mathcal{K}}\psi)(x) := \int_{\Gamma} \gamma_{1,y} G(x-y) \psi(y) ds_y \quad x \in \mathbb{R}^2 \setminus \Gamma,$$

which is well defined for $\psi : \Gamma \rightarrow \mathbb{C}^m$.

In the sequel, we state some important properties of the single and the double layer potentials, but refer to [SaSch04, Chapter 3] and [McL00, Chapter 7] for a detailed analysis.

Theorem 1.2.3 (Single layer potential). *(i) The single layer potential is a linear bounded operator with $\tilde{\mathcal{V}} : H^{-1/2}(\Gamma)^m \rightarrow H_{loc}^1(\mathbb{R}^2)^m$ and $\forall \varphi \in H^{-1/2}(\Gamma)^m$ there holds*

$$L(\tilde{\mathcal{V}}\varphi) = 0 \quad \text{weakly in } \mathbb{R}^2 \setminus \Gamma.$$

(ii) The traces $\gamma_0^{\pm} \tilde{\mathcal{V}} : H^{-1/2}(\Gamma)^m \rightarrow H^{1/2}(\Gamma)^m$ and $\gamma_1^{\pm} \tilde{\mathcal{V}} : H^{-1/2}(\Gamma)^m \rightarrow H^{-1/2}(\Gamma)^m$ are linear bounded operators and satisfy the jump relations

$$\begin{aligned} \llbracket \gamma_0 \tilde{\mathcal{V}}\varphi \rrbracket &:= \gamma_0^+ \tilde{\mathcal{V}}\varphi - \gamma_0^- \tilde{\mathcal{V}}\varphi = 0, \\ \llbracket \gamma_1 \tilde{\mathcal{V}}\varphi \rrbracket &:= \gamma_1^+ \tilde{\mathcal{V}}\varphi - \gamma_1^- \tilde{\mathcal{V}}\varphi = -\varphi. \end{aligned} \tag{1.6}$$

We state a similar result for the double layer potential.

Theorem 1.2.4 (Double layer potential). *(i) The double layer potential is a linear bounded operator with $\tilde{\mathcal{K}} : H^{1/2}(\Gamma)^m \rightarrow H_{loc}^1(\mathbb{R}^2)^m \cap H^1(\Omega)^m$ and $\forall \psi \in H^{1/2}(\Gamma)^m$ there holds*

$$L(\tilde{\mathcal{K}}\psi) = 0 \quad \text{weakly in } \mathbb{R}^2 \setminus \Gamma.$$

(ii) The traces $\gamma_0^{\pm} \tilde{\mathcal{K}} : H^{1/2}(\Gamma)^m \rightarrow H^{1/2}(\Gamma)^m$ and $\gamma_1^{\pm} \tilde{\mathcal{K}} : H^{1/2}(\Gamma)^m \rightarrow H^{-1/2}(\Gamma)^m$ are linear bounded operators and satisfy the jump relations

$$\begin{aligned} \llbracket \gamma_0 \tilde{\mathcal{K}}\psi \rrbracket &:= \gamma_0^+ \tilde{\mathcal{K}}\psi - \gamma_0^- \tilde{\mathcal{K}}\psi = \psi, \\ \llbracket \gamma_1 \tilde{\mathcal{K}}\psi \rrbracket &:= \gamma_1^+ \tilde{\mathcal{K}}\psi - \gamma_1^- \tilde{\mathcal{K}}\psi = 0. \end{aligned} \tag{1.7}$$

In general, not the complete Cauchy data $\varphi := \gamma_1 u$ and $\gamma_0 u$ are known on Γ . While for Dirichlet problems the trace $\gamma_0 u$ on Γ is known (Dirichlet boundary conditions), the co-normal derivative φ is given on Γ for Neumann problems (Neumann boundary conditions). For mixed problems the trace is only known on Γ_D and the co-normal derivative is only known on Γ_N . In order to compute the solution u in Ω the missing Cauchy data have to be determined. Therefore, we

1. Analytical Basics and Notation

derive integral equations by applying the trace operators to the representation formulas (1.2) and (1.4) (or (1.5)), i.e.

$$\gamma_0 u = \sigma_\Omega(\gamma_0 \tilde{\mathcal{V}}\varphi - \gamma_0 \tilde{\mathcal{K}}\psi) \quad (1.8)$$

$$\gamma_1 u = \sigma_\Omega(\gamma_1 \tilde{\mathcal{V}}\varphi - \gamma_1 \tilde{\mathcal{K}}\psi) \quad (1.9)$$

or for the exterior Laplace problem

$$\gamma_0 u = -\gamma_0 \tilde{\mathcal{V}}\varphi + \gamma_0 \tilde{\mathcal{K}}\psi + a_\infty \quad (1.10)$$

$$\gamma_1 u = -\gamma_1 \tilde{\mathcal{V}}\varphi + \gamma_1 \tilde{\mathcal{K}}\psi + a_\infty. \quad (1.11)$$

Here, σ_Ω is defined as in Lemma 1.1.10. The jump relations (1.6) and (1.7) motivate the definition of the following integral operators on the boundary Γ :

- the **single layer operator**: $\mathcal{V} := \gamma_0^- \tilde{\mathcal{V}}$,
- the **double layer operator**: $\mathcal{K} := 1/2 + \gamma_0^- \tilde{\mathcal{K}}$,
- the **adjoint double layer operator**: $\mathcal{K}' := -1/2 + \gamma_1^- \tilde{\mathcal{V}}$,
- the **hypersingular integral operator**: $\mathcal{W} := -\gamma_1^- \tilde{\mathcal{K}}$.

Equations (1.6) and (1.7) directly imply

$$\mathcal{V} = \gamma_0^+ \tilde{\mathcal{V}} \quad \text{and} \quad \mathcal{K}' = 1/2 + \gamma_1^+ \tilde{\mathcal{V}}$$

as well as

$$\mathcal{K} = \gamma_0^+ \tilde{\mathcal{K}} - 1/2 \quad \text{and} \quad \mathcal{W} = -\gamma_1^+ \tilde{\mathcal{K}}.$$

Remark 1.2.5. The operators \mathcal{V} and \mathcal{W} are well-defined for all $x \in \Gamma$, whereas the operators \mathcal{K} and \mathcal{K}' are only defined almost everywhere on Γ , i.e. if Γ is differentiable in a neighborhood. For a corner x we denote by β the interior angle (cf. Figure 1.1) and get the relations

$$\begin{aligned} (\mathcal{K}\psi)(x) &= \left(1 - \frac{\beta}{2\pi}\right) \psi(x) + \gamma_0^- \tilde{\mathcal{K}}\psi(x), \\ (\mathcal{K}'\psi)(x) &= -\frac{\beta}{2\pi} \psi(x) + \gamma_0^+ \tilde{\mathcal{K}}\psi(x), \end{aligned}$$

and

$$\begin{aligned} (\mathcal{K}'\varphi)(x) &:= -\frac{\beta}{2\pi} \varphi(x) + \gamma_1^- \tilde{\mathcal{V}}\varphi(x), \\ (\mathcal{K}\varphi)(x) &:= \left(1 - \frac{\beta}{2\pi}\right) \varphi(x) + \gamma_1^+ \tilde{\mathcal{V}}\varphi(x). \end{aligned}$$

An explicit representation of the integral operators and mapping properties are stated in the following theorem.

Theorem 1.2.6 ([McL00, Theorems 7.1, 7.4]). *(i) The boundary integral operators*

$$\begin{aligned} \mathcal{V} : H^{-1/2}(\Gamma)^m &\rightarrow H^{1/2}(\Gamma)^m, & \mathcal{K} : H^{1/2}(\Gamma)^m &\rightarrow H^{1/2}(\Gamma)^m, \\ \mathcal{K}' : H^{-1/2}(\Gamma)^m &\rightarrow H^{-1/2}(\Gamma)^m, & \mathcal{W} : H^{1/2}(\Gamma)^m &\rightarrow H^{-1/2}(\Gamma)^m \end{aligned}$$

are linear and bounded.

(ii) For $\varphi \in L^\infty(\Gamma)^m$ we get

$$(\mathcal{V}\varphi)(x) = \int_{\Gamma} G(x-y) \varphi(y) ds_y.$$

Let $x \in \Gamma$ and Γ be \mathcal{C}^2 -regular in a neighborhood of x . If we define

$$B(x, \varepsilon) := \{y \in \Gamma : |x - y| < \varepsilon\}, \quad \varepsilon > 0,$$

then we have for all $\varphi \in H^{-1/2}(\Gamma)^m$ and $\psi \in H^{1/2}(\Gamma)^m$

$$\begin{aligned} (\mathcal{K}\psi)(x) &= \lim_{\varepsilon \rightarrow 0} \int_{\Gamma \setminus B(x, \varepsilon)} \gamma_{1,y} G(x-y) \psi(y) ds_y, \\ (\mathcal{K}'\varphi)(x) &= \lim_{\varepsilon \rightarrow 0} \int_{\Gamma \setminus B(x, \varepsilon)} \gamma_{1,x} G(x-y) \varphi(y) ds_y, \\ (\mathcal{W}\psi)(x) &= -f.p. \lim_{\varepsilon \rightarrow 0} \int_{\Gamma \setminus B(x, \varepsilon)} \gamma_{1,x} \gamma_{1,y} G(x-y) \psi(y) ds_y. \end{aligned}$$

By setting $\varphi := \gamma_1^\pm u$ and defining σ_Ω as in Lemma 1.1.10, we rewrite Equations (1.8) and (1.9) and obtain the Caldéron system

$$\begin{pmatrix} u \\ \varphi \end{pmatrix} = \begin{pmatrix} 1/2 - \sigma_\Omega \mathcal{K} & \sigma_\Omega \mathcal{V} \\ \sigma_\Omega \mathcal{W} & 1/2 + \sigma_\Omega \mathcal{K}' \end{pmatrix} \begin{pmatrix} u \\ \varphi \end{pmatrix} \quad (1.12)$$

and for exterior Laplace problems

$$\begin{pmatrix} u \\ \varphi \end{pmatrix} = \begin{pmatrix} 1/2 + \mathcal{K} & -\mathcal{V} \\ -\mathcal{W} & 1/2 - \mathcal{K}' \end{pmatrix} \begin{pmatrix} u \\ \varphi \end{pmatrix} + \begin{pmatrix} a_\infty \\ 0 \end{pmatrix}. \quad (1.13)$$

In the sequel, we describe how the Caldéron system can be used to compute the missing Cauchy data for Dirichlet, Neumann, and mixed problems. For simplicity, we omit the exterior Laplace problem and remark that the constant a_∞ has to be added to the appropriate integral equations.

1. Analytical Basics and Notation

Dirichlet problem. If Dirichlet boundary conditions are imposed, i.e. u is given on $\Gamma_D := \Gamma$, then the first equation of the Caldéron system can be used to compute the missing Neumann data $\varphi := \gamma_1^\pm u$. This leads to Symm's integral equation

$$\sigma_\Omega \mathcal{V}\varphi = (1/2 + \sigma_\Omega \mathcal{K})u. \quad (1.14)$$

We also consider (1.14) in a more general setting $\mathcal{V}\varphi = f, f \in H^{1/2}(\Gamma)^m$.

Neumann problem. For Neumann boundary conditions, i.e. $\varphi := \gamma_1^\pm u$ on $\Gamma_N := \Gamma$, we rearrange the second equation of the Caldéron system and obtain the hypersingular integral equation

$$\sigma_\Omega \mathcal{W}u = (1/2 - \sigma_\Omega \mathcal{K}')\varphi. \quad (1.15)$$

In a general setting we will consider $\mathcal{W}u = f, f \in H^{-1/2}(\Gamma)^m$.

Mixed problem. For mixed boundary value problems the boundary is split into Γ_D and Γ_N with $\Gamma = \Gamma_D \cup \Gamma_N$ and $|\Gamma_D| > 0$. The Dirichlet data $u_D := \gamma_0^\pm u|_{\Gamma_D}$ is imposed on Γ_D and extended to Γ by zero such that $u_D \in H^{1/2}(\Gamma)$. The Neumann data $\varphi_N := \gamma_1^\pm u|_{\Gamma_N}$ is given on Γ_N and extended to Γ by zero such that $\varphi_N \in H^{-1/2}(\Gamma)$. The missing Cauchy data (u_N, φ_D) can be represented by

$$\begin{pmatrix} u_N \\ \varphi_D \end{pmatrix} = \begin{pmatrix} \gamma_0^\pm u \\ \gamma_1^\pm u \end{pmatrix} - \begin{pmatrix} u_D \\ \varphi_N \end{pmatrix}$$

and are computed by rearranging the full Caldéron system as follows

$$\mathcal{A} \begin{pmatrix} u_N \\ \varphi_D \end{pmatrix} = \begin{pmatrix} 1 \\ 2 \end{pmatrix} - \mathcal{A} \begin{pmatrix} u_D \\ \varphi_N \end{pmatrix}, \quad \mathcal{A} := \sigma_\Omega \begin{pmatrix} -\mathcal{K} & \mathcal{V} \\ \mathcal{W} & \mathcal{K}' \end{pmatrix}. \quad (1.16)$$

The operator \mathcal{A} , called the Caldéron projector, maps the space $\mathcal{H} := \tilde{H}^{1/2}(\Gamma_N) \times \tilde{H}^{-1/2}(\Gamma_D)$ to its dual space $\mathcal{H}' := \tilde{H}^{1/2}(\Gamma_D) \times \tilde{H}^{-1/2}(\Gamma_N)$. The duality product of \mathcal{H} and \mathcal{H}' is given by

$$\langle (u_D, \varphi_N), (u_N, \varphi_D) \rangle_{\mathcal{H}' \times \mathcal{H}} := \langle \varphi_D, u_D \rangle_{\Gamma_D} + \langle \varphi_N, u_N \rangle_{\Gamma_N},$$

where $\langle \cdot, \cdot \rangle_{\Gamma_D}$ and $\langle \cdot, \cdot \rangle_{\Gamma_N}$ denote the extended L^2 scalar product on Γ_D and Γ_N . Further, a norm on \mathcal{H} can be defined by

$$\|(u_N, \varphi_D)\|_{\mathcal{H}}^2 := \|u_N\|_{\tilde{H}^{1/2}(\Gamma_N)}^2 + \|\varphi_D\|_{\tilde{H}^{-1/2}(\Gamma_D)}^2.$$

1.3. BIEs for Elliptic Partial Differential Operators

In this section, we introduce boundary integral equations for the three partial differential operators that we consider in this work, namely the Laplace, the Lamé, and the Helmholtz operators. We only summarize the main results, a detailed description and analysis of all three operators can be found in [McL00, Chapters 8, 9 and 10]. For the Helmholtz equation we also refer to [CK83, SaSch04], more details on Lamé problems are given in [Ste03].

Laplace equation. For a function $u : \Omega^\pm \rightarrow \mathbb{R}$ the Laplace operator is given by $Lu := -\Delta u$. The associated bilinear form is given by $b(u, v) = \langle \nabla u, \nabla v \rangle$ and the co-normal derivative coincides with the normal derivative, i.e. $\gamma_1 u = \partial u / \partial \nu$. Here, ν denotes the unit normal vector pointing from the interior domain Ω^- to the exterior domain Ω^+ , see Figure 1.1. A fundamental solution is given by

$$G(x - y) = -\frac{1}{2\pi} \log |x - y|.$$

Under the assumptions of Theorem 1.2.6 the integral operators \mathcal{V} , \mathcal{K} , \mathcal{K}' , and \mathcal{W} have the following explicit representations

$$\begin{aligned} (\mathcal{V}\varphi)(x) &= -\frac{1}{2\pi} \int_{\Gamma} \log |x - y| \varphi(y) ds_y, \\ (\mathcal{K}\psi)(x) &= \frac{1}{2\pi} \int_{\Gamma} \frac{(x - y)^T \nu_y}{|x - y|^2} \psi(y) ds_y, \\ (\mathcal{K}'\varphi)(x) &= -\frac{1}{2\pi} \int_{\Gamma} \frac{(x - y)^T \nu_x}{|x - y|^2} \varphi(y) ds_y \\ (\mathcal{W}\psi)(x) &= -\frac{1}{2\pi} \left(-f.p. \int_{\Gamma} \frac{\nu_x^T \nu_y}{|x - y|^2} \psi(y) ds_y + \int_{\Gamma} \frac{\nu_x^T (x - y) (x - y)^T \nu_y}{|x - y|^4} \psi(y) ds_y \right). \end{aligned}$$

The next theorem summarizes important properties of the integral operators of the Laplace equation.

Theorem 1.3.1 ([McL00, Theorems 8.16, 8.20]). *Let \mathcal{V} , \mathcal{K} , \mathcal{K}' , and \mathcal{W} be the integral operators of the Laplace equation. The following statements hold.*

- (i) *If the capacity of Γ , cap_{Γ} , is smaller than one, the operator \mathcal{V} is $H^{-1/2}$ -elliptic, i.e. there exists $C > 0$ such that*

$$\langle \mathcal{V}\varphi, \varphi \rangle \geq C \|\varphi\|_{H^{-1/2}(\Gamma)}^2 \quad \forall \varphi \in H^{-1/2}(\Gamma).$$

- (ii) *Let $\Gamma_1, \dots, \Gamma_n$ denote the connected pieces of the boundary Γ . The null space of the hyper-singular operator is given by $\ker \mathcal{W} = \text{span}\{\chi_1, \dots, \chi_n\}$, where the indicator functions χ_k are defined by*

$$\chi_k = \begin{cases} 1 & \text{on } \Gamma_k \\ 0 & \text{on } \Gamma \setminus \Gamma_k. \end{cases}$$

1. Analytical Basics and Notation

The operator \mathcal{W} is elliptic on $H_*^{1/2}(\Gamma) := \{v \in H^{1/2}(\Gamma) : \langle v, w \rangle = 0 \quad \forall w \in \ker \mathcal{W}\}$, i.e. there exists $C > 0$ such that

$$\langle \mathcal{W}\psi, \psi \rangle \geq C \|\psi\|_{H_*^{1/2}(\Gamma)}^2 \quad \forall \psi \in H_*^{1/2}(\Gamma).$$

(iii) For all $\psi_1, \psi_2 \in H^{1/2}(\Gamma)$, there holds

$$\langle \mathcal{W}\psi_1, \psi_2 \rangle = \left\langle \mathcal{V} \frac{\partial \psi_1}{\partial s}, \frac{\partial \psi_2}{\partial s} \right\rangle,$$

where $\frac{\partial}{\partial s}$ denotes the arc length derivative.

(iv) The operator \mathcal{K}' is the adjoint of the double layer operator \mathcal{K} , i.e. $\langle \mathcal{K}\psi, \varphi \rangle = \langle \psi, \mathcal{K}'\varphi \rangle$ for all $\varphi \in H^{-1/2}(\Gamma)$, $\psi \in H^{1/2}(\Gamma)$.

For a definition of the capacity of the boundary we refer to [McL00, Theorem 8.15], [SlSp88], and [Dij08], but we mention that $\text{diam}(\Omega^-) < 1$ implies $\text{cap}_\Gamma < 1$. Hence the ellipticity of the single layer operator can be guaranteed by an appropriate scaling of the domain.

Lamé equation. The Lamé equation is a system of elliptic second order partial differential equations, which describes problems in linear elasticity.

We denote by $u : \Omega^- \rightarrow \mathbb{R}^2$ the displacement field of an elastic medium. Furthermore, we introduce the strain tensor $E := \frac{1}{2} (\nabla u + \nabla u^T) \in \mathbb{R}^{2 \times 2}$ and the stress tensor $\sigma \in \mathbb{R}^{2 \times 2}$. For a linear homogenous and isotropic elastic medium, the stain-stress relationship, known as Hook's law, reads

$$\sigma(u) = 2\mu E(u) + \lambda \text{div}(u) \mathbf{I}.$$

Here, we denote by \mathbf{I} the two dimensional identity matrix and by $\lambda, \mu \in \mathbb{R}$ the Lamé coefficients. We assume $\mu > 0$ and $\lambda + 2\mu > 0$ in order to obtain a strongly elliptic partial differential operator.

In the state of equilibrium all forces add up to zero, i.e. there holds

$$\text{div } \sigma + f = 0,$$

where we denote by $f : \Omega \rightarrow \mathbb{R}^2$ the body force density and write

$$\text{div } \sigma := \begin{pmatrix} \partial/\partial x_1 \sigma_{11} + \partial/\partial x_2 \sigma_{12} \\ \partial/\partial x_1 \sigma_{21} + \partial/\partial x_2 \sigma_{22} \end{pmatrix}.$$

The Lamé equation is now given by

$$Lu := -\mu \Delta u - (\lambda + \mu) \nabla(\text{div } u) = f \quad \text{in } \Omega^-.$$

1.3. BIEs for Elliptic Partial Differential Operators

The associated bilinear form reads $b(u, v) = \int_{\Omega^-} \text{tr}(\sigma(u)^T E(v)) dx$. With the first Betty identity the explicit representation of the co-normal derivative can be derived, i.e. $\gamma_1 u = \sigma(u) \nu$, where ν denotes the unit normal vector as depicted in Figure 1.1. Hence, imposing Neumann boundary conditions corresponds to fixing the traction in normal direction on the boundary. An explicit representation of a fundamental solution of the Lamé equation, the Kelvin matrix, reads

$$G(x - y) = \frac{1}{4\pi\mu(\lambda + 2\mu)} \left(-(3\mu + \lambda) \log |x - y| \mathbf{I} + (\lambda + \mu) \frac{(x - y)(x - y)^T}{|x - y|^2} \right). \quad (1.17)$$

For the co-normal derivatives of the fundamental solution and the explicit representation of the integral operators \mathcal{V} , \mathcal{K} , \mathcal{K}' , and \mathcal{W} we refer to Appendix A. We collect the main properties of the integral operators of the Lamé equation in the next theorem.

Theorem 1.3.2 ([McL00, Theorem 10.7], [GS93, Appendix]). *Let \mathcal{V} , \mathcal{K} , \mathcal{K}' , and \mathcal{W} be the integral operators of the Lamé equation.*

(i) *The single layer operator \mathcal{V} is $H^{-1/2}$ -elliptic, i.e. there exists $C > 0$ such that*

$$\langle \mathcal{V}\varphi, \varphi \rangle \geq C \|\varphi\|_{H^{-1/2}(\Gamma)^2}^2 \quad \forall \varphi \in H^{-1/2}(\Gamma)^2.$$

(ii) *Let Ω^- be simply connected. The null space of the hypersingular operator is given by*

$$\ker \mathcal{W} = \text{span}\{(1, 0), (0, 1), (x_2, -x_1) : x \in \Gamma\}.$$

\mathcal{W} is elliptic on $H_^{1/2}(\Gamma)^2 := \{v \in H^{1/2}(\Gamma)^2 : \langle v, w \rangle = 0 \quad \forall w \in \ker \mathcal{W}\}$, i.e. there exists $C > 0$ such that*

$$\langle \mathcal{W}\psi, \psi \rangle \geq C \|\psi\|_{H_*^{1/2}(\Gamma)^2}^2 \quad \forall \psi \in H_*^{1/2}(\Gamma)^2.$$

(iii) *For all $\psi_1, \psi_2 \in H^{1/2}(\Gamma)^2$, we have the identity*

$$\langle \mathcal{W}\psi_1, \psi_2 \rangle = \left\langle \mathcal{V}^* \frac{\partial \psi_1}{\partial s}, \frac{\partial \psi_2}{\partial s} \right\rangle,$$

where $\frac{\partial}{\partial s}$ denotes the arc length derivative and

$$(\mathcal{V}^*\varphi)(x) = \frac{\mu(\mu + \lambda)}{\pi(\lambda + 2\mu)} \int_{\Gamma} \left(-\log |x - y| \mathbf{I} + \frac{(x - y)(x - y)^T}{|x - y|^2} \right) \varphi(y) ds_y. \quad (1.18)$$

(iv) *The operator \mathcal{K}' is the adjoint of the double layer operator \mathcal{K} , i.e. $\langle \mathcal{K}\psi, \varphi \rangle = \langle \psi, \mathcal{K}'\varphi \rangle$ for all $\varphi \in H^{-1/2}(\Gamma)^2$, $\psi \in H^{1/2}(\Gamma)^2$.*

Physically, the null space of the hypersingular operator consists of all rigid body motions, i.e. the translations in x_1 and x_2 direction and the rotation. Hence, the solution of the interior Neumann

1. Analytical Basics and Notation

problem is unique up to strain-free displacements that are comprised of the rigid body motions. For multi-connected domains with holes, the null space is spanned by all rigid body motions of each connected piece of the boundary.

Helmholtz equation. For acoustic wave propagation in a homogenous medium with speed of sound c and damping coefficient γ the velocity potential U satisfies, in the linearized theory, the dissipative wave equation

$$\frac{\partial^2 U}{\partial t^2} + \gamma \frac{\partial U}{\partial t} - c^2 \Delta U = 0. \quad (1.19)$$

The space dependent part $u : \Omega \rightarrow \mathbb{C}$ of a time-harmonic solution of (1.19) with frequency $\omega > 0$ satisfies the Helmholtz equation

$$Lu := -\Delta u - \kappa^2 u = 0. \quad (1.20)$$

Here, $\kappa^2 = \frac{\omega(\omega+i\gamma)}{c^2} \in \mathbb{C} \setminus \{0\}$ is called the wave number, where $\text{Im}(\kappa) \geq 0$ corresponds to damping and $\text{Im}(\kappa) < 0$ corresponds to excitation of the wave. Within this work, we consider damped waves and hence choose κ with $\text{Im}(\kappa) \geq 0$. For $\kappa \in \mathbb{R}$, the Helmholtz operator is self-adjoint.

The sesquilinear form of the Helmholtz operator is given by $b(u, v) = \langle \nabla u, \nabla v \rangle - \int_{\Omega} \overline{\kappa^2 u} v \, dx$. Green's identity directly implies that the co-normal derivative is given by $\gamma_1 u = \partial u / \partial \nu$.

Before we state important properties of the integral operators, we first give a result for the solvability of the interior and exterior Helmholtz problems. Therefore, we define the set of all interior Dirichlet and Neumann eigenvalues of the Laplace operator by

$$M_D := \{\lambda \in \mathbb{C} : \exists v \in H^1(\Omega^-) \setminus \{0\}, -\Delta v = \lambda v \text{ in } \Omega^-, \gamma_0^- v = 0 \text{ on } \Gamma\}, \quad (1.21)$$

$$M_N := \{\lambda \in \mathbb{C} : \exists v \in H^1(\Omega^-) \setminus \{0\}, -\Delta v = \lambda v \text{ in } \Omega^-, \gamma_1^- v = 0 \text{ on } \Gamma\}. \quad (1.22)$$

Theorem 1.3.3 (Interior Helmholtz problem, [CK83, Theorems 3.20, 3.24]). *Let $f \in \tilde{H}^{-1}(\Omega^-)$.*

(i) *For $g \in H^{1/2}(\Gamma)$, the interior Dirichlet problem*

$$-\Delta u - \kappa^2 u = f \quad \text{in } \Omega^-, \quad \gamma_0^- u = g \quad \text{on } \Gamma$$

has a unique solution $u \in H^1(\Omega^-)$ if and only if $\kappa^2 \notin M_D$.

(ii) *For $g \in H^{-1/2}(\Gamma)$, the interior Neumann problem*

$$-\Delta u - \kappa^2 u = f \quad \text{in } \Omega^-, \quad \gamma_1^- u = g \quad \text{on } \Gamma$$

has a unique solution $u \in H^1(\Omega^-)$ if and only if $\kappa^2 \notin M_N$.

Theorem 1.3.4 (Exterior Helmholtz problem, [McL00, Theorem 9.11]). *Let $f \in \tilde{H}^{-1}(\Omega^+)$ have compact support.*

(i) *For $g \in H^{1/2}(\Gamma)$, the exterior Dirichlet problem*

$$-\Delta u - \kappa^2 u = f \quad \text{in } \Omega^+, \quad \gamma_0^+ u = g \quad \text{on } \Gamma$$

has a unique solution $u \in H_{loc}^1(\Omega^+)$, if the radiation condition (1.3) is satisfied.

(ii) *For $g \in H^{-1/2}(\Gamma)$, the exterior Neumann problem*

$$-\Delta u - \kappa^2 u = f \quad \text{in } \Omega^+, \quad \gamma_1^+ u = g \quad \text{on } \Gamma$$

has a unique solution $u \in H_{loc}^1(\Omega^+)$, if the radiation condition (1.3) is satisfied.

An explicit representation of a fundamental solution of the Helmholtz equation is given by the Hankel function

$$G(x - y) = \frac{i}{4} H_0^{(1)}(\kappa|x - y|).$$

The main properties of the Hankel function and the representation of all integral operators are collected in Appendix A.

We state some important properties of the integral operators in the following theorem.

Theorem 1.3.5 ([SaSch04, Theorems 3.9.1, 3.9.8], [CS85b, Lemma 3.9]). *Let \mathcal{V} , \mathcal{K} , \mathcal{K}' , and \mathcal{W} be the integral operators of the Helmholtz equation. The following statements hold.*

(i) *The null space of the single layer operator is given by*

$$\ker \mathcal{V} = \{\gamma_1^- v : -\Delta v = \kappa^2 v \text{ in } \Omega^-, \gamma_0^- v \text{ on } \Gamma\}.$$

The operator \mathcal{V} is invertible if and only if $\kappa^2 \notin M_D$.

(ii) *The single layer operator can be decomposed into an elliptic and a compact operator, i.e.*

$$\mathcal{V} = \mathcal{V}_0 + T_{\mathcal{V}},$$

where \mathcal{V}_0 denotes the single layer operator of the Laplace problem and $T_{\mathcal{V}} : H^{-1/2}(\Gamma) \rightarrow H^{1/2}(\Gamma)$ is compact.

(iii) *There holds $\ker \mathcal{W} = \{\gamma_0^- v : -\Delta v = \kappa^2 v \text{ in } \Omega^-, \gamma_1^- v \text{ on } \Gamma\}$ and hence the hypersingular operator is invertible if and only if $\kappa^2 \notin M_N$.*

(iv) *The hypersingular operator can be decomposed into an elliptic and a compact operator, i.e.*

$$\mathcal{W} = \mathcal{W}_0 + T_{\mathcal{W}},$$

where \mathcal{W}_0 denotes the hypersingular operator of the Laplace problem and $T_{\mathcal{W}} : H^{1/2}(\Gamma) \rightarrow H^{-1/2}(\Gamma)$ is compact.

1. Analytical Basics and Notation

(v) For all $\psi_1, \psi_2 \in H^{1/2}(\Gamma)$, there holds

$$\langle \mathcal{W}\psi_1, \psi_2 \rangle = \left\langle \mathcal{V} \frac{\partial \psi_1}{\partial s}, \frac{\partial \psi_2}{\partial s} \right\rangle - \kappa^2 \langle \mathcal{V}\psi_1 \nu, \psi_2 \nu \rangle,$$

where $\frac{\partial}{\partial s}$ denotes the arc length derivative.

(vi) The operator \mathcal{K}' is the adjoint of the double layer operator \mathcal{K} , i.e. $\langle \mathcal{K}\psi, \varphi \rangle = \overline{\langle \psi, \mathcal{K}'\varphi \rangle}$ for all real-valued functions $\varphi \in H^{-1/2}(\Gamma)$, $\psi \in H^{1/2}(\Gamma)$.

Properties (ii) and (iv) imply that \mathcal{V} and \mathcal{W} are Fredholm operators with index zero. This is used for the proof of the existence of a unique solution in the subsequent sections.

Remark 1.3.6. For all wave numbers $\kappa \in \mathbb{C} \setminus \{0\}$, the existence of a unique solution of exterior problems is guaranteed. Since the integral operators \mathcal{V} and \mathcal{W} are not invertible for all wave numbers, the integral equations (1.14), (1.15), and (1.16) are not solvable and cannot be used for the computation of the missing Cauchy data if $\kappa^2 \in M_D$ or $\kappa^2 \in M_N$.

To remedy this problem there are various different approaches, see [BW65, Pan65, Lei65, BM71] to name a few but not all. We only state the approach by Brakhage and Werner [BW65] for the exterior Dirichlet problem. The idea is to choose $\eta \in \mathbb{R}$ such that $\eta \operatorname{Re}(\kappa) > 0$. For $x \in \Omega^+$ and $\varphi := \gamma_1^+ u$, we set

$$u = \tilde{\mathcal{K}}\varphi - i\eta\tilde{\mathcal{V}}\varphi.$$

It can be proven that the solution u satisfies the Sommerfeld radiation condition and $Lu = 0$ in Ω^+ . The jump relations of the single and the double layer potentials yield the boundary integral equation

$$(1/2 + \mathcal{K} - i\eta\mathcal{V})\varphi = u. \tag{1.23}$$

The invertibility of the operator $1/2 + \mathcal{K} - i\eta\mathcal{V}$ is proven in [BW65] if the boundary Γ is globally smooth. Hence, the missing Neumann data can be computed with (1.23). We stress that for non-smooth boundaries the invertibility of the operator $1/2 + \mathcal{K} - i\eta\mathcal{V}$ is still an open question. The problem is that if Γ is not smooth the potentials $\tilde{\mathcal{V}}$ and $\tilde{\mathcal{K}}$ have different domains of definition. However, we do not go into detail on alternative boundary integral formulations, but assume $\kappa^2 \notin M_D \cup M_N$ throughout this work.

1.4. Triangulation and Discrete Spaces

In order to numerically solve the boundary integral equations introduced in Section 1.2, we consider finite-dimensional subspaces of the involved Sobolev spaces.

Let $\Omega^- \subset \mathbb{R}^2$ be a bounded Lipschitz domain with boundary Γ and its complement $\Omega^+ = \mathbb{R}^2 \setminus \overline{\Omega^-}$. Γ is divided into relative open and disjoint sub boundaries, i.e. the Dirichlet and

Neumann boundary. We consider the cases $\Gamma := \Gamma_D$ (Dirichlet problem), $\Gamma := \Gamma_N$ (Neumann problem) and $\Gamma := \Gamma_D \cup \overline{\Gamma_N}$ (mixed problem). For the discretization of the boundary we introduce a triangulation.

Definition 1.4.1. (i) A triangulation \mathcal{T} is defined by

$$\mathcal{T} := \left\{ T_i, i = 1, \dots, \mathcal{N}_e, \Gamma = \bigcup_{i=1}^{\mathcal{N}_e} T_i, |T_i \cap T_j| = 0 \text{ for } i \neq j. \right\}.$$

We refer to $T_i \in \mathcal{T}$ as boundary elements and call $\mathcal{N}_e = |\mathcal{T}|$ the number of elements. If the boundary is divided into the Dirichlet and Neumann boundaries, we assume that each boundary element $T \in \mathcal{T}$ either belongs to Γ_D or Γ_N and introduce the triangulations of the sub-boundaries by

$$\begin{aligned} \mathcal{T}_D &:= \{T \in \mathcal{T} : |T \cap \Gamma_D| > 0\} \quad \text{and} \\ \mathcal{T}_N &:= \{T \in \mathcal{T} : |T \cap \Gamma_N| > 0\}. \end{aligned}$$

In particular, we have $\mathcal{T} = \mathcal{T}_D \cup \mathcal{T}_N$ and $\mathcal{T}_D \cap \mathcal{T}_N = \emptyset$.

- (ii) For a given triangulation, we denote by M_v the set of all element end-points, which we call nodes, and by $\mathcal{N}_v := |M_v|$ the number of nodes.
- (iii) We assume that each boundary element $T_i \in \mathcal{T}$ is parametrized by a bijective Lipschitz-continuous function $\gamma_i : [-1, 1] \rightarrow T_i$ with smooth inverse.
- (iv) Let $\mathbf{h} \in L^\infty(\Gamma)$ be the mesh-width function with $\mathbf{h}|_{\text{int}(T_i)} = |T_i| =: h_i$, where $|T_i|$ denotes the arc length of the element T_i . Further, we introduce the mesh-width ratio

$$\sigma(\mathbf{h}) := \max \left\{ \frac{h_i}{h_j}, T_i, T_j \in \mathcal{T}, T_i \cap T_j \neq \emptyset \right\}.$$

- (v) Let $\mathbf{p} \in L^\infty(\Gamma)$ be the polynomial degree function with $\mathbf{p}|_{\text{int}(T_i)} =: p_i \in \mathbb{N}_0$.
- (vi) Let $\mathbf{k} \in L^\infty(\Gamma)$ be the regularity function with $\mathbf{k}(x_j) =: k_j \in \mathbb{Z}$ with $\mathbf{k}(x_j) \geq 0$, $x_j \in M_v$.

We are now in the position to introduce the discrete ansatz spaces that we use for the implementation.

Definition 1.4.2. Let $\mathcal{T}, \mathbf{h} \in L^\infty(\Gamma), \mathbf{p} \in L^\infty(\Gamma)$, and $\mathbf{k} \in L^\infty(\Gamma)$ as defined in Definition 1.4.1. We denote the space of all functions that are k_j times continuously differentiable at each node $x_j \in M_v$ by $\mathcal{C}^{\mathbf{k}}(\Gamma), j = 1, \dots, \mathcal{N}_v$. The finite-dimensional ansatz spaces are defined by

$$S(\mathcal{T}, \mathbf{h}, \mathbf{p}, \mathbf{k}) := \{\varphi \in \mathcal{C}^{\mathbf{k}-1}(\Gamma) : \varphi|_{T_i} \circ \gamma_i \in \mathcal{P}_{p_i}([-1, 1]), i = 1, \dots, \mathcal{N}_e\} \quad (1.24)$$

$$R(\mathcal{T}, \mathbf{h}, \mathbf{p}, \mathbf{k}) \subset \{\varphi \in \mathcal{C}^{\mathbf{k}-1}(\Gamma) : \varphi|_{T_i} \circ \gamma_i \in \mathcal{R}_{p_i}([-1, 1]), i = 1, \dots, \mathcal{N}_e\}. \quad (1.25)$$

1. Analytical Basics and Notation

Here, \mathcal{P}_p and \mathcal{R}_p denote the space of all polynomials and rational functions with degree $p \in \mathbb{N}_0$, respectively. We denote the dimension of the ansatz spaces by \mathcal{N} .

Remark 1.4.3. The discrete spaces $S(\mathcal{T}, \mathbf{h}, \mathbf{p}, \mathbf{0}) \subset H^{-1/2}(\Gamma)$ of globally discontinuous functions and $S(\mathcal{T}, \mathbf{h}, \mathbf{p}, \mathbf{1}) \subset H^{1/2}(\Gamma)$ of globally continuous functions are the spaces used for classical Galerkin BEM on polygons. The space $S(\mathcal{T}, \mathbf{h}, \mathbf{p}, \mathbf{p})$ is widely used for collocation methods and the rational space $R(\mathcal{T}, \mathbf{h}, \mathbf{p}, \mathbf{k})$ is used for isogeometric methods (see Section 3.2).

We further introduce the ansatz space $S_{\vartheta}^{\sigma} := S(\mathcal{T}_{\vartheta}, \mathbf{h}_{\vartheta}, \mathbf{p}^{\sigma}, \mathbf{k})$ with respect to a geometrically graded hp -mesh. Given a mesh grading parameter $\vartheta \in (0, 1)$, the boundary Γ is divided geometrically towards a corner. In particular, we obtain $h_i/h_j = \vartheta$ for neighboring elements T_i and T_j , where T_i is the element closer to the corner. The polynomials degree vector \mathbf{p}^{σ} is constructed as follows. At the smallest element near the corner we set $p = 0$ and increase the polynomial degree linearly with slope $\sigma \in \mathbb{N}$. The two examples of a unit circle and a smoothened L-shaped domain, that we consider within the scope of this work, are illustrated in Figure 1.2.

1.5. Collocation Methods

In this section we introduce collocation methods for solving the boundary integral equations (1.14), (1.15), and (1.16). We first derive fully discrete formulations for the Dirichlet, Neumann, and mixed problems and then go into detail on the existence of a unique solution and a priori error estimates.

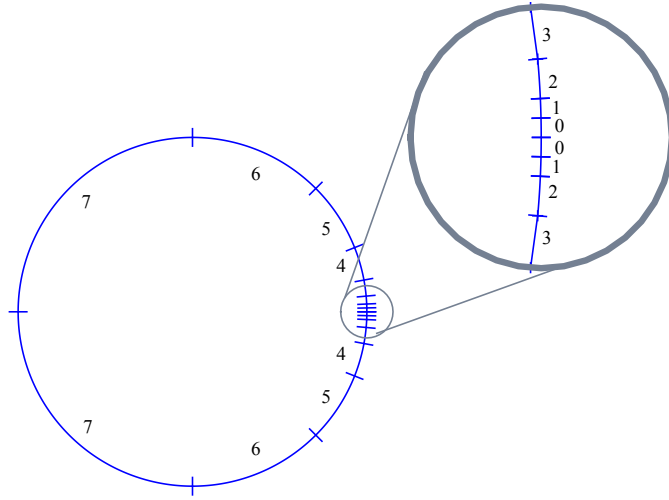
1.5.1. Discrete Collocation BEM

The idea of collocation methods is, that the involved Sobolev spaces are substituted by finite-dimensional subspaces and the integral equation is fulfilled at a discrete number of collocation points.

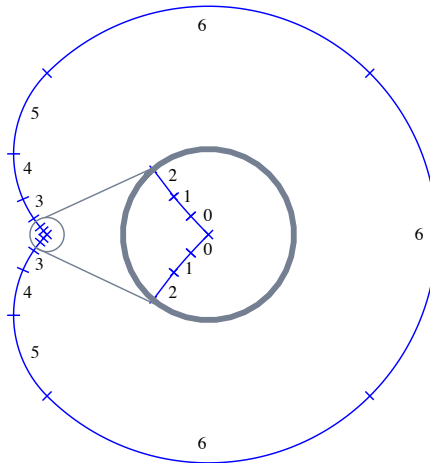
Let $X_{\ell} \subset H^{-1/2}(\Gamma)$ and $Y_{\ell} \subset H^{1/2}(\Gamma)$ be two of the finite-dimensional ansatz spaces defined in Definition 1.4.2 with bases $\{\Phi_1, \dots, \Phi_{\mathcal{N}}\}$ and $\{\Psi_1, \dots, \Psi_{\mathcal{M}}\}$. We denote by $M_{C,X} = \{x_1, \dots, x_{\mathcal{N}}\} \subset \Gamma$ and $M_{C,Y} = \{y_1, \dots, y_{\mathcal{M}}\} \subset \Gamma$ the sets of collocation points with respect to the spaces X_{ℓ} and Y_{ℓ} .

Symm's integral equation. Symm's integral equation reads

$$\sigma_{\Omega}(\mathcal{V}\varphi)(x) = (\sigma_{\Omega}\mathcal{K} + 1/2)u(x), \quad u \in H^{1/2}(\Gamma)$$



(a) Geometric hp -grid on the unit circle. The numbers indicate the polynomial degree on each element.



(b) Geometric hp -grid on the smoothed L-shaped domain. The numbers indicate the polynomial degree on each element.

Figure 1.2.: Examples of geometric hp -grid and polynomial degree vectors with $\vartheta = 0.5$ and $\sigma = 1$, that can be used for geometric hp -refinements.

1. Analytical Basics and Notation

with σ_Ω as in Lemma 1.1.10 or in the general setting

$$(\mathcal{V}\varphi)(x) = f(x), \quad f \in H^{1/2}(\Gamma).$$

The discrete problem is then given by:

Find $\varphi_h \in X_\ell$ such that

$$\begin{aligned} \sigma_\Omega(\mathcal{V}\varphi_h)(x_j) &= (\sigma_\Omega\mathcal{K} + 1/2)u(x_j), \quad j = 1, \dots, \mathcal{N}, \\ (\text{or } (\mathcal{V}\varphi_h)(x_j) &= f(x_j), \quad j = 1, \dots, \mathcal{N}. \end{aligned}$$

Projecting the Dirichlet data on Y_ℓ , i.e. $u_h := \sum_{k=1}^{\mathcal{M}} \mathbf{u}_k \Psi_k$, and writing $\varphi_h = \sum_{k=1}^{\mathcal{N}} \varphi_k \Phi_k$ we obtain the system of linear equations

$$\begin{aligned} \sigma_\Omega \mathbf{V} \boldsymbol{\varphi} &= (\sigma_\Omega \mathbf{K} + 1/2 \mathbf{M}_X) \mathbf{u} \\ (\text{or } \mathbf{V} \boldsymbol{\varphi} &= \mathbf{f}. \end{aligned}$$

Here, $\mathbf{V} := (\mathbf{V}_{jk})_{k,j=1,\dots,\mathcal{N}}$ with $\mathbf{V}_{jk} := (\mathcal{V}\Phi_k)(x_j)$ and $\mathbf{K} := (\mathbf{K}_{jk})_{j=1,\dots,\mathcal{N}}^{k=1,\dots,\mathcal{M}}$ with $\mathbf{K}_{jk} := (\mathcal{K}\Psi_k)(x_j)$ denote the collocation matrices of the single and the double layer operators and the mass matrix is given by $\mathbf{M}_X := (\mathbf{M}_{jk})_{j=1,\dots,\mathcal{N}}^{k=1,\dots,\mathcal{M}}$ and $\mathbf{M}_{jk} := \Psi_k(x_j)$. The entries of the right-hand side vector \mathbf{f} are given by $\mathbf{f}_j = f(x_j)$, $j = 1, \dots, \mathcal{N}$.

The hypersingular integral equation. Recall that the hypersingular integral equation reads

$$\sigma_\Omega(\mathcal{W}u)(x) = (1/2 - \sigma_\Omega\mathcal{K}')\varphi(x), \quad \varphi = \gamma_1^\pm u \in H^{-1/2}(\Gamma)$$

or in the general setting

$$(\mathcal{W}u)(x) = f(x), \quad f \in H^{-1/2}(\Gamma).$$

The discrete problem is then given by:

Find $u_h \in Y_\ell$ such that

$$\begin{aligned} \sigma_\Omega(\mathcal{W}u_h)(y_j) &= (1/2 - \sigma_\Omega\mathcal{K}')\varphi(y_j), \quad j = 1, \dots, \mathcal{M}, \\ (\text{or } (\mathcal{W}u_h)(y_j) &= f(y_j), \quad j = 1, \dots, \mathcal{M}. \end{aligned}$$

Projecting the Neumann data on X_ℓ , i.e. $\varphi_h := \sum_{k=1}^{\mathcal{N}} \varphi_k \Phi_k$, and writing $u_h = \sum_{k=1}^{\mathcal{M}} \mathbf{u}_k \Psi_k$ we obtain the system of linear equations

$$\begin{aligned} \sigma_\Omega \mathbf{W} \mathbf{u} &= (1/2 \mathbf{M}_Y - \sigma_\Omega \mathbf{A}) \boldsymbol{\varphi} \\ (\text{or } \mathbf{W} \mathbf{u} &= \mathbf{f}. \end{aligned}$$

Here, $\mathbf{W} := (\mathbf{W}_{jk})_{k,j=1,\dots,\mathcal{M}}$ with $\mathbf{W}_{jk} := (\mathcal{W}\Psi_k)(y_j)$ and $\mathbf{A} := (\mathbf{A}_{jk})_{j=1,\dots,\mathcal{M}}^{k=1,\dots,\mathcal{N}}$ with $\mathbf{A}_{jk} := (\mathcal{K}'\Phi_k)(y_j)$ denote the collocation matrices of the hypersingular and the adjoint double layer operators. The mass matrix is given by $\mathbf{M}_Y := (\mathbf{M}_{jk})_{j=1,\dots,\mathcal{M}}^{k=1,\dots,\mathcal{N}}$ and $\mathbf{M}_{jk} := \Phi_k(y_j)$ and the entries of the right-hand side vector \mathbf{f} by $\mathbf{f}_j = f(y_j)$, $j = 1, \dots, \mathcal{M}$.

Remark 1.5.1. Since the null space of the hypersingular operator is non-trivial, appropriate conditions have to be introduced in order to solve the discrete problem. Within the scope of this work, we consider the hypersingular integral equation on an open arc for the Laplace equation and imply that the solution u_h vanishes at both endpoints.

Mixed problem. With the notation of Section 1.2 (paragraph mixed problem) the integral equation, which we solve for mixed boundary conditions reads

$$\mathcal{A} \begin{pmatrix} u_N \\ \varphi_D \end{pmatrix} = \left(\frac{1}{2} - \mathcal{A} \right) \begin{pmatrix} u_D \\ \varphi_N \end{pmatrix}. \quad (1.26)$$

We assume $M_{C,X} \subset \Gamma_D$ as well as $M_{C,Y} \subset \Gamma_N$. The ansatz space is given by $Y_{\ell,N} \times X_{\ell,D} \subset \mathcal{H}$. With the notation of the previous two paragraphs we obtain the following discrete problem

$$\sigma_\Omega \begin{pmatrix} -\mathbf{K}_{\Gamma_D \times \Gamma_N} & \mathbf{V}_{\Gamma_D \times \Gamma_D} \\ \mathbf{W}_{\Gamma_N \times \Gamma_N} & \mathbf{A}_{\Gamma_N \times \Gamma_D} \end{pmatrix} \begin{pmatrix} \mathbf{u}_N \\ \varphi_D \end{pmatrix} = \left(\frac{1}{2} \begin{pmatrix} \mathbf{M}_X & \mathbf{0} \\ \mathbf{0} & \mathbf{M}_Y \end{pmatrix} - \sigma_\Omega \begin{pmatrix} -\mathbf{K} & \mathbf{V} \\ \mathbf{W} & \mathbf{A} \end{pmatrix} \right) \begin{pmatrix} \mathbf{u}_D \\ \varphi_N \end{pmatrix}. \quad (1.27)$$

1.5.2. A Priori Error Analysis

In order to derive a priori estimates for all above considered integral equations simultaneously, we consider the general problem

$$Au = f \quad \text{on } \Gamma \quad (1.28)$$

with a bijective Fredholm operator A with index zero, i.e. $A = A_0 + K$ can be decomposed into an elliptic and a compact operator. This assumption guarantees that A satisfies the Gårding inequality. We stress that the single layer and the hypersingular operator for Laplace, Lamé, and Helmholtz problems are of this type, see Theorems 1.3.1, 1.3.2, and 1.3.5.

The following theorem states a result concerning the solvability of the discrete problem and gives an h -asymptotic a priori error estimate for the numerical solution.

Theorem 1.5.2 ([AW83, Theorem 2.1.5]). *Let Γ be analytic and \mathbf{p} be uniform and odd, i.e. $\mathbf{p} = 2j - 1$ with $j \in \mathbb{N}$. We chose α such that $A : H^{j+\alpha}(\Gamma) \rightarrow H^{j-\alpha}(\Gamma)$ and the collocation points to be the nodes, i.e. $M_C := M_v$ with M_v as defined in Definition 1.4.1 (ii).*

Provided $j - \alpha < 1/2$, the discrete problem

$$Au_h(x_k) = f(x_k) \quad \forall x_k \in M_C. \quad (1.29)$$

has a unique solution $u_h \in S(\mathcal{T}, \mathbf{h}, \mathbf{p}, \mathbf{p})$ with

$$\|u - u_h\|_{H^{j+\alpha}(\Gamma)} \leq C \inf_{v_h \in S(\mathcal{T}, \mathbf{h}, \mathbf{p}, \mathbf{p})} \|u - v_h\|_{H^{j+\alpha}(\Gamma)}. \quad (1.30)$$

1. Analytical Basics and Notation

If $u \in H^s(\Gamma)$, $j + \alpha \leq s \leq \alpha$, then

$$\|u - u_h\|_{H^{j+\alpha}(\Gamma)} \leq Ch^{s-j-\alpha} \|u\|_{H^s(\Gamma)}. \quad (1.31)$$

with a constant $C > 0$.

Remark 1.5.3. (i) The proof of Theorem 1.5.2 is based on the derivation of an equivalent Galerkin formulation on which the Céa Lemma can be applied. Using the well-known approximation estimates for the spline space $S(\mathcal{T}, \mathbf{h}, \mathbf{p}, \mathbf{p})$ the a priori estimate (1.31) is obtained. The restriction $j - \alpha < 1/2$ arises since we require $S(\mathcal{T}, \mathbf{h}, \mathbf{p}, \mathbf{p}) \subset H^{j-\alpha}(\Gamma)$ and $\mathcal{A}u_h \in \mathcal{C}(\Gamma)$.

(ii) The theorem requires strong assumptions, i.e. a smooth boundary, only odd degree basis functions of highest regularity and collocation only at end points. Thus, it can only be applied to a small class of problems.

However, similar results are proven in [SW85] for even degree basis functions where the collocation points are chosen as element midpoints. In [CS85a] piecewise smooth boundaries are investigated. Using weighted Sobolev spaces estimates similar to (1.31) are derived for lowest order basis functions, i.e. $\mathbf{p} = 0$ and $\mathbf{p} = 1$. In [Sch86, Dom03] the ε collocation method is introduced which allows to choose more general uniform collocation points. In particular, convergence is proven for collocation points that are shifted by $\varepsilon > 0$ and positioned between the end and mid points.

(iii) An open issue is the convergence and the a priori estimates for non-smooth splines, i.e. for $S(\mathcal{T}, \mathbf{h}, \mathbf{p}, \mathbf{k})$ and $R(\mathcal{T}, \mathbf{h}, \mathbf{p}, \mathbf{k})$ with $\mathbf{k} < \mathbf{p}$. Further, it is not clear how to choose the collocation points for the general case $S(\mathcal{T}, \mathbf{h}, \mathbf{p}, \mathbf{k})$, since more than one collocation point has to be chosen on each element. We will address the optimal choice of the collocation points in Chapter 5.

For Symm's integral equation of Laplace problems on the slit $\Gamma = (-1, 1)$, a p -asymptotic estimate is given in [SIS92]. Therefore, we introduce the Sobolev-type norms for $s \in \mathbb{R}$ by

$$\|u\|_{\hat{H}^s(\Gamma)} := \left(\frac{\pi}{2}\right)^{1/2} \left(\frac{1}{2} |u_0|^2 + \sum_{k=1}^{\infty} k^{2s} |u_k|^2 \right),$$

where u_k , $k \in \mathbb{N}_0$ denote the coefficients of the Chebyshev expansion of u . The space $\hat{H}^s(\Gamma)$ is defined as the closure of the set of all polynomials with respect to this norm. For $\omega(x) = (1 - x^2)^{-1/2}$ and $v = \omega u$, a second Sobolev-type norm is defined by

$$\|v\|_{\overline{H}^s(\Gamma)} := \|u\|_{\hat{H}^s(\Gamma)}.$$

Theorem 1.5.4 ([SlSt92, Theorem 2]). *Let $\Gamma = (-1, 1)$ and $f \in \hat{H}^{t+1}(\Gamma)$. For $p \in \mathbb{N}_0$, there exists a solution $\varphi_h \in \omega\mathcal{P}_p$ of*

$$(\mathcal{V}\varphi_h)(x_j) = f(x_j), \quad j = 1, \dots, p,$$

where x_j denote the zeros of the p -th Chebyshev polynomial. Furthermore, if $t > -1/2$ and $t \geq s$, then for the exact solution $\varphi \in \overline{H}^t(\Gamma)$, there holds

$$\|\varphi - \varphi_h\|_{\overline{H}^s(\Gamma)} \leq c p^{-\min\{t-s, t+1\}} \|f\|_{\hat{H}^{t+1}(\Gamma)}.$$

Remark 1.5.5. A corresponding result is also proven for the hypersingular integral equation on the slit in [ES92]. Here, the basis functions are chosen to be the Chebyshev polynomials of the second kind and their zeros are chosen as the collocation points.

1.6. Galerkin Methods

Galerkin methods are another approach for solving the boundary integral equations derived in Section 1.2. The first part of this section is devoted to the derivation of numerical schemes for the solution of the boundary integral equations with a Galerkin method, while in the second part we state important results for the a priori error estimation.

1.6.1. Discrete Galerkin BEM

Throughout this section let $X_\ell \subset H^{-1/2}(\Gamma)$ and $Y_\ell \subset H^{1/2}(\Gamma)$ be two of the discrete spaces introduced in Definition 1.4.2 with bases $\{\Phi_1, \dots, \Phi_N\}$ and $\{\Psi_1, \dots, \Psi_M\}$, respectively. We investigate the boundary integral equations (1.14), (1.15) and (1.16), separately.

Symm's integral equation. Recall that Symm's integral equation reads

$$\sigma_\Omega(\mathcal{V}\varphi)(x) = (\sigma_\Omega\mathcal{K} + 1/2)u(x), \quad u \in H^{1/2}(\Gamma)$$

with σ_Ω as in Lemma 1.1.10 or in the general setting

$$(\mathcal{V}\varphi)(x) = f(x), \quad f \in H^{1/2}(\Gamma).$$

The variational formulations are given by:

For $u \in H^{1/2}(\Gamma)$ (or $f \in H^{1/2}(\Gamma)$), find $\varphi \in H^{-1/2}(\Gamma)$ such that

$$\begin{aligned} \langle \sigma_\Omega \mathcal{V}\varphi, v \rangle &= \langle (\sigma_\Omega \mathcal{K} + 1/2)u, v \rangle, \quad \forall v \in H^{-1/2}(\Gamma) \\ \text{(or } \langle \mathcal{V}\varphi, v \rangle &= \langle f, v \rangle, \quad \forall v \in H^{-1/2}(\Gamma) \text{).} \end{aligned} \tag{1.32}$$

1. Analytical Basics and Notation

We obtain a discrete problem by considering $X_\ell \subset H^{-1/2}(\Gamma)$ instead of $H^{-1/2}(\Gamma)$ in (1.32): For $u \in H^{1/2}(\Gamma)$ (or $f \in H^{1/2}(\Gamma)$), find $\varphi_h \in X_\ell$ such that

$$\begin{aligned} \sigma_\Omega \langle \mathcal{V}\varphi_h, \Phi_j \rangle &= \langle (\sigma_\Omega \mathcal{K} + 1/2)u, \Phi_j \rangle, \quad \forall j = 1, \dots, \mathcal{N}, \\ (\text{or } \langle \mathcal{V}\varphi_h, \Phi_j \rangle &= \langle f, \Phi_j \rangle, \quad \forall j = 1, \dots, \mathcal{N}). \end{aligned} \quad (1.33)$$

In order to obtain a fully discretized problem, we project the Dirichlet data on Y_ℓ , i.e. $u = \sum_{k=1}^{\mathcal{M}} \mathbf{u}_k \Psi_k$. Writing $\varphi_h = \sum_{k=1}^{\mathcal{N}} \varphi_k \Phi_k$ we get the systems of linear equations

$$\begin{aligned} \sigma_\Omega \mathbf{V} \boldsymbol{\varphi} &= (\sigma_\Omega \mathbf{K} + 1/2 \mathbf{M}) \mathbf{u} \\ (\text{or } \mathbf{V} \boldsymbol{\varphi} &= \mathbf{f}). \end{aligned}$$

Here, the matrices $\mathbf{V} := (\mathbf{V}_{jk})_{j,k=1,\dots,\mathcal{N}}$ with $\mathbf{V}_{jk} := \langle \mathcal{V}\Phi_k, \Phi_j \rangle$ and $\mathbf{K} := (\mathbf{K}_{jk})_{j,k=1,\dots,\mathcal{M}}$ with $\mathbf{K}_{jk} := \langle \mathcal{K}\Psi_k, \Phi_j \rangle$ denote the Galerkin matrices of the single and the double layer operators. The entries of the mass matrix $\mathbf{M} := (\mathbf{M}_{jk})_{j,k=1,\dots,\mathcal{M}}$ are given by $\mathbf{M}_{jk} := \langle \Psi_k, \Phi_j \rangle$. The vector \mathbf{f} is defined by $\mathbf{f}_k = \langle f, \Phi_k \rangle$, $k = 1, \dots, \mathcal{N}$.

The hypersingular integral equation. The hypersingular integral equation (1.15) reads

$$\sigma_\Omega (\mathcal{W}u)(x) = (1/2 - \sigma_\Omega \mathcal{K}')\varphi(x), \quad \varphi = \gamma_1^\pm u \in H^{-1/2}(\Gamma)$$

with σ_Ω as in Lemma 1.1.10 or in the general setting

$$(\mathcal{W}u)(x) = f(x), \quad f \in H^{-1/2}(\Gamma).$$

Since the hypersingular operator \mathcal{W} is $H_*^{1/2}$ -elliptic for the Laplace and the Lamé equation we consider the variational formulation in this space. For Helmholtz problems we set $H_*^{1/2}(\Gamma) = H^{1/2}(\Gamma)$. We have:

For $\varphi \in H^{-1/2}(\Gamma)$ (or $f \in H^{-1/2}(\Gamma)$), find $u \in H_*^{1/2}(\Gamma)$ such that

$$\begin{aligned} \sigma_\Omega \langle \mathcal{W}u, v \rangle &= \langle (1/2 - \sigma_\Omega \mathcal{K}')\varphi, v \rangle, \quad \forall v \in H_*^{1/2}(\Gamma) \\ (\text{or } \langle \mathcal{W}u, v \rangle &= \langle f, v \rangle, \quad \forall v \in H_*^{1/2}(\Gamma)). \end{aligned} \quad (1.34)$$

The formulation (1.34) is not straight-forward to use for the implementation and we therefore introduce a modified sesquilinear form. Let $\{w_j, j = 1, \dots, n\}$ be a basis of $\ker \mathcal{W}$. Then,

$$\langle\langle u, v \rangle\rangle_{W+S} := \langle \mathcal{W}u, v \rangle + \sum_{j=1}^n \langle u, w_j \rangle \langle v, w_j \rangle.$$

The modified variational formulation reads:

For $\varphi \in H^{-1/2}(\Gamma)$ (or $f \in H^{-1/2}(\Gamma)$), find $u \in H^{1/2}(\Gamma)$ such that

$$\begin{aligned} \sigma_\Omega \langle\langle u, v \rangle\rangle_{W+S} &= \langle (1/2 - \sigma_\Omega \mathcal{K}')\varphi, v \rangle, \quad \forall v \in H^{1/2}(\Gamma) \\ (\text{or } \langle\langle u, v \rangle\rangle_{W+S} &= \langle f, v \rangle, \quad \forall v \in H^{1/2}(\Gamma)). \end{aligned} \quad (1.35)$$

The next lemma states the equivalence of both variational formulations.

Lemma 1.6.1 ([Ste03]). *A function $u \in H^{1/2}(\Gamma)$ solves (1.34) if and only if u solves (1.35).*

We obtain a discrete problem by considering $Y_\ell \subset H^{1/2}(\Gamma)$ instead of $H^{1/2}(\Gamma)$ in (1.35):

For $\varphi \in H^{-1/2}(\Gamma)$ (or $f \in H^{-1/2}(\Gamma)$), find $u_h \in Y_\ell$ such that

$$\begin{aligned} \sigma_\Omega \langle\langle u_h, \Psi_j \rangle\rangle_{W+S} &= \langle (1/2 - \sigma_\Omega \mathcal{K}') \varphi, \Psi_j \rangle, \quad \forall j = 1, \dots, \mathcal{M}, \\ (\text{or } \langle\langle u_h, \Psi_j \rangle\rangle_{W+S} &= \langle f, \Psi_j \rangle, \quad \forall j = 1, \dots, \mathcal{M}). \end{aligned} \quad (1.36)$$

In order to obtain a fully discretized problem, we project the Neumann data on X_ℓ , i.e. $\varphi = \sum_{k=1}^{\mathcal{N}} \varphi_k \Phi_k$. Writing $u_h = \sum_{k=1}^{\mathcal{M}} \mathbf{u}_k \Psi_k$ we get the systems of linear equations

$$\begin{aligned} (\mathbf{W} + \mathbf{S})\mathbf{u} &= (1/2 \mathbf{M}^T - \sigma_\Omega \overline{\mathbf{K}}^T) \varphi \\ (\text{or } (\mathbf{W} + \mathbf{S})\mathbf{u} &= \mathbf{f}). \end{aligned}$$

Here, \mathbf{K} , \mathbf{M} , and \mathbf{f} are defined as in the previous paragraph. The matrix $\mathbf{W} := (\mathbf{W}_{jk})_{j,k=1,\dots,\mathcal{M}}$ with $\mathbf{W}_{jk} = \langle \mathcal{W} \Psi_k, \Psi_j \rangle$ is the Galerkin matrix of the hypersingular operator and $\mathbf{S} := (\mathbf{S}_{jk})_{j,k=1,\dots,\mathcal{M}}$ with $\mathbf{S}_{jk} := \sum_{i=1}^n \langle \Psi_k, w_i \rangle \langle \Psi_j, w_i \rangle$ is the stabilization matrix.

Remark 1.6.2. The general solution \tilde{u}_h of the hypersingular integral equation can be represented by

$$\tilde{u}_h = u_h + \sum_{j=1}^n a_j w_j.$$

where u_h solves Equation (1.36). To fix the constants a_j we require the scaling conditions $\langle \tilde{u}_h, w_j \rangle = \alpha_j$, where α_j are arbitrary but fixed. For benchmark examples, where the exact solution u is known, we choose $\alpha_j = \langle u, w_j \rangle$. If $\{w_j, j = 1, \dots, n\}$ is an orthogonal basis of $\ker \mathcal{W}$ we get

$$\alpha_j = \langle u, w_j \rangle = \langle \tilde{u}_h, w_j \rangle = a_j \langle w_j, w_j \rangle$$

and hence $a_j = \frac{\langle u, w_j \rangle}{\langle w_j, w_j \rangle}$. If the exact solution is not known we substitute u by $\mathcal{V}\varphi - \mathcal{K}u_h$.

The mixed problem. With the notation of Section 1.2 (paragraph mixed problem) the boundary integral equation (1.16) for the mixed problem reads

$$\mathcal{A} \begin{pmatrix} u_N \\ \varphi_D \end{pmatrix} = \left(\frac{1}{2} - \mathcal{A} \right) \begin{pmatrix} u_D \\ \varphi_N \end{pmatrix}. \quad (1.37)$$

The variational formulation is given by

$$\langle \mathcal{A}(u_N, \varphi_D), (v, w) \rangle_{\mathcal{H}' \times \mathcal{H}} = \langle (1/2 - \mathcal{A})(u_D, \varphi_N), (v, w) \rangle_{\mathcal{H}' \times \mathcal{H}}, \quad \forall (v, w) \in \mathcal{H}. \quad (1.38)$$

1. Analytical Basics and Notation

To discretize the variational formulation we proceed as in the previous two paragraphs. We replace the space \mathcal{H} by the ansatz space $Y_{\ell,N} \times X_{\ell,D} \subset \mathcal{H}$, where the indices indicate that the spaces are only defined on \mathcal{T}_N and \mathcal{T}_D , respectively. With the projections of the Dirichlet and Neumann data on the ansatz space we obtain the following numerical scheme

$$\tilde{\mathbf{A}} \begin{pmatrix} \varphi_D \\ \mathbf{u}_N \end{pmatrix} = \left(\frac{1}{2} \begin{pmatrix} \mathbf{0} & \mathbf{M} \\ \mathbf{M}^T & \mathbf{0} \end{pmatrix} - \mathbf{A} \right) \begin{pmatrix} \varphi_N \\ \mathbf{u}_D \end{pmatrix} \quad (1.39)$$

with

$$\tilde{\mathbf{A}} := \sigma_\Omega \begin{pmatrix} \mathbf{V}_{\Gamma_D \times \Gamma_D} & -\mathbf{K}_{\Gamma_D \times \Gamma_N} \\ \mathbf{K}_{\Gamma_N \times \Gamma_D}^T & \mathbf{W}_{\Gamma_N \times \Gamma_N} \end{pmatrix} \quad \text{and} \quad \mathbf{A} := \sigma_\Omega \begin{pmatrix} \mathbf{V} & -\mathbf{K} \\ \mathbf{K}^T & \mathbf{W} \end{pmatrix}.$$

The indices in the matrix $\tilde{\mathbf{A}}$ indicate that the Galerkin matrices are restricted to the basis functions with support in Γ_D and Γ_N , respectively.

1.6.2. A Priori Error Analysis

In this section we state a priori error estimates for the discrete solution obtained by solving the variational formulations (1.32), (1.35) and (1.38). We start with stating two results for the unique solvability of the variational formulations in the general Hilbert space framework.

Let X be a Hilbert space with its dual X' and $f \in X'$. We further assume that the linear and bounded operator $A : X \rightarrow X'$ can be decomposed in an elliptic and a compact operator, i.e. $A = A_0 + T$. We consider the variational formulation

$$a(u, v) := \langle A_0 u, v \rangle + \langle T u, v \rangle = \langle f, v \rangle \quad \forall v \in X. \quad (1.40)$$

For $\ell \in \mathbb{N}$, we introduce a sequence of finite dimensional subspaces $X_\ell \subset X$ with $X_\ell \subset X_{\ell+1}$, $\dim X_\ell \rightarrow \infty$ for $\ell \rightarrow \infty$, and $\overline{\bigcup_{\ell \in \mathbb{N}} X_\ell}^{\|\cdot\|_X} = X$. The discrete variational formulation reads

$$a(u_\ell, v_\ell) := \langle A_0 u_\ell, v_\ell \rangle + \langle T u_\ell, v_\ell \rangle = \langle f, v_\ell \rangle \quad \forall v_\ell \in X_\ell. \quad (1.41)$$

The next theorem gives the existence and the quasi-optimality of a unique solution.

Theorem 1.6.3 ([SaSch04, Theorem 4.2.9]). *If the sesquilinear form corresponding to A_0 is X -elliptic and a is injective, i.e.*

$$\langle A_0 u, v \rangle + \langle T u, v \rangle = 0 \quad \forall v \in X \setminus \{0\} \quad \Rightarrow \quad u = 0,$$

then (1.40) has a unique solution $u \in X$ for all $f \in X'$. Furthermore, there exists $\ell_0 \in \mathbb{N}$, such that the discrete variational formulation (1.41) has a unique solution $u_\ell \in X_\ell$ for all $\ell \geq \ell_0$. For $\ell \geq \ell_0$ the solutions u_ℓ converge quasi-optimal to u , i.e.

$$\|u - u_\ell\|_X \leq C \min_{u_\ell \in X_\ell} \|u - v_\ell\|_X. \quad (1.42)$$

In practice, the variational formulation (1.41) cannot be solved exactly, since quadrature rules are applied to numerically evaluate the arising integrals. Therefore, we solve the perturbed variational formulation

$$\tilde{a}(u_\ell, v_\ell) := \langle \tilde{A}_0 u_\ell, v_\ell \rangle + \langle \tilde{T} u_\ell, v_\ell \rangle = \langle \tilde{f}, v_\ell \rangle \quad \forall v_\ell \in X_\ell. \quad (1.43)$$

Before we state the next theorem, called Strang's Lemma, that takes the approximation error into consideration, we introduce a second stronger norm $\|\cdot\|_U$ on X , i.e. $\|u_\ell\|_X \leq C\|u_\ell\|_U$ for all $u_\ell \in X_\ell$.

Theorem 1.6.4 ([SaSch04, Theorem 4.2.1]). *Let the sesquilinear form corresponding to A_0 be X -elliptic and*

$$\langle A_0 u, v \rangle + \langle T u, v \rangle = 0 \quad \forall v \in X \setminus \{0\} \quad \Rightarrow \quad u = 0.$$

If the sesquilinear form \tilde{a} satisfies the stability condition

$$\|a(u_\ell, v_\ell) - \tilde{a}(u_\ell, v_\ell)\| \leq \tilde{C}\|u_\ell\|_X \|v_\ell\|_X \quad \forall u_\ell, v_\ell \in X_\ell$$

and the consistency condition with respect to the stronger norm $\|\cdot\|_U$

$$\|a(u_\ell, v_\ell) - \tilde{a}(u_\ell, v_\ell)\| \leq C_\ell\|u_\ell\|_U \|v_\ell\|_X \quad \forall u_\ell, v_\ell \in X_\ell,$$

then there exists $\ell_0 \in \mathbb{N}$ such that for all $\ell \geq \ell_0$ the perturbed formulation (1.43) is stable and has a unique solution $\tilde{u}_\ell \in X_\ell$ which satisfies

$$\|u - \tilde{u}_\ell\|_X \lesssim \left\{ \inf_{w_\ell \in X_\ell} (\|u - w_\ell\|_X + C_\ell\|w_\ell\|_U) + \sup_{0 \neq v_\ell \in X_\ell} \frac{|\langle f, v_h \rangle - \langle \tilde{f}, v_h \rangle|}{\|v_h\|_X} \right\}. \quad (1.44)$$

We stress that the two theorems stated above can be applied to the integral equations (1.32), (1.35) and (1.38) for Laplace, Lamé, and Helmholtz equations under the assumptions of Theorems 1.3.1, 1.3.2, and 1.3.5. This guarantees the unique solvability and the quasi-optimality of the Galerkin solution for sufficiently large ℓ .

We obtain a priori error estimates by analyzing the approximation properties of the discrete ansatz spaces. The following result for the mixed problem is proven for the Laplace equation on polygonal domains with uniform polynomial degrees \mathbf{p} on quasi-uniform meshes.

Theorem 1.6.5 ([StSu91, Theorem 3.5]). *Let $\Omega \subset \mathbb{R}^2$ be a polygonal domain, $(u_N, \varphi_D) \in \mathcal{H}$ be the solution of (1.38) for $u_D \in H^s(\Gamma_D)$ and $\varphi_N \in H^{s-1}(\Gamma_N)$. Furthermore, let $(u_h, \varphi_h) \in X_\ell := S(\mathcal{T}, \mathbf{h}, \mathbf{p}, \mathbf{1}) \times S(\mathcal{T}, \mathbf{h}, \mathbf{p}, \mathbf{0})$ be the numerical solution of (1.39). Then, for $p \in \mathbb{N}$ large enough, $\mathbf{h} > 0$ small enough, and s large enough and for all $\varepsilon > 0$, there exists $C = C(\varepsilon)$ independent of \mathbf{h} and \mathbf{p} such that*

$$\|u_N - u_h\|_{\tilde{H}^{1/2}(\Gamma_N)} + \|\varphi_D - \varphi_h\|_{\tilde{H}^{-1/2}(\Gamma_N)} \leq C h^\alpha p^{-2\alpha+\varepsilon} (\|u_D\|_{H^s(\Gamma_D)} + \|\varphi_N\|_{H^{s-1}(\Gamma_N)}).$$

Here, $\alpha = \min \left\{ \frac{\pi}{\beta_j}, j = 1, \dots, \mathcal{N}_v \right\}$ where β_j denote the interior angles of the domain Ω .

1. Analytical Basics and Notation

Remark 1.6.6. (i) Similar estimates hold for Symm's integral equation (1.32) and the hyper-singular integral equation (1.35), see [StSu91, Theorem 3.5] and [GH06, Theorem 4.2].

- (ii) The proof is based on the fact that the exact solution behaves like x^α near the corners of the domain, where α depends on the interior angle at the corner. Then, the approximation properties of the discrete ansatz space are used to obtain the a priori error estimate.
- (iii) With the same techniques, regularity results for the solution for Lamé and Helmholtz problems are proven in [StSu89], [HSW85] and [SW84]. Hence, similar estimates are obtained for these problems.
- (iv) The results can be generalized to Lipschitz domains by mapping the line segments to curved elements with a smooth mapping.

The previous theorem shows that increasing the polynomial degree uniformly yields twice the convergence rate as compared to refining the mesh uniformly. With geometrically graded meshes, that are introduced in Section 1.4, exponential convergence is proven in [Heu96].

Theorem 1.6.7 ([Heu96]). *Let \mathcal{T}_ϑ be a geometric mesh with corresponding linear polynomial degree vector \mathbf{p}^σ . Further, let the right-hand side in (1.32) be piecewise analytic and have a polynomial behavior in the corners of Γ . If $\varphi \in H^{-1/2}(\Gamma)$ is the solution of Symm's integral equation (1.32) and $\varphi_h \in S_\vartheta^\sigma = S(\mathcal{T}_\vartheta, \mathbf{h}_\vartheta, \mathbf{p}^\sigma, \mathbf{0})$ is the discrete solution of (1.33), then there holds*

$$\|\varphi - \varphi_h\|_{H^{-1/2}(\Gamma)} \leq C e^{-b\sqrt{\mathcal{N}}}.$$

Here, $\mathcal{N} := \dim S_\vartheta^\sigma$ and C and b only depend on the grading parameters ϑ and σ but not on \mathcal{N} .

Remark 1.6.8. Similar results are proven for the hypersingular integral equation in [Heu96].

2. Orthogonal Polynomials and Gauss Quadrature Rules

For the implementation of high-order BEM, efficient and accurate algorithms for numerical integration are essential. While there are analytical approaches for the computation of the relevant integrals, such as in [Ban13], these approaches require knowledge of the kernel functions and are limited to a polygonal boundary approximation. Since we provide a black box software package, which allows for the computation for general kernels and boundaries, these analytical approaches cannot be used. Hence, we mainly use Gauss quadrature rules for the assembly of the collocation and Galerkin matrices. Besides the Gauss-Legendre quadrature, we also use a Gauss quadrature rule with respect to a logarithmic weight function, which we refer to as Gauss-Log quadrature. Within this chapter consisting of three sections we explore these two types of Gauss quadrature rules.

The first section is devoted to orthogonal polynomials, which are closely related to Gauss quadrature rules. Besides general orthogonal polynomials, we also consider special orthogonal polynomials. Specifically the Legendre polynomials and their antiderivatives known as the Lobatto shape functions are introduced, as we choose these polynomials as basis functions for the polynomial ansatz spaces of NURBS-enhanced methods.

In the next section, we introduce Gauss quadrature rules. In order to evaluate the arising integrals up to a set level of accuracy, the nodes and weights have to be computed up to the same level of accuracy. Since the problem of computing the weights and nodes is generally ill-conditioned, the implementation for high quadrature orders is not straight-forward. We present an approach based on the ideas of [Gau10] that allows for the accurate computation of nodes and weights for the Gauss-Legendre and Gauss-Log quadrature up to 16 significant digits even for high orders. By computing the entries in the Galerkin or collocation matrices with quadrature rules, a consistency error is induced. In order to control the consistency error, such that the convergence rates of the high-order collocation or Galerkin methods are not spoiled, rigorous and sharp error bounds for the quadrature error are needed. While sharp bounds for the Gauss-Legendre quadrature rules are already known, we derive a new estimate for the Gauss-Log quadrature.

2. Orthogonal Polynomials and Gauss Quadrature Rules

Ellipses. In the subsequent sections, we will see that confocal ellipses with foci ± 1 play an important role in the estimation of the quadrature error. The definition of these ellipses is motivated by a conformal mapping, specifically the Joukowski transform. The Joukowski transform maps the exterior of concentric circles with radius greater than one to the exterior of ellipses with foci ± 1 . The transform is given by

$$J : \{w \in \mathbb{C} : |w| > 1\} \rightarrow \mathbb{C} \setminus [-1, 1]$$

$$w \mapsto \frac{1}{2} \left(w + \frac{1}{w} \right).$$

The inverse of the Joukowski transform is given by

$$J^{-1} : \mathbb{C} \setminus [-1, 1] \rightarrow \{w \in \mathbb{C} : |w| > 1\}$$

$$z \mapsto z + \sqrt{z^2 - 1}.$$

We choose the branch of the square root that yields $J^{-1}(\infty) = \infty$. Figure 2.1 shows an example of J . With the Joukowski transform we define complex ellipses with foci ± 1 as follows.

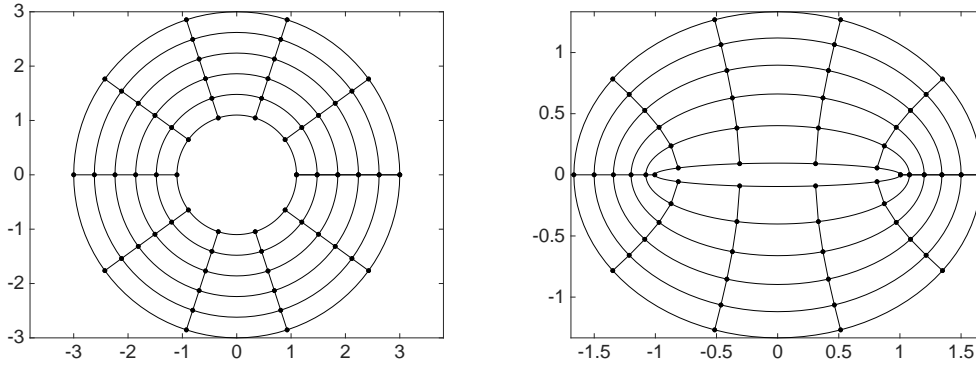


Figure 2.1.: Circular grid (left) mapped to elliptical grid (right) with the conformal Joukowski transform J .

Definition 2.0.9. For $\rho > 1$, we define the open ellipse with foci ± 1 and semi-axis sum ρ by

$$\mathcal{E}_\rho := \left\{ z = \frac{1}{2} \left(w + \frac{1}{w} \right) : w = r \cdot e^{i\varphi}, r \in (1, \rho), \varphi \in [0, 2\pi) \right\} \cup [-1, 1].$$

We denote the real semi-axis by a and the imaginary semi-axis by b with

$$a = \frac{1}{2}(\rho + \rho^{-1}) \quad \text{and} \quad b = \frac{1}{2}(\rho - \rho^{-1}).$$

Remark 2.0.10. The following identities are directly obtained from Definition 2.0.9.

- (i) There holds the following relationship between $z \in \partial\mathcal{E}_\rho$ and the real semi-axis a :

$$a = \frac{|z + 1| + |z - 1|}{2}.$$

(ii) The circumference of the ellipse \mathcal{E}_ρ is bounded by

$$\ell(\mathcal{E}_\rho) < \pi(\rho + \rho^{-1}),$$

see e.g. [DR75] Equation (4.6.1.11).

2.1. Orthogonal Polynomials

Throughout this section, we denote by $\omega \in \mathcal{C}((-1, 1))$ a positive weight function, i.e. $\omega(x) > 0$ for $x \in (-1, 1)$. With the weight function we define a scalar product for $f, g \in \mathcal{C}([-1, 1])$ by

$$(f, g)_\omega := \int_{-1}^1 f(x) g(x) \omega(x) dx.$$

The scalar product induces a norm by $\|f\|_\omega^2 := (f, f)_\omega$. The moments associated to the weight function ω are defined by $\mu_k := (x^k, 1)_\omega$, $k \in \mathbb{N}_0$. In the following definition we introduce orthogonal polynomials.

Definition 2.1.1. Let $(p_n)_{n \in \mathbb{N}_0}$ be a sequence of polynomials with exact degree n and ω be a positive weight function.

(i) $(p_n)_{n \in \mathbb{N}_0}$ is called monic if the leading coefficient of all polynomials equals one, i.e.

$$p_n(x) = x^n + \sum_{k=0}^{n-1} a_k x^k.$$

(ii) $(p_n)_{n \in \mathbb{N}_0}$ is called orthogonal with respect to ω , if

$$(p_n, p_m)_\omega = \|p_n\|_\omega^2 \delta_{nm},$$

where δ_{nm} denotes the Kronecker delta.

(iii) We denote monic orthogonal polynomials with respect to the weight function ω by $\pi_n(x, \omega)$.

If it is clear which weight function is involved we only write $\pi_n(x)$.

The existence and the uniqueness of monic orthogonal polynomials is stated in the following theorem.

Theorem 2.1.2 ([Gau10, Theorem 1.6]). *For every positive weighted scalar product, there exists a unique sequence $(\pi_n)_{n \in \mathbb{N}_0}$ of monic orthogonal polynomials.*

Remark 2.1.3. The uniqueness of orthogonal polynomials $(p_n)_{n \in \mathbb{N}_0}$ is also preserved if we substitute the assumption that $(p_n)_{n \in \mathbb{N}_0}$ are monic by the property $p_n(1) = 1$ for all $n \in \mathbb{N}_0$.

Some useful properties of orthogonal polynomials are collected in the following lemma.

2. Orthogonal Polynomials and Gauss Quadrature Rules

Lemma 2.1.4 ([Gau10]). *Let ω be a positive weight function, $(p_n)_{n \in \mathbb{N}_0}$ be the orthogonal, and $(\pi_n)_{n \in \mathbb{N}_0}$ be the monic orthogonal polynomials with respect to the weighted scalar product.*

- (i) *$(p_n)_{n \in \mathbb{N}_0}$ are linearly independent and hence for $n \in \mathbb{N}_0$ the set $\{p_0, \dots, p_n\}$ forms a basis of \mathcal{P}_n .*
- (ii) *For all $n \in \mathbb{N}$, the zeros of p_n are real, disjoint, and located in $(-1, 1)$. Between two zeros of p_n there is at least one zero of p_m , $m > n$.*
- (iii) *$(\pi_n)_{n \in \mathbb{N}_0}$ satisfy the following three-term recurrence relation*

$$\begin{aligned} \pi_{k+1}(x) &= (x - \alpha_k) \pi_k(x) - \beta_k \pi_{k-1}(x) \quad k \in \mathbb{N}_0, \\ \pi_{-1}(x) &= 0, \quad \pi_0(x) = 1 \end{aligned} \tag{2.1}$$

with

$$\alpha_k = \frac{(x \pi_k, \pi_k)_\omega}{(\pi_k, \pi_k)_\omega}, \quad k \in \mathbb{N}_0, \tag{2.2}$$

$$\beta_k = \frac{(\pi_k, \pi_k)_\omega}{(\pi_{k-1}, \pi_{k-1})_\omega}, \quad k \in \mathbb{N}. \tag{2.3}$$

Remark 2.1.5. Although β_0 can be chosen arbitrarily since $\pi_{-1}(x) = 0$, we define $\beta_0 := (\pi_0, \pi_0)_\omega$, which is used for the computation of Gauss quadrature rules in the subsequent section.

Apart from orthogonal polynomials we are also interested in the associated functions of the second kind.

Definition 2.1.6. For $n \in \mathbb{N}_0$, we define the associated functions of the second kind of π_n on $\mathbb{C} \setminus [-1, 1]$ by

$$\rho_n(z) := \int_{-1}^1 \frac{\pi_n(x)}{z - x} \omega(x) dx.$$

The next lemma states some important properties of ρ_n .

Lemma 2.1.7 ([Gau81]). *The associated functions ρ_n of the second kind are analytic on $\mathbb{C} \setminus [-1, 1]$ and satisfy the same three-term recurrence relation (2.1) as the orthogonal polynomials with initial value $\rho_{-1}(z) = 1$.*

Legendre polynomials and Lobatto shape functions. The Legendre polynomials and the Lobatto shape functions are introduced as special orthogonal polynomials and their antiderivatives. We start by giving a definition of the Legendre polynomials and state some properties.

Definition 2.1.8. For $z \in \mathbb{C}$ and $k \in \mathbb{N}_0$, the Legendre polynomials $P_k(z)$ are the uniquely determined orthogonal polynomials with respect to the weight function $\omega(x) = 1$ with $P_k(1) = 1$, i.e.

$$\int_{-1}^1 P_j(x) P_k(x) dx = \|P_k\|_\omega^2 \delta_{jk}.$$

Lemma 2.1.9. *For $k \in \mathbb{N}_0$, the Legendre polynomials have the following properties.*

(i) **(Recurrence Relation)** *For $z \in \mathbb{C}$ and $k \in \mathbb{N}$, the Legendre polynomials satisfy*

$$\begin{aligned} (k+1)P_{k+1}(z) &= (2k+1)zP_k(z) - kP_{k-1}(z) \\ P_0(z) &= 1, \quad P_1(z) = z. \end{aligned} \tag{2.4}$$

(ii) **(Symmetry)** *For $x \in [-1, 1]$, there holds $P_k(-x) = (-1)^k P_k(x)$. Specifically, the values at the end points are given by $P_k(-1) = (-1)^k$ and $P_k(1) = 1$.*

(iii) **(Norm)** *For the weighted norm, there holds*

$$\|P_k\|_\omega^2 = \frac{2}{2k+1}.$$

(iv) **(Antiderivative)** *For $k \geq 1$, the antiderivative of the Legendre polynomials is given by*

$$\int_{-1}^x P_k(t) dt = \frac{P_{k+1}(x) - P_{k-1}(x)}{2k+1}.$$

(v) **(Maximum on \mathcal{E}_ρ)** *For $\rho > 1$, the Legendre polynomials fulfill*

$$\max_{z \in \mathcal{E}_\rho} |P_k(z)| \leq \rho^k. \tag{2.5}$$

Proof. The first statement is a direct consequence of the recurrence relation (2.1) for the monic orthogonal polynomials and (ii) is obtained by the symmetry of the weight function $\omega(x) = \omega(-x)$. Property (iii) is proven in [Mac67, p. 86]. With the recurrence relation for the derivative $P'_{k+1}(x) - P'_{k-1}(x) = (2k+1)P_k(x)$, $k \geq 1$, which is proven in [Mac67, p. 91], we get (iv). The upper bound (v) is proven in [SaSch97, Proposition 15]. \square

We define the Lobatto shape functions as antiderivatives of the Legendre polynomials. They differ from the similar shape functions in [BS91] just by a scaling factor.

Definition 2.1.10. For $k \in \mathbb{N}$ with $k \geq 3$ and $x \in [-1, 1]$, we define

$$\begin{aligned} N_1(x) &:= \frac{1-x}{2}, \quad N_2(x) := \frac{1+x}{2}, \\ N_k(x) &:= \int_{-1}^x P_{k-2}(t) dt. \end{aligned}$$

For $z \in \mathbb{C}$, we define $N_k(z)$ as the unique analytic extension of $N_k(x)$.

The next lemma summarizes some important properties, that are a direct consequence of the properties of the Legendre polynomials.

Lemma 2.1.11. *Let $x \in [-1, 1]$. The Lobatto shape functions satisfy the following properties.*

2. Orthogonal Polynomials and Gauss Quadrature Rules

(i) **(Relation to Legendre polynomials)** For $k \geq 3$, there holds

$$N_k(x) = \frac{1}{2k-3}(P_{k-1}(x) - P_{k-3}(x)).$$

(ii) **(Recurrence relation)** For $k \geq 4$, the three-term recurrence relation is given by

$$\begin{aligned} k N_{k+1}(x) &= (2k-3)x N_k(x) - (k-3)N_{k-1}(x) \\ N_3(x) &= \frac{1}{2}(x^2-1), \quad N_4(x) = \frac{1}{2}x(x^2-1). \end{aligned} \tag{2.6}$$

(iii) **(Values at ± 1)** For $k \geq 3$, there holds $N_k(\pm 1) = 0$.

Proof. Lemma 2.1.9 (iv) implies part (i). The recurrence relation (ii) is a consequence of (i) and the recurrence relation of the Legendre polynomials. The third property follows from (i) and Lemma 2.1.9 (ii). \square

2.2. Gauss Quadrature Rules

Gauss quadrature rules, i.e. rules of the type

$$\int_{-1}^1 f(x) \omega(x) dx = \sum_{k=1}^n \omega_k f(x_k) + R_n(f), \tag{2.7}$$

are introduced for example in [DR75] for numerical integration. Here, $n \in \mathbb{N}$ is the order of the quadrature rule, the nodes x_k , $k = 1, \dots, n$, are the zeros of the n -th monic orthogonal polynomial π_n associated with the positive weight function ω and the weights ω_k are given by

$$\omega_k = -\frac{k_{n+1}}{k_n} \frac{1}{\pi_{n+1}(x_k) \pi_n'(x_k)}. \tag{2.8}$$

By $R_n(f)$ we denote the remainder of the Gauss quadrature rule. Within the scope of this work we consider Gauss quadrature rules for two different weight functions defined on $(-1, 1)$:

- the Gauss-Legendre quadrature rule with $\omega_{Leg}(x) := 1$,
- the Gauss-Log quadrature with $\omega_{Log}(x) := -\log \frac{x+1}{2}$.

In this section we address two main points. The first point is the computation of the weights and nodes of the quadrature rule. For the accurate numerical integration the nodes and weights have to be computed up to machine precision for large integers n . In order to avoid that round-off errors affect the first 16 significant digits, Maple is used for the implementation, which allows computations with multiple precision arithmetic. Second, we state sharp and reliable error bounds for the absolute quadrature error, which are used to control the consistency error induced by numerical integration. While for Gauss-Legendre rules the computation of weights and nodes as well as sharp error bounds are well known, there are no corresponding results for Gauss-Log rules. In the remainder of this section, we first describe the computation of both Gauss rules before we give sharp error bounds for the absolute quadrature error.

2.2.1. Computation of Gauss Quadrature Rules

If the coefficients α_k and β_k in (2.1) of the orthogonal polynomials associated to the weight function ω are known, the nodes and weights of the related Gauss rule can be computed with an algorithm presented in [GW69]. It is proven that the nodes x_k are the eigenvalues of the matrix J_n with

$$J_n := \begin{pmatrix} \alpha_0 & \sqrt{\beta_1} & & & 0 \\ \sqrt{\beta_1} & \alpha_1 & \sqrt{\beta_2} & & \\ & \sqrt{\beta_2} & \alpha_2 & \ddots & \\ & & \ddots & \ddots & \sqrt{\beta_{n-1}} \\ 0 & & & \sqrt{\beta_{n-1}} & \alpha_{n-1} \end{pmatrix} \in \mathbb{R}^{n \times n}, \quad (2.9)$$

(see for example [Gau10]). The corresponding weights can be computed from the eigenvectors of J_n . If we denote by v_1, \dots, v_n an orthonormal system of eigenvectors, the weights are given by $\omega_k = v_{k,1}^2$ [GW69]. However, the eigenvectors do not have to be computed explicitly, since the weights have the following representation.

Lemma 2.2.1 ([Gau10, Theorem 1.31]). *The weights satisfy*

$$\omega_k = \left(\sum_{j=0}^{n-1} \tilde{\pi}_j(x_k)^2 \right)^{-1}, \quad k = 1, \dots, n. \quad (2.10)$$

Here, the orthonormal polynomials $\tilde{\pi}_k$ are defined by the recurrence

$$\begin{aligned} \tilde{\pi}_{k+1}(x) &= (x - \alpha_k) \frac{\tilde{\pi}_k(x)}{\sqrt{\beta_{k+1}}} - \beta_k \frac{\tilde{\pi}_{k-1}(x)}{\sqrt{\beta_{k+1}\beta_k}}, \\ \tilde{\pi}_{-1}(x) &= 0, \quad \tilde{\pi}_0(x) = \frac{1}{\sqrt{\beta_0}}. \end{aligned} \quad (2.11)$$

Listing 2.1 shows a Maple code for the computation of the weights with (2.10). The procedure `compWeigth` requires the zeros `xi` of π_n and the vectors `ak` and `bk` containing α_k and $\sqrt{\beta_k}$, respectively, as input parameters and returns the vector `w` containing the weights. The orthogonal polynomials $\tilde{\pi}_j$ are evaluated efficiently with the three-term recurrence relation (2.11).

Listing 2.1: Maple code for the computation of the weights for Gauss quadrature rules.

```
1 compWeights:=proc(xi::Vector, ak::Vector, sbk::Vector)::Vector;
2 # xi -> vector of roots of n-th orthogonal polynomial
3 # ak -> vector of first coefficient of three-term recurrence
4 # sbk -> vector of square roots of second coefficient of
5 # three-term recurrence
```

2. Orthogonal Polynomials and Gauss Quadrature Rules

```

6
7  local j,k,n,w,p0,p1,p2,tmp;
8  n:=Dimension(xi):
9  w:=Vector(1..n,0);
10 for k from 1 to n do
11     p0:=1 / sbk[1];
12     tmp:=p0*p0;
13     if n>1 then
14         p1:= (xi[k]-ak[1])*p0 / sbk[2];
15         for j from 1 to n-1 do
16             p2:=((xi[k]-ak[j+1])*p1-sbk[j+1]*p0) / sbk[j+2];
17             tmp := tmp+p2*p2;
18             p0:=p1;
19             p1:=p2;
20         end do;
21     end if;
22     w[k]:=1 / tmp;
23 end do;

```

For the Gauss-Legendre quadrature rule with weight function ω_{Leg} , the coefficients of the monic orthogonal polynomials are given by

$$\alpha_k = 0, \quad \beta_k = \begin{cases} 2, & k = 0 \\ \frac{1}{4-k^2}, & k \geq 1. \end{cases}$$

Thus, the quadrature rule can be computed with (2.9) and (2.10). Listing 2.2 shows an excerpt of the Maple script for the computation of the Gauss-Legendre quadrature rule. After having computed the coefficients α_k and β_k of the orthogonal polynomials (line 1), the symmetric tridiagonal Jacobi matrix J_n is assembled (lines 2-13). The nodes and weights are obtained by computing the eigenvalues of J_n and calling the procedure `compWeights` from Listing 2.1.

Listing 2.2: Excerpt of a Maple code for the computation of the Gauss-Legendre quadrature rule.

```

1  A := coeffLegendre(n, a, b):
2  for j to RowDimension(A) do
3      A[j, 2] := sqrt(A[j, 2]):
4  end do:
5  if n = 1 then
6      Jn := A[1, 1]:
7  else
8      Jn := Matrix([convert(A(2 .. n, 2), list),

```



```

9             convert(A(1 .. n, 1), list),
10            convert(A(2 .. n, 2), list)],
11            shape = band[1, 1], scan = band[1, 1],
12            shape = symmetric):
13 end if:
14 EW := Eigenvalues(Jn):
15 W := compWeights(EW, A[1 .. n, 1], A[1 .. n+1, 2]):
    
```

For the log-weight function ω_{Log} , the coefficients α_k and β_k of the orthogonal polynomials have to be computed recursively. In [Che59] an algorithm is presented, the so-called Chebyshev algorithm, that can be used to compute the coefficients α_k and β_k via the moments μ_k . However, the problem of computing the coefficients by the moments is ill-conditioned for ω_{Log} and computations are only possible for small integers n .

To remedy this problem we introduce modified moments and use a modification of the Chebyshev algorithm, which is presented in [Gau10, Algorithm 2.1]. The modified moments with respect to the scaled Legendre polynomials $\tilde{P}_k(x) := \frac{2^n (n!)^2}{(2n)!} P_k(x)$ are defined by

$$m_k := \left(\tilde{P}_k, 1 \right)_{\omega_{Log}}, \quad k = 0, \dots, n. \quad (2.12)$$

Remark 2.2.2. For the definition of the modified moments m_k also other sets of monic polynomials can be used, as long as they satisfy a three-term recurrence relation of the form (2.1) with known coefficients α_k and β_k . Our choice of the scaled Legendre polynomials is motivated by two facts. First, orthogonal polynomials have good stability properties in many practical applications and hence we expect to obtain a well-conditioned problem. Second, there are closed formulas for the modified moments, which are given in the subsequent theorem.

Theorem 2.2.3 ([BF14]). *Let $\alpha, \beta > -1$, $n \in \mathbb{N}_0$ and $P_n^{(\alpha, \beta)}$ denote the Jacobi polynomials. Then, for $n = 0$*

$$\begin{aligned} & \int_{-1}^1 (1-t)^\alpha (1+t)^\beta \log\left(\frac{1+t}{2}\right) P_0^{(\alpha, \beta)}(t) dt \\ &= -2^{\alpha+\beta+1} \frac{\Gamma(\alpha+1) \Gamma(\beta+1)}{\Gamma(\alpha+\beta+2)} \left(\psi(\alpha+\beta+2) - \psi(\beta+1) \right) \end{aligned} \quad (2.13)$$

and for $n > 0$

$$\begin{aligned} & \int_{-1}^1 (1-t)^\alpha (1+t)^\beta \log\left(\frac{1+t}{2}\right) P_n^{(\alpha, \beta)}(t) dt \\ &= (-1)^{n-1} 2^{\alpha+\beta+1} \frac{\Gamma(n+\alpha+1) \Gamma(\beta+1)}{n \Gamma(n+\alpha+\beta+2)}. \end{aligned} \quad (2.14)$$

Here, we denote by $\Gamma(x)$ the gamma function, and by $\psi(x) := \frac{d}{dx} \ln(\Gamma(x))$ the digamma function.

2. Orthogonal Polynomials and Gauss Quadrature Rules

Remark 2.2.4. Theorem 2.2.3 can be used to compute the modified moments

$$m_k^{(\alpha, \beta)} := \left(\tilde{P}_k^{(\alpha, \beta)}, 1 \right)_{\omega_{Log}^{(\alpha, \beta)}}$$

with respect to the scaled Jacobi polynomials

$$\tilde{P}_n^{(\alpha, \beta)}(x) = 2^n \frac{\Gamma(n+1) \Gamma(n+\alpha+\beta+1)}{\Gamma(2n+\alpha+\beta+1)} P_n^{(\alpha, \beta)}(x)$$

for the more general weight function

$$\omega_{Log}^{(\alpha, \beta)}(x) = -(1-x)^\alpha (1+x)^\beta \log\left(\frac{1+x}{2}\right), \quad \alpha, \beta > -1.$$

For $\alpha = \beta = 0$, the general case reduces to the modified moments (2.12).

Listing 2.3: Maple code for the computation of the modified moments $m_k^{(\alpha, \beta)}$

```

1 modMom := proc (n::integer, a::numeric, b::numeric)::Vector;
2   local k, m, tmp;
3   m := Vector(1 .. n+1, 0);
4   tmp := 2^(a+b+1)*GAMMA(a+1)*GAMMA(b+1)/GAMMA(a+b+2);
5   m[1] := tmp*(Psi(a+b+2)-Psi(b+1));
6   m[2] := -2*tmp*(a+1)/(a+b+2)^2;
7   for k from 2 to n do
8       m[k+1] := -2*m[k]*(a+b+k)*(k-1)*(a+k) /
9               ((a+b+k+1)*(a+b+2*k-1)*(a+b+2*k));
10  end do;
11  m;
12 end proc;

```

Listing 2.3 shows a Maple code for the computation of the modified moments $m_k^{(\alpha, \beta)}$ with the formulas given in Theorem 2.2.3. In order to save computational time, the modified moments are computed recursively. For $k \geq 2$, there holds

$$\begin{aligned}
m_k^{(\alpha, \beta)} &= (-1)^{k-1} 2^{k+\alpha+\beta+1} \frac{\Gamma(k+1) \Gamma(k+\alpha+\beta+1)}{\Gamma(2k+\alpha+\beta+1)} \frac{\Gamma(k+\alpha+1) \Gamma(\beta+1)}{k \Gamma(k+\alpha+\beta+2)} \\
&= (-1)^{k-1} 2^{k+\alpha+\beta+1} \frac{k \Gamma(k) (k+\alpha+\beta) \Gamma(k+\alpha+\beta)}{(2k+\alpha+\beta)(2k+\alpha+\beta-1) \Gamma(2k+\alpha+\beta-1)} \\
&\quad \cdot \frac{(k+\alpha) \Gamma(k+\alpha) \Gamma(\beta+1)}{k (k+\alpha+\beta+1) \Gamma(k+\alpha+\beta+1)} \\
&= -m_{k-1}^{(\alpha, \beta)} \frac{2(k-1)(k+\alpha+\beta)(k+\alpha)}{(2k+\alpha+\beta)(2k+\alpha+\beta-1)(k+\alpha+\beta+1)},
\end{aligned}$$

where we used the functional equation of the gamma function, i.e. $x \Gamma(x) = \Gamma(x+1)$.

Listing 2.4 shows a Maple code for the computation of the coefficients α_k and β_k of the orthogonal polynomials with respect to the weight function $\omega_{Log}^{(\alpha, \beta)}$. The modified Chebyshev

algorithm `modifiedChebyshev`, which is implemented in [Gau06], computes the coefficients $\{\alpha_k, \beta_k\}_{k=0,\dots,n}$ using the modified moments $\{m_k^{(\alpha,\beta)}\}_{k=0,\dots,2n+1}$ and the coefficients $\{a_k, b_k\}_{k=0,\dots,2n}$ of the scaled Jacobi polynomials $\tilde{P}_k^{(\alpha,\beta)}$. The coefficients are computed in the procedure `coeffJacobi` according to the following formulas

$$\begin{aligned} a_k &= \frac{\beta^2 - \alpha^2}{(2k + \alpha + \beta)(2k + \alpha + \beta + 2)}, k \in \mathbb{N}_0, \\ b_0 &= \frac{2^{\alpha+\beta+1} \Gamma(\alpha + 1) \Gamma(\beta + 1)}{\Gamma(\alpha + \beta + 2)}, \\ b_k &= \frac{4k(k + \alpha)(k + \beta)(k + \alpha + \beta)}{(2k + \alpha + \beta)^2(2k + \alpha + \beta + 1)(2k + \alpha + \beta - 1)}, k \geq 1. \end{aligned}$$

Listing 2.4: Computation of the coefficients α_k and β_k for the log-weight function.

```

1 m := modMom(2*n+1, a, b):
2 ab := coeffJacobi(2*n, a, b):
3 A := modifiedChebyshev(m, ab[1], ab[2]):
    
```

Replacing the first line in Listing 2.2 by the code of Listing 2.4 the Gauss-Log rule can be computed efficiently and stable even for large integers n . Table 2.1 shows the computational times for the computation of Gauss-Log quadrature rules, where the nodes and weights are computed up to an accuracy of 16 significant digits. For all computations 36 digits are used. We see that our implementation allows the computation of the Gauss-Log rule of order $n = 2048$ in approximately 2.5 minutes. Further, the overall computational time is dominated by the computation of the eigenvalues, the time for computing the modified moments is negligible.

2.2.2. Error Bounds for Gauss Quadrature Rules

In order to control the consistency error, which is induced by the numerical integration in BEM, it is of main importance to have a computable, sharp, and reliable estimate for the quadrature error. For $(2n)$ -times continuously differentiable functions the following representation of the remainder can be proven.

Theorem 2.2.5 ([Gau10, Theorem 1.48]). *Let $n \in \mathbb{N}$, $f \in \mathcal{C}^{2n}([-1, 1])$ and $(\pi_n)_{n \in \mathbb{N}_0}$ be the monic orthogonal polynomials corresponding to the positive weight function ω . Then*

$$R_n(f) = \frac{f^{(2n)}(\xi)}{(2n)!} \|\pi_n\|_{\omega}^2, \quad \xi \in (-1, 1). \quad (2.15)$$

Remark 2.2.6. (i) Equation (2.15) implies that the n -th order Gauss quadrature rule is exact for all polynomials of degree $2n - 1$. Among all interpolatory quadrature rules of order n this is optimal.

2. Orthogonal Polynomials and Gauss Quadrature Rules

order n	computational time [s]			
	mod. moments m_k	mod. Cheb. alg.	nodes x_k	weights ω_k
64	0.046	0.050	0.057	0.054
128	0.005	0.130	0.222	0.090
256	0.005	0.424	0.846	0.404
512	0.008	1.744	3.245	1.805
1024	0.013	6.806	15.182	7.159
2048	0.111	28.812	87.092	30.876

Table 2.1.: Computational times in seconds for the computation of Gauss-Log quadrature rules with Maple. The nodes and weights are computed up to an accuracy of 16 significant digits. All computations are performed on a desktop computer with a 3.5 GHz Intel Core i7 processor, 32GB DDR3 RAM and OSX 10.9.5 operating system.

- (ii) Estimating the expression $\max_{\xi \in (-1,1)} |f^{(2n)}(\xi)|$ we obtain an upper bound for the quadrature error. However, the bound requires knowledge of high-order derivatives of the integrand, which is not provided for the application to BEM. In the sequel, we thus derive derivative-free error bounds for analytic integrands.

Throughout this section, we denote by f an analytic function on the domain $D \subset \mathbb{C}$ containing $[-1, 1]$ in its interior. Based on the Cauchy integral theorem the following derivative-free representation of the remainder is given in [Gau10].

Theorem 2.2.7 ([Gau10, Theorem 2.48]). *Let $n \in \mathbb{N}$, ω be a positive weight function and C be a contour in D with positive orientation that encircles the real interval $[-1, 1]$. Then, the remainder can be expressed by*

$$R_n(f) = \frac{1}{2\pi i} \oint_C K_n(z) f(z) dz. \quad (2.16)$$

Here, the kernel K_n is given by

$$K_n(z) := \frac{\rho_n(z)}{\pi_n(z)}. \quad (2.17)$$

With Theorem 2.2.7 we obtain the error bound

$$|R_n(f)| = \frac{\ell(C)}{2\pi} \max_{z \in C} |K_n(z)| \max_{z \in C} |f(z)|, \quad (2.18)$$

where $\ell(C)$ denotes the length of the contour C .

Remark 2.2.8. The bound (2.18) significantly depends on the contour C . In the literature, see e.g. [Gau10, Gau92, Sch97, GV83], there are used two classes of contours, concentric circles

and confocal ellipses. For the application to BEM there occur meromorphic integrands that may contain poles near the interval $[-1, 1]$. Therefore, we derive estimates with respect to confocal ellipses, i.e. $C := \partial\mathcal{E}_\rho$ with \mathcal{E}_ρ as defined in Definition 2.0.9, as the poles can be avoided by choosing $\rho > 1$ sufficiently small.

While the second maximum in (2.18) depends on the integrand f , the first maximum only depends on the quadrature rule. Hence, general error bounds for the quadrature rule are obtained by deriving estimates for $\max_{z \in \partial\mathcal{E}_\rho} |K_n(z)|$. Contour plots of the kernels K_n for the weight functions ω_{Leg} and ω_{Log} are given in Figure 2.2.

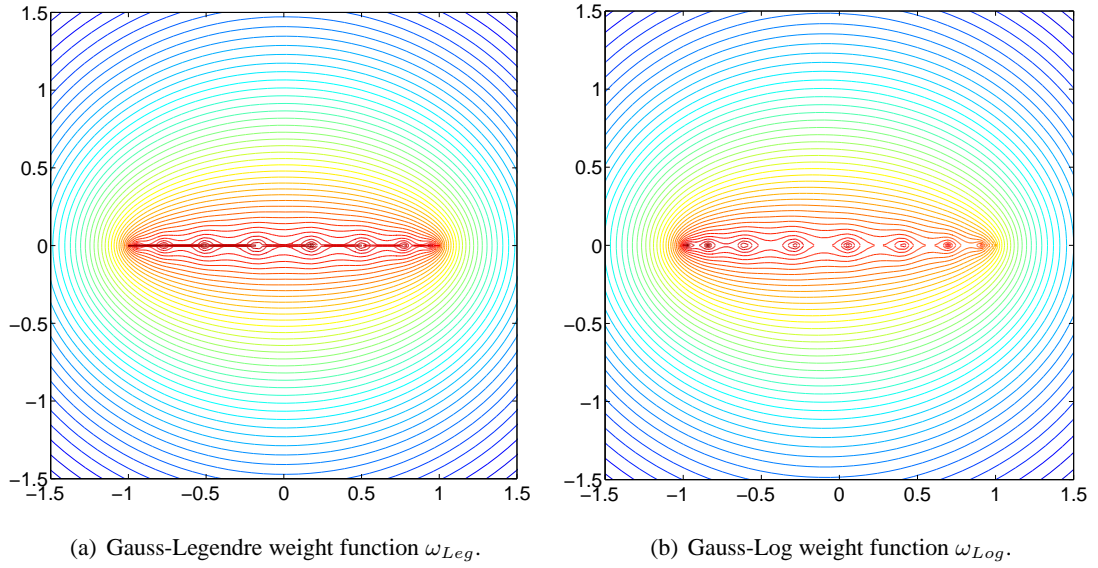


Figure 2.2.: Contour plot of the kernel K_n for $n = 8$ for different weight functions.

The following lemma collects some useful properties of the kernel.

Lemma 2.2.9. *Let $n \in \mathbb{N}$, ω be a positive weight function and K_n as defined in (2.17). Then, the following properties hold.*

- (i) K_n is analytic on $\mathbb{C} \setminus [-1, 1]$ and has n simple poles in $(-1, 1)$.
- (ii) For $z \rightarrow \infty$ there holds

$$K_n(z) = \mathcal{O}(z^{-2n-1}). \quad (2.19)$$

Proof. The first property is a direct consequence of Lemma 2.1.4 (ii), the second statement is proven in [Gau10, Equation (1.3.43)]. \square

With property (ii) in the above lemma, we have an asymptotic estimate of the kernel for general weight functions on large ellipses. However, we are also interested in reliable error bounds and

2. Orthogonal Polynomials and Gauss Quadrature Rules

thus in the behavior of the kernel for small ellipses. We therefore analyze the kernel K_n with respect to the weight functions ω_{Leg} and ω_{Log} more closely. For the Gauss-Legendre weight function ω_{Leg} we have the following result.

Lemma 2.2.10 ([DR75, Equation (4.6.1.10)]). *Let $n \in \mathbb{N}$ be sufficient large and K_n be the kernel associated to ω_{Leg} . Then, there holds*

$$K_n(z) \cong \frac{2\pi}{(z + (z^2 - 1)^{1/2})^{2n+1}}, \quad (2.20)$$

where the symbol " \cong " means that the quotient of the left-hand and the right-hand side approaches to one for $n \rightarrow \infty$.

With the asymptotic estimate (2.20), the well-known error bound for the Gauss-Legendre quadrature is a direct consequence.

Theorem 2.2.11. *Let $n \in \mathbb{N}$ be sufficiently large, $\rho > 1$ and f be analytic in \mathcal{E}_ρ . Then, the error of the n -th order Gauss-Legendre quadrature rule is bounded by*

$$|R_n(f)| \leq \frac{\pi(\tilde{\rho} + \tilde{\rho}^{-1})}{\tilde{\rho}^{2n+1}} \max_{z \in \partial\mathcal{E}_{\tilde{\rho}}} |f(z)|, \quad 1 < \tilde{\rho} < \rho. \quad (2.21)$$

Proof. For $z \in \partial\mathcal{E}_{\tilde{\rho}}$ we have $|z + (z^2 - 1)^{1/2}| = \tilde{\rho}$. With (2.20) and the inequality $\ell(\mathcal{E}_{\tilde{\rho}}) < \pi(\tilde{\rho} + \tilde{\rho}^{-1})$ we conclude the proof. \square

Remark 2.2.12. (i) Theorem 2.2.11 shows that the Gauss-Legendre quadrature converges exponentially with respect to the quadrature order for analytic integrands.

(ii) The asymptotic estimate of the kernel (2.20) yields a sharp error bound, provided the second maximum in (2.18) can be estimated sharply.

(iii) The optimal bound is obtained by

$$|R_n(f)| \leq \inf_{1 < \tilde{\rho} < \rho} \left(\frac{\pi(\tilde{\rho} + \tilde{\rho}^{-1})}{\tilde{\rho}^{2n+1}} \max_{z \in \partial\mathcal{E}_{\tilde{\rho}}} |f(z)| \right).$$

However, computing the optimal error bound for the a priori determination of the quadrature error is inefficient and hence generally omitted. Furthermore, for controlling the consistency error induced by the quadrature rules for Galerkin or collocation methods, we are mainly interested in the asymptotic behavior of the quadrature error. Hence, we choose $\tilde{\rho} \rightarrow \rho$ although $\lim_{\tilde{\rho} \rightarrow \rho} \max_{z \in \partial\mathcal{E}_{\tilde{\rho}}} |f(z)|$ may tend to infinity, if f contains a pole on $\partial\mathcal{E}_\rho$.

We now investigate the kernel, which is associated to the weight function ω_{Log} . Since there are no closed formulas for the kernel, and hence no asymptotic estimates, we start by investigating

the behavior of K_1 on confocal ellipses. The first coefficient α_0 of the three-term recurrence relation is given by

$$\alpha_0 = \frac{(t \pi_0, \pi_0)_{\omega_{Log}}}{(\pi_0, \pi_0)_{\omega_{Log}}} = -\frac{1}{2}$$

and hence

$$\begin{aligned} \pi_1(z) &= z - \alpha_0 = z + \frac{1}{2} \\ \rho_1(z) &= - \int_{-1}^1 \frac{t + 1/2}{z - t} \log \left(\frac{1+t}{2} \right) dt = \left(z + \frac{1}{2} \right) \operatorname{dilog} \left(\frac{z-1}{z+1} \right) - 2. \end{aligned} \quad (2.22)$$

Remark 2.2.13. The di-logarithm is defined by

$$\operatorname{dilog}(z) = \int_1^z \frac{\log t}{1-t} dt.$$

Note the following relationship to the poly-logarithm $\operatorname{dilog}(z) = \operatorname{Li}_2(1-z)$.

With (2.22) we get

$$K_1(z) = \operatorname{dilog} \left(\frac{z-1}{z+1} \right) - \frac{2}{z + \frac{1}{2}}.$$

We see that K_1 has singularities for $z = -1$ and $z = -\frac{1}{2}$. Since the algebraic singularity $z = -\frac{1}{2}$ is stronger, the maximum value of K_1 near the real interval $[-1, 1]$ is located in the vicinity of $-\frac{1}{2}$. On ellipses \mathcal{E}_ρ , i.e. $z := z(\varphi) = \frac{1}{2} (\rho e^{i\varphi} + \rho^{-1} e^{-i\varphi})$, this yields

$$\operatorname{argmax}_{\varphi \in [0, 2\pi)} |K_1(z(\varphi))| \rightarrow \arccos \left(-\frac{1}{2} \right) = \frac{2}{3} \pi, \quad \text{as } \rho \rightarrow 1.$$

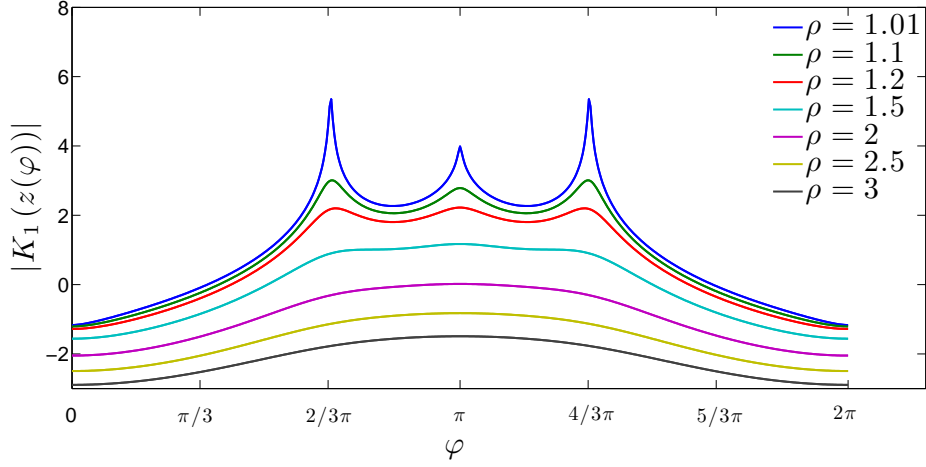
For large values of ρ the value of K_1 is determined by the dilog-term. Hence, the maximum of the kernel is attained on the negative real axis for sufficient large ρ , i.e.

$$\operatorname{argmax}_{\varphi \in [0, 2\pi)} |K_1(z(\varphi))| = \pi.$$

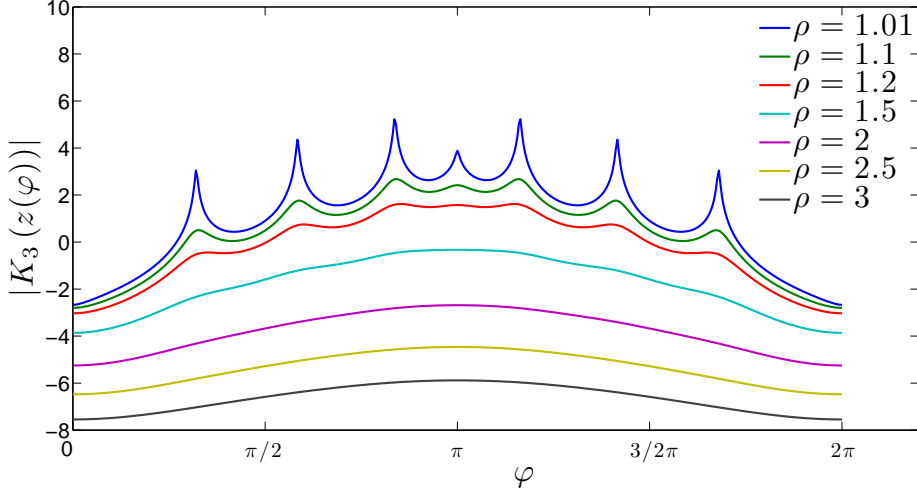
Figure 2.3 (a) shows the values of $|K_1(z(\varphi))|$ over φ on different ellipses \mathcal{E}_ρ . We see that the behavior of the kernel coincides with our theoretical considerations, i.e. for small $\rho \approx 1$ the maximum is attained for $\varphi \approx \frac{2}{3}\pi$ and due to the symmetry with respect to the real axis at $\varphi \approx \frac{4}{3}\pi$.

Similar results are also obtained for the higher order kernels K_n , $n > 1$. Figure 2.3 (b) shows the results for $n = 3$. We see that for small ρ we have peaks that correspond to the zeros $-1 < x_0 < \dots < x_n < 1$ of π_n . In particular, the maximal peak of K_n is located in the neighborhood of the zero x_0 closest to -1 . Lemma 2.1.4 (ii) implies that $x_0 \rightarrow -1$ as $n \rightarrow \infty$ and hence the maximum value of the kernel is attained at $\varphi \approx \pi$ for sufficiently large n and small ρ . For large values of ρ , the numerical examples indicate that the maximum is attained for

2. Orthogonal Polynomials and Gauss Quadrature Rules



(a) Kernel for $n = 1$.



(b) Kernel for $n = 3$.

Figure 2.3.: Kernel $|K_n(z(\varphi))|$ with $z(\varphi) = \frac{1}{2}(\rho e^{i\varphi} + \rho^{-1}e^{-i\varphi})$ over φ for different values of $\rho > 1$.

$\varphi = \pi$.

Since we do not know an analytical result for the maximum of the kernel for $n \geq 1$, we derive an upper bound based on numerical experiments. In order to obtain a simple bound for the kernel, we choose the following approach:

$$\max_{z \in \mathcal{E}_\rho} |K_n(z)| \leq \frac{c}{(\rho - 1)(\rho + 1)\rho^{2n-1}}, \quad c > 0. \quad (2.23)$$

We note that the bound (2.23) describes the behavior of the kernel that is observed in Figure 2.3. In particular, the singularity of the kernel at x_0 , which is relevant for the maximum value of the kernel on \mathcal{E}_ρ , is considered in the bound by the term $(\rho - 1)^{-1}$. Furthermore, for large values of

ρ the bound behaves like $\mathcal{O}(\rho^{-2n-1})$, which coincides with the behavior that is proven for the kernel in (2.19).

Remark 2.2.14. For the subsequent numerical experiments, the associated functions of the second kind ρ_n have to be evaluated for large order n . Although ρ_n satisfies the same three-term recurrence relation as π_n , the recurrence is unstable for ρ_n and hence inappropriate for the evaluation.

The instability can be explained by minimal solutions. A solution f_n of a difference equation $y_{k+1} = (z - \alpha_k)y_k - \beta_k y_{k-1}$, $k \in \mathbb{N}_0$, is said to be minimal if

$$\lim_{n \rightarrow \infty} \frac{f_n}{y_n} \rightarrow 0$$

for all linearly independent solutions y_n of the difference equation. In [Gau10, Theorem 1.43], it is proven that ρ_n is a minimal solution of the recurrence relation (2.1) for $z \in \mathbb{C} \setminus [-1, 1]$.

For the evaluation of minimal solutions a stable algorithm based on continued fractions is given in [Gau81] and a MATLAB code is provided by [Gau06], which is used for the numerical experiments in the remainder of this section.

In order to obtain an explicit upper bound for the kernel, we determine c numerically. Therefore, we define

$$c_n(\rho) := \max_{z \in \mathcal{E}_\rho} |K_n(z)| (\rho - 1)(\rho + 1) \rho^{2n-1}$$

and investigate the dependency of $c_n(\rho)$ on ρ and n . We start by investigating $c_n(\rho)$ with respect to ρ . The results are illustrated in Figure 2.4, where $c_n(\rho)$ is plotted against ρ . For the test case we choose $\rho \geq 1.01$ and $n \leq 512$, which covers most practical applications. Both plots in

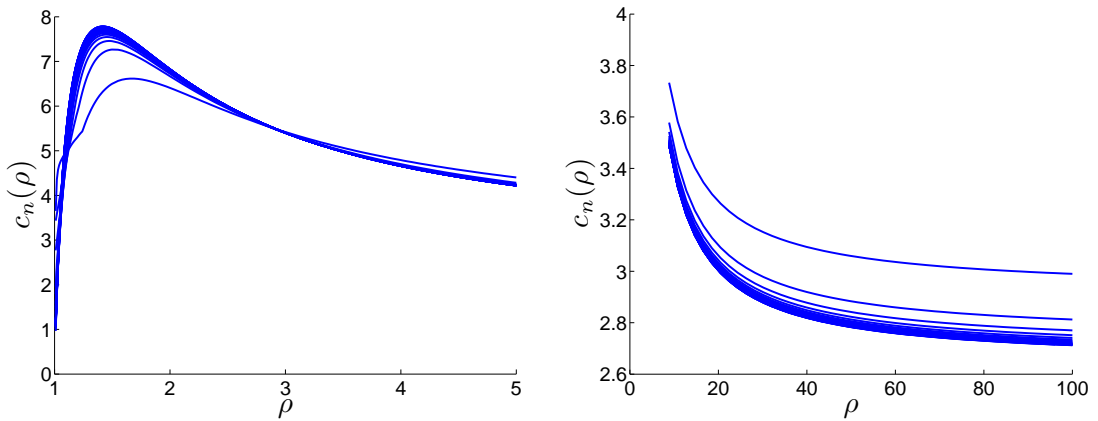


Figure 2.4.: $c_n(\rho)$ over ρ for $n \leq 512$, small values of ρ (left) and large values of ρ (right).

Figure 2.4 show that for all $n \leq 512$, $c_n(\rho)$ behaves similarly. It reaches the maximum point for $\rho \in [1, 2]$ and stabilizes for large values of ρ . In particular, $c_n(\rho)$ is bounded for all values of n

2. Orthogonal Polynomials and Gauss Quadrature Rules

and

$$\frac{\max_{\rho > 1.01} c_n(\rho)}{\min_{\rho > 1.01} c_n(\rho)} < 8,$$

which means that the bound of K_n overestimates the real value at most by a factor of 8.

In the next step we investigate the dependency of $\max_{\rho > 1.01} c_n(\rho)$ on n . The results are illustrated in Figure 2.5. We see that $\max_{\rho > 1.01} c_n(\rho)$ is bounded for all values of n and remains

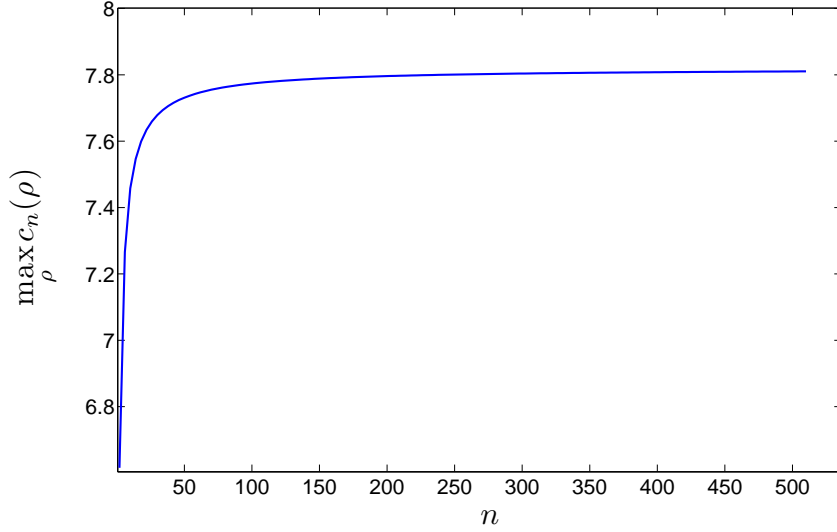


Figure 2.5.: $\max_{\rho \in [1.01, 100]} c_n(\rho)$ over n .

constant for large values of n . Thus, by choosing $c = 8$ in (2.23) we obtain a reliable bound for the kernel K_n , $n < 2048$. The resulting error bound is given in the next "theorem".

"Theorem" 2.2.15. *Let $\rho > 1$ and f be analytic in \mathcal{E}_ρ . Then, the error of the n -th order Gauss-Log quadrature rule is bounded by*

$$|R_n(f)| \leq 4 \frac{(\tilde{\rho}^2 + 1)}{(\tilde{\rho}^2 - 1)} \tilde{\rho}^{-2n} \max_{z \in \partial \mathcal{E}_{\tilde{\rho}}} |f(z)|, \quad 1 < \tilde{\rho} < \rho. \quad (2.24)$$

Proof. With (2.18), (2.23) and $1 < \tilde{\rho} < \rho$ there holds

$$\begin{aligned} |R_n(f)| &= \frac{\ell(\mathcal{E}_{\tilde{\rho}})}{2\pi} \max_{z \in \partial \mathcal{E}_{\tilde{\rho}}} |K_n(z)| \max_{z \in \partial \mathcal{E}_{\tilde{\rho}}} |f(z)| \\ &\leq \frac{8\pi(\tilde{\rho} + \tilde{\rho}^{-1})}{2\pi(\tilde{\rho} - 1)(\tilde{\rho} + 1)\tilde{\rho}^{2n-1}} \max_{z \in \partial \mathcal{E}_{\tilde{\rho}}} |f(z)| \\ &= 4 \frac{(\tilde{\rho}^2 + 1)}{(\tilde{\rho}^2 - 1)} \tilde{\rho}^{-2n} \max_{z \in \partial \mathcal{E}_{\tilde{\rho}}} |f(z)|. \end{aligned}$$

□

Remark 2.2.16. The numerical experiments indicate that the bound in Theorem 2.2.15 is reliable for all $\rho > 1.01$ and $n \leq 2048$. However, Figure 2.4 shows that the error may be overestimated by a factor of 8 in some cases. Better bounds can be obtained by further parameter

optimization with respect to ρ and n . Since the constant in (2.24) is only included logarithmically in the consistency estimates for BEM, we use the simple bound (2.24) for our application.

For the computation of the Galerkin entries, we also apply tensor quadrature rules. Therefore, we generalize the results of Theorems 2.2.11 and 2.2.15.

Theorem 2.2.17. *Let $n := (n_1, n_2) \in \mathbb{N}^2$, $\omega^{(i)} \in \{\omega_{Leg}, \omega_{Log}\}$, and $x_k^{(i)}$ and $\omega_k^{(i)}$ be the nodes and weights with respect to the weight function $\omega^{(i)}$, $i \in \{1, 2\}$. Furthermore, the tensor quadrature rule is given by*

$$\int_{-1}^1 \int_{-1}^1 f(x, y) \omega_1(x) dx \omega_2(y) dy = \sum_{j=1}^{n_1} \omega_j^{(1)} \sum_{k=1}^{n_2} \omega_k^{(2)} f(x_j^{(1)}, x_k^{(2)}) + R_n(f).$$

If $f(\cdot, y)$ is analytic on \mathcal{E}_{ρ_1} for all $y \in [-1, 1]$ and if $f(x, \cdot)$ is analytic on \mathcal{E}_{ρ_2} for all $x \in [-1, 1]$, $\rho_1, \rho_2 > 1$, then there holds

$$|R_n(f)| \leq \mu_0^{(1)} \max_{x \in [-1, 1]} C_{\omega^{(2)}}(\rho_2, n_2, f(x, \cdot)) + \mu_0^{(2)} \max_{y \in [-1, 1]} C_{\omega^{(1)}}(\rho_1, n_1, f(\cdot, y)).$$

Here, we denote by $\mu_0^{(i)}$ the zeroth moment with respect to $\omega^{(i)}$ and by $C_{\omega^{(i)}}(\rho_i, n_i, f)$ the bound for the remainder of the n_i -th order Gauss quadrature rule with respect to $\omega^{(i)}$, which is given in Theorems 2.2.11 and 2.2.15, respectively.

Proof. The proof is based on the idea of [SaSch97, Proposition 14]. We have

$$\begin{aligned} R_n(f) &= \int_{-1}^1 \int_{-1}^1 f(x, y) \omega^{(1)}(x) dx \omega^{(2)}(y) dy - \sum_{j=1}^{n_1} \omega_j^{(1)} \sum_{k=1}^{n_2} \omega_k^{(2)} f(x_j^{(1)}, x_k^{(2)}) \\ &= \int_{-1}^1 \int_{-1}^1 f(x, y) \omega^{(1)}(x) dx \omega^{(2)}(y) dy - \int_{-1}^1 \sum_{k=1}^{n_2} \omega_k^{(2)} f(x, x_k^{(2)}) \omega^{(1)}(x) dx \\ &\quad + \int_{-1}^1 \sum_{k=1}^{n_2} \omega_k^{(2)} f(x, x_k^{(2)}) \omega^{(1)}(x) dx - \sum_{j=1}^{n_1} \omega_j^{(1)} \sum_{k=1}^{n_2} \omega_k^{(2)} f(x_j^{(1)}, x_k^{(2)}). \end{aligned}$$

Applying the triangle inequality we get

$$\begin{aligned} |R_n(f)| &\leq \left| \int_{-1}^1 \int_{-1}^1 f(x, y) \omega^{(1)}(x) dx \omega^{(2)}(y) dy - \int_{-1}^1 \sum_{k=1}^{n_2} \omega_k^{(2)} f(x, x_k^{(2)}) \omega^{(1)}(x) dx \right| \\ &\quad + \left| \int_{-1}^1 \sum_{k=1}^{n_2} \omega_k^{(2)} f(x, x_k^{(2)}) \omega^{(1)}(x) dx - \sum_{j=1}^{n_1} \omega_j^{(1)} \sum_{k=1}^{n_2} \omega_k^{(2)} f(x_j^{(1)}, x_k^{(2)}) \right| \\ &\leq \left| \int_{-1}^1 \left[\int_{-1}^1 f(x, y) \omega^{(2)}(y) dy - \sum_{k=1}^{n_2} \omega_k^{(2)} f(x, x_k^{(2)}) \right] \omega^{(1)}(x) dx \right| \\ &\quad + \left| \sum_{k=1}^{n_2} \omega_k^{(2)} \left[\int_{-1}^1 f(x, x_k^{(2)}) \omega^{(1)}(x) dx - \sum_{j=1}^{n_1} \omega_j^{(1)} f(x_j^{(1)}, x_k^{(2)}) \right] \right| \\ &\leq \mu_0^{(1)} \max_{x \in [-1, 1]} |R_{n_2}^{(2)}(f(x, \cdot))| + \mu_0^{(2)} \max_{y \in [-1, 1]} |R_{n_1}^{(1)}(f(\cdot, y))|. \end{aligned}$$

2. Orthogonal Polynomials and Gauss Quadrature Rules

Here, $R_n^{(1)}$ and $R_n^{(2)}$ denote the remainders for the integration with respect to x and y , respectively. Since the integrand f is analytic on $[-1, 1] \times \mathcal{E}_{\rho_2}$ and $\mathcal{E}_{\rho_1} \times [-1, 1]$ we can apply Theorems 2.2.11 and 2.2.15, which completes the proof.

□

3. High-Order NURBS-Based Boundary Element Methods

Discrete ansatz spaces arise when solving the boundary integral equations introduced in Section 1.2. In standard BEM implementations, e.g. [BBF13, AEF⁺14, ŠBA⁺15], the boundary Γ is approximated by a polygon Γ_h and piecewise polynomial basis functions are chosen for the ansatz space. For high-order collocation or Galerkin methods, which use ansatz functions with high polynomial degrees, the geometric error induced by the boundary approximation diminishes the convergence rates. In order to preserve the optimal convergence rates there are different approaches depending on the choice of the bases used for the boundary representation and the ansatz space. Throughout this work, we consider three approaches, **isoparametric**, **isogeometric** and **NURBS-enhanced** methods. These three approaches and their dependency on the functions chosen for the boundary parametrization and ansatz space are summarized in Table 3.1.

		ansatz space	
		polynomial	NURBS
boundary param.	polynomial	isoparametric	
	NURBS	NURBS-enhanced	isogeometric

Table 3.1.: Different versions of BEM depending on the choice of the basis functions used for the boundary parametrization and the ansatz space.

Isoparametric methods, which were introduced in [Zie71], approximate the boundary Γ by the same polynomial basis functions that are used for the ansatz space. While the geometrical error decays with the same order as the collocation or Galerkin error for the hypersingular integral equation, the convergence rates are in general diminished by the geometrical error for Symm's integral equation.

Isogeometric analysis, first introduced in [HCB05], extends the idea of isoparametric methods by using a common basis for the boundary parametrization and the ansatz space without inducing a geometrical error. In practice, the geometry is designed in computer-aided design (CAD)

3. High-Order NURBS-Based Boundary Element Methods

software and represented with NURBS basis functions. Therefore, the same NURBS basis is also used for the ansatz space, which in general results in a rational ansatz space.

The new isogeometric approach has several advantages as compared to conventional methods. While in conventional methods the exact representation of the geometry is approximated by piecewise polynomial meshes, this mesh generation process is eliminated in isogeometric analysis by directly using the CAD representation of the geometry. It is mentioned in [HCB05] that mesh generation takes a huge amount of the overall simulation process, hence the simulation time is significantly reduced in isogeometric methods. Moreover, no communication with CAD is required for repeated mesh refinement, since the exact mesh can be directly refined using simple algorithms available for NURBS. Another advantage is that besides the classical h - and p -refinements, where the triangulation is refined and the polynomial degree of the basis functions is increased, new refinement algorithms are developed based on the variable global regularity of the NURBS basis functions.

Although isogeometric analysis has found many applications to the finite element method (FEM), see e.g. [CHB09, WFC08, BH08, BCZ⁺06, BBH⁺10, CRB⁺06], the most suitable method for isogeometric analysis is BEM. Usually, the geometry is defined by its surface parametrization in CAD and a volume mesh has to be generated for the application to finite elements. Since BEM requires the discretization of only the domain's boundary, no additional volume mesh has to be generated. However, the application of isogeometric analysis to BEM has been investigated only very recently in e.g. [SSE⁺13, SBT⁺12, FGP15].

Finally, we also consider the **NURBS-enhanced** approach, which was introduced for FEM in [SFH08] and further examined in [SFH11]. NURBS-enhanced methods combine the classical methods with the idea of eliminating the geometrical error as done in isogeometric methods. While the geometry is represented exactly using NURBS curves, a polynomial basis is chosen for the ansatz space. Hence, the advantages of isogeometric methods - i.e. the absence of a geometrical error, the elimination of the mesh generation process as well as the elimination of the communication with CAD during the mesh refinement process - are transferred to NURBS-enhanced methods.

The original idea of NURBS-enhanced FEM was to preserve the efficiency of conventional FEM implementations by using the standard integration for the polynomial ansatz functions on interior elements. While for the application to BEM there is generally no gain in efficiency as compared to isogeometric methods, stability properties are enhanced for high-order methods, specifically by using Legendre polynomials and their antiderivatives as basis functions for the polynomial ansatz space.

Since both isogeometric and NURBS-enhanced methods are based on a NURBS representation of the boundary, we refer to both methods as NURBS-based methods within the scope of this work. In order to define the bases for the discrete ansatz spaces of NURBS-based BEM, we first

introduce NURBS curves used for the boundary parametrization. We then introduce the discrete ansatz spaces used for the implementation and conclude this chapter by describing different strategies of mesh refinement.

3.1. Non-Uniform Rational B-Splines

For the introduction of NURBS, we are guided by [PT97] and [Far99]. We only state the main properties of the NURBS basis functions and curves as well as fundamental algorithms used for mesh refinement.

Definition 3.1.1. Let $q, n \in \mathbb{N}_0$.

- (i) For $-1 = \xi_0 \leq \dots \leq \xi_{n+q} = 1$, we introduce a non-uniform knot vector $\Xi := \{\xi_0, \dots, \xi_{n+q}\}$, which we call open if $\xi_0 = \dots = \xi_q$ and $\xi_{n-1} = \dots = \xi_{n+q}$. Further, we define the unique knot vector $\tilde{\Xi} = \{\zeta_0, \dots, \zeta_m\}$ with $\zeta_0 < \dots < \zeta_m$ and associate with each unique knot ζ_j a multiplicity r_j such that

$$\Xi = \underbrace{\{\zeta_0, \dots, \zeta_0\}}_{r_0 \text{ times}}, \dots, \underbrace{\{\zeta_m, \dots, \zeta_m\}}_{r_m \text{ times}}.$$

In particular, we have $\sum_{j=0}^m r_j = n + q + 1$. We assume $r_j \leq q + 1$ and refer to ζ_j as nodes, $j = 1, \dots, m$.

- (ii) For $i = 0, \dots, n + q$ and $\xi \in [-1, 1]$, we define the b-spline basis functions recursively by

$$\begin{aligned} \mathcal{B}_{i,0}(\xi) &:= \begin{cases} 1, & \xi_i \leq \xi < \xi_{i+1} \\ 0, & \text{else.} \end{cases} \\ \mathcal{B}_{i,q}(\xi) &:= \frac{\xi - \xi_i}{\xi_{i+q} - \xi_i} \mathcal{B}_{i,q-1}(\xi) + \frac{\xi_{i+q+1} - \xi}{\xi_{i+q+1} - \xi_{i+1}} \mathcal{B}_{i+1,q-1}(\xi). \end{aligned} \quad (3.1)$$

- (iii) Let $\omega_k > 0$, $k = 0, \dots, n$, be positive weights. We define the weight function ω by

$$\omega(\xi) := \sum_{k=0}^n \omega_k \mathcal{B}_{k,q}(\xi)$$

and the NURBS basis functions by

$$\mathcal{R}_{k,q}(\xi) := \frac{\omega_k}{\omega(\xi)} \mathcal{B}_{k,q}(\xi).$$

- (iv) For control points $Q_k \in \mathbb{R}^2$, $k = 0, \dots, n$, we define the NURBS curve by

$$\begin{aligned} \gamma &: [-1, 1] \rightarrow \mathbb{R}^2 \\ \xi &\mapsto \gamma(\xi) := \sum_{k=0}^n \mathcal{R}_{k,q}(\xi) Q_k. \end{aligned}$$

3. High-Order NURBS-Based Boundary Element Methods

Remark 3.1.2. Most common geometries like circles, ellipses, and conics can be represented exactly using NURBS curves (see e.g. [PT97] Chapter 7). Hence, in many computer aided design (CAD) software programs NURBS curves are used for the internal representation of the geometries.

Example 3.1.3. The NURBS parametrization of a quarter circle with degree $q = 2$ is given by

$$\begin{aligned}\Xi &= \{-1, -1, -1, 1, 1, 1\} \\ \{\omega_k\}_{k=0,\dots,2} &= \left\{1, \frac{1}{\sqrt{2}}, 1\right\} \\ \{Q_k\}_{k=0,\dots,2} &= \{(0, 0), (1, 1), (0, 1)\}.\end{aligned}\tag{3.2}$$

The unit circle can be parametrized by concatenating four quarter circles. We obtain

$$\begin{aligned}\Xi &= \left\{-1, -1, -1, -\frac{1}{2}, -\frac{1}{2}, 0, 0, \frac{1}{2}, \frac{1}{2}, 1, 1, 1\right\} \\ \{\omega_k\}_{k=0,\dots,8} &= \left\{1, \frac{1}{\sqrt{2}}, 1, \frac{1}{\sqrt{2}}, 1, \frac{1}{\sqrt{2}}, 1, \frac{1}{\sqrt{2}}, 1\right\} \\ \{Q_k\}_{k=0,\dots,8} &= \{(1, 0), (1, 1), (0, 1), (-1, 1), (-1, 0), (-1, -1), (0, -1), (1, -1), (1, 0)\}.\end{aligned}\tag{3.3}$$

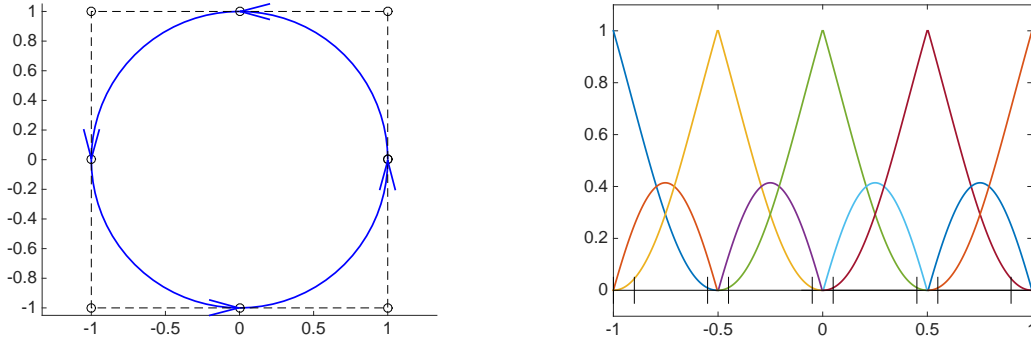


Figure 3.1.: NURBS parametrization of the unit circle with control polygon (left) and corresponding rational basis functions (right).

The following lemma collects some useful properties of NURBS and b-spline basis functions and curves.

Lemma 3.1.4. *With the notation of Definition 3.1.1 the following properties hold.*

- (i) *The b-spline and NURBS basis functions form a partition of unity, i.e. $\sum_{k=0}^n \mathcal{B}_{k,q}(\xi) = \sum_{k=0}^n \mathcal{R}_{k,q}(\xi) = 1$ for $\xi \in [-1, 1]$.*

- (ii) *The b-spline and NURBS basis functions have local support, i.e. $\text{supp } \mathcal{B}_{k,q} = \text{supp } \mathcal{R}_{k,q} = [\xi_k, \xi_{k+q+1})$.*
- (iii) *The b-spline and NURBS basis functions are $q - r_j$ times continuously differentiable at ζ_j , $j = 0, \dots, m$.*
- (iv) *The b-spline basis functions $\mathcal{B}_{k,q}$, $k = 0, \dots, n$, form a basis of the space of all piecewise polynomials of degree q , which are $q - r_j$ times continuously differentiable at ζ_j , $j = 0, \dots, m$.*
- (v) *The derivative of the b-spline basis functions is given by*

$$\mathcal{B}'_{k,q} = q \left(\frac{\mathcal{B}_{i,q-1}}{\xi_{k+q} - \xi_k} - \frac{\mathcal{B}_{i+1,q-1}}{\xi_{k+q+1} - \xi_{k+1}} \right).$$
- (vi) *If $\omega_0 = \dots = \omega_n = 1$, then $\omega(\xi) \equiv 1$ and the NURBS basis functions reduce to the b-spline basis functions.*
- (vii) *At all nodes ζ_j the NURBS curve γ is $q - r_j$ times continuously differentiable.*
- (viii) *Both components of $\gamma|_{[\zeta_j, \zeta_{j+1}]}$ ($j = 0, \dots, m$) are rational functions of degree q with non-vanishing denominator.*
- (ix) *Let $\omega_{\min} = \min_{k=0, \dots, n} \omega_k$ and $\omega_{\max} = \max_{k=0, \dots, n} \omega_k$. The derivative is bounded by*

$$\max_{\xi \in [-1, 1]} |\dot{\gamma}(\xi)| \leq n \left(\frac{\omega_{\max}}{\omega_{\min}} \right)^2 \max_{0 < j \leq n} \frac{\|Q_j - Q_{j-1}\|}{\xi_{j+q-1} - \xi_{j-1}}.$$

Proof. A proof of (i)-(viii) is given in [PT97] and the estimate in (ix) is proven in [Far99, page 164]. \square

In the following we introduce some basic geometric algorithms, which we will use for mesh refinement in Section 3.3. A detailed derivation of all algorithms is given in [PT97, Chapter 5]. Let $\gamma(t) = \sum_{k=0}^n \mathcal{R}_{k,q}(t) Q_k$ be a q -th degree NURBS curve associated with the open knot vector Ξ , weights ω_k and control points $Q_k := (q_k^{(1)}, q_k^{(2)})$. The two dimensional NURBS curve is projected in the three dimensional space by defining the weighted control points

$$Q_k^\omega := (\omega_k q_k^{(1)}, \omega_k q_k^{(2)}, \omega_k) \quad (3.4)$$

and setting

$$\gamma^\omega(t) := \sum_{k=0}^n \mathcal{B}_{k,p}(t) Q_k^\omega.$$

All subsequently presented algorithms only use the three-dimensional projection $\gamma^\omega(t)$ of $\gamma(t)$.

3. High-Order NURBS-Based Boundary Element Methods

Knot Insertion. Knot insertion is a fundamental algorithm that can be used for subdividing NURBS curves and changing the regularity of the NURBS basis functions. Additional knots are inserted into the knot vector Ξ without changing the curve parametrically or geometrically.

Inserting the knot $\bar{\xi} \in [\xi_k, \xi_{k+1})$ into Ξ we obtain the new knot vector

$$\hat{\Xi} := \{\xi_0, \dots, \xi_k, \bar{\xi}, \xi_{k+1}, \dots, \xi_{n+p}\}.$$

Hence, the number of NURBS basis functions associated to $\hat{\Xi}$ is increased by one, i.e. the NURBS curve has a representation

$$\gamma^\omega(t) = \sum_{j=0}^{n+1} \hat{\mathcal{B}}_{j,q} \hat{Q}_j^\omega.$$

The new weighted control points $\hat{Q}_j^\omega, j = 0, \dots, n+1$, can be computed by

$$\hat{Q}_j^\omega = \alpha_j Q_j^\omega + (1 - \alpha_j) Q_{j-1}^\omega \quad (3.5)$$

with

$$\alpha_j = \begin{cases} 1, & j \leq k-p \\ \frac{\bar{\xi} - \xi_j}{\xi_{j+p} - \xi_j}, & k-p+1 \leq j \leq k \\ 0, & j \geq k+1. \end{cases}$$

Hence, inserting a knot into the knot vector changes the basis representing the curve but not the curve itself. This implies, that the continuity of the curve remains unchanged while due to property (iii) in Lemma 3.1.4 the continuity of the basis functions is reduced by inserting additional knots in the knot vector. Therefore, the knot insertion algorithm allows to control the regularity of the basis functions without changing the regularity of the curve.

Furthermore, repeating an existing knot until its multiplicity equals $q+1$ splits the curve. Repeating this procedure for all interior knots yields a rational Bezier splitting of the NURBS curve.

Knot Removal. Knot removal is the inverse process of knot insertion. An interior node $\zeta \in \Xi$ with multiplicity r is called removable if the curve γ^ω is $p-r+1$ times continuously differentiable in ζ , i.e. additional regularity of the curve is assumed.

Let $\zeta \in \Xi$ be a removable node with multiplicity $r > 1$ and $k \in \{0, \dots, n+q\}$ be the index with $\zeta = \xi_k \neq \xi_{k+1}$. The new weighted control points \hat{Q}_k^ω can be computed by

$$\begin{aligned} \hat{Q}_i^\omega &= \frac{Q_i^\omega - (1 - \alpha_i) Q_{i-1}^\omega}{\alpha_i} & k-q \leq i \leq \frac{1}{2}(2k-q-r-1), \\ \hat{Q}_j^\omega &= \frac{Q_j^\omega - (1 - \alpha_j) Q_{j-1}^\omega}{\alpha_j} & \frac{1}{2}(2k-q-r+2) \leq j \leq k-r \end{aligned}$$

with $\alpha_\ell := \frac{\xi_k - \xi_\ell}{\xi_{\ell+q+1} - \xi_\ell}$. Again, the curve is neither changed geometrically nor parametrically but the regularity of the basis functions at ζ is increased by one.

Degree Elevation. Elevating the degree of a curve by $s \in \mathbb{N}$ without changing the curve geometrically or parametrically is called degree elevation, i.e.

$$\gamma^\omega(t) = \sum_{j=0}^{\hat{n}} \hat{B}_{j,q+s} \hat{Q}_j^{\hat{\omega}}.$$

Since the curve is not changed parametrically, the continuity of the curve at the nodes $\zeta \in \tilde{\Xi}$ has to remain unchanged. Property (vii) in Lemma 3.1.4 implies that the multiplicity of each knot in the knot vector has to be increased by s , i.e.

$$\hat{\Xi} = \{\hat{\xi}_0, \dots, \hat{\xi}_{n+q+s(m+1)}\} := \underbrace{\{\zeta_0, \dots, \zeta_0\}}_{r_0+s \text{ times}}, \dots, \underbrace{\{\zeta_m, \dots, \zeta_m\}}_{r_m+s \text{ times}}.$$

For the computation of the new weights and control points Algorithm 3.1 can be used, which is introduced in [PT97, Chapter 5.5].

Algorithm 3.1 Computation of new control points and weights for degree elevation

INPUT: q -th degree NURBS curve defined by Ξ , Q_k and ω_k , $k = 1, \dots, n$.

OUTPUT: $(q + s)$ -th degree NURBS curve defined by $\hat{\Xi}$, \hat{Q}_k and $\hat{\omega}_k$, $k = 1, \dots, n + sm$.

- 1: Extract the Bezier segments of the curve by repeating all interior knots $(q + 1)$ times using the knot insertion algorithm.
 - 2: Degree elevate each Bezier segment.
 - 3: Remove all interior knots until $\hat{r}_j = r_j + s$ using the knot removal algorithm.
-

3.2. Discrete Ansatz Spaces

Let $\Omega \subset \mathbb{R}^2$ be a Lipschitz domain with boundary $\Gamma := \partial\Omega$. We introduce a triangulation and its parametrization in the following definition.

Definition 3.2.1. (i) Let $\mathcal{N}_e \in \mathbb{N}$ and $\gamma : [-1, 1] \rightarrow \Gamma$ be the q -th degree NURBS parametrization of Γ with open knot vector

$$\Xi = \underbrace{\{\zeta_0, \dots, \zeta_0\}}_{r_0 \text{ times}}, \dots, \underbrace{\{\zeta_{\mathcal{N}_e}, \dots, \zeta_{\mathcal{N}_e}\}}_{r_{\mathcal{N}_e} \text{ times}},$$

weights ω_k , and control points Q_k , $k = 0, \dots, n$, as given in Definition 3.1.1. For $i = 1, \dots, \mathcal{N}_e$, we introduce boundary elements $T_i := \gamma([\zeta_{i-1}, \zeta_i])$, which form a triangulation $\mathcal{T} = \{T_i, i = 1, \dots, \mathcal{N}_e\}$ of Γ as in Definition 1.4.1.

3. High-Order NURBS-Based Boundary Element Methods

(ii) We denote the number of vertices of the triangulation \mathcal{T} by \mathcal{N}_v .

(iii) For each element $T_i \in \mathcal{T}, i = 1, \dots, \mathcal{N}_e$, we define its local parametrization by

$$\begin{aligned} \gamma_i : [-1, 1] &\rightarrow T_i \\ t &\mapsto \gamma_i(t) := \gamma \left(\frac{(t+1)(\zeta_i - \zeta_{i-1})}{2} + \zeta_{i-1} \right). \end{aligned}$$

(iv) Let $\mathbf{h} \in L^\infty(\Gamma)$ be the mesh width function with $\mathbf{h}|_{\text{int}(T_i)} = |T_i| =: h_i$, where $|T_i| := \int_{\zeta_{i-1}}^{\zeta_i} |\dot{\gamma}(t)| dt$ denotes the arc length of the element T_i . Further, we introduce the mesh-width ratio

$$\sigma(\mathbf{h}) := \max \left\{ \frac{h_i}{h_j}, T_i, T_j \in \mathcal{T}, T_i \cap T_j \neq \emptyset \right\}.$$

(v) Let $\mathbf{p} \in L^\infty(\Gamma)$ be the polynomial degree function with $\mathbf{p}|_{T_i} =: p_i \in \mathbb{N}_0$. If the polynomial degree function is uniform, i.e. $p_1 = \dots = p_{\mathcal{N}_e}$, we write $p = \mathbf{p}$.

(vi) Let $\mathbf{k} \in L^\infty(\Gamma)$ be the regularity function with $\mathbf{k}|_{T_i} = q - r_i + 1$.

Remark 3.2.2. Throughout this work, we assume that either $\Gamma \subset \mathbb{R}^2$ is an open arc or Γ is closed and $\mathcal{N}_e > 1$. This assumption implies that the local parametrizations $\gamma_i, i = 1, \dots, \mathcal{N}_e$, are bijective.

Now we are in the position to introduce the bases for the different ansatz spaces. We start with the isoparametric and isogeometric ansatz spaces, where we use transformed b-spline and NURBS basis functions.

Definition 3.2.3. Let γ be the NURBS parametrization of Γ as given in Definition 3.2.1. Further, let $\tilde{\mathcal{R}}_k := \mathcal{R}_{k,q} \circ \gamma^{-1}, k = 0, \dots, n$, where $\mathcal{R}_{k,q}$ are the NURBS basis functions of degree q defined by the same knot vector and weights that are used for γ . We define the rational ansatz space by

$$R(\mathcal{T}, \mathbf{h}, q, \mathbf{k}) := \text{span} \{ \tilde{\mathcal{R}}_k, k = 0, \dots, n \}. \quad (3.6)$$

Remark 3.2.4. (i) The ansatz space for isoparametric methods is obtained by setting all weights $\omega_k=1, k = 0, \dots, n$. Then, the rational ansatz space $R(\mathcal{T}, \mathbf{h}, q, \mathbf{k})$ changes over the polynomial ansatz space $S(\mathcal{T}, \mathbf{h}, q, \mathbf{k})$ introduced in Section 1.4.

(ii) Using NURBS and b-spline basis functions, respectively, allows for the easy construction of ansatz spaces with variable and high-order global regularity. Therefore, b-spline basis functions are often used for collocation methods, where the high-order regularity is needed in the theoretical analysis.

For the construction of the ansatz spaces for NURBS-enhanced methods, we use transformed Legendre polynomials and Lobatto shape functions.

Definition 3.2.5. Let \mathcal{T} and γ be defined as in Definition 3.2.1.

- (i) For $i = 1, \dots, \mathcal{N}_e$, we define $\tilde{P}_k^{(i)} := P_k \circ \gamma_i^{-1}$, $k \in \mathbb{N}_0$, and $\tilde{N}_k^{(i)} := N_k \circ \gamma_i^{-1}$, $k \in \mathbb{N}$, where P_k and N_k are the Legendre polynomials and Lobatto shape functions as defined in Definitions 2.1.8 and 2.1.10, respectively.
- (ii) The basis of the ansatz space $S(\mathcal{T}, \mathbf{h}, \mathbf{p}, \mathbf{0})$ is given by

$$\bigcup_{i=1}^{\mathcal{N}_e} \{\tilde{P}_0^{(i)}, \dots, \tilde{P}_{p_i}^{(i)}\} \quad (3.7)$$

and the basis of the ansatz space $S(\mathcal{T}, \mathbf{h}, \mathbf{p}, \mathbf{1})$ is given by

$$\{\tilde{\mathcal{H}}_1, \dots, \tilde{\mathcal{H}}_{\mathcal{N}_v}\} \cup \left(\bigcup_{i=1}^{\mathcal{N}_e} \{\tilde{N}_3^{(i)}, \dots, \tilde{N}_{p_i+1}^{(i)}\} \right), \quad (3.8)$$

where $\tilde{\mathcal{H}}_j \circ \gamma \in \mathcal{P}_1([-1, 1])$ with $\tilde{\mathcal{H}}_j(\gamma(\zeta_k)) = \delta_{jk}$ denote the hat functions, $j = 1, \dots, \mathcal{N}_v$.

Remark 3.2.6. (i) In [Heu92] and [HS96] the condition number of the single layer Galerkin matrix for polygonal boundaries is analyzed. In particular, it is proven that taking the Legendre basis as defined in (3.7) yields condition numbers of order $\mathcal{O}(\mathbf{p}^\alpha)$ with $\alpha = 3$. The numerical results presented in [Ban13] indicate that the condition number only grows linearly in \mathbf{p} if a diagonal scaling is applied to the Galerkin matrix. Similar results are also observed in our numerical examples for curved boundaries in the later chapters.

- (ii) Although the Legendre polynomials and the Lobatto shape function yield good condition numbers in the Galerkin matrix, it is difficult to construct ansatz spaces with higher global regularity. Hence, these basis functions are only used for the ansatz spaces $S(\mathcal{T}, \mathbf{h}, \mathbf{p}, \mathbf{0})$ and $S(\mathcal{T}, \mathbf{h}, \mathbf{p}, \mathbf{1})$.
- (iii) Since Lamé problems are two-dimensional problems the ansatz spaces are defined by the tensor product $X_\ell \times X_\ell$, where $X_\ell = \{\Phi_k, k = 1, \dots, \mathcal{N}\}$ denotes one of the above defined ansatz spaces. The basis of the tensor product space is then given by $\{(\Phi_k, 0), (0, \Phi_k), k = 1, \dots, \mathcal{N}\}$.

Example 3.2.7. Let Γ be an open arc parametrized by the NURBS curve with degree $q = 2$, knot vector $\Xi = [-1, -1, -1, -0.5, 0, 0, 1, 1, 1]$, weights $\{\omega_k\}_{k=0, \dots, 5} = \{1, 2, 1, 0.5, 1, 3\}$ and control points $\{Q_k\}_{k=0, \dots, 5} = \{(1, 0), (2, 2), (3, -1), (5, 2.5), (6, 2), (7, 0)\}$. The polynomial degree vector is given by $\mathbf{p} = [1, 3, 2]$. The NURBS curve with control polygon and the basis functions of the three ansatz spaces $R(\mathcal{T}, \mathbf{h}, q, \mathbf{k})$, $S(\mathcal{T}, \mathbf{h}, \mathbf{p}, \mathbf{0})$ and $S(\mathcal{T}, \mathbf{h}, \mathbf{p}, \mathbf{1})$ are depicted in the Figures 3.2 and 3.3.

3. High-Order NURBS-Based Boundary Element Methods

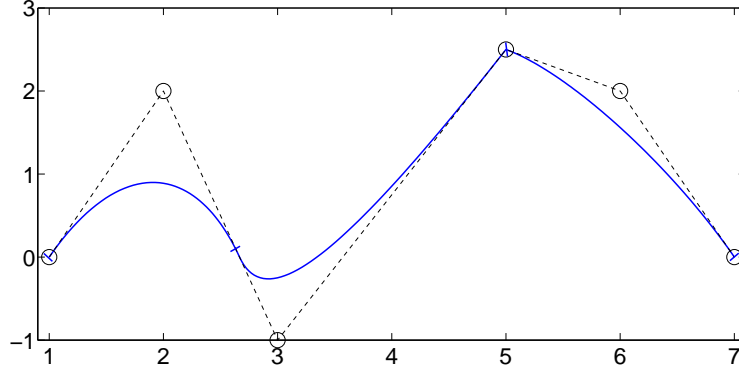


Figure 3.2.: NURBS curve as defined in Example 3.2.7 with control polygon (dashed).

In the remainder of this section, we derive some important properties of the NURBS parametrizations γ_i that are used for the implementation of collocation and Galerkin methods. In particular, we prove that the local parametrizations are analytically extendable and determine their domain of analyticity.

Lemma 3.2.8. *For $\rho > 1$, let \mathcal{E}_ρ denote the ellipse with foci ± 1 as defined in Definition 2.0.9.*

(i) $\gamma_i : [-1, 1] \rightarrow T_i$ is bijective and there exists $\alpha_i > 0$, such that for all $s, t \in [-1, 1]$

$$\alpha_i^{-1} < \min_{\xi \in [-1, 1]} |\dot{\gamma}_i(\xi)| \leq \frac{|\gamma_i(t) - \gamma_i(s)|}{|t - s|} \leq \max_{\xi \in [-1, 1]} |\dot{\gamma}_i(\xi)| < \alpha_i.$$

(ii) For a sufficiently small arc length h_i , we get

$$\frac{h_i}{2} \leq \max_{\xi \in [-1, 1]} |\dot{\gamma}_i(\xi)| \leq q \frac{\omega_{\max}}{\omega_{\min}} h_i.$$

(iii) There exists $\rho_1 > 1$ such that both components of γ_i are analytically extendable to the complex ellipse \mathcal{E}_{ρ_1} with semi-axis sum ρ_1 .

(iv) There exists $\rho_2 > 1$ such that $|\dot{\gamma}_i|$ is analytically extendable to the complex ellipse \mathcal{E}_{ρ_2} with semi-axis sum ρ_2 .

Proof. (i) With Remark 3.2.2 and $T_i \in \mathcal{T}$, and since Ω is a Lipschitz domain there exists a bi-Lipschitz continuous parametrization, which implies (i).

(ii) For the first inequality, we obtain

$$\frac{h_i}{2} = \frac{1}{2} \int_{-1}^1 |\dot{\gamma}_i(t)| dt \leq \max_{\xi \in [-1, 1]} |\dot{\gamma}_i(\xi)|.$$

For the second inequality, we assume a rational Bezier representation with control points \tilde{Q}_k and weights $\tilde{\omega}_k$ of γ_i , which can be obtained by inserting the knots ζ_{i-1} and ζ_i up to

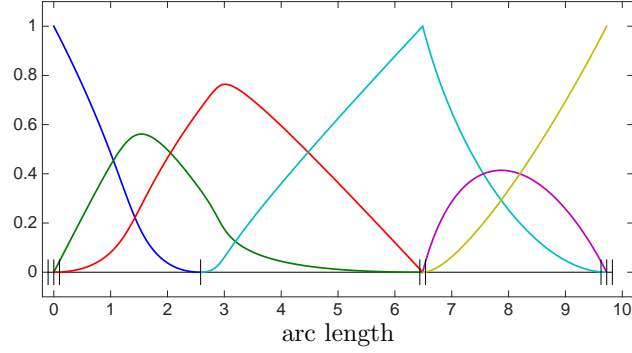
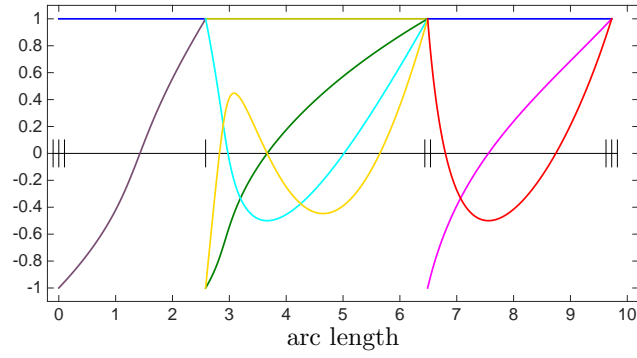
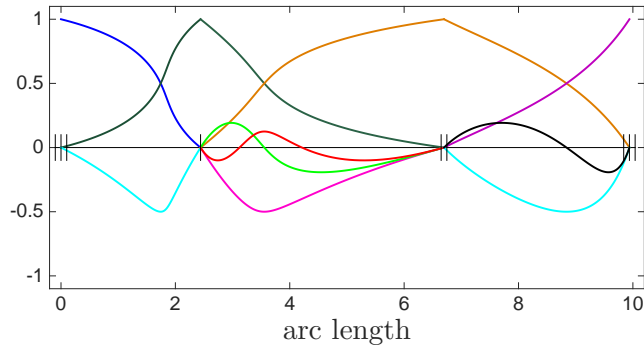

 (a) NURBS basis functions $\tilde{\mathcal{R}}_k$, $k = 0, \dots, 5$.

 (b) Legendre basis functions $\tilde{P}_k^{(i)}$, $i = 1, \dots, 4$, $k = 0, \dots, p_i$.

 (c) Lobatto basis functions $\tilde{N}_k^{(i)}$, $i = 1, \dots, 4$, $k = 3, \dots, p_i + 1$, and hat functions $\tilde{\mathcal{H}}_k$, $k = 1, \dots, 4$, respectively.

Figure 3.3.: Basis functions of the ansatz spaces in Definitions 3.2.3 and 3.2.5 plotted over the arc length of the boundary. The vertical bars on the x-axes denote the multiplicity of the knot in the knot vector.

3. High-Order NURBS-Based Boundary Element Methods

multiplicity $q + 1$. In [PK94] it is proven that $\tilde{Q}_k = \gamma_i(\xi_k) + \mathcal{O}(h^2)$. Hence, we get with Lemma 3.1.4 (ix)

$$\begin{aligned} \max_{\xi \in [-1, 1]} |\dot{\gamma}_i(\xi)| &\leq q \frac{\omega_{\max}}{\omega_{\min}} \max_{0 \leq k, j < n} \|\tilde{Q}_k - \tilde{Q}_j\| \\ &\leq q \frac{\omega_{\max}}{\omega_{\min}} \max_{0 \leq k < q} \|\gamma_i(\xi_k) - \gamma_i(\xi_j)\| + \mathcal{O}(h_i^2) \\ &\leq q \frac{\omega_{\max}}{\omega_{\min}} h_i + \mathcal{O}(h_i^2). \end{aligned}$$

For sufficiently small h_i we get $\max_{\xi \in [-1, 1]} |\dot{\gamma}_i(\xi)| \leq q \frac{\omega_{\max}}{\omega_{\min}} h_i$.

(iii) Due to (viii) in Lemma 3.1.4 both components of γ_i are rational functions with poles $z_j \in \mathbb{C} \setminus [-1, 1]$ ($j = 1, \dots, q$). Thus, there exists $\rho_1 > 1$ such that $z_j \notin \mathcal{E}_{\rho_1}$ and hence γ_i can be analytically extended to \mathcal{E}_{ρ_1} .

(iv) Since both components of γ_i are analytically extendable to \mathcal{E}_{ρ_1} , both components of $\dot{\gamma}_i$ are analytically extendable to \mathcal{E}_{ρ_1} .

Let $f(t) := [\dot{\gamma}_{i,1}(t)]^2 + [\dot{\gamma}_{i,2}(t)]^2$. Then, f is an analytic function on \mathcal{E}_{ρ_1} and with (i) we get $f(t) \neq 0$ for all $t \in [-1, 1]$. Due to the continuity of f there exists $1 < \rho_2 \leq \rho_1$ with $f(t) \neq 0$ for $t \in \mathcal{E}_{\rho_2}$. With [FB06, Theorem II.2.9] there exists a holomorphic function $h : \mathcal{E}_{\rho_2} \rightarrow \mathbb{C}$ with $h^2 = f$ on \mathcal{E}_{ρ_2} . The holomorphic function h is the unique analytic extension of $|\dot{\gamma}_i|$, since $h(t) = |\dot{\gamma}_i(t)|$ for $t \in [-1, 1]$ ([FB06], Theorem III.3.2)).

□

Definition 3.2.9. Let $i = 1, \dots, \mathcal{N}_e$ and γ_i be the local parametrization of T_i . We denote by \mathcal{E}_{ρ_i} the ellipse with maximum semi-axis sum ρ_i as defined in Definition 2.0.9, in which both components of γ_i and $|\dot{\gamma}_i|$ are analytically extendable. Further, we identify γ_i and $|\dot{\gamma}_i|$ by their analytic extensions if no ambiguity occurs.

Proposition 3.2.10. *The derivative $\dot{\gamma}$ of a q -th degree NURBS parametrization is a piecewise rational function with numerator of degree $2(q - 1)$.*

Proof. Defining $P(t) := \sum_{k=0}^n \mathcal{B}_{k,q}(t) \omega_k Q_k$ we have

$$\dot{\gamma}(t) = \frac{\omega(t) P'(t) - \omega'(t) P(t)}{\omega(t)^2}.$$

The derivative of the b-spline polynomials is given by $\mathcal{B}'_{k,q}(t) = q \left(\frac{\mathcal{B}_{k,q-1}(t)}{\xi_{k+q} - \xi_k} - \frac{\mathcal{B}_{k+1,q-1}(t)}{\xi_{k+q+1} - \xi_{k+1}} \right)$

(Lemma 3.1.4 (v)). Therefore, we get

$$\begin{aligned}
\omega(t) P'(t) - \omega'(t) P(t) &= q \sum_{k=0}^n \sum_{j=0}^n \omega_k \omega_j Q_k \left(\frac{\mathcal{B}_{k,q-1}(t)}{\xi_{k+q} - \xi_k} - \frac{\mathcal{B}_{k+1,q-1}(t)}{\xi_{k+q+1} - \xi_{k+1}} \right) \mathcal{B}_{j,q}(t) \\
&\quad - q \sum_{k=0}^n \sum_{j=0}^n \omega_k \omega_j Q_j \left(\frac{\mathcal{B}_{k,q-1}(t)}{\xi_{k+q} - \xi_k} - \frac{\mathcal{B}_{k+1,q-1}(t)}{\xi_{k+q+1} - \xi_{k+1}} \right) \mathcal{B}_{j,q}(t) \\
&= q \sum_{k=0}^n \sum_{j=0}^n \omega_k \omega_j (Q_k - Q_j) \left(\frac{\mathcal{B}_{k,q-1}(t)}{\xi_{k+q} - \xi_k} - \frac{\mathcal{B}_{k+1,q-1}(t)}{\xi_{k+q+1} - \xi_{k+1}} \right) \mathcal{B}_{j,q}(t) \\
&=: q \sum_{k=0}^n \sum_{j=0}^n \alpha_{j,k} \left(\frac{\mathcal{B}_{k,q-1}(t)}{\xi_{k+q} - \xi_k} - \frac{\mathcal{B}_{k+1,q-1}(t)}{\xi_{k+q+1} - \xi_{k+1}} \right) \mathcal{B}_{j,q}(t)
\end{aligned}$$

with $\alpha_{jk} := \omega_k \omega_j (Q_k - Q_j)$. Since $\alpha_{jk} = -\alpha_{kj}$ we have

$$\begin{aligned}
\omega(t) P'(t) - \omega'(t) P(t) &= q \sum_{k=0}^n \sum_{j=k+1}^n \alpha_{j,k} \left[\left(\frac{\mathcal{B}_{k,q-1}(t)}{\xi_{k+q} - \xi_k} - \frac{\mathcal{B}_{k+1,q-1}(t)}{\xi_{k+q+1} - \xi_{k+1}} \right) \mathcal{B}_{j,q}(t) \right. \\
&\quad \left. - \left(\frac{\mathcal{B}_{j,q-1}(t)}{\xi_{j+q} - \xi_j} - \frac{\mathcal{B}_{j+1,q-1}(t)}{\xi_{j+q+1} - \xi_{j+1}} \right) \mathcal{B}_{k,q}(t) \right].
\end{aligned}$$

Applying the recurrence relation (3.1) we get

$$\begin{aligned}
&\left(\frac{\mathcal{B}_{k,q-1}(t)}{\xi_{k+q} - \xi_k} - \frac{\mathcal{B}_{k+1,q-1}(t)}{\xi_{k+q+1} - \xi_{k+1}} \right) \mathcal{B}_{j,q}(t) - \left(\frac{\mathcal{B}_{j,q-1}(t)}{\xi_{j+q} - \xi_j} - \frac{\mathcal{B}_{j+1,q-1}(t)}{\xi_{j+q+1} - \xi_{j+1}} \right) \mathcal{B}_{k,q}(t) \\
&= \left(\frac{\mathcal{B}_{k,q-1}(t)}{\xi_{k+q} - \xi_k} - \frac{\mathcal{B}_{k+1,q-1}(t)}{\xi_{k+q+1} - \xi_{k+1}} \right) \left(\frac{t - \xi_j}{\xi_{j+q} - \xi_j} \mathcal{B}_{j,q-1}(t) + \frac{\xi_{j+q+1} - t}{\xi_{j+q+1} - \xi_{j+1}} \mathcal{B}_{j+1,q-1}(t) \right) \\
&\quad - \left(\frac{\mathcal{B}_{j,q-1}(t)}{\xi_{j+q} - \xi_j} - \frac{\mathcal{B}_{j+1,q-1}(t)}{\xi_{j+q+1} - \xi_{j+1}} \right) \left(\frac{t - \xi_k}{\xi_{k+q} - \xi_k} \mathcal{B}_{k,q-1}(t) + \frac{\xi_{k+q+1} - t}{\xi_{k+q+1} - \xi_{k+1}} \mathcal{B}_{k+1,q-1}(t) \right) \\
&= \left(\frac{\mathcal{B}_{k,q-1}(t)}{\xi_{k+q} - \xi_k} - \frac{\mathcal{B}_{k+1,q-1}(t)}{\xi_{k+q+1} - \xi_{k+1}} \right) \left(-\frac{\xi_j}{\xi_{j+q} - \xi_j} \mathcal{B}_{j,q-1}(t) + \frac{\xi_{j+q+1}}{\xi_{j+q+1} - \xi_{j+1}} \mathcal{B}_{j+1,q-1}(t) \right) \\
&\quad - \left(\frac{\mathcal{B}_{j,q-1}(t)}{\xi_{j+q} - \xi_j} - \frac{\mathcal{B}_{j+1,q-1}(t)}{\xi_{j+q+1} - \xi_{j+1}} \right) \left(-\frac{\xi_k}{\xi_{k+q} - \xi_k} \mathcal{B}_{k,q-1}(t) + \frac{\xi_{k+q+1}}{\xi_{k+q+1} - \xi_{k+1}} \mathcal{B}_{k+1,q-1}(t) \right).
\end{aligned}$$

Finally, we obtain $\omega(t) P'(t) - \omega'(t) P(t) \in \mathcal{P}_{2(q-1)}([-1, 1])$.

□

Remark 3.2.11 (Computation of the domain of analyticity). As we see in the subsequent chapters it is necessary to explicitly determine the domain of analyticity of the local parametrization γ_i . In particular, we compute the semi-axis sum ρ_i as defined in Definition 3.2.9 in order to obtain accurate error bounds for the quadrature rules. According to the proof of Lemma 3.2.8 (ii) and (iii) we have to compute the complex zeros and the poles of the rational function $f(z) := [\dot{\gamma}_{i,1}(z)]^2 + [\dot{\gamma}_{i,2}(z)]^2$. If we denote the numerator of $\dot{\gamma}_i$ by $g = (g_1, g_2)$ and the denominator by ω_i we have

$$f(z) = \frac{g_1(z)^2 + g_2(z)^2}{\omega_i(z)^4}.$$

3. High-Order NURBS-Based Boundary Element Methods

The poles of $f(z)$ correspond to the roots of $\omega_i(z)$. Since $\omega_i(z)$ is a polynomial of order q we have closed formulas only for $q \leq 4$ and for higher order splines we can compute the roots numerically, e.g. via an eigenvalue problem.

Since the numerator of f is a polynomial with real coefficients, the roots ζ_j , $j = 1, \dots, 4q - 2$, are complex conjugate. In order to determine the semi-axis sum ρ_i , we only have to compute one zero of the complex conjugate pairs. Therefore, we write

$$g_1(z)^2 + g_2(z)^2 = [g_1(z) + i g_2(z)] [g_1(z) - i g_2(z)].$$

Since the coefficients of g_k , $k \in \{1, 2\}$, are real, we have

$$\overline{g_1(z) + i g_2(z)} = g_1(\bar{z}) - i g_2(\bar{z}).$$

This implies that if ζ_j is a zero of $g_1(z) + i g_2(z)$, then $\bar{\zeta}_j$ is a zero of $g_1(z) - i g_2(z)$. Thus, it is sufficient to compute the complex roots of the polynomial $g_1(z) + i g_2(z)$. Due to Proposition 3.2.10 we compute the roots of a $2(q - 1)$ -th degree polynomial and analytic formulas for the roots are given for $q \leq 3$.

Let M denote the set of all roots and poles of f . According to Remark 2.0.10 (i) the real semi-axis of \mathcal{E}_{ρ_i} is given by

$$a = \min_{z_k \in M} \frac{|z_k + 1| + |z_k - 1|}{2}$$

and finally $\rho_i = a + \sqrt{a^2 - 1}$.

The following lemma gives an estimate for the maximum value of $|\dot{\gamma}_i(z)|$ on confocal ellipses lying in the domain of analyticity.

Lemma 3.2.12. *Let $1 < \rho < \rho_i$ and $a, a_i > 1$ denote the real semi axis of the ellipses \mathcal{E}_ρ and \mathcal{E}_{ρ_i} . Then, there holds*

$$\max_{z \in \partial \mathcal{E}_\rho} |\dot{\gamma}_i(z)| \leq \frac{(a_i + a)^{2(q-1)}}{(a_i - a)^{2q}} \frac{(a_i - 1)^{2q}}{(a_i + 1)^{2(q-1)}} \max_{z \in [-1, 1]} |\dot{\gamma}_i(z)| =: c h_i.$$

Proof. Due to the definition of the ellipse \mathcal{E}_{ρ_i} , $\dot{\gamma}_i(z)$ contains no roots and poles in \mathcal{E}_{ρ_i} . However, at least one root or pole is located in $\partial \mathcal{E}_{\rho_i}$. In the worst case, we have a root of multiplicity $2(q - 1)$ (degree of the numerator of $\dot{\gamma}_i$) located at $-a_i$ and simultaneously a pole of order $2q$ (degree of the denominator of $\dot{\gamma}_i$) located at a_i . In this case, $|\dot{\gamma}_i(z)|$ behaves like $\frac{(a_i + a)^{2(q-1)}}{(a_i - a)^{2q}}$. If the maximum on $[-1, 1]$ is attained at the right end, we obtain the upper bound

$$\max_{z \in \partial \mathcal{E}_\rho} |\dot{\gamma}_i(z)| \leq \frac{(a_i + a)^{2(q-1)}}{(a_i - a)^{2q}} \frac{(a_i - 1)^{2q}}{(a_i + 1)^{2(q-1)}} \max_{z \in [-1, 1]} |\dot{\gamma}_i(z)| =: c h_i.$$

Here, we applied Lemma 3.2.8 in the last step. \square

Remark 3.2.13. The estimate in Lemma 3.2.12 is a worst case estimate. While there are boundary parametrizations for which the estimate is sharp, the estimate is generally very coarse.

3.3. Boundary Meshes and Refinement

We construct a sequence of discrete ansatz spaces $S(\mathcal{T}_\ell, \mathbf{h}_\ell, \mathbf{p}_\ell, \mathbf{k}_\ell)$ and $R(\mathcal{T}_\ell, \mathbf{h}_\ell, q_\ell, \mathbf{k}_\ell)$, $\ell \in \mathbb{N}$, during the mesh refinement process. In order to increase the dimension of the discrete ansatz spaces, there are different types of mesh refinements. Besides the classical h - and p -refinement, we also consider the uniform k -refinement for the isogeometric ansatz space $R(\mathcal{T}_\ell, \mathbf{h}_\ell, q_\ell, \mathbf{k}_\ell)$, which is originally introduced in [HCB05] and [CHR07]. Furthermore, we go into detail on the construction of geometrically graded meshes on the unit circle and a round L-shaped domain, which are introduced in Section 1.4.

Uniform h -refinement. In uniform h -methods we refine the boundary mesh \mathcal{T} uniformly by splitting each element $T \in \mathcal{T}$ into two sons T' and T'' . For NURBS-enhanced methods both sons inherit the polynomial degree p of T .

For the splitting of elements, a new knot is inserted in each knot interval of the knot vector Ξ_ℓ , i.e.

$$\Xi_\ell = \{\xi_0, \dots, \xi_{n+q}\} \rightarrow \Xi_{\ell+1} = \{\bar{\xi}_0, \dots, \bar{\xi}_{n+q+\mathcal{N}_e}\}.$$

The new control points and weights are computed using the knot insertion algorithm introduced in Section 3.1 such that the curves are neither changed geometrically nor parametrically.

Remark 3.3.1. Since the parametrization remains unchanged by using the knot insertion algorithm, the domain of analyticity of the new local parametrizations can directly be computed without solving the root finding problem described in Remark 3.2.11 in the following way:

Let γ_i be the local parametrization of T_i and M_i denote the set of all roots and poles of $\dot{\gamma}_i$ as introduced in Remark 3.2.11. Refining the mesh by inserting $\bar{\zeta}$ into $[\zeta_i, \zeta_{i+1}]$ the local parametrization $\gamma_i^{(\ell)}$ and $\gamma_i^{(r)}$ of the new elements $T_i^{(\ell)}$ and $T_i^{(r)}$ with $\gamma_i^{(\ell)}([-1, 1]) = T_i^{(\ell)}$ and $\gamma_i^{(r)}([-1, 1]) = T_i^{(r)}$ can be represented by

$$\begin{aligned} \gamma_i^{(\ell)}(t) &:= \gamma_i \left(\frac{(t+1)(\bar{\zeta} - \zeta_i)}{\zeta_{i+1} - \zeta_i} - 1 \right) \\ \gamma_i^{(r)}(t) &:= \gamma_i \left(\frac{(t-1)(\zeta_{i+1} - \bar{\zeta})}{\zeta_{i+1} - \zeta_i} + 1 \right). \end{aligned}$$

Hence, with $z \in M_i$, $z^{(\ell)} \in M_i^{(\ell)}$ and $z^{(r)} \in M_i^{(r)}$ we have the following relationship

$$\begin{aligned} z^{(\ell)} &= \frac{\zeta_{i+1} - \zeta_i}{\bar{\zeta} - \zeta_i} z + \frac{\zeta_{i+1} - \bar{\zeta}}{\bar{\zeta} - \zeta_i} \\ z^{(r)} &= \frac{\zeta_{i+1} - \zeta_i}{\zeta_{i+1} - \bar{\zeta}} z + \frac{\zeta_i - \bar{\zeta}}{\zeta_{i+1} - \bar{\zeta}}. \end{aligned}$$

The semi-axis sums $\rho_i^{(\ell)}$ and $\rho_i^{(r)}$ can be computed with the sets $M_i^{(\ell)}$ and $M_i^{(r)}$ as in Remark 3.2.11.

3. High-Order NURBS-Based Boundary Element Methods

An open issue in h -refinement is how to choose the new knots. The easiest way is to half each element such that a uniform mesh is created during the refinement process and the mesh-width ratio $\sigma(\mathbf{h})$ is not blowing up. However, since the parametrization not only depends on the control points but also on the weights, refining the knot vector uniformly does not refine the boundary mesh uniformly. An approach based on point inversion for approximately halving the element size is presented in [HCB05]. The idea is to compute the point $P := \frac{1}{2} (\gamma(\zeta_k) + \gamma(\zeta_{k+1}))$ and determine $\bar{\xi}$ such that $\bar{\xi} = \arg\min_{t \in [-1, 1]} \|\gamma(t) - P\|$.

As it is proven in Remark 3.3.1, the smoothness of the parametrization depends on the knot that is inserted. Hence, another strategy is to choose the knot so that the smoothness of the resulting local parametrization is optimally increased, i.e.

$$\bar{\xi} := \arg \max_{t \in [\zeta_i, \zeta_{i+1}]} \min\{\rho'_i(t), \rho''_i(t)\}.$$

This strategy of choosing $\bar{\xi}$ has the advantage that the order of the quadrature rules used for the numerical integration is decreased. Although the mesh width ratio $\sigma(\mathbf{h})$ remains bounded during the mesh refinement using this strategy, we obtain no uniform mesh.

Uniform p -refinement. We increase the discrete ansatz space by uniformly increasing the degree of the basis functions, i.e. $\mathbf{p}_\ell \rightarrow \mathbf{p}_{\ell+1} = 2\mathbf{p}_\ell + 1$ for NURBS-enhanced methods and $q_\ell \rightarrow q_{\ell+1} = q_\ell + 1$ for isogeometric methods. Hence, for NURBS-enhanced methods we do not change the boundary parametrization since the basis of the ansatz space is independent of the basis used for the boundary approximation. For isogeometric and isoparametric methods we increase the degree of the NURBS basis functions that are also used for the boundary approximation. In order to compute the new control points and weights without changing the curves geometrically or parametrically, the degree elevation Algorithm 3.1 is used. Hence, the dimension of the ansatz space is increase by \mathcal{N}_v .

Since only the NURBS basis functions and the control points but not the parametrization itself are changed, the domain of analyticity of the local parametrization remains unchanged both for NURBS-enhanced and isogeometric methods.

Uniform k -refinement. The idea of k -refinement, which has no analogue in classical BEM, is that the global regularity of the basis functions can be controlled by the multiplicity of the interior knots in the open knot vector Ξ_ℓ . In order to increase the regularity of the basis functions we assume that the boundary is smooth enough such that no geometrical error is induced by increasing the regularity of the basis. Further, the knot vector Ξ_ℓ is required to contain interior knots. If there are no interior knots, the basis function already have \mathcal{C}^∞ -regularity and uniform k -refinement corresponds to uniform p -refinement. We proceed as in Algorithm 3.2. After the degree elevation in the first step the regularity of the basis functions is unchanged, i.e. the basis

Algorithm 3.2 Uniform k -refinement

INPUT: q -th degree NURBS curve defined by Ξ_ℓ , Q_k^ℓ and ω_k^ℓ , $k = 0, \dots, n$.

OUTPUT: $(q + 1)$ -th degree NURBS curve defined by $\Xi_{\ell+1}$, $Q_k^{\ell+1}$ and ω_k^ℓ , $k = 0, \dots, n + 1$.

- 1: Degree elevate the curve using Algorithm 3.1.
- 2: Remove all interior knots in the knot vector one time:

$$\begin{aligned} \Xi_\ell &= \{\underbrace{\zeta_0, \dots, \zeta_0}_{r_0 \text{ times}}, \dots, \underbrace{\zeta_{\mathcal{N}_e}, \dots, \zeta_{\mathcal{N}_e}}_{r_{\mathcal{N}_e} \text{ times}}\} \\ &\rightarrow \Xi_{\ell+1} = \{\underbrace{\zeta_0, \dots, \zeta_0}_{r_0+1 \text{ times}}, \underbrace{\zeta_1, \dots, \zeta_1}_{r_1 \text{ times}}, \dots, \underbrace{\zeta_{\mathcal{N}_e-1}, \dots, \zeta_{\mathcal{N}_e-1}}_{r_{\mathcal{N}_e-1} \text{ times}}, \underbrace{\zeta_{\mathcal{N}_e}, \dots, \zeta_{\mathcal{N}_e}}_{r_{\mathcal{N}_e}+1 \text{ times}}\} \end{aligned}$$

Compute the corresponding control points and weights with the knot removal algorithm.

functions are $q + 1 - (r_k + 1) = q - r_k$ times continuously differentiable at ζ_k . Removing all interior knots one time yields $(q - r_k + 1)$ regularity at the interior node ζ_k .

The dimension of the resulting ansatz space is given by

$$\dim R(\mathcal{T}_{\ell+1}, \mathbf{h}_{\ell+1}, q_{\ell+1}, \mathbf{k}_{\ell+1}) = \dim R(\mathcal{T}_\ell, \mathbf{h}_\ell, q_\ell, \mathbf{k}_\ell) + 1.$$

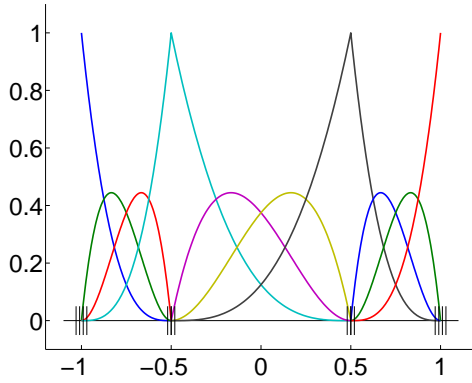
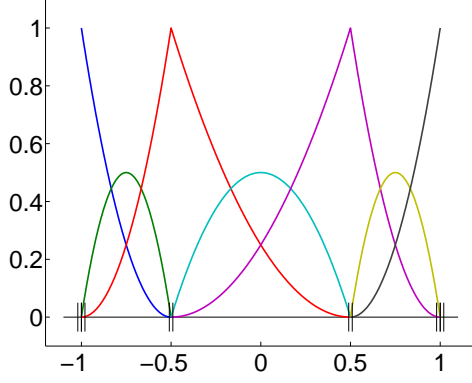
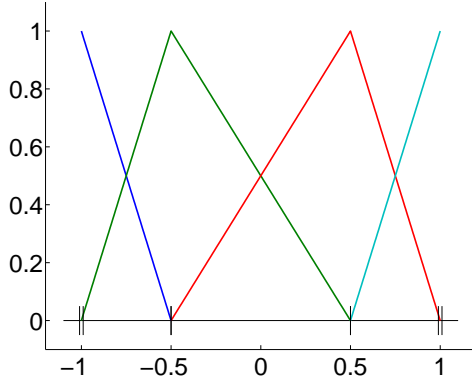
A comparison of the basis functions obtained by uniform p - and k -refinements is given in Figure 3.4.

Geometric hp -refinement. The geometrically graded hp -meshes, which are introduced in Section 1.4, are created using the knot insertion algorithm. We consider the unit circle $\Gamma := \{x \in \mathbb{R}^2 : \|x\|_2 = 1\}$, the procedure for the L-shaped domain is similar.

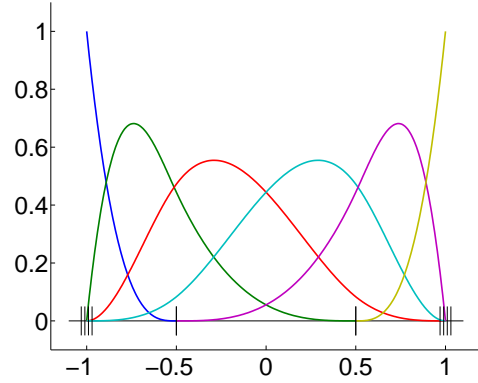
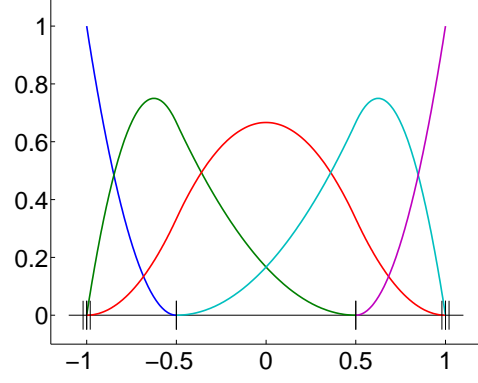
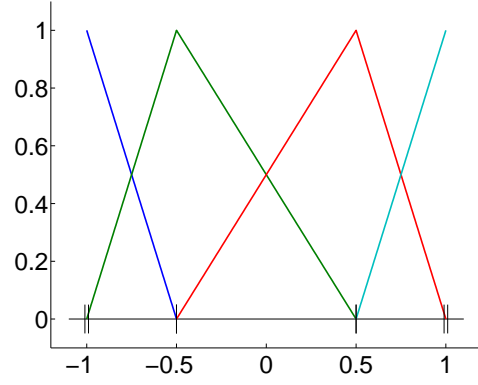
For $m \in \mathbb{N}$ and $\vartheta \in (0, 1)$, we define a geometrically graded mesh on the parameter domain by $\Xi = \{-1, -1, -1, -x_m, \dots, -x_1, -0.5, -0.5, 0, 0, 0.5, 0.5, x_1, \dots, x_m, 1, 1, 1\}$ with $x_k = 1 - \frac{\vartheta^k}{2}$, $k = 1, \dots, m$. The control points and weights of the parametrization are computed by inserting the knots $\pm x_k$, $k = 1, \dots, m$, into the initial knot vector Ξ , which is defined in Example 3.1.3. Due to the symmetry of the weights in the initial mesh, we obtain $h_i/h_j = \vartheta$ for all neighboring elements T_i and T_j , where T_i is closer to the singularity.

In the end of this section, we proof that the different mesh refinements introduced above produce a nested sequence of ansatz spaces. This property is a necessary assumption for the a priori estimates stated in Section 1.6.2. While this is clear for the polynomial ansatz spaces, for general rational ansatz spaces this assumption is not satisfied.

3. High-Order NURBS-Based Boundary Element Methods



(a) Basis functions for uniform p -refinement.



(b) Basis functions for uniform k -refinement.

Figure 3.4.: Comparison of uniform p - and k -refinements. The initial knot vector and the weights are given by $\Xi = \{-1, -1, -0.5, 0.5, 1, 1\}$ and $\omega_1 = \omega_2 = \omega_3 = \omega_4 = 1$.

Lemma 3.3.2. *Let $R_\ell(\mathcal{T}_\ell, \mathbf{h}_\ell, q_\ell, \mathbf{k}_\ell)$, $\ell \in \mathbb{N}$, be the sequence of NURBS ansatz spaces as defined in Definition 3.2.3 which are created by uniform h - or p -refinement. Then, there holds $R_\ell(\mathcal{T}_\ell, \mathbf{h}_\ell, q_\ell, \mathbf{k}_\ell) \subset R_{\ell+1}(\mathcal{T}_{\ell+1}, \mathbf{h}_{\ell+1}, q_{\ell+1}, \mathbf{k}_{\ell+1})$.*

Proof. Due to the definition of the NURBS basis functions we obtain for $f \in R_\ell(\mathcal{T}_\ell, \mathbf{h}_\ell, q_\ell, \mathbf{k}_\ell)$

$$f(t) = \frac{1}{\omega_\ell(t)} \tilde{f}(t)$$

with the weight function ω_ℓ and $\tilde{f} \in S_\ell(\mathcal{T}_\ell, \mathbf{h}_\ell, q_\ell, \mathbf{k}_\ell)$. For all introduced mesh refinements the weights are computed such that $\omega_\ell = \omega_{\ell+1}$. With $S_\ell(\mathcal{T}_\ell, \mathbf{h}_\ell, q_\ell, \mathbf{k}_\ell) \subset S_{\ell+1}(\mathcal{T}_{\ell+1}, \mathbf{h}_{\ell+1}, q_{\ell+1}, \mathbf{k}_{\ell+1})$ we obtain that $f \in R_{\ell+1}(\mathcal{T}_{\ell+1}, \mathbf{h}_{\ell+1}, q_{\ell+1}, \mathbf{k}_{\ell+1})$. \square

Remark 3.3.3. The sequence of ansatz spaces produced by uniform k -refinement is not nested. Hence, Theorem 1.6.3 cannot be applied and convergence and quasi-optimality for k -refinement is still an open question.

4. Numerical Integration for High-Order NURBS-Based BEM

The efficient evaluation of the arising integrals in NURBS-based boundary element methods is numerically challenging. First, the boundary is parametrized by arbitrary NURBS curves, therefore the use of analytic formulae for the numerical integration is not possible. Hence, the arising integrals have to be evaluated approximately, which induces a consistency error. Second, besides regular integrals also singular and nearly singular integrals have to be evaluated accurately for high-order basis functions. Theorem 1.6.7 states that the Galerkin error decays exponentially with respect to the degrees of freedom on geometrically graded meshes. The numerical results in Chapter 5 show a similar decay for collocation methods. In order to obtain algorithms for the numerical integration with algebraic complexity, that preserve the exponential convergence of the collocation and the Galerkin errors, the quadrature error has to decay exponentially for all integrals, too.

This chapter is organized as follows. The first section gives an overview on existing approaches for the numerical evaluation of integrals arising in BEM.

In the second section, we discuss the evaluation of the boundary integral operators, that are introduced in Section 1.2. We derive evaluation schemes that can be applied to the evaluation of all boundary integral operators of Laplace, Lamé, and Helmholtz problems for general NURBS boundary parametrizations and for all discrete ansatz spaces introduced in Section 3.2. In the case of NURBS-enhanced methods we also present algorithms that are efficient for high degrees of the polynomial basis functions. For all algorithms, we proof an exponential decay of the approximation errors with respect to the evaluation order. In particular, we show that the convergence rates are optimal in the sense that they only depend on the smoothness of the boundary parametrization but not on the kernel function and the evaluation point. While the error estimates presented are in general h -asymptotic estimates, for NURBS-enhanced methods, we additionally give estimates that are explicit in the polynomial degree p of the basis functions and can be used for uniform p - and hp - methods.

We discuss the assembly of the Galerkin matrices that are introduced in Section 1.6.1 in the last part of this chapter. Therefore, we present algorithms for the evaluation of the arising double

4. Numerical Integration for High-Order NURBS-Based BEM

integrals that converge exponentially with respect to the evaluation order for general boundary parametrizations and all considered ansatz spaces. For the regularization of the singular integrands coordinate transforms are introduced. The remaining logarithmic singularity is evaluated with the Gauss-Log quadrature that is introduced in Section 2.2. Further, we give error estimates for the evaluation of all integrals that are explicit in the mesh size h , and for NURBS-enhanced methods also explicit in the polynomial degree p . In the end of this section, we derive a relationship of the absolute evaluation error and the induced consistency error. Combining this relationship and the error estimates, we are able to give a priori estimates for the evaluation order for all integral operators, such that the consistency error does not deteriorate the convergence rates of the Galerkin method.

4.1. Existing Approaches for the Numerical Integration in BEM

For the evaluation of integrals arising in BEM, there are three different types of approaches: **analytic** approaches for the exact integration, **numerical** approaches that use quadrature rules for the approximate integration, and **semi-analytic** approaches. In the following we give an overview on the different approaches. This overview is by no means complete.

Analytic formulae are often used for the evaluation of singular and nearly singular integrals, since the integrals can be evaluated exactly without any further regularization. However, in order to be able to derive analytic formulae, knowledge on the kernel function and a simple boundary parametrization is required, which limits the field of applications. For polygonal boundaries and polynomial basis functions, analytic approaches for the numerical integration are presented in e.g. [RS07, Ban13, Mai96, Mai97, ST99]. While in [RS07] analytic formulae for the evaluation of the Galerkin entries arising in lowest order BEM for Laplace and Lamé problems are given, the works of Maischak and Bantle focus on high-order BEM. Therefore, the evaluation of the arising integrals is reduced to the evaluation of some elementary integrals, for which analytic formulae can be derived. In [Ban13], the evaluation of the boundary integral operators and the assembly of the Galerkin matrices for the Laplace problem are reduced to the evaluation of the modified associated Legendre functions of second kind and their antiderivatives. Further, the efficient and stable evaluation for high orders with recurrence relations is discussed. This approach can also be extended to Lamé and Helmholtz problems. In [Mai96, Mai97], a similar approach for all three partial differential operators is presented for two- and three-dimensional BEM. As compared to the approach of [Ban13] the elementary integrals are defined via monomials instead of Legendre polynomials. Due to the arising cancellation effects multiple precision libraries are used for the evaluation.

4.1. Existing Approaches for the Numerical Integration in BEM

The idea of **semi-analytic approaches** is to extend the field of application of the analytic formulae by interpolation of the kernel functions and approximation of the curved boundaries by affine elements. The arising singular and nearly singular integrals are then evaluated analytically or with a combination of analytic formulae and quadrature rules. In [Sau92, HS93, SIS98, NWW⁺05, GG90, GKR⁺92], semi-analytic approaches for the evaluation of the Galerkin entries are presented for piecewise smooth boundaries and general kernel functions. Besides the expansion of the kernel and the interpolation of the curved boundary elements, coordinate transformations are introduced for the regularization of the singularities. The resulting integrals are then evaluated semi-analytically. However, for high-order kernel expansions and basis functions these methods become inefficient and cancellation effects arise in the analytic evaluation of the integrals [ST99].

For the **numerical integration** with Gauss quadrature rules, the absolute quadrature error decays exponentially with respect to the quadrature order for analytic integrands, see Theorems 2.2.11 and 2.2.15. Furthermore, quadrature rules can be applied to all regular integrands without any additional knowledge on the kernel function and the boundary parametrization and have hence a wide field of application. However, it is proven in [LR84] that the quadrature error only decays algebraically for weakly singular integrals, for strongly singular integrals the quadrature rules do not converge at all. For the efficient numerical evaluation of singular integrals, there are basically three different methods: the evaluation with adapted quadrature rules, the application of composite rules, and the regularization of the integrand with coordinate transformations.

Adapted quadrature rules are special quadrature rules, where the weak singularity of the integrand is considered to be the weight function of the quadrature rule and an exponential decay of the error is achieved. If the quadrature rules can be calculated a priori, the application of adapted quadrature rules provides an efficient possibility for the evaluation of weakly singular integrals. In particular, for the logarithmic singularities, which typically arises in twodimensional boundary element methods, the Gauss-Log quadrature rules, which are introduced in Section 2.2, can be used.

The idea of composite rules, which are presented in [Sch94], is to introduce a mesh, that is geometrically graded towards the singularity. On each interval of the mesh a Gauss-Legendre quadrature of variable order is applied, i.e. the lowest order is chosen on the interval closest to the singularity and the order increases linearly for increasing distance to the singularity. In [Sch94] an exponential convergence is proven for a wide class of singular integrands. However, the factor of the exponential convergence significantly depends on the grading parameters and optimal parameters that yield a fast exponential convergence cannot be determined for general integrands.

By applying appropriate coordinate transformations, singular integrands are regularized, since

4. Numerical Integration for High-Order NURBS-Based BEM

the singularity is cancelled out by the Jacobian determinant of the transformation. In [Duf82], a coordinate transformation, called Duffy transformation, for the integration over a triangle is given, which regularizes integrands containing algebraic corner singularities. Amongst others, this coordinate transformation is used in [SaSch97], where quadrature rules for the three-dimensional Galerkin BEM with general kernel functions and general piecewise smooth boundary parametrizations are presented. The Duffy transformation and a subsequent composite rule are applied to the integrand and exponential convergence for a general class of kernel functions is proven. These quadrature rules are widely used in three-dimensional boundary element implementations, see e.g. [HK12, ŠBA⁺15, MMR⁺14].

While the singular case can be treated efficiently with quadrature rules, the nearly singular case is numerically challenging, since the application of quadrature rules yields a very slow exponential, almost algebraic convergence. In two-dimensional BEM, the nearly singular integrands are of the type

$$f(x) \log(x^2 + c^2) \quad \text{and} \quad \frac{f(x)}{x^2 + c^2} \quad (4.1)$$

with $c \ll 1$. Constructing adapted quadrature rules is inefficient, since the nodes and weights depend on c and cannot be pre-computed. For the application of composite rules, which also yield exponential convergence depending on the grading parameters, c has to be known explicitly. In the setting of NURBS-based BEM this is equivalent to computing the point on the NURBS curve which is closest to the evaluation point by the point inversion algorithm. This is generally inefficient.

In [SIS198, Tel86, TM74] different types of coordinate transforms for the regularization of integrands of type (4.1) are given. Besides the power and the Telles ([Tel86]) transformation, which are polynomial transformations, also trigonometric coordinates transformations (tan-transformation, [SIS198]) and double exponential formulae (tanh-sinh-transformations [TM74]) are presented. While the near singularity is not cancelled out, the domain of analyticity is increased by the coordinate transforms, which yields an acceleration of the convergence speed if a Gauss-Legendre quadrature is applied. This is depicted for the power transformation $g(t) = t^2$ in Figure 4.1, where it is shown that the ellipses \mathcal{E}_ρ contained in the domain of analyticity of the transformed integrand (blue) are significantly larger than the ellipses contained in the domain of analyticity of the original integrand. A comparison of all mentioned coordinate transformations is illustrated in Figure 4.2, where a significant acceleration of the convergence speed can be observed. However, the application of coordinate transforms has two drawbacks. First, the coordinate transformations require the knowledge of c , which affects the efficiency. Second, the convergence speed depends on c , which still yields a slow exponential convergence for very small c .

4.1. Existing Approaches for the Numerical Integration in BEM

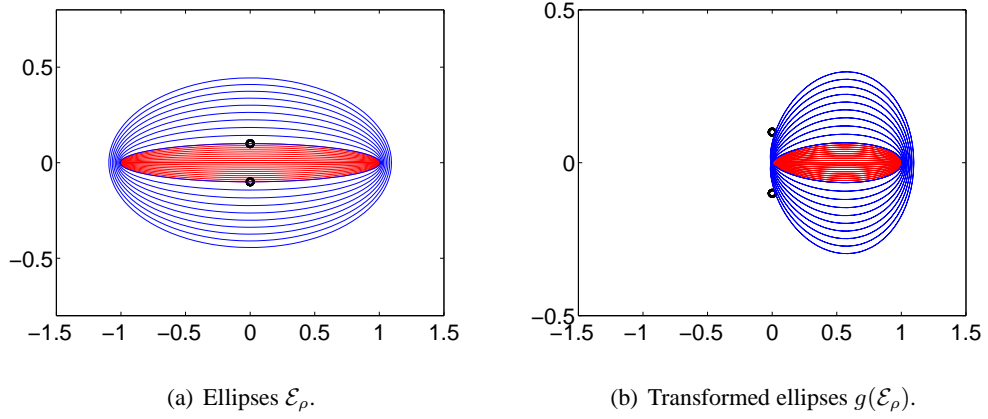


Figure 4.1.: Ellipses \mathcal{E}_ρ contained in the domain of analyticity of the original integrand (red), and of the transformed integrand (blue) for the power transformation $g(t) = t^2$ and $c = 0.1$. The black dots denote the singularities of the integrand.

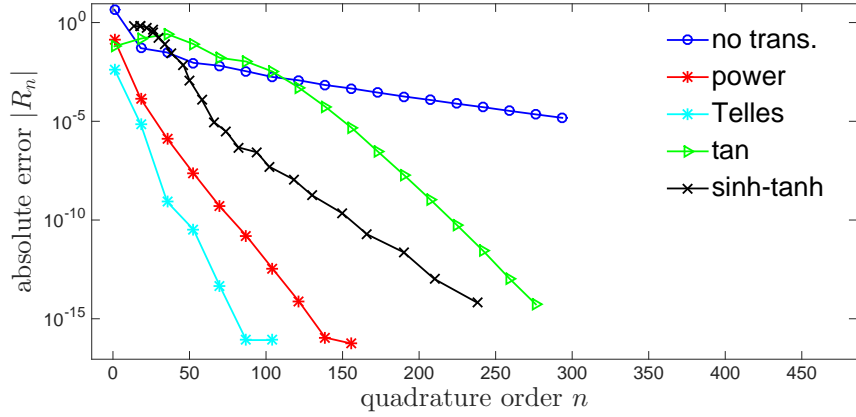


Figure 4.2.: Absolute error $|R_n|$ over quadrature order n for different coordinate transformation applied to the logarithmic integrand of type (4.1) with $c = 0.01$ and logarithmically scaled y -axis.

For the evaluation of the boundary integral operators, we derive a semi-analytic approach, where the singularities and the near singularities are extracted of the integrand and integrated analytically. While the above mentioned semi-analytic approaches become unstable for high order expansions, our algorithm is numerically stable even for high interpolation orders. This is achieved by exploiting the general structure of NURBS curves, which allows to reduce the evaluation of the boundary integral operators to the evaluation of elementary integrals discussed in [Ban13]. These integrals can be evaluated in an efficient and stable way for high orders.

For the assembly of the Galerkin matrices, we introduce coordinate transformations for the regularization of the singular integrands, which are similar to the coordinate transformations pre-

4. Numerical Integration for High-Order NURBS-Based BEM

sented in [SaSch97] for three-dimensional BEM. However, instead of using composite rules for the integration of the remaining singular integrals, we evaluate the integrals containing a logarithmic singularity with a Gauss-Log quadrature. This yields a fast exponential convergence for these integrals and polynomial integrands are integrated exactly.

4.2. Evaluation of Boundary Integral Operators

Apart from the assembly of the collocation matrices \mathbf{V} , \mathbf{K} , \mathbf{A} , and \mathbf{W} introduced in Section 1.5.1, the potentials $\tilde{\mathcal{V}}$, $\tilde{\mathcal{K}}$ and their co-normal derivatives have to be evaluated for the computation of the solution and its co-normal derivative within the domain Ω . Hence, we discuss the evaluation of the integral operators for all $x \in \mathbb{R}^2$, which covers both cases.

Depending on the ansatz space, we have basis functions with local support, i.e. $\tilde{P}_k^{(i)}$ and $\tilde{N}_k^{(i)}$, and basis functions whose support contains more than one element, i.e. $\tilde{\mathcal{H}}_k$ and $\tilde{\mathcal{R}}_k$. Since the basis function with non-local support have reduced regularity at the element edges, see Lemma 3.1.4 (ii), we split the integration at all element edges and add up the local contributions. For $T_i \in \mathcal{T}$ and $x \in \mathbb{R}^2$, we investigate the evaluation of

$$A_k^{(i)}(x) := \int_{T_i} \tilde{K}(x-y) \Phi_k^{(i)}(y) ds_y, \quad k = 0, \dots, p_i. \quad (4.2)$$

Here, we denote by $\Phi_k^{(i)}$ the non-vanishing basis functions on T_i of one of the discrete spaces introduced in Definitions 3.2.3 and 3.2.5, and by $\tilde{K}(x-y)$ the kernel function of the integral operator. We assume the following representation of the kernel

$$\tilde{K}(x-y) := g_{-1}(x-y) + g_0(x-y) \log |x-y| + \sum_{\ell=1}^N g_\ell(x-y) |x-y|^{-2\ell} \quad (4.3)$$

with functions g_ℓ , $\ell \geq -1$, that are analytic on \mathbb{C} .

Remark 4.2.1. The fundamental solutions of Laplace, Lamé, and Helmholtz equations and their co-normal derivatives are of the form (4.3). For an explicit representation of all kernel functions and the corresponding representations of the functions g_ℓ we refer to Appendix A.

Plugging in the local parametrization of T_i we get with $K(x, t) := \tilde{K}(x - \gamma_i(t))$

$$A_k^{(i)}(x) := \int_{-1}^1 K(x, t) \Phi_k(t) |\dot{\gamma}_i(t)| dt.$$

Since the regularity of the kernel function K has a big impact on the numerical integration, we first analyze K , before we go into detail on the evaluation of $A_k^{(i)}(x)$.

The representation (4.3) of K implies that K is weakly singular and singular if $x \in T_i$, while K is regular for $x \notin T_i$. However, also in the regular case the domain of analyticity of K significantly depends on the parametrization γ_i and the mutual location of x and T_i , which is proven in the subsequent lemma.

Lemma 4.2.2. *Let $x \notin T_i$, $D := \text{dist}\{T_i, x\} > 0$ and \mathcal{E}_{ρ_i} as defined in Definition 3.2.9. Then, the kernel function $K(x, t)$ is analytically extendable on $\mathcal{E}_{\rho_i} \cap \mathcal{E}_{\rho_1}$ with real semi-axis $a_1 = 1 + c \frac{D}{h_i}$. The constant $c > 0$ is independent of h_i and D , but still depends on the parametrization γ_i .*

Proof. By assumption, the functions $g_\ell(z)$, $\ell = -1, \dots, N$, in representation (4.3) are analytic for $z \in \mathbb{C}$ and γ_i is analytically extendable on \mathcal{E}_{ρ_i} . Hence, $g_\ell(x - \gamma_i(t))$ is analytic for $t \in \mathcal{E}_{\rho_i}$. Let $f(t) := (x_1 - \gamma_{i,1}(t))^2 + (x_2 - \gamma_{i,2}(t))^2$. Since f is analytic on \mathcal{E}_{ρ_i} and $f(t) = |x - \gamma_i(t)|^2$ on $[-1, 1]$, f is the unique analytic extension of $|x - \gamma_i(t)|^2$ on \mathcal{E}_{ρ_i} . Hence, $\log(f)$ and $f^{-\ell}$ are analytic on $\mathcal{E}_{\rho_1} \cap \mathcal{E}_{\rho_i}$, where $\rho_1 > 1$ is chosen such that $f(t) > 0$ for all $t \in \mathcal{E}_{\rho_1}$. Since $f(t) \geq D$ for $t \in [-1, 1]$, the real semi-axis a_1 of \mathcal{E}_{ρ_1} is given by

$$a_1 = 1 + \frac{D}{\max_{z \in \mathcal{E}_{\tilde{\rho}}} |\dot{\gamma}_i(z)|}$$

with $1 < \rho_1 \leq \tilde{\rho} < \rho_i$. With Lemma 3.2.12 we have $\max_{z \in \mathcal{E}_{\tilde{\rho}}} |\dot{\gamma}_i(z)| \leq \tilde{c} h_i$ and conclude the proof. \square

Lemma 4.2.2 motivates, that besides the singular case with $x \in T_i$, we also differentiate the near-field case, in which the domain of analyticity of the kernel is spoiled by x ($\rho_1 < \rho_i$), and the far-field case, in which the size of the domain of analyticity of the kernel does not depend on x ($\rho_1 \geq \rho_i$).

The proof of Lemma 4.2.2 shows that the estimate is a worst case estimate and generally pessimistic. Therefore, we are interested in the computation of the maximum ellipse contained in the domain of analyticity. Since the domain of analyticity of the kernel is limited by the zeros of the analytic function $|x - \gamma_i(t)|^2$, we state the following result concerning the position of these zeros.

Lemma 4.2.3. *Let $T_i \in \mathcal{T}$, γ_i be its parametrization and $x \in \mathbb{R}^2 \setminus T_i$. Then, there exists at most one pair of complex conjugate numbers $z, \bar{z} \in \mathcal{E}_{\rho_i}$ with $|x - \gamma_i(\bar{z})|^2 = |x - \gamma_i(z)|^2 = 0$. Further, the zeros z and \bar{z} have multiplicity one if they exist. (If z is real, $z = \bar{z}$ and we have one zero with multiplicity two).*

Proof. It is proven in Lemma 4.2.2 that $f(z) = |x - \gamma_i(z)|^2$ is analytically extendable to \mathcal{E}_{ρ_i} . By analogy to Remark 3.2.11 we write

$$|x - \gamma_i(z)|^2 = [(x_1 - \gamma_{i,1}(z)) + i(x_2 - \gamma_{i,2}(z))] [(x_1 - \gamma_{i,1}(z)) - i(x_2 - \gamma_{i,2}(z))].$$

Since $x \in \mathbb{R}^2$ and γ_i has real coefficients, we have the following property: If z_1 is a zero of $[(x_1 - \gamma_{i,1}(z)) + i(x_2 - \gamma_{i,2}(z))]$, then \bar{z}_1 is a zero of $[(x_1 - \gamma_{i,1}(z)) - i(x_2 - \gamma_{i,2}(z))]$ and vice versa. Therefore, it is sufficient to show that $g(z) := [(x_1 - \gamma_{i,1}(z)) + i(x_2 - \gamma_{i,2}(z))]$ has

4. Numerical Integration for High-Order NURBS-Based BEM

at most one zero in \mathcal{E}_{ρ_i} .

There holds

$$g'(z) = -\dot{\gamma}_{i,1}(z) - i \dot{\gamma}_{i,2}(z).$$

Due to Remark 3.2.11 $g'(z) \neq 0$ on \mathcal{E}_{ρ_i} and with [Jae99, Section 3.4] g is locally injective on \mathcal{E}_{ρ_i} . This implies that there exists at most one zero, i.e. $0 = g(z_1) = g(z_2) \Rightarrow z_1 = z_2$. Since g' does not vanish on \mathcal{E}_{ρ_i} , the zero has multiplicity one if it exists. \square

With the result of the previous lemmas we now introduce the following classification for the evaluation point x .

Definition 4.2.4. For $x \in \mathbb{R}^2$, let $z_j \in \mathbb{C}$, $j = 1, \dots, q_i$, denote the zeros of $|x - \dot{\gamma}_i(z)|^2$. We define

- (i) the set of all far-field points M_f by

$$M_f := \{x \in \mathbb{R}^2 : z_j \notin \mathcal{E}_{\rho_i}, j = 1, \dots, q_i\},$$

- (ii) the set of all near-field points M_n by

$$M_n := \{x \in \mathbb{R}^2 : \exists z_j \in \mathcal{E}_{\rho_i} \setminus [-1, 1]\},$$

- (iii) and the set of all singular points M_s by

$$M_s := \{x \in \mathbb{R}^2 : \exists z_j \in [-1, 1]\} = T_i.$$

Remark 4.2.5. (i) In order to classify the evaluation points x , the zeros z_j of $|x - \gamma_i(z)|^2$ have to be computed explicitly. As it is shown in the proof of Lemma 4.2.3, it is sufficient to compute the zeros of the complex polynomial

$$g(z) := \omega_i(z) [(x_1 - \gamma_{i,1}(z)) + i(x_2 - \gamma_{i,2}(z))]$$

with the same degree q_i as the parametrization. Here, we denote by ω_i the denominator of γ_i . Thus, there are closed formulae for $q_i \leq 4$, which are the most common cases, and for higher order parametrizations, the zeros can be calculated numerically, e.g. via an eigenvalue problem.

- (ii) In the standard implementation, the dependency of the regularity of the kernel on the parametrization γ_i is ignored for the classification of far-field points. The criterion, which is used in e.g. [NWW⁺05, ST99], is the ratio of the distance $D > 0$ and the arc length h_i , i.e.

$$x \in M_f, \text{ if } D > \varepsilon h_i \text{ for a given tolerance } \varepsilon > 0. \quad (4.4)$$

The representation of a_1 in Lemma 4.2.2 implies, that this criterion works well for large distances D , since in this case the size of the domain of analyticity of the kernel is dominated by D . However, for small distances, the regularity is mainly determined by the derivative of the parametrization, which may be non-smooth for general NURBS curves. Hence, the dependency on the parametrization cannot be ignored for NURBS curves, if reliable statements concerning the regularity of the kernel are needed. This is also exemplified in Figure 4.3, which shows the domain of analyticity and the set of all far-field points for the quarter circle as defined in Example 3.1.3.

- (iii) Comparing the complexity of computing the distance D with the complexity of computing the zeros z_j , we obtain the following result.

For the computation of the distance D , the parameter $t_0 := \operatorname{argmin}_{t \in [-1,1]} |x - \gamma_i(t)|$ has to be computed explicitly. This is equivalent to the computation of the roots of a polynomial with degree $3q_i - 1$, see e.g. [CZS⁺07]. Hence, the computation of the zeros z_j according to (i) is more efficient. Furthermore, we will see in the subsequent sections that in the near-field and the singular case the additional information of the root $z_j \in \mathcal{E}_{\rho_i}$ is not only used for the classification of the evaluation points, but also for the regularization of the integrals.

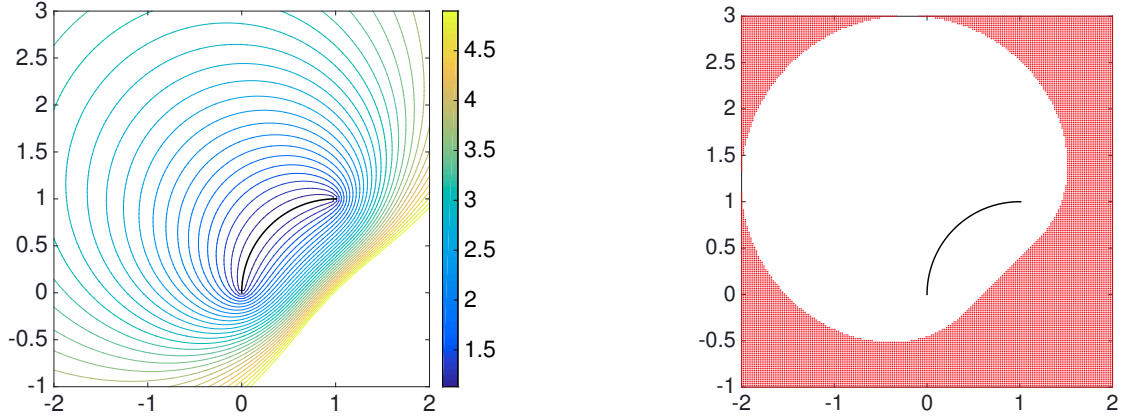


Figure 4.3.: Semi-axis sum of the largest ellipse contained in the domain of analyticity of the kernel (left) and set M_f of all far-field points (right) for the quarter circle T_i , which is parametrized by the NURBS curve defined in Example 3.1.3.

Algorithm 4.1 shows the classification of the evaluation points x_ℓ , $\ell = 1, \dots, n$. We additionally introduce a tolerance $\varepsilon \in (0, 1]$ for the classification, as for parametrizations γ_i containing a pole on $\partial\mathcal{E}_{\rho_i}$ there exist many evaluation points for which the zeros z_j are located closely to this pole. For these points the far-field algorithm with almost optimal convergence is more efficient

4. Numerical Integration for High-Order NURBS-Based BEM

as the near-field evaluation with optimal convergence. Choosing $\varepsilon < 1$ classifies these points as far-field points, specifically setting $\varepsilon = 0$ in Algorithm 4.1 corresponds to the classification of all points as far-field points. Having computed the zeros z_j of $|x_\ell - \gamma_i(t)|^2$, we determine the real semi-axis a of the maximum ellipse that does not contain any zero z_j . For $a = 1$ there exists a zero $z_j \in [-1, 1]$ and we are hence in the singular case, for $1 < a < \varepsilon \left(\frac{1+\rho_i^2}{2\rho_i} - 1 \right) + 1$ we are in the near-field case, since $\frac{1+\rho_i^2}{2\rho_i}$ corresponds to the real semi-axis of \mathcal{E}_{ρ_i} . In the remainder of this section we discuss the evaluation of the integrals $A_k^{(i)}(x)$ for all three cases, separately.

Algorithm 4.1 Algorithm for the Classification of the Evaluation Points

INPUT: Evaluation points $x_\ell, \ell = 1, \dots, n$, semi-axis sum $\rho_i > 1$ of γ_i , and tolerance $\varepsilon \in (0, 1]$.

OUTPUT: The sets M_f, M_n and M_s of far-field, near-field and singular points.

```

1: for  $\ell$  from 1 to n do
2:   Compute the zeros  $z_1, \dots, z_{q_i}$  of  $|x_\ell - \gamma_i(t)|^2$  according to Remark 4.2.5 (i)
3:   Compute  $a = \min_{j=1, \dots, q_i} \frac{|z_j+1|+|z_j-1|}{2}$ 
4:   if  $a = 1$  then
5:      $x_\ell \in M_s$ .
6:   end if
7:   if  $1 < a < \varepsilon \left( \frac{1+\rho_i^2}{2\rho_i} - 1 \right) + 1$  then
8:      $x_\ell \in M_n$ .
9:   else
10:     $x_\ell \in M_f$ .
11:   end if
12: end for

```

4.2.1. Far-field Case

We assume that the kernel function is analytic on \mathcal{E}_{ρ_i} . If $\varepsilon < 1$ is chosen for the classification, ρ_i has to be substituted by $\rho_{i,\varepsilon} := \varepsilon(a_i - 1) + 1 + \sqrt{\varepsilon^2(a_i - 1)^2 + 2\varepsilon(a_i - 1)}$, where a_i denotes the real semi-axis of \mathcal{E}_{ρ_i} . For the evaluation of $A_k^{(i)}(x)$ with the Gauss-Legendre quadrature, an exponential convergence of the absolute quadrature error is proven in the subsequent lemma.

Lemma 4.2.6. *Let $T_i \in \mathcal{T}$, γ_i denote its parametrization and $x \in M_f$. The absolute error $|R_n(x)|$ for the evaluation of $A_k^{(i)}(x)$ with a Gauss-Legendre quadrature rule of order $n \in \mathbb{N}$ is bounded by*

$$|R_n(x)| \leq c h_i \rho^{-2n-1}, \quad 1 < \rho < \rho_i, \quad (4.5)$$

4.2. Evaluation of Boundary Integral Operators

with a constant $c > 0$ independent of h_i , but still depending on γ_i and the basis functions Φ_k .

Proof. Since $x \in M_f$, the kernel and hence the integrand is analytic on \mathcal{E}_{ρ_i} and we can apply Theorem 2.2.11. With Lemma 3.2.12, there holds for $1 < \rho < \rho_i$

$$\max_{z \in \mathcal{E}_\rho} |K(\gamma_i(t), x) |\dot{\gamma}_i(z)| | \leq c_1 h_i \quad (4.6)$$

with $c_1 > 0$ independent of h_i . Since the kernel function and the basis functions are bounded, we obtain (4.5). \square

Remark 4.2.7. For the Legendre polynomials, $\Phi_k := P_k$, and the Lobatto shape functions, $\Phi_k := N_k$, we apply the estimates given in Lemma 2.1.9 (vi) and 2.1.11 (iv) and obtain

$$|R_n(x)| \leq \tilde{c} h_i \rho^{-2n+k-1}, \quad 1 < \rho < \rho_i.$$

Here, the constant \tilde{c} is also independent of the polynomial degree k .

The Gauss-Legendre quadrature yields a fast exponential convergence of the quadrature error for the general representation of the kernel (4.3) and all types of basis functions. This allows the easy implementation in the far-field case. However, for both NURBS-enhanced and isogeometric methods we propose two alternative approaches with less complexity as compared to the Gauss-Legendre quadrature. Both approaches are based on the interpolation of the kernel and exploit the properties of the basis functions.

NURBS-enhanced methods. For simplicity, we restrict to consider the case $\Phi_k = P_k$, corresponding results for the Lobatto shape functions are obtained in a similar way. Let $I_n(x, t)$ denote the n -th degree Legendre expansion of $K(x, t) |\dot{\gamma}_i(t)|$, i.e.

$$K(x, t) |\dot{\gamma}_i(t)| \approx I_n(x, t) := \sum_{\mu=0}^n \alpha_\mu(x) P_\mu(t). \quad (4.7)$$

Plugging in the interpolation polynomial we obtain for all $k = 0, \dots, p_i$

$$\begin{aligned} \int_{-1}^1 K(x, t) |\dot{\gamma}_i(t)| P_k(t) dt &\approx \sum_{\mu=0}^n \alpha_\mu(x) \int_{-1}^1 P_\mu(t) P_k(t) dt \\ &= \begin{cases} \frac{2}{2k+1} \alpha_k(x), & n \geq k \\ 0, & \text{otherwise.} \end{cases} \end{aligned}$$

Here, we used the orthogonality of the Legendre polynomials with respect to the L^2 scalar product in the last step. Computing the coefficients $\alpha_\mu(x)$, $\mu = 0, \dots, n$, we can evaluate all integrals $\{A_k^{(i)}(x)\}_{k=0, \dots, p_i}$, simultaneously. For directly computing the interpolation polynomial in the Legendre representation, $\mathcal{O}(n^2)$ operations are needed. Therefore, we follow the algorithm

4. Numerical Integration for High-Order NURBS-Based BEM

given in [AR91], which only has a complexity of $\mathcal{O}(n \log n)$. A Pseudo-code is given in Algorithm 4.2.

The coefficients $\alpha_\mu := \alpha_\mu(x)$, $\mu = 0, \dots, n$, are computed in three steps. First, we evaluate the function f at the zeros of the $(n+1)$ -th Chebyshev polynomial and obtain the vector $\mathbf{f} \in \mathbb{R}^{n+1}$. Second, we apply the discrete cosine transform to \mathbf{f} , see [RY90], and obtain the coefficients $\tilde{\alpha}_\mu$ with respect to the Chebyshev basis. In the third step, we apply a basis transformation, which corresponds to a matrix-vector multiplication. The exact coefficient matrix \mathbf{M} is given by

$$M_{ij} := \begin{cases} 1, & \text{if } i = j = 0 \\ \frac{\sqrt{\pi}}{2\Lambda(i)}, & \text{if } 0 < i = j < n \\ \frac{-j(i+1/2)}{(j+i+1)(j-i)} \Lambda\left(\frac{j-i-2}{2}\right) \Lambda\left(\frac{j+i+1}{2}\right) & \text{if } 0 \leq i < j < n \text{ and } i+j \text{ even} \\ 0, & \text{otherwise} \end{cases} \quad (4.8)$$

with

$$\Lambda(z) := \frac{\Gamma(z + 1/2)}{\Gamma(z + 1)}.$$

A proof can be found in [AR91, Section 2.3]. Further, the authors present an algorithm of linear complexity that calculates the matrix-vector product by approximating the coefficient matrix up to a given tolerance $\varepsilon > 0$ by an \mathcal{H}^2 -matrix.

Algorithm 4.2 Algorithm for the Computation of the Legendre Interpolation

INPUT: Function f , order n .

OUTPUT: Vector $\mathbf{a} \in \mathbb{R}^{n+1}$ containing the coefficients α_μ , $\mu = 0, \dots, n$.

- 1: Evaluate f at $t_\mu = \cos\left(\frac{(\mu+1/2)\pi}{n+1}\right)$, $\mu = 0, \dots, n$
 $\mathbf{f} \leftarrow f(\mathbf{t})$.
 - 2: Apply discrete cosine transformation to \mathbf{f}
 $\tilde{\mathbf{a}} \leftarrow \text{dct}(\mathbf{f})$.
 - 3: Transform the coefficients to Legendre basis
 $\mathbf{a} \leftarrow \mathbf{M}\tilde{\mathbf{a}}$.
-

Remark 4.2.8. With the algorithm presented in [AR91] we have an overall complexity of $\mathcal{O}(n \log n)$. However, the linear complexity of the \mathcal{H}^2 -matrix approach for the basis transformation is dominated by the constant and is only profitable for high interpolation orders n .

The next lemma gives an upper bound for the absolute error arising in the evaluation $A_k^{(i)}(x)$ by interpolation.

Lemma 4.2.9. *Let $n \in \mathbb{N}$, $x \in M_f$, $I_n(x, t)$ as defined in (4.7) and*

$$|R_n(x)| := \left| A_k^{(i)}(x) - \int_{-1}^1 I_n(x, t) P_k(t) dt \right|$$

denote the absolute error for the evaluation of $A_k^{(i)}(x)$. Then, there exists $c > 0$ independent of h_i such that

$$|R_n(x)| \leq ch_i \frac{1}{(\rho - 1)\rho^{n+1}} \max_{z \in \partial\mathcal{E}_\rho} |K(x, z)|, \quad 1 < \rho < \rho_i. \quad (4.9)$$

Proof. Recall that $K(x, t)|\dot{\gamma}_i(t)|$ is analytic on $\mathcal{E}_{\rho_i} \supset [-1, 1]$. In particular, the kernel is continuous on $[-1, 1]$ and hence we can represent the kernel by a Chebyshev series, see [Riv90, Theorem 3.4]. There holds

$$K(x, t)|\dot{\gamma}_i(t)| = \sum_{\mu=0}^{\infty} \tilde{\alpha}_\mu(x) T_\mu(t), \quad (4.10)$$

where the coefficients $\tilde{\alpha}_\mu$ are bounded by

$$|\tilde{\alpha}_\mu(x)| \leq 2 \max_{z \in \partial\mathcal{E}_\rho} |K(x, z)| |\dot{\gamma}_i(z)| \rho^{-\mu}, \quad 1 < \rho < \rho_i.$$

A proof is given in [Riv90, Theorem 3.8]. With $\max_{z \in \partial\mathcal{E}_\rho} |\dot{\gamma}_i(z)| \leq \tilde{c} h_i$ and (4.10), the interpolation error

$$\begin{aligned} |E_n(x)| &:= \max_{t \in [-1, 1]} \left| K(x, t)|\dot{\gamma}_i(t)| - \sum_{\mu=0}^n \tilde{\alpha}_\mu(x) T_\mu(t) \right| \\ &\leq \sum_{\mu=n+1}^{\infty} |\tilde{\alpha}_\mu(x)| \leq 2\tilde{c} \frac{h_i}{(\rho - 1)\rho^{n+1}} \max_{z \in \partial\mathcal{E}_\rho} |K(x, z)|. \end{aligned} \quad (4.11)$$

where we used $|T_\mu(t)| \leq 1$. With the Hölder inequality, we get

$$|R_n(x)| \leq |E_n(x)| \int_{-1}^1 |P_k(t)| dt \leq 4\tilde{c} \frac{h_i}{(\rho - 1)\rho^{n+1}} \max_{z \in \partial\mathcal{E}_\rho} |K(x, z)|.$$

□

Remark 4.2.10. (i) The method based on the interpolation of the kernel has two advantages as compared to the Gauss-Legendre quadrature, if ansatz functions with large polynomial degrees are considered. First, Lemma 4.2.9 shows that the remainder $|R_n(x)|$ does not depend on the polynomial degree p_i of the basis functions, since only the kernel is interpolated in (4.7). For high-order methods with a large polynomial degree p_i , a small number of interpolation points $n \ll p_i$ suffices, since the kernel is smooth in the far-field case. For the Gauss-Legendre quadrature Lemma 4.2.6 implies, that the quadrature order $n > \frac{p_i-1}{2}$ is needed in order to reduce the quadrature error. The second advantage is, that

4. Numerical Integration for High-Order NURBS-Based BEM

also the complexity for the evaluation of $\{A_k^{(i)}\}_{k=0,\dots,p_i}$ is independent of p_i , since all integrals are evaluated simultaneously by using the orthogonality of the Legendre polynomials. In particular, the complexity of $\mathcal{O}(n p_i)$ of the Gauss-Legendre quadrature is reduced to $\mathcal{O}(n \log n)$, where the interpolation order is smaller as compared to the quadrature order. Hence, the interpolation method shows to be very efficient for uniform p - and hp -refinements.

- (ii) Since the Lobatto shape functions are closely related to the Legendre polynomials, see Lemma 2.1.11 (i), the method introduced above can also be generalized to $\Phi_k = N_k$.

Isogeometric methods. For the numerical integration in isogeometric FEM, quadrature rules are constructed that exactly integrate all basis functions of the NURBS ansatz space, see e.g. [ACH⁺12]. As compared to the Gauss-Legendre quadrature, less function evaluations are needed if the basis functions have a high inter-element regularity.

We extend this approach to the application to BEM by considering a patch $\mathcal{P} \subset \mathcal{T}$ that may contain more than one element. Let $\Phi_\ell \in S(\mathcal{P}, \mathbf{h}|_{\mathcal{P}}, q, \mathbf{k}|_{\mathcal{P}})$, $\ell = 1, \dots, m$, denote all non-vanishing b-spline basis functions on the patch \mathcal{P} . Furthermore, we assume that the patch \mathcal{P} is parametrized by a \mathcal{C}^∞ -regular b-spline curve $\gamma_{\mathcal{P}}$ and that $x \in \mathbb{R}^2$ is a far-field point for the whole patch. By analogy to (4.7), we denote by $I_n(x, t)$ the interpolation polynomial of the kernel and the parametrization of the patch, i.e.

$$K(x, t) |\dot{\gamma}_{\mathcal{P}}(t)| \approx I_n(x, t)$$

with $K(x, t) := \tilde{K}(x, \gamma_{\mathcal{P}}(t))$. Plugging in the interpolation polynomial, we obtain

$$\int_{-1}^1 K(x, t) |\dot{\gamma}_{\mathcal{P}}(t)| \Phi_\ell(t) dt \approx \sum_{\mu=0}^n \alpha_\mu \int_{-1}^1 P_\mu(t) \Phi_\ell(t) dt.$$

Since $P_\mu(t) \Phi_\ell(t) \in S(\mathcal{P}, \mathbf{h}|_{\mathcal{P}}, q + n, \mathbf{k}|_{\mathcal{P}})$, $\mu = 0, \dots, n$ and $\ell = 1, \dots, m$, a quadrature rule that exactly integrates all functions in $S(\mathcal{P}, \mathbf{h}|_{\mathcal{P}}, q + n, \mathbf{k}|_{\mathcal{P}})$ can be used for the exact evaluation of the integral on the right-hand side. If the basis functions have uniform regularity $\mathbf{k} \geq 0$, the optimal interpolatory quadrature rule, which is also called generalized Gauss rule, is of order $N := \lceil \dim S(\mathcal{P}, \mathbf{h}|_{\mathcal{P}}, q + n, \mathbf{k}|_{\mathcal{P}}) / 2 \rceil$, i.e.

$$\int_{-1}^1 f(t) dt = \sum_{k=1}^N \omega_k f(t_k), \quad \forall f \in S(\mathcal{P}, \mathbf{h}|_{\mathcal{P}}, q + n, \mathbf{k}|_{\mathcal{P}}).$$

Remark 4.2.11. (i) For the exact integration with the Gauss-Legendre quadrature, $\frac{|\mathcal{P}|(q+n+1)}{2}$ function evaluations are needed, where we denote by $|\mathcal{P}|$ the number of elements contained in the patch.

The space $S(\mathcal{P}, \mathbf{h}|_{\mathcal{P}}, q + n, \mathbf{k}|_{\mathcal{P}})$ is spanned by b-splines defined on a periodic knot vector, i.e. there holds $\dim S(\mathcal{P}, \mathbf{h}|_{\mathcal{P}}, q + n, \mathbf{k}|_{\mathcal{P}}) = |\mathcal{P}|(n + q - k) - k - 1$. Hence, the order of

the optimal interpolatory quadrature rule depends on the regularity of the basis functions. While for discontinuous basis functions the same order $\left\lceil \frac{|\mathcal{P}|(n+q+1)}{2} \right\rceil$ as for the Gauss-Legendre quadrature is needed, only $\left\lceil \frac{|\mathcal{P}|(n+1)-q}{2} \right\rceil$ function evaluations are needed for the basis functions with maximum regularity.

- (ii) The main issue of this approach is the computation of the nodes and weights of the optimal quadrature rules. While in [MRW96] the existence and uniqueness of generalized Gauss rules is proven for special families of functions, so-called Chebyshev systems, this result cannot be applied to the B-spline basis. Hence, existence and uniqueness of the quadrature rule in the general case are still an open question.
- (iii) The computation of the generalized Gauss rule corresponds to the solution of a non-linear problem. Hence, the nodes and weights have to be computed a priori, which limits the fields of application to some special cases, i.e. uniform knot vectors with the same multiplicity of all interior knots. In [ACH⁺12], an algorithm based on the Newton iteration for uniform periodic and open knot vectors is presented.

4.2.2. Near-Field Case

The near-field case is the numerically most challenging case, since for small distances $D := \text{dist}\{T_i, x\}$ the kernel is nearly singular. While for singular integrals the singularity can be cancelled out by coordinate transforms or adapted quadrature rules can be applied, it is not possible to find similar coordinate transforms and quadrature rules independent of the evaluation point x in the nearly singular case.

We propose a semi-analytic approach, which is based on the analytic integration introduced in [Ban13, Section 2.3]. Therefore, we define the modified associated Legendre functions.

Definition 4.2.12 ([Ban13, Definition 2.3.1]). (i) For $z \in \mathbb{C} \setminus (-\infty, 1]$, we define

$$\tilde{Q}_k^{-1}(z) := \int_{-1}^1 P_k(t) \log(z - t) dt$$

and for $x \in (-\infty, 1]$ we define

$$\tilde{Q}_k^{-1}(x) := \frac{1}{2} \lim_{\varepsilon \rightarrow 0} \left(\tilde{Q}_k^{-1}(x + \varepsilon i) + \tilde{Q}_k^{-1}(x - \varepsilon i) \right).$$

(ii) For $m \in \mathbb{N}_0$ and $z \in \mathbb{C} \setminus (-1, 1)$, we define

$$\tilde{Q}_k^m(z) := \int_{-1}^1 \frac{P_k(t)}{(z - t)^{m+1}} dt$$

and for $x \in [-1, 1]$ we define

$$\tilde{Q}_k^m(x) := \frac{1}{2} \lim_{\varepsilon \rightarrow 0} \left(\tilde{Q}_k^m(x + \varepsilon i) + \tilde{Q}_k^m(x - \varepsilon i) \right).$$

4. Numerical Integration for High-Order NURBS-Based BEM

Remark 4.2.13. (i) The accurate and efficient evaluation of the integrals $\tilde{Q}_k^m(z)$ is discussed in [Ban13] for all $z \in \mathbb{C} \setminus \{-1, 1\}$. Therefore, the following recurrence relation is derived

$$(k - m + 1)\tilde{Q}_{k+1}^m(z) = (2k + 1)z\tilde{Q}_k^m(z) - (k + m)\tilde{Q}_{k-1}^m(z), \quad m, k \in \mathbb{N}. \quad (4.12)$$

With this recurrence relation and Gautschi's continued fraction algorithm all integrals can be evaluated up to double machine precision for large values of k in an efficient way.

- (ii) The definition of the modified associated Legendre functions can be extended to $z \in \{-1, 1\}$ in the sense of the Hadamard finite part. With a modification of the recurrence relation (4.12), where the coefficients of the infinite algebraic terms have to be considered separately, $\tilde{Q}_k^m(\pm 1)$ can also be evaluated in an efficient and accurate way for high orders k .

In the following, we reduce the evaluation of $A_k^{(i)}(x)$ to the computation of the modified associated Legendre functions by interpolation. Since the domain of analyticity of the kernel is limited by the complex conjugate zeros of $|x - \gamma_i(t)|^2$, see Lemmas 4.2.2 and 4.2.3, the interpolation of the whole kernel only yields very slow convergence of the interpolation error. Hence, we split the kernel function K into regular and nearly singular parts and only interpolate the regular parts.

Definition 4.2.14. For $T_i \in \mathcal{T}$ with its parametrization γ_i and $x \in M_n$, we denote by $z_x \in \mathcal{E}_{\rho_i}$ one of the complex conjugate zeros of $|x - \gamma_i(t)|^2$.

The following proposition is a direct consequence of Lemmas 4.2.2 and 4.2.3.

Proposition 4.2.15. Let $x \in M_n$ and γ_i be the parametrization of $T_i \in \mathcal{T}$ as defined in Definition 3.2.1. Then, the function

$$f(t) := \frac{|x - \gamma_i(t)|^2}{|t - z_x|^2}$$

is analytic on \mathcal{E}_{ρ_i} and $0 \notin f(\mathcal{E}_{\rho_i})$.

Using the result of the previous lemma, we now split the kernel function $K(x, t)$ in regular and nearly singular parts:

$$\begin{aligned} K(x, t) &= g_{-1}(x - \gamma_i(t)) + g_0(x - \gamma_i(t)) \log |x - \gamma_i(t)|^2 + \sum_{\ell=1}^N g_\ell(x - \gamma_i(t)) |x - \gamma_i(t)|^{-2\ell} \\ &= g_{-1}(x - \gamma_i(t)) + g_0(x - \gamma_i(t)) \log \frac{|x - \gamma_i(t)|^2}{|z_x - t|^2} + g_0(x - \gamma_i(t)) \log |z_x - t|^2 \\ &\quad + \sum_{\ell=1}^N \left(g_\ell(x - \gamma_i(t)) \frac{|z_x - t|^{2\ell}}{|x - \gamma_i(t)|^{2\ell}} \right) \frac{1}{|z_x - t|^{2\ell}} \\ &=: f_{-1}(x - \gamma_i(t)) + f_0(x - \gamma_i(t)) \log |z_x - t|^2 + \sum_{\ell=1}^N f_\ell(x - \gamma_i(t)) \frac{1}{|z_x - t|^{2\ell}}. \end{aligned} \quad (4.13)$$

4.2. Evaluation of Boundary Integral Operators

With Proposition 4.2.15 the functions f_ℓ , $\ell = -1, \dots, N$, are analytic on \mathcal{E}_{ρ_i} . The integral corresponding to f_{-1} can be evaluated efficiently as in the far-field case. The nearly singular integrals are given by

$$\begin{aligned} I_0(x) &:= \int_{-1}^1 f_0(x - \gamma_i(t)) \log |t - z_x|^2 |\dot{\gamma}_i(t)| \Phi_k(t) dt, \\ I_\ell(x) &:= \int_{-1}^1 f_\ell(x - \gamma_i(t)) \frac{1}{|t - z_x|^{2\ell}} |\dot{\gamma}_i(t)| \Phi_k(t) dt, \quad \ell = 1, \dots, N. \end{aligned} \quad (4.14)$$

For the computation of the nearly singular integrals we need the following preliminary lemma.

Lemma 4.2.16. *Let $\ell \in \mathbb{N}$, $t \in \mathbb{R}$ and $z \in \mathbb{C} \setminus \mathbb{R}$. Then, there holds*

$$\frac{1}{(z-t)^\ell (\bar{z}-t)^\ell} = \sum_{\mu=1}^{\ell} \varrho_\mu(z) \left(\frac{1}{(z-t)^\mu} + (-1)^\mu \frac{1}{(\bar{z}-t)^\mu} \right). \quad (4.15)$$

Proof. We proof the statement by induction over ℓ . For $\ell = 1$ we have

$$\frac{1}{(z-t)(\bar{z}-t)} = -\frac{1}{2 \operatorname{Im}(z) i} \left(\frac{1}{z-t} - \frac{1}{\bar{z}-t} \right) \quad (4.16)$$

and hence (4.15) holds. If we assume that (4.15) holds for $(\ell-1)$, we get with (4.16)

$$\begin{aligned} \frac{1}{(z-t)^\ell (\bar{z}-t)^\ell} &= \frac{1}{(z-t)(\bar{z}-t)} \sum_{\mu=1}^{\ell-1} \varrho_\mu(z) \left(\frac{1}{(z-t)^\mu} + (-1)^\mu \frac{1}{(\bar{z}-t)^\mu} \right) \\ &= -\frac{1}{2 \operatorname{Im}(z) i} \left(\frac{1}{z-t} - \frac{1}{\bar{z}-t} \right) \sum_{\mu=1}^{\ell-1} \varrho_\mu(z) \left(\frac{1}{(z-t)^\mu} + (-1)^\mu \frac{1}{(\bar{z}-t)^\mu} \right) \\ &= \sum_{\mu=1}^{\ell-1} \left(-\frac{\varrho_\mu(z)}{2 \operatorname{Im}(z) i} \right) \left(\frac{1}{(z-t)^{\mu+1}} + (-1)^{\mu+1} \frac{1}{(\bar{z}-t)^{\mu+1}} \right) \\ &\quad + \sum_{\mu=1}^{\ell-1} \left(-\frac{\varrho_\mu(z)}{2 \operatorname{Im}(z) i} \right) \left((-1)^\mu \frac{1}{(\bar{z}-t)^\mu (z-t)} - \frac{1}{(\bar{z}-t)(z-t)^\mu} \right). \end{aligned} \quad (4.17)$$

Investigating the expressions in the second sum we obtain by applying (4.16) recursively

$$\begin{aligned} \frac{1}{(\bar{z}-t)^\mu (z-t)} &= -\frac{1}{2 \operatorname{Im}(z) i} \left(\frac{1}{z-t} - \frac{1}{\bar{z}-t} \right) \frac{1}{(\bar{z}-t)^{\mu-1}} \\ &= -\frac{1}{2 \operatorname{Im}(z) i} \left(-\frac{1}{(\bar{z}-t)^\mu} + \frac{1}{(z-t)(\bar{z}-t)^{\mu-1}} \right) \\ &= \dots = \sum_{k=1}^{\mu} \left(-\frac{1}{2 \operatorname{Im}(z) i} \right)^{\mu-k+1} \frac{1}{(\bar{z}-t)^k} \end{aligned}$$

and with similar arguments

$$\frac{1}{(\bar{z}-t)(z-t)^\mu} = \dots = -\sum_{k=1}^{\mu} \left(\frac{1}{2 \operatorname{Im}(z) i} \right)^{\mu-k+1} \frac{1}{(z-t)^k}.$$

4. Numerical Integration for High-Order NURBS-Based BEM

Hence, the second sum in (4.17) can be written as

$$\begin{aligned}
& \sum_{\mu=1}^{\ell-1} \left(-\frac{\varrho_{\mu}(z)}{2 \operatorname{Im}(z) i} \right) \left((-1)^{\mu} \frac{1}{(\bar{z}-t)^{\mu}(z-t)} - \frac{1}{(\bar{z}-t)(z-t)^{\mu}} \right) \\
&= \sum_{\mu=1}^{\ell-1} \left(-\frac{\varrho_{\mu}(z)}{2 \operatorname{Im}(z) i} \right) \sum_{k=1}^{\mu} \left(\frac{1}{2 \operatorname{Im}(z) i} \right)^{\mu-k+1} \left(\frac{1}{(z-t)^k} + (-1)^k \frac{1}{(\bar{z}-t)^k} \right) \\
&= \sum_{\mu=1}^{\ell-1} \left(-\sum_{k=\mu}^{\ell-1} \frac{\varrho_k(z)}{(2 \operatorname{Im}(z) i)^{k-\mu+2}} \right) \left(\frac{1}{(z-t)^{\mu}} + (-1)^{\mu} \frac{1}{(\bar{z}-t)^{\mu}} \right).
\end{aligned}$$

Finally, we get

$$\begin{aligned}
\frac{1}{(z-t)^{\ell}(\bar{z}-t)^{\ell}} &= \sum_{\mu=1}^{\ell-1} \left(-\frac{\varrho_{\mu}(z)}{2 \operatorname{Im}(z) i} \right) \left(\frac{1}{(z-t)^{\mu+1}} + (-1)^{\mu+1} \frac{1}{(\bar{z}-t)^{\mu+1}} \right) \\
&\quad + \sum_{\mu=1}^{\ell-1} \left(-\sum_{k=\mu}^{\ell-1} \frac{\varrho_k(z)}{(2 \operatorname{Im}(z) i)^{k-\mu+2}} \right) \left(\frac{1}{(z-t)^{\mu}} + (-1)^{\mu} \frac{1}{(\bar{z}-t)^{\mu}} \right) \\
&= \sum_{\mu=1}^{\ell} \varrho_{\mu}^{*} \left(\frac{1}{(z-t)^{\mu}} + (-1)^{\mu} \frac{1}{(\bar{z}-t)^{\mu}} \right)
\end{aligned}$$

with

$$\varrho_{\mu}^{*} := \begin{cases} -\sum_{k=1}^{\ell-1} \frac{\varrho_k(z)}{(2 \operatorname{Im}(z) i)^{k+1}}, & \mu = 1 \\ -\left(\frac{\varrho_{\mu-1}(z)}{2 \operatorname{Im}(z) i} + \sum_{k=\mu}^{\ell-1} \frac{\varrho_k(z)}{(2 \operatorname{Im}(z) i)^{k-\mu+2}} \right), & \mu = 2, \dots, \ell-1 \\ -\frac{\varrho_{\ell-1}}{2 \operatorname{Im}(z) i}, & \mu = \ell. \end{cases} \quad (4.18)$$

□

Remark 4.2.17. For $\mu = 1, \dots, \ell$, the coefficients ϱ_{μ} in Lemma 4.2.16 satisfy $|\varrho_{\mu}| = \mathcal{O}(\operatorname{Im}(z)^{2\ell-\mu})$.

For $\ell = 1$ this is proven by Equation (4.16), for $\ell > 1$ the statement follows by induction and the representation (4.18) of ϱ_{μ}^{*} .

For the numerical evaluation of the nearly singular integrals (4.14), we expand the regular parts of the integrand into a Legendre sum, i.e. for $n \in \mathbb{N}$ we get

$$f_{\ell}(x - \gamma_i(t)) |\dot{\gamma}_i(t)| \Phi_k(t) \approx \sum_{\mu=0}^n \alpha_{\mu}^{(\ell)} P_{\mu}(t). \quad (4.19)$$

The coefficients $\alpha_{\mu}^{(\ell)} := \alpha_{\mu}^{(\ell)}(x)$ of the Legendre expansion are computed with Algorithm 4.2. Plugging in the interpolation polynomial, we can reduce the evaluation of the critical integrals to the computation of modified associated Legendre functions as follows:

$$\begin{aligned}
I_0(x) &\approx \sum_{\mu=0}^n \alpha_{\mu}^{(0)} \int_{-1}^1 P_{\mu}(t) \log |z_x - t|^2 dt = \sum_{\mu=0}^n \alpha_{\mu}^{(0)} \int_{-1}^1 P_{\mu}(t) \log(z_x - t)(\bar{z}_x - t) dt \\
&= 2 \sum_{\mu=0}^n \alpha_{\mu}^{(0)} \operatorname{Re}(\tilde{Q}_{\mu}^{-1}(z_x)).
\end{aligned} \quad (4.20)$$

4.2. Evaluation of Boundary Integral Operators

For the algebraic terms with $\ell = 1, \dots, N$ we distinguish between real values of z_x and complex values of z_x . For $z_x \in \mathbb{R} \setminus [-1, 1]$, we have

$$I_\ell(x) \approx \sum_{\mu=0}^n \alpha_\mu^{(\ell)} \int_{-1}^1 P_\mu(t) \frac{1}{|z_x - t|^{2\ell}} dt = \sum_{\mu=0}^n \alpha_\mu^{(\ell)} \tilde{Q}_\mu^{2\ell-1}(z_x). \quad (4.21)$$

For complex $z_x \in \mathbb{C} \setminus \mathbb{R}$, we apply the partial fraction decomposition (4.15) and obtain

$$\begin{aligned} I_\ell(x) &\approx \sum_{\mu=0}^n \alpha_\mu^{(\ell)} \int_{-1}^1 P_\mu(t) \frac{1}{|z_x - t|^{2\ell}} dt \\ &= \sum_{\mu=0}^n \alpha_\mu^{(\ell)} \sum_{j=1}^{\ell} \varrho_j(z_x) \int_{-1}^1 P_\mu(t) \left(\frac{1}{(z_x - t)^j} + (-1)^j \frac{1}{(\bar{z}_x - t)^j} \right) dt \end{aligned} \quad (4.22)$$

For even integers j , we get

$$\int_{-1}^1 P_\mu(t) \left(\frac{1}{(z_x - t)^j} + \frac{1}{(\bar{z}_x - t)^j} \right) dt = 2 \operatorname{Re} \left(\tilde{Q}_\mu^{j-1}(z_x) \right)$$

and for odd integers j we obtain

$$\int_{-1}^1 P_\mu(t) \left(\frac{1}{(z_x - t)^j} - \frac{1}{(\bar{z}_x - t)^j} \right) dt = 2i \operatorname{Im} \left(\tilde{Q}_\mu^{j-1}(z_x) \right),$$

which yields

$$I_\ell(x) \approx 2 \sum_{\mu=0}^n \alpha_\mu^{(\ell)} \left(\sum_{j=1, j \text{ odd}}^{\ell} i \varrho_j(z_x) \operatorname{Im} \left(\tilde{Q}_\mu^{j-1}(z_x) \right) + \sum_{j=1, j \text{ even}}^{\ell} \varrho_j(z_x) \operatorname{Re} \left(\tilde{Q}_\mu^{j-1}(z_x) \right) \right).$$

While the modified associated Legendre functions \tilde{Q}_k^j can be evaluated exactly (up to 15 significant digits, see [Ban13]), it remains to investigate the error, which is introduced by the interpolation. The following Lemma gives an upper bound for the overall error of the evaluation according to (4.20), (4.21), and (4.22).

Lemma 4.2.18. *Let γ_i be the parametrization of $T_i \in \mathcal{T}$, $x \in M_n$ be a near-field point and z_x as defined in Definition 4.2.14. For $n \in \mathbb{N}$, the remainder $|R_n^{(\ell)}(x)|$ of the evaluation of the integrals (4.14) according to (4.20), (4.21), and (4.22) is bounded by*

$$|R_n^{(\ell)}(x)| \leq c \, c_\ell(x) \, h_i \frac{1}{\rho - 1} \rho^{-n-1}, \quad 1 < \rho < \rho_i. \quad (4.23)$$

The constant c is independent of h_i but still depending on the basis functions Φ_k , and

$$c_\ell(x) := \begin{cases} \int_{-1}^1 |\log |z_x - t|| dt, & \ell = 0 \\ \int_{-1}^1 \frac{1}{|z_x - t|^{2\ell}} dt, & \ell > 0. \end{cases}$$

4. Numerical Integration for High-Order NURBS-Based BEM

Proof. Due to Proposition 4.2.15 for all $\ell = 0, \dots, N$, the interpolants are analytic on \mathcal{E}_{ρ_i} . With the same arguments as in the proof of Lemma 4.2.9 and $1 < \rho < \rho_i$, the interpolation error $|E_n^{(\ell)}(x)|$ of the Legendre sum (4.19) is bounded by

$$|E_n^{(\ell)}(x)| := \max_{t \in [-1, 1]} \left| f_\ell(x - \gamma_i(t)) |\dot{\gamma}_i(t)| \Phi_k(t) - \sum_{\iota=0}^n \alpha_\mu^{(\ell)} P_\mu(t) \right| \leq c h_i \frac{1}{\rho - 1} \rho^{-n-1}$$

with $c > 0$ independent of h_i and the distance D . Applying the Hölder inequality we get for $\ell = 0$

$$\begin{aligned} |R_n^{(0)}(x)| &\leq |E_n^{(0)}(x)| \int_{-1}^1 |\log |t - z_x|| dt \\ &\leq c h_i \frac{1}{\rho - 1} \rho^{-n-1} \int_{-1}^1 |\log |t - z_x|| dt \end{aligned}$$

and

$$\begin{aligned} |R_n^{(\ell)}(x)| &\leq |E_n^{(\ell)}(x)| \int_{-1}^1 \frac{1}{|t - z_x|^{2\ell}} dt \\ &\leq c h_i \frac{1}{\rho - 1} \rho^{-n-1} \int_{-1}^1 \frac{1}{|t - z_x|^{2\ell}} dt. \end{aligned}$$

□

Corollary 4.2.19. For $x \in M_n$, the absolute error $|R_n(x)|$ of the evaluation of $A_k^{(i)}(x)$ according to (4.20), (4.21), and (4.22) is bounded by

$$|R_n(x)| \leq \tilde{c}(x) h_i \frac{1}{\rho - 1} \rho^{-n-1}, \quad 1 < \rho < \rho_i. \quad (4.24)$$

Remark 4.2.20. For the Legendre polynomials, $\Phi_k = P_k$, and the Lobatto shape functions, $\Phi_k = N_k$, we apply the estimates given in Lemma 2.1.9 (vi) and 2.1.11 (iv) and obtain

$$|R_n(x)| \leq \tilde{c} h_i \frac{1}{\rho - 1} \rho^{-n+k-1}, \quad 1 < \rho < \rho_i.$$

Here, the constant \tilde{c} is independent of h_i and the polynomial degree k .

Remark 4.2.21. (i) For the evaluation of $A_k^{(i)}(x)$ in the near-field case, the remainder $|R_n(x)|$ asymptotically behaves like $\mathcal{O}(\rho^{-n-1})$ with a convergence factor $1 < \rho < \rho_i$ only depending on the boundary parametrization but not on the evaluation point x . This yields a fast decay of the absolute error even for small distances D . However, the constant $c_\ell(x)$ in (4.23) depends on the evaluation point x . Remark 4.2.17 implies that $c_\ell(x) = \mathcal{O}(D^{-2\ell+1})$ as $D \rightarrow 0$.

(ii) For NURBS-enhanced methods, the complexity for the evaluation of $\{A_k^{(i)}\}_{k=0, \dots, p_i}$ with n interpolation points is $\mathcal{O}(p_i n \log n)$, since the basis functions Φ_k are also interpolated in

(4.19), Furthermore, the bound (4.24) for $|R_n(x)|$ depends on the polynomial degree of the basis functions. Hence, the advantage that the complexity and the decay of the remainder are independent of p_i , which we obtain in the far-field case, cannot be transferred to the near-field case.

- (iii) As compared to the Gauss-Legendre quadrature, the interpolation generally only yields half the convergence rate with respect to the order n . However, since we only interpolate the regular parts of the kernel and integrate the nearly singular parts analytically, the interpolation order is much smaller than the quadrature order, when a Gauss-Legendre quadrature is applied for the evaluation of $A_k^{(i)}(x)$. We will see in Section 5.2.2 that the convergence of the Gauss-Legendre quadrature rules is even slower if the integrand is additionally regularized with coordinate transforms.
- (iv) For the single layer operator of the Laplace equation, there holds $g_0(x - y) = -\frac{1}{2\pi}$ and $g_\ell(x - y) = 0$, $\ell \in \mathbb{N}$. Hence, the coefficients $\alpha_\mu^{(\ell)}$ in (4.19) are independent of the evaluation point x and the Legendre expansion of the kernel only has to be computed once for all evaluation points. However, this does not apply to the single layer operator of the Lamé and Helmholtz equations and double layer operators of all three PDEs.

4.2.3. Identical Case

Let $x \in T_i$ and $z_x \in [-1, 1]$ as defined in Definition 4.2.14. The modified associated Legendre functions $\tilde{Q}_k^m(z)$ are also defined on $[-1, 1]$ in the sense of the Cauchy principle values and the Hadamard finite parts, see Definition 4.2.12. Furthermore, efficient algorithms for the evaluation are given in [Ban13]. Hence, we can proceed as in the near-field case for the evaluation of $A_k^{(i)}(x)$. All results concerning the complexity and the absolute error remain valid, except for the constant c_ℓ in Lemma 4.2.18, which changes to

$$c_\ell(x) := \begin{cases} p.v. \int_{-1}^1 |\log |z_x - t|| dt, & \ell = 0 \\ f.p. \int_{-1}^1 \frac{1}{|z_x - t|^{2\ell}} dt, & \ell > 0. \end{cases}$$

Remark 4.2.22. Since the nearly singular and singular cases do not have to be distinguished and all type of singularities are evaluated in a similar way, we obtain a simple implementation for all kernel functions of the general type (4.26). However, for some special cases there are also alternative methods for the evaluation of the nearly singular integrals $I_\ell(x)$, $\ell = 0, \dots, N$ as defined in (4.14), which we present in the following.

- (i) For the integral I_0 containing the logarithmic singularity, i.e.

$$I_0(x) = \int_{-1}^1 f_0(x - \gamma_i(t)) \log |t - z_x|^2 |\dot{\gamma}_i(t)| \Phi_k(t) dt =: \int_{-1}^1 \tilde{f}(t) \log |t - z_x| dt$$

4. Numerical Integration for High-Order NURBS-Based BEM

the Gauss-Log quadrature, which is introduced in Section 2.2, can be used for the evaluation. For this purpose, we split the integration at z_x and apply affine transforms to the resulting integrals, such that the logarithmic singularity is located at -1. We get

$$\begin{aligned} I_0(x) &= \log(1 - z_x) \frac{1 - z_x}{2} \int_{-1}^1 \tilde{f} \left(\frac{1 - z_x}{2} t + \frac{1 + z_x}{2} \right) dt \\ &\quad + \log(1 + z_x) \frac{1 + z_x}{2} \int_{-1}^1 \tilde{f} \left(-\frac{1 + z_x}{2} t - \frac{1 - z_x}{2} \right) dt \\ &\quad + \int_{-1}^1 \log \left(\frac{1 + t}{2} \right) \left[\tilde{f} \left(\frac{1 - z_x}{2} t + \frac{1 + z_x}{2} \right) + \tilde{f} \left(-\frac{1 + z_x}{2} t - \frac{1 - z_x}{2} \right) \right] dt. \end{aligned}$$

The first two integrals can be evaluated as in the far-field case, while the third integral is evaluated with a Gauss-Log quadrature. Since the function \tilde{f} is analytic on \mathcal{E}_{ρ_i} , Theorem 2.2.15 implies that the absolute quadrature error for the third integral decays with $\mathcal{O}(\rho_i^{-2n-1})$, which is twice the convergence rate with respect to the order n as compared to the interpolation approach. Furthermore, the complexity for the evaluation reduces from $\mathcal{O}(n \log n)$ of the interpolation to $\mathcal{O}(n)$ for the Gauss-Log quadrature.

- (ii) For the evaluation of $I_1(x)$, the approach presented in [GC87] can be used when additionally assuming that $f_1(x - \gamma_i(t)) = (z_x - t) \hat{f}_1(x - \gamma_i(t))$ with $\hat{f}_1(z_x - \gamma_i(t)) \neq 0$. This is satisfied for the double layer operators of Laplace, Lamé and Helmholtz equations. Hence, we get

$$p.v. I_1(x) = p.v. \int_{-1}^1 \hat{f}_1(x - \gamma_i(t)) |\dot{\gamma}_i(t)| \Phi_k(t) \frac{1}{z_x - t} dt =: p.v. \int_{-1}^1 \tilde{f}(t) \frac{1}{z_x - t} dt.$$

There holds

$$\begin{aligned} p.v. I_1(x) &= \int_{-1}^1 \frac{\tilde{f}(t) - \tilde{f}(z_x)}{z_x - t} dt + p.v. \int_{-1}^1 \frac{\tilde{f}(z_x)}{z_x - t} dt \\ &= \int_{-1}^1 \frac{\tilde{f}(t) - \tilde{f}(z_x)}{z_x - t} dt + \tilde{f}(z_x) \log \frac{z_x - 1}{z_x + 1}. \end{aligned}$$

Since the first integrand is analytic on \mathcal{E}_{ρ_i} the Gauss-Legendre quadrature yields exponential convergence with twice the convergence rate as compared to the interpolation method if the integrand is evaluated appropriately at z_x .

- (iii) A similar algorithm for the evaluation of the hypersingular integrals I_ℓ , $\ell > 1$, is presented in [PA92]. Here, higher order Taylor expansions of f are used for the semi-analytic

evaluation, i.e. for $\ell = 2$ with $\tilde{f}(z_x) \neq 0$ and $\tilde{f}'(z_x) \neq 0$

$$\begin{aligned} f.p. I_2(x) &= f.p. \int_{-1}^1 \frac{\tilde{f}(t) - \tilde{f}(z_x) - \tilde{f}'(z_x)(z_x - t)}{(z_x - t)^2} dt \\ &\quad + f.p. \int_{-1}^1 \frac{\tilde{f}(z_x)}{(z_x - t)^2} dt + p.v. \int_{-1}^1 \frac{\tilde{f}'(z_x)}{z_x - t} dt \\ &= \int_{-1}^1 \frac{\tilde{f}(t) - \tilde{f}(z_x) - \tilde{f}'(z_x)(z_x - t)}{(z_x - t)^2} dt + \tilde{f}(z_x) \frac{2}{z_x^2 - 1} + \tilde{f}'(z_x) \log \frac{z_x - 1}{z_x + 1}. \end{aligned}$$

4.3. Computation of Galerkin Entries

In this section we discuss the assembly of the Galerkin matrices \mathbf{V} , \mathbf{K} , and \mathbf{W} that are introduced in Section 1.6.1. For the evaluation of the arising double integrals, we split the integration at all element edges. For the non-local basis functions, we add up the local contributions. For a fixed element combination of boundary elements $T_i, T_j \in \mathcal{T}$, we have to evaluate the integrals

$$A_{k,\ell}^{(i,j)} := \int_{T_i} \Phi_k^{(i)}(x) \int_{T_j} \Psi_\ell^{(j)}(y) \tilde{K}(x - y) ds_y ds_x. \quad (4.25)$$

Here, we denote by $\Phi_k^{(i)}$ and $\Psi_\ell^{(j)}$ the basis functions of the discrete ansatz spaces as defined in Definitions 3.2.3 and 3.2.5. The kernel function \tilde{K} is of the type

$$\begin{aligned} \tilde{K}(x - y) &= g_0(x - y) + g_1(x - y) \log |x - y| \\ &\quad + g_2(x - y) \frac{(x - y)^T \nu_y}{|x - y|^2} + g_3(x - y) \frac{(x - y)^T \tau_y}{|x - y|^2}, \end{aligned} \quad (4.26)$$

where we denote by ν_y and τ_y the outer unit normal and tangential vectors at $y \in \Gamma$. Furthermore, we assume that the functions $g_n(z)$, $n = 0, \dots, 3$, are analytic on $z \in \mathbb{C} \setminus \{0\}$ and analytically extendable to $z = 0$ and $g_3(x - y) = g_3(y - x)$.

Remark 4.3.1. The entries of \mathbf{V} and \mathbf{K} of the Laplace, Lamé and Helmholtz operators are of the form (4.25) with kernel functions (4.26), see Appendix A. For the assembly of \mathbf{W} , we use the relationship between the hypersingular and the single layer operator, see Theorems 1.3.1 (iii), 1.3.2 (iii), and 1.3.5 (v). Hence, the Galerkin matrices for all partial differential operators are included in the subsequent analysis.

Plugging in the local parametrizations of T_i and T_j , which are defined in Definition 3.2.1, we obtain with $K(s, t) := \tilde{K}(\gamma_i(s) - \gamma_j(t))$

$$A_{k,\ell}^{(i,j)} := \int_{-1}^1 \int_{-1}^1 \Phi_k(s) \Psi_\ell(t) K(s, t) |\dot{\gamma}_i(s)| |\dot{\gamma}_j(t)| dt ds. \quad (4.27)$$

Since the kernel function contains singularities if T_i and T_j have common points, we differentiate the following cases:

4. Numerical Integration for High-Order NURBS-Based BEM

- far-field elements: $T_i \cap T_j = \emptyset$, i.e. $D := \text{dist}\{T_i, T_j\} > 0$.
- neighboring elements: $T_i \cap T_j \neq \emptyset$ and $|T_i \cap T_j| = 0$, i.e. the elements have one common node.
- identical elements: $T_i = T_j$.

In the remainder of this section, we discuss the evaluation of the double integrals in (4.27) and give error estimates for the absolute error. For all three cases, we proof that the absolute error decays exponentially with respect to the function evaluations. This is fundamental for high-order methods that yield an exponential decay of the Galerkin error. The last part of this section is devoted to the derivation of a priori estimates for the quadrature orders by estimating the consistency error induced by numerical integration.

4.3.1. Far-field Elements

Throughout this section, we denote by $D > 0$ the minimal distance of the elements T_i and T_j . Since the kernel is regular in this setting, the tensor Gauss-Legendre quadrature yields an exponential decay of the quadrature error and is hence the intuitive choice for the evaluation. After having proven an explicit bound for the quadrature error, we also propose alternative algorithms for the numerical integration in NURBS-enhanced methods.

We start with proving the analyticity of the kernel function.

Lemma 4.3.2. *Let h_i, h_j denote the arc lengths of T_i, T_j , and $\mathcal{E}_{\rho_i}, \mathcal{E}_{\rho_j}$ be as defined in Definition 3.2.9.*

- (i) *For all $t \in [-1, 1]$, the kernel $K(s, t)$ is real analytic on $[-1, 1]$ with respect to s and admits an analytic extension to $\mathcal{E}_{\rho_1} \cap \mathcal{E}_{\rho_i}$, where \mathcal{E}_{ρ_1} is defined by its real semi-axis $a_1 = 1 + c_i \frac{D}{h_i}$.*
- (ii) *For all $s \in [-1, 1]$, the kernel $K(s, t)$ is real analytic on $[-1, 1]$ with respect to t and admits an analytic extension to $\mathcal{E}_{\rho_2} \cap \mathcal{E}_{\rho_j}$, where \mathcal{E}_{ρ_2} is defined by its real semi-axis $a_2 = 1 + c_j \frac{D}{h_j}$.*

The constants c_i and c_j only depend on the parametrizations γ_i and γ_j , respectively, but are independent of h_i and h_j .

Proof. Let $t \in [-1, 1]$ be fixed. Setting $x := \gamma_j(t)$, Lemma 4.2.2 implies that $K(s, t)$ is analytically extendable on $\mathcal{E}_{\rho_i} \cap \mathcal{E}_{\rho_1}$ with real semi-axis $a_1 = 1 + c_i \frac{D_t}{h_i}$ and $D_t := \text{dist}\{\gamma_j(t), T_i\} > 0$. With $D = \min_{t \in [-1, 1]} D_t$ we obtain (i). Statement (ii) can be proven analogously. \square

Remark 4.3.3. The previous lemma shows that the regularity of the kernel depends on the ratio of the distance and the arc length of the elements. Depending on the position of T_i and T_j the maximum domains of analyticity \mathcal{E}_{ρ_i} and \mathcal{E}_{ρ_j} , respectively, may be decreased. This is the main

difference to the far-field case for the evaluation of the integral operators discussed in Section 4.2, where the maximum regularity of the kernel is guaranteed for all far-field points.

The following lemma gives an estimate for the absolute error of the Gauss-Legendre quadrature.

Lemma 4.3.4. *Let $n := (n_1, n_2) \in \mathbb{N}^2$ and $\rho_1, \rho_2 > 1$ such that the domains $\partial\mathcal{E}_{\rho_1} \times [-1, 1]$ and $[-1, 1] \times \partial\mathcal{E}_{\rho_2}$ are contained in the domain of analyticity of the kernel K . Furthermore, we denote by $|R_n|$ the absolute quadrature error of the tensor Gauss-Legendre quadrature of order n for the integral (4.25).*

Then, there exist constants $C_1, C_2 > 0$ depending on the distance, the parametrizations γ_i and γ_j and the basis functions, but independent of h_i and h_j such that

$$|R_n| \leq h_i h_j \left(C_1 \rho_1^{-2n_1-1} + C_2 \rho_2^{-2n_2-1} \right). \quad (4.28)$$

Proof. With Lemma 4.3.2 and the analyticity of the basis functions, the integrand is analytic on $\mathcal{E}_{\rho_1} \times [-1, 1]$ and $[-1, 1] \times \mathcal{E}_{\rho_2}$ and we thus apply Theorem 2.2.17. In order to obtain (4.28) it remains to estimate the maximum of the integrand on the domains of analyticity. For the kernel function, there holds

$$\begin{aligned} \max_{(s,t) \in \partial\mathcal{E}_{\rho_1} \times [-1,1]} |K(s,t)| &\leq \alpha_0 + \alpha_1 |\log D| + \alpha_2 \frac{1}{D} \\ \max_{(s,t) \in [-1,1] \times \partial\mathcal{E}_{\rho_2}} |K(s,t)| &\leq \beta_0 + \beta_1 |\log D| + \beta_2 \frac{1}{D}. \end{aligned}$$

The constants $\alpha_k, \beta_k > 0, k = 0, 1, 2$, depend on the coefficient functions g_n and the parametrizations but are independent of the distance D and the arc lengths h_i and h_j of the elements. The maximum value of the basis functions on $\partial\mathcal{E}_{\rho_1}$ and $\partial\mathcal{E}_{\rho_2}$ is bounded and independent of h_i and h_j . With Lemma 3.2.12 we get

$$\max_{z \in \partial\mathcal{E}_{\rho_1}} |\dot{\gamma}_i(z)| \leq ch_i \quad \text{and} \quad \max_{z \in \partial\mathcal{E}_{\rho_2}} |\dot{\gamma}_j(z)| \leq ch_j$$

and conclude the proof. \square

Corollary 4.3.5. *For the Legendre polynomials, i.e. $\Phi_k = P_k$ and $\Psi_\ell = P_\ell$, and the Lobatto shape functions, i.e. $\Phi_k = N_k$ and $\Psi_\ell = N_\ell$, there holds*

$$|R_n| \leq h_i h_j \left(C_1 \rho_1^{-2n_1+k-1} + C_2 \rho_2^{-2n_2+\ell-1} \right),$$

where the constants C_1 and C_2 only dependent on the parametrizations γ_i and γ_j and the distance of the elements, but are independent of the polynomial degrees k and ℓ .

Proof. Follows directly from the estimates given in Lemmas 2.1.9 (vi) and 2.1.11 (iv). \square

4. Numerical Integration for High-Order NURBS-Based BEM

NURBS-enhanced methods. For the Legendre and the Lobatto bases, we generalize the approach of expanding the kernel into a Legendre series, which is introduced in Section 4.2 for the evaluation of the boundary integral operators. By taking advantage of the smoothness of the kernel for far-field elements and the orthogonality of the Legendre polynomials and the Lobatto shape functions, we obtain a complexity for the evaluation of $A_{k,\ell}^{(i,j)}$, $k, \ell = 1, \dots, p$, that is independent of the polynomial degree p .

For simplicity, we only describe the interpolation for the Legendre basis, i.e. $\Phi_k := P_k$ and $\Psi_\ell := P_\ell$. Let the tensor Legendre expansion be given by

$$K(s, t) |\dot{\gamma}_i(s)| |\dot{\gamma}_j(t)| \approx I_n(s, t) := \sum_{\mu=0}^{n_1} \sum_{\nu=0}^{n_2} \alpha_{\mu\nu} P_\mu(s) P_\nu(t). \quad (4.29)$$

Plugging in the Legendre expansion we obtain

$$\begin{aligned} & \int_{-1}^1 P_k(s) \int_{-1}^1 P_\ell(t) K(s, t) |\dot{\gamma}_i(s)| |\dot{\gamma}_j(t)| dt ds \\ & \approx \sum_{\mu=0}^{n_1} \sum_{\nu=0}^{n_2} \alpha_{\mu\nu} \int_{-1}^1 P_\mu(s) P_k(s) ds \int_{-1}^1 P_\nu(t) P_\ell(t) dt \\ & = \begin{cases} \alpha_{k\ell} \frac{4}{(2k+1)(2\ell+1)}, & k \leq n_1 \quad \text{and} \quad j \leq n_2 \\ 0, & \text{otherwise.} \end{cases} \end{aligned} \quad (4.30)$$

Hence, for evaluating all integrals $A_{k,\ell}^{(i,j)}$, $k, \ell = 0, \dots, p$, simultaneously we only have to compute the coefficients of the Legendre expansion. Similarly to Algorithm 4.2 for the one-dimensional case, we compute the coefficients in two steps. First, we compute the coefficients $\tilde{\alpha}_{\mu\nu}$ with respect to the Chebyshev basis. Therefore, we evaluate $K(s, t) |\dot{\gamma}_i(s)| |\dot{\gamma}_j(t)|$ at

$$(s_\nu, t_\mu), \quad \nu = 1, \dots, n_1 \quad \text{and} \quad \mu = 1, \dots, n_2,$$

where s_ν and t_μ denote the zeros of the $(n_1 + 1)$ -th and $(n_2 + 1)$ -th Chebyshev polynomials, respectively. We then apply the discrete cosine transform on the rows and columns.

Second, the basis transformation to the Legendre polynomials is realized by the multiplication of the coefficient matrix with the transformation matrix \mathbf{M} defined in (4.8) from the left and right.

Remark 4.3.6 (Complexity). For $n := n_1 = n_2$, we have an overall complexity of $\mathcal{O}(n^2 \log n)$: The two-dimensional discrete cosine transform has a complexity of $\mathcal{O}(n^2 \log n)$, since the discrete cosine transform is applied two times to a $(n \times n)$ -matrix. The basis transformation to the

Legendre basis corresponds to two matrix-matrix multiplications. If the algorithm of [AR91] is used for the \mathcal{H}^2 -matrix approximation of the transformation matrix, we also obtain a complexity of $\mathcal{O}(n^2)$.

As compared to the tensor Gauss-Legendre quadrature we can reduce the complexity from $\mathcal{O}(n^3)$ to $\mathcal{O}(n^2 \log n)$. Furthermore, the interpolation order only depends on the smoothness of the kernel and the boundary parametrization and is independent of the polynomial degree p . Hence, the interpolation approach becomes very efficient for the uniform p -refinement, i.e. if the kernel is smooth and the polynomial degrees of the basis functions are large.

The following Lemma gives an estimate for the absolute evaluation error.

Lemma 4.3.7. *Let $T_i, T_j \in \mathcal{T}$ with $D = \text{dist}\{T_i, T_j\} > 0$ and $\rho_1, \rho_2 > 1$ such that the expression $K(s, t) |\dot{\gamma}_i(s)| |\dot{\gamma}_j(t)|$ is analytically extendable on $\overline{\mathcal{E}_{\rho_1}} \times \overline{\mathcal{E}_{\rho_2}}$. For $n \in \mathbb{N}^2$, let I_n be the Legendre sum as defined in (4.29). If we denote by $|R_n|$ the absolute error of the evaluation of the double integral (4.25) according to (4.30), then there holds*

$$|R_n| \leq Ch_i h_j \max_{(s,t) \in \partial \mathcal{E}_{\rho_1} \times \partial \mathcal{E}_{\rho_2}} |K(s, t)| \left(\frac{1}{(\rho_1 - 1) \rho_1^{n_1+1}} + \frac{1}{(\rho_2 - 1) \rho_2^{n_2+1}} \right).$$

Proof. Let $\sum_{\mu=0}^{n_1} \alpha_\mu(t) P_\mu(s)$ denote the Legendre expansion of $K(s, t) |\dot{\gamma}_i(s)| |\dot{\gamma}_j(t)|$ with respect to s . Then, we obtain for the interpolation error of I_n

$$\begin{aligned} \left| K(s, t) |\dot{\gamma}_i(s)| |\dot{\gamma}_j(t)| - I_n \right| &\leq \left| K(s, t) |\dot{\gamma}_i(s)| |\dot{\gamma}_j(t)| - \sum_{\mu=0}^{n_1} \alpha_\mu(t) P_\mu(s) \right| \\ &\quad + \left| \sum_{\mu=0}^{n_1} \alpha_\mu(t) P_\mu(s) - I_n \right|. \end{aligned}$$

By analogy to the proof of Lemma 4.2.9 we obtain for the first term

$$\left| K(s, t) |\dot{\gamma}_i(s)| |\dot{\gamma}_j(t)| - \sum_{\mu=0}^{n_1} \alpha_\mu(t) P_\mu(s) \right| \leq \tilde{c}_1 \frac{h_i h_j}{(\rho_1 - 1) \rho_1^{n_1+1}} \max_{(s,t) \in \partial \mathcal{E}_{\rho_1} \times \partial \mathcal{E}_{\rho_2}} |K(s, t)|.$$

For the second term we get with (4.11)

$$\begin{aligned} \left| \sum_{\mu=0}^{n_1} \alpha_\mu(t) P_\mu(s) - I_n \right| &= \left| \sum_{\mu=0}^{n_1} \left(\alpha_\mu(t) - \sum_{\nu=0}^{n_2} \alpha_{\mu,\nu} P_\nu(t) \right) P_\mu(s) \right| \\ &\leq \max_{t \in \partial \mathcal{E}_{\rho_2}} |\alpha_\mu(t)| \frac{1}{(\rho_2 - 1) \rho_2^{n_2+1}} \sum_{\mu=0}^{n_1} |P_\mu(s)| \\ &\leq (n_1 + 1) \max_{(s,t) \in \partial \mathcal{E}_{\rho_1} \times \partial \mathcal{E}_{\rho_2}} |K(s, t) |\dot{\gamma}_i(s)| |\dot{\gamma}_j(t)| | \frac{1}{(\rho_2 - 1) \rho_2^{n_2+1}} \\ &\leq \tilde{c}_2 (n_1 + 1) \max_{(s,t) \in \partial \mathcal{E}_{\rho_1} \times \partial \mathcal{E}_{\rho_2}} |K(s, t)| \frac{h_i h_j}{(\rho_2 - 1) \rho_2^{n_2+1}}. \end{aligned}$$

4. Numerical Integration for High-Order NURBS-Based BEM

With

$$|R_n| \leq 4 \left| K(s, t) |\dot{\gamma}_i(s)| |\dot{\gamma}_j(t)| - I_n \right|$$

we conclude the proof. \square

Remark 4.3.8. (i) In [Heu96] and [Ban13], it is observed that the entries in the far-field block $A_{k,\ell}^{(i,j)}$ decay rapidly with respect to the polynomial degrees k and ℓ of the Legendre polynomials. For the implementation, the small entries, that do not significantly affect the overall error, are simply neglected. This yields a data compression scheme for the far-field blocks. The interpolation approach presented above yields a similar compression scheme, since small entries are automatically neglected by exploiting the orthogonality of the Legendre polynomials.

(ii) As compared to the Gauss-Legendre quadrature, the convergence is slower, since the kernel K has to be analytically extendable in $\mathcal{E}_{\rho_1} \times \mathcal{E}_{\rho_2}$ as compared to $\mathcal{E}_{\rho_1} \times [-1, 1]$ and $[-1, 1] \times \mathcal{E}_{\rho_2}$, respectively. Hence, the semi-axis sums ρ_1 and ρ_2 cannot be estimated by the formulas given in Lemma 4.3.2 and the computation is in general expensive.

4.3.2. Neighboring elements

Let $T_i, T_j \in \mathcal{T}$ be neighboring elements that have one common node. Without loss of generality we assume that the local parametrizations of T_i and T_j satisfy $\gamma_j(1) = \gamma_i(-1)$, the case $\gamma_j(-1) = \gamma_i(1)$ can be treated analogously. Plugging in the local parametrizations into the representation of the kernel function (4.26) we get

$$\begin{aligned} K(s, t) &= g_0(\gamma_i(s) - \gamma_j(t)) + g_1(\gamma_i(s) - \gamma_j(t)) \log |\gamma_i(s) - \gamma_j(t)| \\ &\quad + g_2(\gamma_i(s) - \gamma_j(t)) \frac{(\gamma_i(s) - \gamma_j(t))^T \nu_j(t)}{|\gamma_i(s) - \gamma_j(t)|^2} \\ &\quad + g_3(\gamma_i(s) - \gamma_j(t)) \frac{(\gamma_i(s) - \gamma_j(t))^T \tau_j(t)}{|\gamma_i(s) - \gamma_j(t)|^2}, \end{aligned} \tag{4.31}$$

which implies that the kernel $K(s, t)$ has algebraic and logarithmic corner singularities at $(s, t) = (-1, 1)$. Thus, the integrand has to be regularized in order to achieve an exponential decay of the evaluation error. Therefore, we first introduce a coordinate transformation, discuss the evaluation of the integral (4.25) with quadrature rules, and proof the exponential decay of the quadrature errors. Finally, we derive analytic formulas for the evaluation of (4.25) for NURBS-enhanced methods and linear boundary parametrizations.

For the regularization of the integrand we introduce the following coordinate transformation:

$$\begin{aligned} \int_{-1}^1 \int_{-1}^1 f(s, t) ds dt &= \int_{-1}^1 \int_{-1}^1 f\left(-v, 1 - \frac{(1+u)(1-v)}{2}\right) \frac{1-v}{2} ds dt \\ &+ \int_{-1}^1 \int_{-1}^1 f\left(\frac{(1+u)(1-v)}{2} - 1, v\right) \frac{1-v}{2} ds dt. \end{aligned} \quad (4.32)$$

Figure 4.3.2 shows a geometrical interpretation of the transform. In the first step, the integration domain is split along the diagonal going through the singular vertex. Second, both triangles are transformed to the unit square by a transformation, which is similar to the one introduced in [Duf82] for the regularization of vertex singularities and called Duffy transformation. In the last step, the first square is reflected with respect to the diagonal such that the top edge is the singular edge. For both transformations, the Jacobian determinant is given by $\frac{1-v}{2}$, which implies (4.32).

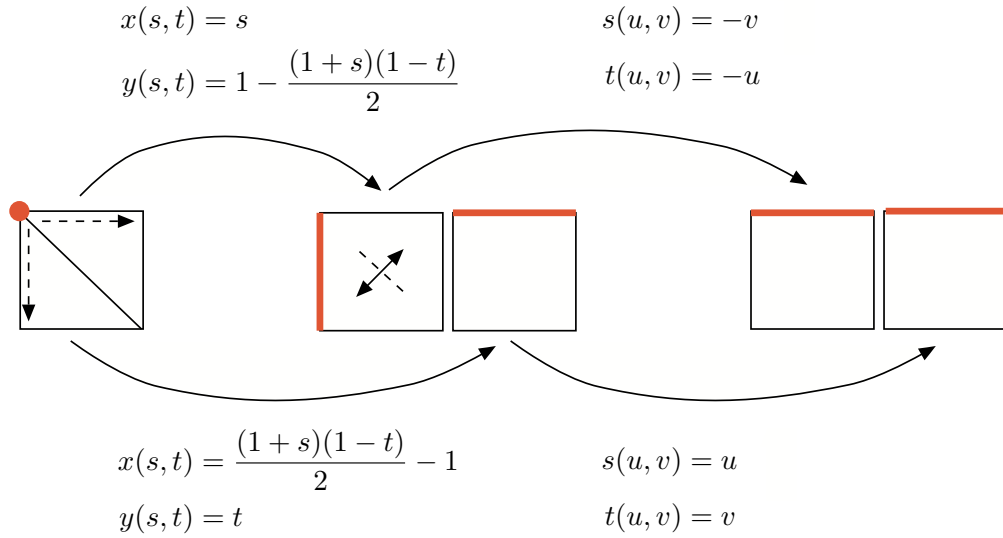


Figure 4.4.: Coordinate transformation for neighboring elements. The red corner and edges indicate the singularity.

Remark 4.3.9. The transformation given in (4.32) is specially designed for the regularization of algebraic singularities of order one. We will show in the sequel, that the Jacobian determinant $\frac{1-v}{2}$ cancels out the algebraic singularities in the kernel function and we obtain regular expressions. However, the logarithmic term multiplied with the Jacobian determinant is continuously extendable to the top edge $v = 1$, but not real analytic. In [LR84] it is proven that the Gauss-Legendre quadrature yields an algebraic convergence for these types of integrands. Hence, the logarithmic term has to be treated separately.

4. Numerical Integration for High-Order NURBS-Based BEM

Since the algebraic terms in the representation are regular after the transformation, we apply a tensor Gauss-Legendre quadrature. For the integration of the logarithmic term arising from the lower triangle, we additionally introduce the following splitting

$$\begin{aligned} & \log \left| \gamma_i \left(\frac{(1+u)(1-v)}{2} - 1 \right) - \gamma_j(v) \right| \\ &= \log \left(\frac{2 \left| \gamma_i \left(\frac{(1+u)(1-v)}{2} - 1 \right) - \gamma_j(v) \right|}{1-v} \right) + \log \left(\frac{1-v}{2} \right). \end{aligned} \quad (4.33)$$

A similar splitting is also introduced for the upper triangle. We will prove that the first term in (4.33) is regular and can be evaluated with a tensor Gauss-Legendre quadrature. The second term contains the logarithmic singularity and the corresponding integral has to be evaluated with a combination of Gauss-Legendre quadrature with respect to u and a Gauss-Log quadrature with respect to v . Overall, we have to evaluate four integrals.

Remark 4.3.10. A similar coordinate transformation is also introduced in [SaSch97] for the Galerkin entries in three-dimensional BEM. In contrast to our approach of evaluating the weakly singular integrals with adapted quadrature rules, a composite rule is applied in order to achieve an exponential decay of the quadrature error.

In the following, we analyze the regularity of the transformed kernel function and then derive estimates for the quadrature errors. In particular, we prove an exponential decay of the quadrature error for all four integrals. For the subsequent analysis of the kernel, we only consider the two integrals arising from the lower triangle, the same arguments also apply to the two integrals coming from the upper triangle.

For notational convenience we define

$$K \left(\frac{(1+u)(1-v)}{2} - 1, v \right) =: \hat{K}_1(u, v) + \hat{K}_2(u, v) \log \left(\frac{1-v}{2} \right), \quad (4.34)$$

where $\hat{K}_1(u, v)$ contains all terms of the transformed kernel that are evaluated with a Gauss-Legendre quadrature.

Proposition 4.3.11. *Let $\theta(u, v) := \frac{(1+u)(1-v)}{2} - 1$ and \mathcal{E}_ρ as defined in Definition 2.0.9 with $\rho > 1$. Then, we obtain*

$$\theta(\mathcal{E}_\rho, [-1, 1]) \subset \mathcal{E}_\rho \quad \text{and} \quad \theta([-1, 1], \mathcal{E}_\rho) \subset \mathcal{E}_\rho.$$

Proof. Let a be the real semi-axis of \mathcal{E}_ρ , $u \in \mathcal{E}_\rho$ and $v \in [-1, 1]$. Since $\theta(u, v) = \frac{1-v}{2} u - \frac{1+v}{2}$, f corresponds to a scaling of \mathcal{E}_ρ with a scaling factor $\frac{1-v}{2} \leq 1$ and a subsequent translation in the direction of the real axis by $-\frac{1+v}{2} \leq 0$. Hence, it suffices to show that $\theta(-a, v) \in \mathcal{E}_\rho$ for all $v \in [-1, 1]$. We get $\theta(-a, v) = -\frac{1-v}{2} a - \frac{1+v}{2} > -a$ since $a > 1$. The second statement can be proven with similar arguments. \square

We now estimate the domain, in which the kernel $(1-v)\hat{K}_1$ is analytically extendable.

Lemma 4.3.12. *Let $\hat{K}_1(u, v)$ be as defined in (4.34).*

- (i) *For all $v \in [-1, 1]$, the term $(1-v)\hat{K}_1(u, v)$ is real analytic on $[-1, 1]$ with respect to u and admits an analytic extension to $\mathcal{E}_{\rho_1} \cap \mathcal{E}_{\rho_i}$ with real semi axis $a_1 = 1 + c_1 \frac{D}{h_i}$.*
- (ii) *For all $u \in [-1, 1]$, the term $(1-v)\hat{K}_1(u, v)$ is real analytic on $[-1, 1]$ with respect to v and admits an analytic extension to $\mathcal{E}_{\rho_2} \cap \mathcal{E}_{\rho_i} \cap \mathcal{E}_{\rho_j}$ with real semi axis $a_2 = 1 + c_2 \frac{D}{\max\{h_i, h_j\}}$.*

The constants $c_1, c_2 > 0$ only depend on the parametrizations γ_i and γ_j , the constant $D > 0$ depends on the angle between the elements T_i and T_j .

Proof. Due to Definition 3.2.9 γ_i and γ_j are analytically extendable to \mathcal{E}_{ρ_i} and \mathcal{E}_{ρ_j} , respectively. Proposition 4.3.11 implies that $\gamma_i \left(\frac{(1+u)(1-v)}{2} - 1 \right)$ is analytically extendable to $[-1, 1] \times \mathcal{E}_{\rho_i}$ and $\mathcal{E}_{\rho_i} \times [-1, 1]$. Further, the expression

$$\gamma_i \left(\frac{(1+u)(1-v)}{2} - 1 \right) - \gamma_j(v)$$

and by assumption the coefficient functions

$$g_\mu \left(\gamma_i \left(\frac{(1+u)(1-v)}{2} - 1 \right) - \gamma_j(v) \right), \quad \mu = 0, \dots, 3,$$

are analytically extendable to $[-1, 1] \times (\mathcal{E}_{\rho_i} \cap \mathcal{E}_{\rho_j})$ and $\mathcal{E}_{\rho_i} \times [-1, 1]$. Hence, it remains to investigate the logarithmic and the algebraic terms in the representation (4.26) of the kernel. We first proof that these terms are real analytic on $[-1, 1]^2$ and then estimate the ellipse, in which these terms can be analytically extended.

The Taylor expansion of γ_i at -1 and of γ_j at 1 is given by

$$\begin{aligned} \gamma_i \left(\frac{(1+u)(1-v)}{2} - 1 \right) - \gamma_j(v) &= \dot{\gamma}_i(-1) \frac{(1+u)(1-v)}{2} + \mathcal{O} \left(\frac{(1+u)^2(1-v)^2}{4} \right) \\ &\quad - \dot{\gamma}_j(1)(v-1) - \mathcal{O}((v-1)^2) \\ &= (1-v) \left(\dot{\gamma}_i(-1) \frac{(1+u)}{2} + \dot{\gamma}_j(1) + \mathcal{O}(1-v) \right) \\ &=: (1-v) h(u, v). \end{aligned} \tag{4.35}$$

Plugging in the Taylor expansion (4.35) we obtain for the algebraic terms of the kernel multiplied with the Jacobian determinant $\frac{1-v}{2}$

$$\frac{1-v}{2} \frac{\left(\gamma_i \left(\frac{(1+u)(1-v)}{2} - 1 \right) - \gamma_j(v) \right)^T \nu_j(v)}{\left| \gamma_i \left(\frac{(1+u)(1-v)}{2} - 1 \right) - \gamma_j(v) \right|^2} = \frac{h(u, v)^T \nu_j(v)}{2 |h(u, v)|^2} \tag{4.36}$$

4. Numerical Integration for High-Order NURBS-Based BEM

and

$$\frac{1-v}{2} \frac{\left(\gamma_i \left(\frac{(1+u)(1-v)}{2} - 1 \right) - \gamma_j(v) \right)^T \tau_j(v)}{\left| \gamma_i \left(\frac{(1+u)(1-v)}{2} - 1 \right) - \gamma_j(v) \right|^2} = \frac{h(u,v)^T \tau_j(v)}{2 |h(u,v)|^2}. \quad (4.37)$$

Further, we get for the logarithmic term

$$\log \frac{\left| \gamma_i \left(\frac{(1+u)(1-v)}{2} - 1 \right) - \gamma_j(v) \right|}{1-v} = \log |h(u,v)|. \quad (4.38)$$

The function $h(u,v)$ does not vanish on $[-1, 1]^2$, since $h(u, 1) = \dot{\gamma}_i(-1) \frac{(1+u)}{2} + \dot{\gamma}_j(1) = 0$ if and only if the angle between both elements T_i and T_j vanishes, which is not possible for Lipschitz boundaries.

Therefore, all three terms (4.36), (4.37) and (4.38) are real analytic on $[-1, 1]^2$ and there exists $\rho_1, \rho_2 > 1$ such that they are analytically extendable on $\mathcal{E}_{\rho_1} \times [-1, 1]$ and $[-1, 1] \times \mathcal{E}_{\rho_2}$.

In the sequel we proof the representation of both real semi-axes a_1 and a_2 . Let

$$D := \min_{u \in [-1, 1]} \min_{v \in [-1, 1]} |h(u, v)| > 0. \quad (4.39)$$

(i) Let $v \in [-1, 1]$ be fixed. There holds

$$\frac{\partial}{\partial u} h(u, v) = \frac{\frac{1-v}{2} \dot{\gamma}_i \left(\frac{(1+u)(1-v)}{2} - 1 \right)}{1-v} = \frac{\dot{\gamma}_i \left(\frac{(1+u)(1-v)}{2} - 1 \right)}{2}.$$

With Lemma 3.2.12 we get

$$\left| \frac{\partial}{\partial u} h(u, v) \right| \leq \frac{c h_i}{2}.$$

Hence, $|h(u, v)| > 0$ for all $u \in \mathcal{E}_{\rho_1}$ with real semi-axis $a_1 = 1 + \frac{2}{c} \frac{D}{h_i}$, which implies the analyticity of the kernel on $\mathcal{E}_{\rho_1} \cap \mathcal{E}_{\rho_i}$ with respect to u .

(ii) Let $u \in [-1, 1]$ be fixed. Since for $v \notin [-1, 1]$

$$|h(u, v)| = 0 \Leftrightarrow |f(v)| := \left| \gamma_i \left(\frac{(1+u)(1-v)}{2} - 1 \right) - \gamma_j(v) \right| = 0$$

we restrict to investigate f . There holds

$$\frac{\partial}{\partial v} f(v) = -\frac{1+u}{2} \dot{\gamma}_i \left(\frac{(1+u)(1-v)}{2} - 1 \right) - \dot{\gamma}_j(v),$$

which implies that

$$\left| \frac{\partial}{\partial v} f(v) \right| \leq 2c_i h_i + c_j h_j.$$

Here, we applied Lemma 3.2.12. Hence, $|h(u, v)| > 0$ for all $v \in \mathcal{E}_{\rho_2}$ with real semi-axis $a_2 = 1 + \frac{D}{2c_i h_i + c_j h_j}$, which implies the analyticity of the kernel on $\mathcal{E}_{\rho_2} \cap \mathcal{E}_{\rho_i} \cap \mathcal{E}_{\rho_j}$ with respect to v .

□

Remark 4.3.13. (i) The proof of Lemma 4.3.12 shows, that the maximum domain of analyticity may be decreased by the zeros of

$$\frac{\gamma_i \left(\frac{(1+u)(1-v)}{2} - 1 \right) - \gamma_j(v)}{1-v}. \quad (4.40)$$

According to Lemma 4.2.3, for all fixed $v \in [-1, 1]$ there exists at most one pair of complex conjugate zeros $z(v) \in \mathcal{E}_{\rho_i}$ with respect to u . Depending on the angle between both elements and the ratio of the arc lengths, the zeros $z(v)$ may be positioned close to the interval $[-1, 1]$, which results in a small domain of analyticity of the integrand. This fact is exemplified in Figure 4.5. For the evaluation of the corresponding integrals with a Gauss-Legendre quadrature, we hence expect a slow exponential convergence.

Although $z(v)$ can be computed for all $v \in [-1, 1]$, it is generally not possible to derive an explicit representation of $z(v)$. Hence, we cannot regularize the integrand as it is done for the evaluation of the boundary integral operators in the near-field case in Section 4.2.

- (ii) The estimate for the semi axis sums ρ_1 and ρ_2 are worst case estimates and hence in general coarse. The numerical examples in Chapter 5 will show, that ρ_1 and ρ_2 are smaller than the actual semi axis sums of the domains of analyticity. However, Lemma 4.3.12 gives a reliable and computable bound for the domain of analyticity.

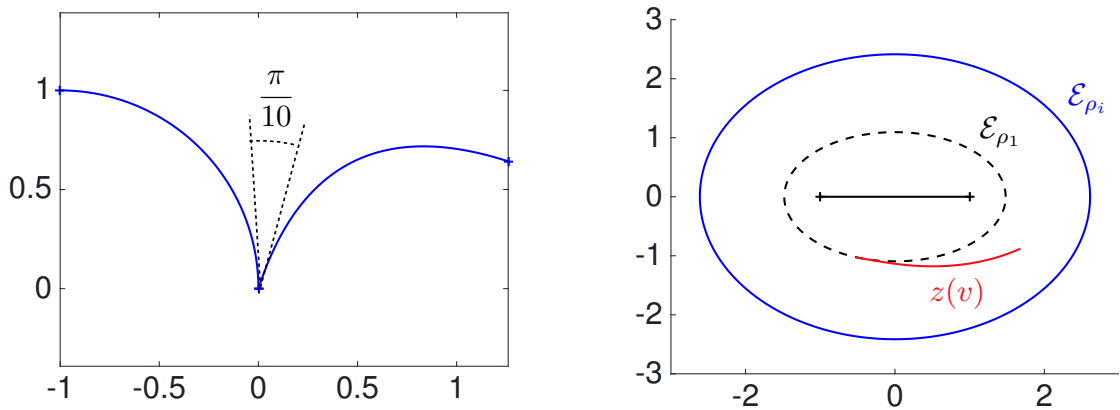


Figure 4.5.: Neighboring Elements T_i and T_j with interior angle $\pi/10$ parametrized by the NURBS curves defined in Example 3.1.3 (left figure). The right figure shows \mathcal{E}_{ρ_i} (blue), the maximum ellipse \mathcal{E}_{ρ_1} in which the expression (4.40) is analytic with respect to u (black dashed), and the zeros $z(v)$ of (4.40) for $v \in [-1, 1]$ (red).

Now we are in the position to derive estimates for the quadrature errors.

4. Numerical Integration for High-Order NURBS-Based BEM

Lemma 4.3.14. *Let $n \in \mathbb{N}^2$ and $\rho_1, \rho_2 > 1$ be the semi-axis sums of \mathcal{E}_{ρ_1} and \mathcal{E}_{ρ_2} such that $\frac{1-v}{2} \hat{K}_1(u, v)$ is analytically extendable on $\overline{\mathcal{E}_{\rho_1}} \times [-1, 1]$ and $[-1, 1] \times \overline{\mathcal{E}_{\rho_2}}$. Further, let $|R_n|$ denote the absolute quadrature error of the Gauss-Legendre quadrature rule applied to the integral*

$$\int_{-1}^1 \int_{-1}^1 \frac{1-v}{2} \hat{K}_1(u, v) \Phi_k \left(\frac{(1+u)(1-v)}{2} - 1 \right) \Psi_\ell(v) \left| \dot{\gamma}_i \left(\frac{(1+u)(1-v)}{2} - 1 \right) \right| |\dot{\gamma}_j(v)| du dv.$$

Then, there holds

$$|R_n| \leq h_i h_j \left(C_1 \rho_1^{-2n_1-1} + C_2 \rho_2^{-2n_2-1} \right) \quad (4.41)$$

with constants $C_1, C_2 > 0$ depending on the basis function, the parametrizations γ_i and γ_j , but independent of h_i and h_j .

Proof. Since the basis functions Φ_k and Ψ_ℓ and the parametrizations γ_i and γ_j are analytic, the kernel and hence the whole integrand is analytic on $\mathcal{E}_{\rho_1} \times [-1, 1]$ and $[-1, 1] \times \mathcal{E}_{\rho_2}$, respectively. In order to apply Theorem 2.2.17, it remains to estimate the maximum value of the integrand on the domains of analyticity.

Let $h(u, v)$ be defined as in (4.35) and $D = \max_{(u,v) \in [-1,1]^2} |h(u, v)|$. With the Cauchy-Schwartz inequality we obtain

$$\begin{aligned} \frac{|h(u, v)^T \nu_j(v)|}{|h(u, v)|^2} &\leq \frac{1}{|h(u, v)|} \\ \frac{|h(u, v)^T \tau_j(v)|}{|h(u, v)|^2} &\leq \frac{1}{|h(u, v)|}. \end{aligned}$$

Hence, the kernel can be bounded by

$$\max_{(u,v) \in [-1,1] \times \partial \mathcal{E}_{\rho_2}} \left| \frac{1-v}{2} \hat{K}_1(u, v) \right| \leq \alpha_1 |\log D| + \alpha_2 \frac{1}{D}, \quad (4.42)$$

where the constants $\alpha_1 > 0$ and $\alpha_2 > 0$ depend on the parametrizations γ_i and γ_j . With Lemma 3.2.12 we get

$$\begin{aligned} \max_{(u,v) \in [-1,1] \times \partial \mathcal{E}_{\rho_2}} \left| \dot{\gamma}_i \left(\frac{(1+u)(1-v)}{2} - 1 \right) \right| &\leq \alpha_3 h_i \\ \max_{(u,v) \in [-1,1] \times \partial \mathcal{E}_{\rho_2}} |\dot{\gamma}_j(v)| &\leq \alpha_4 h_j. \end{aligned} \quad (4.43)$$

Similar estimates to (4.42) and (4.43) can be proven on $\partial \mathcal{E}_{\rho_1} \times [-1, 1]$.

With Theorem 2.2.17 there exist constants C_1 and C_2 independent of h_i and h_j , but depending on γ_i, γ_j , and D , such that

$$|R_n| \leq h_i h_j \left(C_1 \rho_1^{-2n_1-1} + C_2 \rho_2^{-2n_2-1} \right).$$

□

For the integral corresponding to the second term in (4.34), which is evaluated with a combination of Gauss-Legendre and Gauss-Log quadratures, the next lemma gives an upper bound for the quadrature error.

Lemma 4.3.15. *Let $n \in \mathbb{N}^2$ and $\rho_i, \rho_j > 1$ as defined in Definition 3.2.9 and $1 < \rho_1 < \rho_i$ and $1 < \rho_2 < \min\{\rho_i, \rho_j\}$. Further, let $|R_n|$ denote the absolute error of the Gauss-Legendre and Gauss-Log quadrature rules applied to the integral*

$$\int_{-1}^1 \log\left(\frac{1-v}{2}\right) \int_{-1}^1 \frac{1-v}{2} \hat{K}_2(u, v) \Phi_k\left(\frac{(1+u)(1-v)}{2} - 1\right) \Psi_\ell(v) \left| \dot{\gamma}_i\left(\frac{(1+u)(1-v)}{2} - 1\right) \right| |\dot{\gamma}_j(v)| du dv.$$

Then, there holds

$$|R_n| \leq h_i h_j \left(C_1 \rho_1^{-2n_1-1} + C_2 \rho_2^{-2n_2-1} \right) \quad (4.44)$$

with constants $C_1, C_2 > 0$ depending of the parametrizations γ_1 and γ_j , but independent of h_i and h_j .

Proof. Let $\omega(v) := \log\left(\frac{1-v}{2}\right)$ be the weight function of the Gauss-Log quadrature rule in v -direction.

By assumption $\hat{K}_2(u, v) = g_1\left(\gamma_i\left(\frac{(1+u)(1-v)}{2} - 1\right) - \gamma_j(v)\right)$ is analytically extendable on $\mathcal{E}_{\rho_1} \times [-1, 1]$ and $[-1, 1] \times \mathcal{E}_{\rho_2}$. Since the basis functions and the local parametrizations are also analytic on these domains, the whole integrand (except for the weight function ω) is analytic and Theorem 2.2.17 can be applied. With (4.43) and the boundedness of the basis functions and $\hat{K}_2(u, v)$, we obtain

$$|R_n| \leq h_i h_j \left(C_1 \rho_1^{-2n_1-1} + C_2 \rho_2^{-2n_2-1} \right)$$

and conclude the proof. \square

Corollary 4.3.16. *For the polynomial basis functions used for NURBS-enhanced BEM, we obtain for (4.41) and (4.44)*

$$|R_n| \leq h_i h_j \left(\tilde{C}_1 \rho_1^{-2n_1+k-1} + \tilde{C}_2 \rho_2^{-2n_2+k+\ell-1} \right).$$

Here, the constants \tilde{C}_1, \tilde{C}_2 are also independent of the polynomial degrees k and ℓ of the basis functions.

Proof. The statement follows directly from the estimates given in Lemmas 2.1.9 (vi) and 2.1.11 (iv). \square

4. Numerical Integration for High-Order NURBS-Based BEM

NURBS-Enhanced BEM. For neighboring elements T_i and T_j with affine parametrizations and polynomial basis functions, we present an analytic method for the computation of the Galerkin entries based on the coordinate transformation introduced above, which provides an alternative to the evaluation presented in [Ban13]. We exploit the fact that for affine parametrizations we can split the kernel function into terms of u and v . Therefore, the integral can be split in a singular integral, a nearly singular integral and a regular integral, which can be treated separately.

For simplicity, we only consider the logarithmic part in the representation of the kernel function, i.e.

$$I_{k,\ell} := \frac{|T_i||T_j|}{4} \int_{-1}^1 \int_{-1}^1 \log \left| \gamma_i \left(\frac{(1+u)(1-v)}{2} - 1 \right) - \gamma_j(v) \right| P_k \left(\frac{(1+u)(1-v)}{2} - 1 \right) P_\ell(v) \frac{1-v}{2} dudv.$$

For linear elements, we obtain with the Taylor expansion (4.35)

$$\gamma_i \left(\frac{(1+u)(1-v)}{2} - 1 \right) - \gamma_j(v) = (1-v) \left(\dot{\gamma}_i(-1) \frac{1+u}{2} + \dot{\gamma}_j(1) \right). \quad (4.45)$$

Therefore, we get

$$\begin{aligned} & \left| \gamma_i \left(\frac{(1+u)(1-v)}{2} - 1 \right) - \gamma_j(v) \right|^2 \\ &= (1-v)^2 \left(\frac{|\dot{\gamma}_i(-1)|^2}{4} (1+u)^2 + (1+u) \dot{\gamma}_i(-1)^T \dot{\gamma}_j(1) + |\dot{\gamma}_j(1)|^2 \right) \\ &= |\dot{\gamma}_i(-1)|^2 \frac{(1-v)^2}{4} (z-u)(\bar{z}-u), \end{aligned}$$

where the complex zero z is given by

$$\begin{aligned} z &= \frac{-\dot{\gamma}_i(-1)^T \dot{\gamma}_j(1) - \sqrt{(\dot{\gamma}_i(-1)^T \dot{\gamma}_j(1))^2 - |\dot{\gamma}_i(-1)|^2 |\dot{\gamma}_j(1)|^2}}{1/2 |\dot{\gamma}_i(-1)|^2} - 1 \\ &= \frac{-2 \dot{\gamma}_i(-1)^T \dot{\gamma}_j(1) - 2i (\dot{\gamma}_i(-1) \times \dot{\gamma}_j(1))}{|\dot{\gamma}_i(-1)|^2} - 1. \end{aligned} \quad (4.46)$$

Remark 4.3.17. The representation (4.46) of z shows, that for collinear elements T_i and T_j there holds $z \in \mathbb{R}$. Furthermore, if the angle between both elements vanishes and $|T_j| \leq |T_i|$ then $z \in [-1, 1]$, i.e. for identical elements with $\gamma_i(s) = \gamma_j(-s)$ we obtain $z = 1$. Hence, apart from the singular edge $v = -1$ we obtain a second singular edge $u = 1$ in the integration domain.

Splitting the logarithmic term, we obtain for $I_{k,\ell}$

$$\begin{aligned} I_{k,\ell} &= \frac{|T_i||T_j|}{4} \left(\log(|\dot{\gamma}_i(-1)|^2) \int_{-1}^1 \int_{-1}^1 P_k \left(\frac{(1+u)(1-v)}{2} - 1 \right) P_\ell(v) \frac{1-v}{2} dudv \right. \\ &\quad + 2 \int_{-1}^1 \int_{-1}^1 \log \left(\frac{1-v}{2} \right) P_k \left(\frac{(1+u)(1-v)}{2} - 1 \right) P_\ell(v) \frac{1-v}{2} dudv \\ &\quad \left. + \int_{-1}^1 \int_{-1}^1 \log((z-u)(\bar{z}-u)) P_k \left(\frac{(1+u)(1-v)}{2} - 1 \right) P_\ell(v) \frac{1-v}{2} dudv \right) \\ &=: \frac{|T_i||T_j|}{4} \left(I_{k,\ell}^{(1)} + 2 I_{k,\ell}^{(2)} + I_{k,\ell}^{(3)} \right). \end{aligned}$$

While the first integral $I_{k,\ell}^{(1)}$ is regular, the second integral $I_{k,\ell}^{(2)}$ contains the logarithmic singularity. The last integral $I_{k,\ell}^{(3)}$ contains the nearly singular part, which is responsible for the slow convergence of quadrature rules if z is positioned close to the interval $[-1, 1]$.

We discuss the evaluation of all three integrals separately and start with deriving analytic formulas for $I_{k,\ell}^{(1)}$ in the next lemma.

Lemma 4.3.18. *For $k, \ell \in \mathbb{N}_0$, there holds*

$$\begin{aligned} &\int_{-1}^1 \int_{-1}^1 P_k \left(\frac{(1+u)(1-v)}{2} - 1 \right) P_\ell(v) \frac{1-v}{2} dudv \\ &= \begin{cases} 2, & k = \ell = 0 \\ (-1)^{k+1} \left(\delta_{k,\ell-1} \frac{2}{(2k+1)(2k+3)} - \delta_{k,\ell+1} \frac{2}{(2\ell+1)(2\ell+3)} \right), & k \geq 1, \ell \geq 1 \end{cases} \end{aligned}$$

For the second integral, we apply a Gauss-Log quadrature in v and a Gauss-Legendre quadrature in u . Since $P_k \left(\frac{(1+u)(1-v)}{2} - 1 \right) P_\ell(v) \frac{1-v}{2} \in \mathcal{P}_k([-1, 1])$ with respect to u and $P_k \left(\frac{(1+u)(1-v)}{2} - 1 \right) P_\ell(v) \frac{1-v}{2} \in \mathcal{P}_{k+\ell+1}([-1, 1])$ with respect to v , we choose the quadrature order according to $n = (\lceil \frac{k+1}{2} \rceil, \lceil \frac{k+\ell}{2} \rceil + 1)$, such that $I_{k,\ell}^{(2)}$ is integrated exactly.

For the third integral, we write

$$P_k \left(\frac{(1+u)(1-v)}{2} - 1 \right) = \sum_{\mu=0}^k \alpha_\mu^{(k)}(v) P_\mu(u).$$

The coefficients can be computed with the discrete cosine transform according to Algorithm 4.2.

Plugging in the Legendre expansion we obtain

$$\begin{aligned} I_{k,\ell}^{(3)} &= \sum_{\mu=0}^k \int_{-1}^1 \alpha_\mu^{(k)}(v) P_\ell(v) \frac{1-v}{2} dv \int_{-1}^1 \log((z-u)(\bar{z}-u)) P_\mu(u) du \\ &= 2 \sum_{\mu=0}^k \int_{-1}^1 \alpha_\mu^{(k)}(v) P_\ell(v) \frac{1-v}{2} dv \operatorname{Re} \left(\int_{-1}^1 \log(z-u) P_\mu(u) du \right) \\ &= 2 \sum_{\mu=0}^k \int_{-1}^1 \alpha_\mu^{(k)}(v) P_\ell(v) \frac{1-v}{2} dv \operatorname{Re} \left(\tilde{Q}_\mu^{-1}(z) \right), \end{aligned}$$

4. Numerical Integration for High-Order NURBS-Based BEM

where the modified associated Legendre functions of second kind $\tilde{Q}_\mu^{-1}(z)$ are defined as in Definition 4.2.12.

Remark 4.3.19. (i) Only the third integral $I_{k,\ell}^{(3)}$ depends on the mutual position of T_i and T_j and has to be computed for all combinations of neighboring elements. However, the integrals $I_{k,\ell}^{(1)}$ and $I_{k,\ell}^{(2)}$ only depend on the basis functions and can be precomputed once for the maximum polynomial degree.

(ii) The functions $\tilde{Q}_\mu^{-1}(z)$ are also defined for $z \in \mathbb{C} \setminus \{-1, 1\}$ and can be extended to $z = \pm 1$ in the sense of the Hadamard finite parts. Therefore, the case of identical elements can be treated similarly and has not to be distinguished for this special setting of linear elements.

(iii) This approach can also be extended to the algebraic terms of the kernel function, by applying the partial fraction decomposition proven in Lemma 4.2.16. Here, the algebraic singularity is cancelled out by the Jacobi determinant of the transformation and only the nearly singular integral has to be evaluated.

4.3.3. Identical Elements

In the case of identical elements $T_i = T_j$ with $\gamma_i = \gamma_j$, the kernel has an edge singularity on the diagonal, i.e. for $s = t$. In order to regularize the integrand we introduce the following transformation:

$$\begin{aligned} \int_{-1}^1 \int_{-1}^1 f(s, t) \, ds \, dt &= \int_{-1}^1 \int_{-1}^1 f\left(\theta_1(u, v), \theta_2(u, v)\right) \frac{1-v}{2} \, du \, dv \\ &\quad + \int_{-1}^1 \int_{-1}^1 f\left(\theta_2(u, v), \theta_1(u, v)\right) \frac{1-v}{2} \, du \, dv. \end{aligned} \quad (4.47)$$

with

$$\theta_1(u, v) := \frac{(1+u)(1-v)}{2} - 1 \quad \text{and} \quad \theta_2(u, v) = 1 - \frac{(1-u)(1-v)}{2}. \quad (4.48)$$

Figure 4.6 shows the geometrical interpretation of the transformation. In the first step the integration domain is rotated and split along the singular diagonal. Second, both triangles are transformed to the unit square by a transformation, which is similar to the one introduced in [Duf82]. In the last step, the second square is flipped horizontal such that the bottom edge is the singular edge. For both transformations, the Jacobian determinant is given by $\frac{1-v}{2}$ which implies (4.47).

Remark 4.3.20. While for neighboring elements the Jacobian determinant of the transformation cancels out the algebraic singularities, this is not true for the transformation introduced in (4.48). However, we will proof in the sequel that this transformation also regularizes the algebraic edge

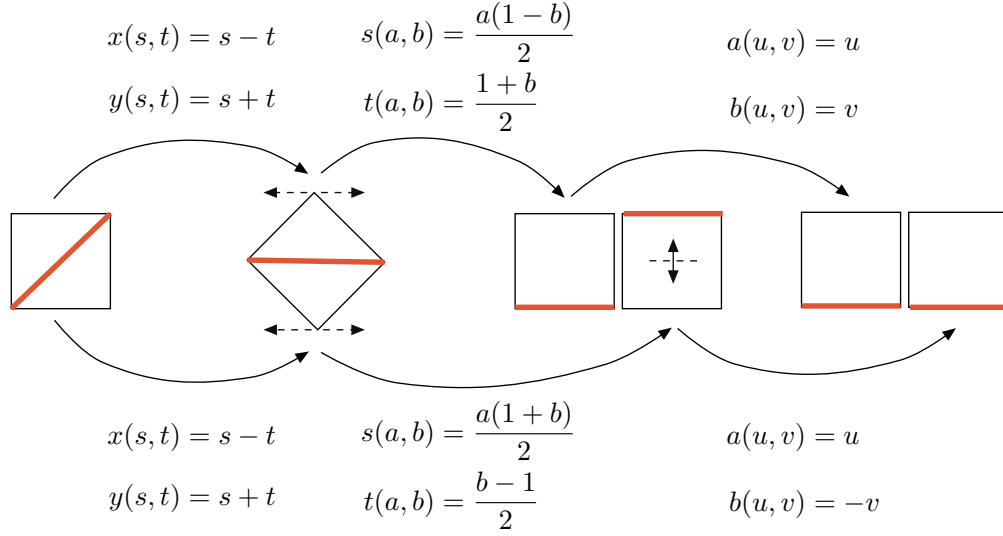


Figure 4.6.: Coordinate transformation for identical elements. The singular edges are depicted in red.

singularity of the kernel K , whereby the singular parts are cancelled out by adding up both integrands. For the logarithmic singularity, we proceed similarly to the case of neighboring elements and introduce the following splitting for the transformation of the upper triangle

$$\begin{aligned} \log |\gamma_i(\theta_1(u, v)) - \gamma_i(\theta_2(u, v))| &= \log \frac{2 |\gamma_i(\theta_1(u, v)) - \gamma_i(\theta_2(u, v))|}{v+1} \\ &+ \log \left(\frac{v+1}{2} \right). \end{aligned} \quad (4.49)$$

A similar splitting is introduced for the lower triangle. We prove that the first part is regular while the second part contains the logarithmic singularity.

The regular parts of the kernel function, i.e. the algebraic terms in (4.26) as well as the first logarithmic term in (4.49), are evaluated by a tensor Gauss-Legendre quadrature. The second term in (4.49) is evaluated with a combination of Gauss-Legendre quadrature in u and a Gauss-Log quadrature in v , where the logarithmic singularity is considered to be the weight function. For notational convenience we define

$$\begin{aligned} K\left(\theta_1(u, v), \theta_2(u, v)\right) &=: \hat{K}_1^{(1)}(u, v) + \hat{K}_2^{(1)}(u, v) \log \left(\frac{1+v}{2} \right), \\ K\left(\theta_2(u, v), \theta_1(u, v)\right) &=: \hat{K}_1^{(2)}(u, v) + \hat{K}_2^{(2)}(u, v) \log \left(\frac{1+v}{2} \right), \end{aligned} \quad (4.50)$$

where $\hat{K}_1^{(1)}(u, v)$ and $\hat{K}_1^{(2)}(u, v)$ contain the parts of the kernel that are evaluated with the Gauss-Legendre quadrature.

4. Numerical Integration for High-Order NURBS-Based BEM

In the remainder of this section, we proof the analyticity of the integrand for identical elements and derive upper bounds for the quadrature errors. In particular, we prove the exponential decay of the quadrature error with respect to the quadrature order. Therefore, we need the following preliminary result.

Proposition 4.3.21. *Let \mathcal{E}_ρ denote the ellipse with semi axis sum $\rho > 1$ as defined in Definition 2.0.9 and θ_1 and θ_2 as defined in (4.48). Then, there holds*

$$\theta_1([-1, 1], \mathcal{E}_\rho) \subset \mathcal{E}_\rho, \quad \theta_1(\mathcal{E}_\rho, [-1, 1]) \subset \mathcal{E}_\rho$$

and

$$\theta_2([-1, 1], \mathcal{E}_\rho) \subset \mathcal{E}_\rho, \quad \theta_2(\mathcal{E}_\rho, [-1, 1]) \subset \mathcal{E}_\rho.$$

Proof. The statements can be proven with similar arguments as used in the proof of Proposition 4.3.11. \square

Lemma 4.3.22. *Let \mathcal{E}_{ρ_i} as defined in Definition 3.2.9 and $\hat{K}_1^{(1)}(u, v)$ and $\hat{K}_1^{(2)}(u, v)$ as defined in (4.50). Then, $\hat{K}_1^{(1)}(u, v)$ and $\hat{K}_1^{(2)}(u, v)$ are analytically extendable to $[-1, 1] \times (\mathcal{E}_{\rho_i} \setminus \{-1\})$ and $\mathcal{E}_{\rho_i} \times (-1, 1]$ and contain a simple pole for $v = -1$.*

Proof. We only proof the statement for $\hat{K}_1^{(1)}(u, v)$, the proof for $\hat{K}_1^{(2)}(u, v)$ is similar.

Due to Definition 3.2.9 γ_i is analytically extendable to \mathcal{E}_{ρ_i} . Proposition 4.3.21 implies that $\gamma_i(\theta_1(u, v))$ and $\gamma_i(\theta_2(u, v))$ are analytically extendable to $[-1, 1] \times \mathcal{E}_{\rho_i}$ and $\mathcal{E}_{\rho_i} \times [-1, 1]$. Since, by assumption, the coefficient functions g_μ , $\mu = 0, \dots, 3$, in (4.26) are analytic, the expression

$$g_\mu(\gamma_i(\theta_1(u, v)) - \gamma_i(\theta_2(u, v))), \quad \mu = 0, \dots, 3,$$

is analytically extendable to $[-1, 1] \times \mathcal{E}_{\rho_i}$ and $\mathcal{E}_{\rho_i} \times [-1, 1]$. Hence, it remains to investigate the logarithmic and the algebraic terms in the representation (4.26) of the kernel.

Due to Lemma 4.2.3 γ_i is injective on \mathcal{E}_{ρ_i} . Hence, for fixed $(s, t) \in [-1, 1] \times \mathcal{E}_{\rho_i}$ and $(s, t) \in \mathcal{E}_{\rho_i} \times [-1, 1]$, $\gamma_i(s) - \gamma_i(t) = 0$ if and only if $s = t$. Plugging in the transformation we get

$$\theta_1(u, v) = \theta_2(u, v) \Leftrightarrow v = -1.$$

Hence, the logarithmic term in the splitting (4.49)

$$\log \left(\frac{|\gamma_i(\theta_1(u, v)) - \gamma_i(\theta_2(u, v))|}{|1 + v|} \right)$$

is analytically extendable on $\mathcal{E}_{\rho_i} \times [-1, 1]$ and $[-1, 1] \times \mathcal{E}_{\rho_i}$. The algebraic terms

$$\frac{(\gamma_i(\theta_1(u, v)) - \gamma_i(\theta_2(u, v)))^T \nu_i(\theta_2(u, v))}{|\gamma_i(\theta_1(u, v)) - \gamma_i(\theta_2(u, v))|^2} \quad \text{and} \quad \frac{(\gamma_i(\theta_1(u, v)) - \gamma_i(\theta_2(u, v)))^T \tau_i(\theta_2(u, v))}{|\gamma_i(\theta_1(u, v)) - \gamma_i(\theta_2(u, v))|^2}$$

contain a pole for $v = -1$. With the Taylor series of $\gamma_i(s)$ at t and plugging in the transformation (4.48), we obtain

$$\gamma_i(\theta_1(u, v)) - \gamma_i(\theta_2(u, v)) = (v + 1) (\dot{\gamma}_i(\theta_2(u, v)) + \ddot{\gamma}_i(\theta_2(u, v))(v + 1) + \mathcal{O}((v + 1)^2)).$$

Plugging in the Taylor series, the algebraic terms read

$$\frac{(\gamma_i(\theta_1(u, v)) - \gamma_i(\theta_2(u, v)))^T \nu_i(\theta_2(u, v))}{|\gamma_i(\theta_1(u, v)) - \gamma_i(\theta_2(u, v))|^2} = \frac{(\dot{\gamma}_i(\theta_2(u, v)) + \mathcal{O}(v + 1))^T \nu_i(\theta_2(u, v))}{|\dot{\gamma}_i(\theta_2(u, v)) + \mathcal{O}(v + 1)|^2}$$

and

$$\frac{(\gamma_i(\theta_1(u, v)) - \gamma_i(\theta_2(u, v)))^T \tau_i(\theta_2(u, v))}{|\gamma_i(\theta_1(u, v)) - \gamma_i(\theta_2(u, v))|^2} = \frac{1}{v + 1} \frac{(\dot{\gamma}_i(\theta_2(u, v)) + \mathcal{O}(v + 1))^T \tau_i(\theta_2(u, v))}{|\dot{\gamma}_i(\theta_2(u, v)) + \mathcal{O}(v + 1)|^2}.$$

Note that we use $\gamma_i(t)^T \nu_i(t) = 0$ for the first term. Hence, $\hat{K}_1(u, v)$ contains a simple pole for $v = -1$. \square

Corollary 4.3.23. *The expression $\hat{K}_1^{(1)}(u, v) + \hat{K}_1^{(2)}(u, v)$ is analytically extendable to $\mathcal{E}_{\rho_i} \times [-1, 1]$ and $[-1, 1] \times \mathcal{E}_{\rho_i}$.*

Proof. Due to the proof of Lemma 4.3.22 we only investigate the term of $\hat{K}_1^{(1)}(u, v) + \hat{K}_1^{(2)}(u, v)$, which contains the algebraic singularity, i.e.

$$\begin{aligned} f(u, v) &:= \frac{1}{v + 1} \left(g_3(\theta_1(u, v) - \theta_2(u, v)) \frac{(\dot{\gamma}_i(\theta_2(u, v)) + \mathcal{O}(v + 1))^T \tau_i(\theta_2(u, v))}{|\dot{\gamma}_i(\theta_2(u, v)) + \mathcal{O}(v + 1)|^2} \right. \\ &\quad \left. + g_3(\theta_2(u, v) - \theta_1(u, v)) \frac{(-\dot{\gamma}_i(\theta_2(u, v)) - \mathcal{O}(v + 1))^T \tau_i(\theta_1(u, v))}{|\dot{\gamma}_i(\theta_1(u, v)) + \mathcal{O}(v + 1)|^2} \right) \\ &= \frac{g_3(\theta_1(u, v) - \theta_2(u, v))}{v + 1} \left(\frac{(\dot{\gamma}_i(\theta_2(u, v)) + \mathcal{O}(v + 1))^T (\tau_i(\theta_2(u, v)) - \tau_i(\theta_1(u, v)))}{|\dot{\gamma}_i(\theta_2(u, v)) + \mathcal{O}(v + 1)|^2} \right), \end{aligned}$$

where we used the symmetry property of g_3 . Since $\theta_1(u, -1) = \theta_2(u, -1) = u$, the term in brackets vanishes as $v \rightarrow -1$ and hence $\lim_{v \rightarrow -1} f(u, v) < \infty$. \square

We are now in the position to give an estimate for the integral that is evaluated with the tensor Gauss-Legendre quadrature.

Lemma 4.3.24. *Let $n \in \mathbb{N}^2$, \mathcal{E}_{ρ_i} as defined in Definition 3.2.9, $1 < \rho < \rho_i$, and Φ_k and Ψ_ℓ denote the basis functions introduced in Definitions 3.2.3 and 3.2.5. Further, let $\hat{K}_1^{(1)}(u, v)$ and $\hat{K}_1^{(2)}(u, v)$ be as defined in (4.50) and $|R_n|$ denote the absolute error of the n -th order Gauss-Legendre quadrature applied to the integral*

$$\begin{aligned} &\int_{-1}^1 \int_{-1}^1 \left[\hat{K}_1^{(1)}(u, v) \Phi_k(\theta_1(u, v)) \Psi_\ell(\theta_2(u, v)) \right. \\ &\quad \left. + \hat{K}_1^{(2)}(u, v) \Phi_k(\theta_2(u, v)) \Psi_\ell(\theta_1(u, v)) \right] |\dot{\gamma}_i(\theta_1(u, v))| |\dot{\gamma}_i(\theta_2(u, v))| \frac{1 - v}{2} du dv. \end{aligned}$$

4. Numerical Integration for High-Order NURBS-Based BEM

Then, there exist constants $C_1, C_2 > 0$ independent of h_i such that

$$|R_n| \leq h_i^2 (C_1 \rho^{-2n_1-1} + C_2 \rho^{-2n_2-1}). \quad (4.51)$$

Proof. With Lemma 4.3.22 and Corollary 4.3.23 and the analyticity of the basis functions, the integrand is analytic on $[-1, 1] \times \mathcal{E}_\rho$ and $\mathcal{E}_\rho \times [-1, 1]$, respectively. Since the basis functions Φ_k and Ψ_ℓ and the terms $\hat{K}_1^{(1)}$ and $\hat{K}_1^{(2)}$ are bounded on $[-1, 1] \times \mathcal{E}_\rho$ and $\mathcal{E}_\rho \times [-1, 1]$, we obtain with Lemma 3.2.12 that the integrand is bounded by $C_1 h_i^2$ on $\partial\mathcal{E}_\rho \times [-1, 1]$ and by $C_2 h_i^2$ on $[-1, 1] \times \partial\mathcal{E}_\rho$. Here, $C_1, C_2 > 0$ are independent of h_i . With Theorem 2.2.17 we obtain

$$|R_n| \leq h_i^2 (C_1 \rho^{-2n_1-1} + C_2 \rho^{-2n_2-1}).$$

□

For the integrals evaluated with the Gauss-Legendre and the Gauss-Log quadrature, the next Lemma gives an estimate for the absolute error.

Lemma 4.3.25. *Let $n \in \mathbb{N}^2$, \mathcal{E}_{ρ_i} as defined in Definition 3.2.9, $1 < \rho < \rho_i$, and Φ_k and Ψ_ℓ denote the basis functions introduced in Definitions 3.2.3 and 3.2.5. Further, let $\hat{K}_2^{(1)}(u, v)$ and $\hat{K}_2^{(2)}(u, v)$ be as defined in (4.50) and $|R_n|$ denote the absolute error of the n_1 -th order Gauss-Legendre quadrature in u and the n_2 -th order Gauss-Log quadrature in v applied to*

$$\int_{-1}^1 \int_{-1}^1 \left[\hat{K}_2^{(1)}(u, v) \Phi_k(\theta_1(u, v)) \Psi_\ell(\theta_2(u, v)) + \hat{K}_2^{(2)}(u, v) \Phi_k(\theta_2(u, v)) \Psi_\ell(\theta_1(u, v)) \right] |\dot{\gamma}_i(\theta_1(u, v))| |\dot{\gamma}_i(\theta_2(u, v))| \frac{1-v}{2} \log \left(\frac{1+v}{2} \right) du dv.$$

Then, there exist $C_1, C_2 > 0$ independent of h_i such that

$$|R_n| \leq h_i^2 (C_1 \rho^{-2n_1-1} + C_2 \rho^{-2n_2-1}). \quad (4.52)$$

Proof. For the Gauss-Log quadrature the weight function is given by $\omega(x) = \log \left(\frac{1+x}{2} \right)$. By assumption the expressions

$$\begin{aligned} \hat{K}_2^{(1)}(u, v) &= g_1 (\gamma_i(\theta_1(u, v)) - \gamma_i(\theta_2(u, v))) \\ \hat{K}_2^{(2)}(u, v) &= g_1 (\gamma_i(\theta_2(u, v)) - \gamma_i(\theta_1(u, v))) \end{aligned}$$

and thus the integrand (except for the log-term) are analytic and bounded on $\mathcal{E}_\rho \times [-1, 1]$ and $[-1, 1] \times \mathcal{E}_\rho$. With Lemma 3.2.12 and Theorem 2.2.17 we obtain

$$|R_n| \leq h_i^2 (C_1 \rho^{-2n_1-1} + C_2 \rho^{-2n_2-1}).$$

□

Corollary 4.3.26. *For the polynomial basis functions used for NURBS-enhanced BEM, we obtain for (4.51) and (4.52)*

$$|R_n| \leq h_i^2 \left(\tilde{C}_1 \rho^{-2n_1+k+\ell-1} + \tilde{C}_2 \rho^{-2n_2+k+\ell-1} \right).$$

Here, the constants \tilde{C}_1, \tilde{C}_2 are also independent of the polynomial degrees k and ℓ of the basis functions.

Proof. The statement directly follows by the estimates given in Lemmas 2.1.9 (vi) and 2.1.11 (iv). \square

4.3.4. Consistency Error Analysis

After having discussed the computation of the Galerkin entries via interpolation and quadrature rules, we investigate the effect of the absolute errors in the Galerkin matrices on the consistency error in Strang's Lemma 1.6.4. We then give a priori estimates for the interpolation and quadrature orders, such that the induced consistency errors do not spoil the convergence rates of the Galerkin methods.

In the general framework of Section 1.6 we consider a Hilbert space X with its dual X' , $f \in X'$ and a linear and bounded operator $A : X \rightarrow X'$. We denote by $X_\ell \subset X$ one of the discrete ansatz spaces as defined in Definitions 3.2.3 and 3.2.5, and by $\{\Phi_1, \dots, \Phi_{\mathcal{N}}\}$ a basis of X_ℓ . The discrete variational formulation is given by

$$a(u_h, v_h) := \langle Au_h, v_h \rangle = \langle f, v_h \rangle \quad \forall v_h \in X_\ell.$$

Let $\mathcal{I} = \{1, \dots, \mathcal{N}\}$ be the set of all degrees of freedom. Writing $u_h = \sum_{k=1}^{\mathcal{N}} \mathbf{u}_k \Phi_k$ and $v_h = \sum_{k=1}^{\mathcal{N}} \mathbf{v}_k \Phi_k$, we obtain

$$a(u_h, v_h) = \sum_{j,k \in \mathcal{I}} \mathbf{u}_j \mathbf{A}_{j,k} \mathbf{v}_k = \mathbf{u}^T \mathbf{A} \mathbf{v}. \quad (4.53)$$

Here, \mathbf{A} denotes the Galerkin Matrix of the integral operator A , which is defined for all considered integral operators in Section 1.6.1. In a similar way we obtain for the perturbed sesquilinear form $\tilde{a}(u_h, v_h)$

$$\tilde{a}(u_h, v_h) = \sum_{j,k \in \mathcal{I}} \mathbf{u}_j \tilde{\mathbf{A}}_{j,k} \mathbf{v}_k = \mathbf{u}^T \tilde{\mathbf{A}} \mathbf{v}, \quad (4.54)$$

where $\tilde{\mathbf{A}}$ denotes the numerically computed Galerkin matrix. Strang's Lemma 1.6.4 implies that the consistency error, which is induced by the perturbed sesquilinear form \tilde{a} , is given by

$$\sup_{u_h, v_h \in X_\ell} \frac{|a(u_h, v_h) - \tilde{a}(u_h, v_h)|}{\|u_h\|_U \|v_h\|_X},$$

4. Numerical Integration for High-Order NURBS-Based BEM

where $\|\cdot\|_U$ is a stronger norm on X , i.e. $\|u_h\|_U \leq C\|u_h\|_X$ for all $u_h \in X_\ell$. The consistency error induced by the right-hand side is given by

$$\sup_{v_h \in X_\ell} \frac{|\langle f, v_h \rangle - \langle \tilde{f}, v_h \rangle|}{\|v_h\|_X},$$

Remark 4.3.27. (i) For the solution of Symm's integral equation (1.33), the operator $A := \mathcal{V}$ is the single layer operator. The Hilbert space involved is $X = H^{-1/2}(\Gamma)$, and the norm is given by $\|\cdot\|_X := \|\cdot\|_{H^{-1/2}(\Gamma)}$. Since all discrete ansatz spaces considered in this work are subsets of $L^2(\Gamma)$ we can choose the L^2 norm as stronger norm, i.e. $\|\cdot\|_U := \|\cdot\|_{L^2(\Gamma)}$. For the hypersingular integral equation, the operator $A := \mathcal{W}$ is the hypersingular integral operator. Since the variational formulation (1.36) is posed in $X := H^{1/2}(\Gamma)$ we choose $\|\cdot\|_X = \|\cdot\|_U = \|\cdot\|_{H^{1/2}(\Gamma)}$.

(ii) Throughout this section, we assume $\mathbf{p} > 0$.

Before we start with estimating the consistency error for Symm's and the hypersingular integral equation, we first state some preliminary results. In particular, for $u_h \in X_\ell$ we state an inverse-type inequality and proof the equivalence of the ℓ^2 norm of its coefficient vector \mathbf{u} and the L^2 norm.

The following lemma states an inverse-type inequality for the polynomial ansatz spaces. For the rational ansatz-spaces a corresponding result is still open.

Lemma 4.3.28 ([Geo07, Theorem 3.9]). *Let X_ℓ be a polynomial ansatz space, $0 < s < 1$, $-\infty < \underline{\alpha} < \overline{\alpha} < \infty$ and $-\infty < \underline{\beta} < \overline{\beta} < \infty$. Then, there holds*

$$\left\| \frac{\mathbf{h}^{s+\alpha}}{\mathbf{p}^{2s+\beta}} u_h \right\|_{L^2(\Gamma)} \lesssim \left\| \frac{\mathbf{h}^\alpha}{\mathbf{p}^\beta} u_h \right\|_{H^{-s}(\Gamma)}, \quad \forall u_h \in X_\ell \quad (4.55)$$

uniformly in $\alpha \in [\underline{\alpha}, \overline{\alpha}]$ and $\beta \in [\underline{\beta}, \overline{\beta}]$.

The following lemma, which is proven in [SaSch04, Corollary 5.3.28], shows the equivalence of the L^2 norm and the ℓ_2 norm $\|\cdot\|_2$ of the coefficient vector. The proof is cited here, as it is used to derive further estimates for the Legendre and Lobatto basis functions.

Lemma 4.3.29. *Let $T_i \in \mathcal{T}$ and γ_i be its NURBS parametrization, $\mathcal{I}_{T_i} := \{k \in \mathcal{I} : |\text{supp } \Phi_k \cap T_i| > 0\}$ and $|\mathcal{I}_{T_i}|$ denote the cardinality of \mathcal{I}_{T_i} . Further, let \mathbf{u}_{T_i} be the local coefficient vector of $u_h \in X_\ell$ on T_i . If $\max_{T \in \mathcal{T}} |\mathcal{I}_T| < \infty$ and the eigenvalues λ of*

$$\mathbf{M} := \left(\int_{-1}^1 (\Phi_k \circ \gamma_i)(t) (\Phi_j \circ \gamma_i)(t) dt \right)_{k,j \in \mathcal{I}_{T_i}}$$

satisfy $0 < \lambda_{\min} \leq \lambda \leq \lambda_{\max} < \infty$, then there holds

$$c\|u_h\|_{L^2(T_i)} \leq h_i^{1/2} \|\mathbf{u}_{T_i}\|_2 \leq C\|u_h\|_{L^2(T_i)}, \quad \forall u_h \in X_\ell. \quad (4.56)$$

The constants $c > 0$ and $C > 0$ are independent of h_i but still depending on the degree of the basis functions.

Proof. For $u_h|_{T_i} := \sum_{k \in \mathcal{I}_{T_i}} \mathbf{u}_k^{(T_i)} \Phi_k$, we obtain

$$\|u_h\|_{L^2(T_i)}^2 = \int_{T_i} \left(\sum_{k \in \mathcal{I}_{T_i}} \mathbf{u}_k^{(T_i)} \Phi_k(x) \right)^2 dx = \int_{-1}^1 \left(\sum_{k \in \mathcal{I}_{T_i}} \mathbf{u}_k^{(T_i)} (\Phi_k \circ \gamma_i)(t) \right)^2 |\dot{\gamma}_i(t)| dt.$$

With Lemma 3.2.12 and the definition of the matrix \mathbf{M} we obtain

$$\|u_h\|_{L^2(T_i)}^2 \geq \tilde{c} h_i \mathbf{u}_{T_i}^T \mathbf{M} \mathbf{u}_{T_i} \geq \tilde{c} h_i \lambda_{\min} \|\mathbf{u}_{T_i}\|_2^2.$$

$$\|u_h\|_{L^2(T_i)}^2 \leq \tilde{C} h_i \mathbf{u}_{T_i}^T \mathbf{M} \mathbf{u}_{T_i} \leq \tilde{C} h_i \lambda_{\max} \|\mathbf{u}_{T_i}\|_2^2.$$

□

Remark 4.3.30. The lemma stated above can be applied to all sets of bases that are considered in this work. Since the polynomial basis functions (Legendre, Lobatto and b-splines basis functions) form a basis on $\mathcal{P}_{p_i}([-1, 1])$ and the L^2 scalar product is a scalar product on $\mathcal{P}_{p_i}([-1, 1])$, the matrix \mathbf{M} is positive definite for these bases. For the NURBS basis functions we write

$$\begin{aligned} & \int_{-1}^1 \mathcal{R}_k \left(\frac{t+1}{2} (\zeta_{j-1} - \zeta_j) + \zeta_{j-1} \right) \mathcal{R}_j \left(\frac{t+1}{2} (\zeta_{j-1} - \zeta_j) + \zeta_{j-1} \right) dt \\ &= \int_{-1}^1 \omega_k \mathcal{B}_k \left(\frac{t+1}{2} (\zeta_{j-1} - \zeta_j) + \zeta_{j-1} \right) \omega_j \mathcal{B}_j \left(\frac{t+1}{2} (\zeta_{j-1} - \zeta_j) + \zeta_{j-1} \right) \frac{1}{(\omega(t))^2} dt \\ &=: (\omega_k \mathcal{B}_k, \omega_j \mathcal{B}_j)_{L_{\omega}^2(-1,1)}, \end{aligned}$$

where ω_j, ω_k denote the weights and $\omega(x)$ denotes the weight functions of the NURBS basis functions. Since $(\omega(x))^2 > 0$ we have a weighted scalar product $(\omega_k \mathcal{B}_k, \omega_j \mathcal{B}_j)_{L_{\omega}^2(-1,1)}$ on $\mathcal{P}_{p_i}([-1, 1])$, which yields the positivity of \mathbf{M} for the NURBS basis functions.

While the constants in Lemma 4.3.29 are independent of the arc length h_i , the eigenvalues λ_{\min} and λ_{\max} of \mathbf{M} still depend on the polynomial degree p_i of the basis functions. In order to obtain consistency estimates for uniform p - and hp -refinements for NURBS-enhanced BEM, we have to determine the dependency on p_i explicitly. A corresponding result is stated in the following corollary.

Corollary 4.3.31. *For the ansatz space $S(\mathcal{T}, \mathbf{h}, \mathbf{p}, \mathbf{0})$ spanned by the Legendre basis we obtain*

$$c \|u_h\|_{L^2(T_i)} \leq h_i^{1/2} \|\mathbf{u}_{T_i}\|_2 \leq C p_i^{1/2} \|u_h\|_{L^2(T_i)}, \quad \forall u_h \in X_{\ell}. \quad (4.57)$$

The constants are independent of h_i and p_i . For the discrete ansatz space $S(\mathcal{T}, \mathbf{h}, \mathbf{p}, \mathbf{1})$ spanned by the Lobatto basis, we get the following estimate

$$c \|u_h\|_{L^2(T_i)} \leq h_i^{1/2} \|\mathbf{u}_{T_i}\|_2 \leq C p_i^{5/2} \|u_h\|_{L^2(T_i)}, \quad \forall u_h \in X_{\ell} \quad (4.58)$$

with c, C independent of h_i and p_i .

4. Numerical Integration for High-Order NURBS-Based BEM

Proof. Since the independency of the constants of h_i is already proven in Lemma 4.3.29, we only need to proof the independency of p_i . Due to the orthogonality of the Legendre polynomials we obtain

$$\mathbf{M} := \left(\int_{-1}^1 P_k(t) P_j(t) dt \right)_{k,j=0,\dots,p_i} = \text{diag} \left(\frac{2}{2k+1}, k = 0, \dots, p_i \right).$$

Hence, the minimum and maximum eigenvalues of \mathbf{M} are given by $\lambda_{\min} = \frac{2}{2p_i+1} = \mathcal{O}(p_i^{-1})$ and $\lambda_{\max} = 2$, which directly implies the first inequality.

For the Lobatto shape functions, we first prove an inequality in the H^1 norm and then apply an estimate between the H^1 and L^2 norms. With the relationship (i) in Lemma 2.1.11, we obtain for the Lobatto shape functions

$$\mathbf{M} := \underbrace{\left(\begin{array}{cc|cccc} \frac{2}{3} & \frac{1}{3} & -\frac{1}{3} & \frac{1}{15} & 0 & \dots & 0 \\ \frac{1}{3} & \frac{2}{3} & -\frac{1}{3} & -\frac{1}{15} & 0 & \dots & 0 \\ \hline -\frac{1}{3} & -\frac{1}{3} & * & 0 & * & & 0 \\ \frac{1}{15} & -\frac{1}{15} & 0 & * & 0 & * & \\ 0 & 0 & * & 0 & * & 0 & * \\ \vdots & \vdots & & * & 0 & * & 0 \\ 0 & 0 & 0 & & * & 0 & * \end{array} \right)}_{\widetilde{\mathbf{M}}},$$

where the matrix $\widetilde{\mathbf{M}}$ is given by

$$\begin{aligned} \widetilde{\mathbf{M}}_{j,k} &= \frac{4}{(2k+3)(2k+1)(2k-1)} \delta_{j,k} \\ &\quad - \frac{2}{(2k+5)(2k+3)(2k+1)} \delta_{j,k+2} - \frac{2}{(2k+1)(2k-1)(2k-3)} \delta_{j,k-2}. \end{aligned}$$

Furthermore, we define the matrix \mathbf{A} by

$$\mathbf{A} := \left(\int_{-1}^1 N'_j(t) N'_k(t) dt \right)_{j,k=1,\dots,p_i+1}.$$

With the definition of the Lobatto shape functions and the orthogonality of the Legendre polynomials, we get

$$\mathbf{A} := \underbrace{\left(\begin{array}{cc|ccc} \frac{1}{2} & -\frac{1}{2} & 0 & \dots & 0 \\ -\frac{1}{2} & \frac{1}{2} & 0 & \dots & 0 \\ \hline 0 & 0 & * & & 0 \\ \vdots & \vdots & & * & \\ 0 & 0 & 0 & & * \end{array} \right)}_{\widetilde{\mathbf{A}}},$$

with $\tilde{\mathbf{A}}_{j,k} = \text{diag} \left(\frac{2}{2k+1} \right)$. For $u_h \in S(\mathcal{T}, \mathbf{h}, \mathbf{p}, \mathbf{1})$ we get

$$\|u_h\|_{H^1(T_i)}^2 = \|u_h\|_{L^2(T_i)}^2 + \|u_h'\|_{L^2(T_i)}^2 \geq \lambda_{\min} \|\mathbf{u}\|_2^2 \quad (4.59)$$

$$\|u_h\|_{H^1(T_i)}^2 = \|u_h\|_{L^2(T_i)}^2 + \|u_h'\|_{L^2(T_i)}^2 \leq \lambda_{\max} \|\mathbf{u}\|_2^2. \quad (4.60)$$

Here, λ_{\min} and λ_{\max} denote the minimum and maximum eigenvalues of $(\mathbf{A} + \mathbf{M})$. Applying Gershgorin's Theorem [Sch88] we can estimate the minimum eigenvalue by

$$\begin{aligned} \lambda_{\min} &\geq \min \left\{ \frac{3}{5}, \frac{26}{105}, \frac{4 + 2(2p_i + 3)(2p_i - 1)}{(2p_i + 3)(2p_i + 1)(2p_i - 1)} - \frac{2}{(2p_i + 1)(2p_i - 1)(2p_i - 3)} \right\} \\ &= \mathcal{O}(p_i^{-1}) \end{aligned} \quad (4.61)$$

and the maximum eigenvalue by

$$\begin{aligned} \lambda_{\max} &\leq \max \left\{ \frac{26}{15}, \frac{34}{21}, \frac{4 + 2(2p_i + 3)(2p_i - 1)}{(2p_i + 3)(2p_i + 1)(2p_i - 1)} + \frac{2}{(2p_i + 1)(2p_i - 1)(2p_i - 3)} \right\} \\ &\leq 2. \end{aligned} \quad (4.62)$$

With Equations (4.59), (4.61), and the inverse inequality proven in [Geo07, Theorem 3.3], we get

$$\|\mathbf{u}\|_2 \leq \tilde{C} p_i^{1/2} \|u_h\|_{H^1(T_i)} \leq C p_i^{5/2} \|u_h\|_{L^2(T_i)}.$$

With Equations (4.60), (4.62), and the Poincaré inequality $\|u_h'\|_{L^2(T_i)} \geq \bar{c} \|u_h\|_{L^2(T_i)}$, which is proven in [Sch98, Theorem A.25], we get

$$\|\mathbf{u}\|_2 \geq \tilde{c} \|u_h\|_{H^1(T_i)} \geq c \|u_h\|_{L^2(T_i)}.$$

Both constants $c, C > 0$ are independent of p_i . \square

We are now in the position to give an estimate of the consistency error for Symm's and the hypersingular integral equations, where we restrict to the polynomial ansatz spaces $S(\mathcal{T}, \mathbf{h}, \mathbf{p}, \mathbf{k})$.

Symm's integral equation. The following lemma gives an estimate how the absolute quadrature error in the Galerkin matrix of the single layer operator affects the consistency error of the sesquilinear form.

Lemma 4.3.32. *If the absolute error in the Galerkin entries of the single layer operator \mathbf{V} is bounded by*

$$|\mathbf{V}_{jk} - \tilde{\mathbf{V}}_{jk}| \leq \varepsilon h_j^{1/2} h_k, \quad j, k \in \mathcal{I},$$

then the induced consistency error of the sesquilinear form is bounded by

$$\frac{|a(u_h, v_h) - \tilde{a}(u_h, v_h)|}{\|u_h\|_{L^2(\Gamma)} \|v_h\|_{H^{-1/2}(\Gamma)}} \lesssim \mathcal{N} \varepsilon.$$

The constant is independent of \mathbf{h} but still depending on \mathbf{p} .

4. Numerical Integration for High-Order NURBS-Based BEM

Proof. With the Cauchy-Schwartz inequality we obtain

$$\begin{aligned} |a(u_h, v_h) - \tilde{a}(u_h, v_h)| &\leq \varepsilon \sum_{j \in \mathcal{I}} h_j^{1/2} |\mathbf{u}_j| \sum_{k \in \mathcal{I}} h_k |\mathbf{v}_k| \\ &\leq \varepsilon \left(\sum_{j \in \mathcal{I}} h_j |\mathbf{u}_j|^2 \right)^{1/2} \left(\sum_{k \in \mathcal{I}} h_k^2 |\mathbf{v}_k|^2 \right)^{1/2} |\mathcal{I}|. \end{aligned} \quad (4.63)$$

With Lemma 4.3.29 we obtain for the first sum in (4.63)

$$\begin{aligned} \sum_{j \in \mathcal{I}} h_j |\mathbf{u}_j|^2 &= \sum_{T_i \in \mathcal{T}} h_i \sum_{k \in \mathcal{I}_{T_i}} |\mathbf{u}_k|^2 \\ &\lesssim \sum_{T_i \in \mathcal{T}} \|u_h\|_{L^2(T_i)}^2 = \|u_h\|_{L^2(\Gamma)}^2. \end{aligned}$$

For the second sum in (4.63) we additionally apply the inverse inequality (4.55) and obtain

$$\begin{aligned} \sum_{k \in \mathcal{I}} h_k^2 |\mathbf{v}_k|^2 &\lesssim \sum_{T_i \in \mathcal{T}} h_i \|v_h\|_{L^2(T_i)}^2 = \sum_{T_i \in \mathcal{T}} \|h_i^{1/2} v_h\|_{L^2(T_i)}^2 \\ &= \|\mathbf{h}^{1/2} v_h\|_{L^2(\Gamma)}^2 \lesssim \|v_h\|_{H^{-1/2}(\Gamma)}^2. \end{aligned} \quad (4.64)$$

Hence, we get

$$\frac{|a(u_h, v_h) - \tilde{a}(u_h, v_h)|}{\|u_h\|_{L^2(\Gamma)} \|v_h\|_{H^{-1/2}(\Gamma)}} \lesssim \mathcal{N}\varepsilon.$$

□

Corollary 4.3.33. *If the absolute error in the Galerkin entries of the single layer operator \mathbf{V} with respect to the Legendre basis is bounded by*

$$|\mathbf{V}_{jk} - \tilde{\mathbf{V}}_{jk}| \leq \varepsilon h_j^{1/2} p_j^{-1/2} h_k p_k^{-3/2}, \quad j, k \in \mathcal{I},$$

then the induced consistency error of the sesquilinear form is given by

$$\frac{|a(u_h, v_h) - \tilde{a}(u_h, v_h)|}{\|u_h\|_{L^2(\Gamma)} \|v_h\|_{H^{-1/2}(\Gamma)}} \lesssim \mathcal{N}\varepsilon.$$

The constant is independent of \mathbf{h} and \mathbf{p} .

Proof. With Corollary 4.3.31 and the inverse estimate (4.55) we obtain

$$\begin{aligned} \sum_{j \in \mathcal{I}} h_j p_j^{-1} |\mathbf{u}_j|^2 &= \sum_{T_i \in \mathcal{T}} h_i p_i^{-1} \sum_{k \in \mathcal{I}_{T_i}} |\mathbf{u}_k|^2 \\ &\lesssim \sum_{T_i \in \mathcal{T}} \|u_h\|_{L^2(T_i)}^2 = \|u_h\|_{L^2(\Gamma)}^2 \end{aligned}$$

and

$$\begin{aligned}
\sum_{k \in \mathcal{I}} h_k^2 p_k^{-3} |\mathbf{v}_k|^2 &= \sum_{T_i \in \mathcal{T}} h_i^2 p_i^{-3} \sum_{k \in \mathcal{I}_{T_i}} |\mathbf{v}_k|^2 \\
&\lesssim \sum_{T_i \in \mathcal{T}} h_i p_i^{-2} \|v_h\|_{L^2(T_i)}^2 = \sum_{T_i \in \mathcal{T}} \left\| \frac{h_i^{1/2}}{p_i} v_h \right\|_{L^2(T_i)}^2 \\
&= \left\| \frac{\mathbf{h}^{1/2}}{\mathbf{p}} v_h \right\|_{L^2(\Gamma)}^2 \lesssim \|v_h\|_{H^{-1/2}(\Gamma)}^2.
\end{aligned} \tag{4.65}$$

□

The next lemma states a relationship of the absolute error of the Galerkin matrix of the double layer operator and the consistency error induced by the right-hand side. Let $u_D \in Y_\ell \subset H^{1/2}(\Gamma)$ denote the discretized Dirichlet datum, $\{\Psi_1, \dots, \Psi_{\mathcal{M}}\}$ denote a basis of Y_ℓ , and $\mathcal{J} = \{1, \dots, \mathcal{M}\}$ denote an index set.

Lemma 4.3.34. *If the absolute error in the Galerkin entries of the double layer operator \mathbf{K} is bounded by*

$$|\mathbf{K}_{jk} - \tilde{\mathbf{K}}_{jk}| \leq \varepsilon h_j h_k^{1/2}, \quad j \in \mathcal{I}, k \in \mathcal{J},$$

then the induced consistency error of the right-hand side $f := (\mathbf{K} + \frac{1}{2})\mathbf{u}_D$ in Symm's integral equation is bounded by

$$\frac{|\langle f, v_h \rangle - \langle \tilde{f}, v_h \rangle|}{\|v_h\|_{H^{-1/2}(\Gamma)}} \lesssim \mathcal{N}^{1/2} \mathcal{M}^{1/2} \varepsilon \|u_D\|_{L^2(\Gamma)}.$$

The constant is independent of \mathbf{h} but still depending on \mathbf{p} .

Proof. For all $v_h \in X_\ell$, there holds

$$\begin{aligned}
|\langle f, v_h \rangle - \langle \tilde{f}, v_h \rangle| &= |\mathbf{v}^T (\mathbf{K} - \tilde{\mathbf{K}}) \mathbf{u}_D| \leq \varepsilon \sum_{j \in \mathcal{I}} |\mathbf{v}_j| h_j \sum_{k \in \mathcal{J}} |\mathbf{u}_{D,k}| h_k^{1/2} \\
&\leq \varepsilon \mathcal{N}^{1/2} \mathcal{M}^{1/2} \left(\sum_{j \in \mathcal{I}} |\mathbf{v}_j|^2 h_j^2 \right)^{1/2} \left(\sum_{k \in \mathcal{J}} |\mathbf{u}_{D,k}|^2 h_k \right)^{1/2}.
\end{aligned} \tag{4.66}$$

With (4.64) we obtain for the first sum in (4.66)

$$\sum_{j \in \mathcal{I}} h_j^2 |\mathbf{v}_j|^2 \lesssim \|v_h\|_{H^{-1/2}(\Gamma)}^2.$$

Applying Lemma 4.3.29 on the second sum in (4.66), we finally obtain

$$|\langle f, v_h \rangle - \langle \tilde{f}, v_h \rangle| \leq \varepsilon \mathcal{N}^{1/2} \mathcal{M}^{1/2} \|v_h\|_{H^{-1/2}(\Gamma)} \|u_D\|_{L^2(\Gamma)}.$$

□

4. Numerical Integration for High-Order NURBS-Based BEM

Corollary 4.3.35. *If the absolute error in the Galerkin entries of the double layer operator \mathbf{K} with respect to the Legendre basis for X_ℓ and the Lobatto basis for Y_ℓ is bounded by*

$$|\mathbf{K}_{jk} - \widetilde{\mathbf{K}}_{jk}| \leq \varepsilon h_j h_k^{1/2} p_j^{-3/2} p_k^{-5/2}, \quad j \in \mathcal{I}, k \in \mathcal{J},$$

then the induced consistency error of the right-hand side $f := (\mathbf{K} + \frac{1}{2})\mathbf{u}_D$ in Symm's integral equation is bounded by

$$\frac{|\langle f, v_h \rangle - \langle \widetilde{f}, v_h \rangle|}{\|v_h\|_{H^{-1/2}(\Gamma)}} \lesssim \mathcal{N}^{1/2} \mathcal{M}^{1/2} \varepsilon \|u_D\|_{L^2(\Gamma)}.$$

The constant is independent of \mathbf{h} but still depending on \mathbf{p} .

Proof. With (4.65) we obtain for the first sum in (4.66)

$$\sum_{j \in \mathcal{I}} h_j^2 p_j^{-3} |\mathbf{v}_j|^2 \lesssim \|v_h\|_{H^{-1/2}(\Gamma)}^2.$$

With Corollary 4.3.31 the second sum of (4.66) simplifies to

$$\begin{aligned} \sum_{k \in \mathcal{J}} h_k p_k^{-5} |\mathbf{u}_{D,k}|^2 &= \sum_{T_i \in \mathcal{T}} h_i p_i^{-5} \sum_{k \in \mathcal{J}_{T_i}} |\mathbf{u}_{D,k}|^2 \\ &\lesssim \sum_{T_i \in \mathcal{T}} \|u_D\|_{L^2(T_i)}^2 = \|u_D\|_{L^2(\Gamma)}^2. \end{aligned}$$

□

The hypersingular integral equation. The effect of the perturbations in the Galerkin matrix of the hypersingular operator on the consistency error induced by the sesquilinear form in the hypersingular integral equation is estimated in the next lemma.

Lemma 4.3.36. *If the absolute error in the Galerkin entries of the hypersingular operator \mathbf{W} is bounded by*

$$|\mathbf{W}_{jk} - \widetilde{\mathbf{W}}_{jk}| \leq \varepsilon, \quad j, k \in \mathcal{I},$$

then the induced consistency error of the sesquilinear form is given by

$$\frac{|a(u_h, v_h) - \widetilde{a}(u_h, v_h)|}{\|u_h\|_{H^{1/2}(\Gamma)} \|v_h\|_{H^{1/2}(\Gamma)}} \lesssim \mathcal{N} \varepsilon.$$

The constant is independent of \mathbf{h} but still depending on \mathbf{p} .

Proof. With the Cauchy-Schwartz inequality we obtain

$$\begin{aligned} |a(u_h, v_h) - \widetilde{a}(u_h, v_h)| &\leq \varepsilon \sum_{j \in \mathcal{I}} |\mathbf{u}_j| \sum_{k \in \mathcal{I}} |\mathbf{v}_k| \\ &\leq \varepsilon \left(\sum_{j \in \mathcal{I}} |\mathbf{u}_j|^2 \right)^{1/2} \left(\sum_{k \in \mathcal{I}} |\mathbf{v}_k|^2 \right)^{1/2} |\mathcal{I}|. \end{aligned} \quad (4.67)$$

With Lemma 4.3.29 we obtain for the first sum of (4.67)

$$\begin{aligned}
 \sum_{j \in \mathcal{I}} |\mathbf{u}_j|^2 &= \sum_{T_i \in \mathcal{T}} \sum_{k \in \mathcal{I}_{T_i}} |\mathbf{u}_k|^2 \\
 &\lesssim \sum_{T_i \in \mathcal{T}} h_i^{-1} \|u_h\|_{L^2(T_i)}^2 = \sum_{T_i \in \mathcal{T}} \|h_i^{-1/2} u_h\|_{L^2(T_i)}^2 \\
 &= \|\mathbf{h}^{-1/2} u_h\|_{L^2(\Gamma)}^2 \lesssim \|u_h\|_{H^{1/2}(\Gamma)}^2.
 \end{aligned} \tag{4.68}$$

Applying the same arguments to the second sum of (4.67), we get

$$\frac{|a(u_h, v_h) - \tilde{a}(u_h, v_h)|}{\|u_h\|_{H^{1/2}(\Gamma)} \|v_h\|_{H^{1/2}(\Gamma)}} \lesssim \mathcal{N}\varepsilon.$$

□

Corollary 4.3.37. *If the absolute error in the Galerkin entries of the hypersingular operator \mathbf{W} with respect to the Lobatto basis functions is bounded by*

$$|\mathbf{W}_{jk} - \widetilde{\mathbf{W}}_{jk}| \leq \varepsilon p_j^{-3/2} p_k^{-3/2}, \quad j, k \in \mathcal{I},$$

then the induced consistency error of the sesquilinear form is given by

$$\frac{|a(u_h, v_h) - \tilde{a}(u_h, v_h)|}{\|u_h\|_{H^{1/2}(\Gamma)} \|v_h\|_{H^{1/2}(\Gamma)}} \lesssim \mathcal{N}\varepsilon.$$

The constant is independent of \mathbf{h} and \mathbf{p} .

Proof. With Corollary 4.3.31, we obtain similarly to Equation (4.68)

$$\begin{aligned}
 \sum_{j \in \mathcal{I}} p_j^{-3} |\mathbf{u}_j|^2 &= \sum_{T_i \in \mathcal{T}} p_i^{-3} \sum_{k \in \mathcal{I}_{T_i}} |\mathbf{u}_k|^2 \\
 &\lesssim \sum_{T_i \in \mathcal{T}} \frac{p_i^2}{h_i} \|u_h\|_{L^2(T_i)}^2 = \sum_{T_i \in \mathcal{T}} \left\| \frac{p_i}{h_i^{1/2}} u_h \right\|_{L^2(T_i)}^2 \\
 &= \left\| \frac{\mathbf{p}}{\mathbf{h}^{1/2}} u_h \right\|_{L^2(\Gamma)}^2 \lesssim \|u_h\|_{H^{1/2}(\Gamma)}^2,
 \end{aligned} \tag{4.69}$$

with a constant independent of \mathbf{h} and \mathbf{p} .

□

For the investigation of the consistency error induced by the right-hand side of the hypersingular integral operator, we define the discrete space $Y_\ell \subset H^{-1/2}(\Gamma)$ with basis $\{\Psi_1, \dots, \Psi_M\}$ and corresponding index set $\mathcal{J} := \{1, \dots, M\}$.

Lemma 4.3.38. *Let $\varphi \in Y_\ell$ denote the discretized Neumann datum. If the absolute error in the Galerkin entries of the double layer operator \mathbf{K} is bounded by*

$$|\mathbf{K}_{jk} - \widetilde{\mathbf{K}}_{jk}| \leq \varepsilon h_j^{1/2}, \quad j, k \in \mathcal{I},$$

4. Numerical Integration for High-Order NURBS-Based BEM

then the induced consistency error of the right-hand side $f := (\frac{1}{2}\mathbf{M} - \mathbf{K}^T)\varphi$ in the hypersingular integral equation is bounded by

$$\frac{|\langle f, v_h \rangle - \langle \tilde{f}, v_h \rangle|}{\|v_h\|_{H^{1/2}(\Gamma)}} \lesssim \mathcal{N}^{1/2} \mathcal{M}^{1/2} \varepsilon \|\varphi\|_{L^2(\Gamma)}.$$

The constant is independent of \mathbf{h} but still depending on \mathbf{p} .

Proof. For all $v_h \in X_\ell$, there holds

$$\begin{aligned} |\langle f, v_h \rangle - \langle \tilde{f}, v_h \rangle| &= |\mathbf{v}^T (\mathbf{K}^T - \tilde{\mathbf{K}}^T) \varphi| \leq \varepsilon \sum_{j \in \mathcal{J}} |\varphi_j| h_j^{1/2} \sum_{k \in \mathcal{I}} |\mathbf{v}_k| \\ &\leq \varepsilon \mathcal{N}^{1/2} \mathcal{M}^{1/2} \left(\sum_{j \in \mathcal{J}} |\varphi_j|^2 h_j \right)^{1/2} \left(\sum_{k \in \mathcal{I}} |\mathbf{v}_k|^2 \right)^{1/2}. \end{aligned}$$

With similar arguments as in (4.68) we get

$$\sum_{k \in \mathcal{I}} |\mathbf{v}_k|^2 \lesssim \|v_h\|_{H^{1/2}(\Gamma)}^2.$$

Further, Lemma 4.3.29 yields

$$\sum_{j \in \mathcal{J}} |\varphi_j|^2 h_j \lesssim \|\varphi\|_{L^2(\Gamma)}^2$$

and we finally get

$$|\langle f, v_h \rangle - \langle \tilde{f}, v_h \rangle| \leq \varepsilon \mathcal{N}^{1/2} \mathcal{M}^{1/2} \|v_h\|_{H^{1/2}(\Gamma)} \|\varphi\|_{L^2(\Gamma)}.$$

□

Corollary 4.3.39. *If the absolute error in the Galerkin entries of the double layer operator \mathbf{K} with respect to the Legendre basis $\Phi_k = P_k$ and the Lobatto basis $\Psi_j = N_j$ is bounded by*

$$|\mathbf{K}_{jk} - \tilde{\mathbf{K}}_{jk}| \leq \varepsilon h_j^{1/2} p_j^{-1/2} p_k^{-3/2}, \quad j \in \mathcal{I}, k \in \mathcal{J},$$

then the induced consistency error of the right-hand side $f := (1/2\mathbf{M} - \mathbf{K}')\varphi$ in the hypersingular integral equation is bounded by

$$\frac{|\langle f, v_h \rangle - \langle \tilde{f}, v_h \rangle|}{\|v_h\|_{H^{-1/2}(\Gamma)}} \lesssim \mathcal{N}^{1/2} \mathcal{M}^{1/2} \varepsilon \|\varphi\|_{L^2(\Gamma)}.$$

The constant is independent of \mathbf{h} and \mathbf{p} .

Proof. Corollary 4.3.31 implies that

$$\sum_{j \in \mathcal{J}} h_j p_j^{-1} |\varphi_j|^2 \lesssim \|\varphi\|_{L^2(\Gamma)}^2$$

and with Equation (4.69) we get

$$\sum_{k \in \mathcal{I}} p_k^{-3} |\mathbf{v}_k|^2 \lesssim \|v_h\|_{H^{1/2}(\Gamma)}^2.$$

□

Quadrature and interpolation orders. Recall that the error estimates for the absolute quadrature errors for far-field, neighboring, and identical elements read

$$|R_n| \leq h_i h_j \left(C_1 \rho_1^{-2n_1-1} + C_2 \rho_2^{-2n_2-1} \right).$$

Here, we assume that the kernel functions are analytically extendable on $\overline{\mathcal{E}_{\rho_1}} \times [-1, 1]$ and $[-1, 1] \times \overline{\mathcal{E}_{\rho_2}}$ and for the interpolation method on $\overline{\mathcal{E}_{\rho_1}} \times \overline{\mathcal{E}_{\rho_2}}$. Further, we assume that the Galerkin error behaves like $\varepsilon(\mathcal{N})$, where \mathcal{N} denotes the degrees of freedom. With the estimates for $|R_n|$ and the estimates for the consistency errors presented in this section, we can a priori determine the quadrature and interpolation orders such that the consistency error in Strang's Lemma does not spoil the convergence rates of the Galerkin error. Specifically n is chosen such that $|R_n| \lesssim \varepsilon(\mathcal{N})$.

Remark 4.3.40. The a priori estimate presented in Theorem 1.6.5 indicates that $\varepsilon(\mathcal{N}) = \mathcal{N}^{-\alpha-1}$ for uniform h -methods and $\varepsilon(\mathcal{N}) = \mathcal{N}^{-2\alpha-1}$ for uniform p -methods, where α depends on the interior angles of the domain.

For geometric hp -methods, Theorem 1.6.7 indicates that $\varepsilon(\mathcal{N}) = e^{-b\sqrt{\mathcal{N}}}$, where b depends on the grading parameters σ and ϑ .

Tables 4.1-4.3 give an overview on the quadrature orders for all Galerkin matrices for the different combinations of boundary elements. For the NURBS basis functions we set $p_i = p_j = q$ but remark that the constants in all estimates still depend on the weight function ω and hence on q .

4. Numerical Integration for High-Order NURBS-Based BEM

Let

$$\tilde{C} := -\log(\varepsilon(\mathcal{N})) + \frac{1}{2}\log(h_i h_j) + \frac{1}{2}\log(p_i p_j) - \frac{1}{2}\log(\max\{h_i, h_j\}) + \log(\min\{p_i, p_j\}).$$

\mathbf{V}	order n
far-field elements (quadrature)	$n_1 \geq \frac{\tilde{C} + \log(C_1)}{2\log(\rho_1)} + \frac{p_i - 1}{2}$ $n_2 \geq \frac{\tilde{C} + \log(C_2)}{2\log(\rho_2)} + \frac{p_j - 1}{2}$
far-field elements (interpolation)	$n_1 \geq \frac{\tilde{C} + \log(C_1)}{\log(\rho_1)}$ $n_2 \geq \frac{\tilde{C} + \log(C_2)}{\log(\rho_2)}$
neighboring elements	$n_1 \geq \frac{\tilde{C} + \log(C_1)}{2\log(\rho_1)} + \frac{\max\{p_i, p_j\} - 1}{2}$ $n_2 \geq \frac{\tilde{C} + \log(C_2)}{2\log(\rho_2)} + \frac{p_i + p_j - 1}{2}$
identical elements	$n_1 \geq \frac{\tilde{C} + \log(C_1)}{2\log(\rho_1)} + \frac{p_i + p_j - 1}{2}$ $n_2 \geq \frac{\tilde{C} + \log(C_2)}{2\log(\rho_2)} + \frac{p_i + p_j - 1}{2}$

Table 4.1.: Quadrature and interpolation orders that are chosen for the assembly of the single layer Galerkin matrix \mathbf{V} . We denote the order with respect to s and u by n_1 and with respect to t and v by n_2 .

Let

$$\tilde{C} := -\log(\varepsilon(\mathcal{N})) + \frac{1}{2}\log(h_j) + \frac{1}{2}\log(p_i^3 p_j^5).$$

K	order n
far-field elements (quadrature)	$n_1 \geq \frac{\tilde{C} + \log(C_1)}{2\log(\rho_1)} + \frac{p_i - 1}{2}$ $n_2 \geq \frac{\tilde{C} + \log(C_2)}{2\log(\rho_2)} + \frac{p_j - 1}{2}$
far-field elements (interpolation)	$n_1 \geq \frac{\tilde{C} + \log(C_1)}{\log(\rho_1)}$ $n_2 \geq \frac{\tilde{C} + \log(C_2)}{\log(\rho_2)}$
neighboring elements	$n_1 \geq \frac{\tilde{C} + \log(C_1)}{2\log(\rho_1)} + \frac{\max\{p_i, p_j\} - 1}{2}$ $n_2 \geq \frac{\tilde{C} + \log(C_2)}{2\log(\rho_2)} + \frac{p_i + p_j - 1}{2}$
identical elements	$n_1 \geq \frac{\tilde{C} + \log(C_1)}{2\log(\rho_1)} + \frac{p_i + p_j - 1}{2}$ $n_2 \geq \frac{\tilde{C} + \log(C_2)}{2\log(\rho_2)} + \frac{p_i + p_j - 1}{2}$

Table 4.2.: Quadrature and interpolation orders that are chosen for the assembly of the double layer Galerkin matrix **K**. We denote the order with respect to s and u by n_1 and with respect to t and v by n_2 .

4. Numerical Integration for High-Order NURBS-Based BEM

Let

$$\tilde{C} := -\log(\varepsilon(\mathcal{N})) + \log(h_i h_j) + \frac{3}{2} \log(p_i p_j).$$

\mathbf{W}	order n
far-field elements (quadrature)	$n_1 \geq \frac{\tilde{C} + \log(C_1)}{2 \log(\rho_1)} + \frac{p_i - 1}{2}$ $n_2 \geq \frac{\tilde{C} + \log(C_2)}{2 \log(\rho_2)} + \frac{p_j - 1}{2}$
far-field elements (interpolation)	$n_1 \geq \frac{\tilde{C} + \log(C_1)}{\log(\rho_1)}$ $n_2 \geq \frac{\tilde{C} + \log(C_2)}{\log(\rho_2)}$
neighboring elements	$n_1 \geq \frac{\tilde{C} + \log(C_1)}{2 \log(\rho_1)} + \frac{\max\{p_i, p_j\} - 1}{2}$ $n_2 \geq \frac{\tilde{C} + \log(C_2)}{2 \log(\rho_2)} + \frac{p_i + p_j - 1}{2}$
identical elements	$n_1 \geq \frac{\tilde{C} + \log(C_1)}{2 \log(\rho_1)} + \frac{p_i + p_j - 1}{2}$ $n_2 \geq \frac{\tilde{C} + \log(C_2)}{2 \log(\rho_2)} + \frac{p_i + p_j - 1}{2}$

Table 4.3.: Quadrature and interpolation orders that are chosen for the assembly of the Galerkin matrix \mathbf{W} of the hypersingular integral operator. We denote the order with respect to s and u by n_1 and with respect to t and v by n_2 .

5. Implementation and Numerical Results

The implementation of NURBS-based boundary element methods for the solution of the integral equations defined in Section 1.2 is discussed in this chapter. It is the goal to provide an implementation that has a wide field of application. In particular, we focus on an implementation that allows for the use of different kernel functions, different basis functions for the ansatz space, including polynomial and rational basis functions, and the use of collocation and Galerkin methods. Apart from Laplace, Lamé, and Helmholtz problems, for which our implementation can be used, also other fundamental solutions of a similar type should be incorporated easily. Hence, the assembly of the collocation and Galerkin matrices should be implemented as black box.

We would like to stress that unlike in most previous works, we use the exact boundary representation via NURBS for all computations, which allows for the solution of integral equations on complex geometries. Particularly, our implementation can be used for multi-connected boundaries with corners. For NURBS-enhanced methods, where an exact NURBS parametrization of the boundary and a Legendre basis for the polynomial ansatz space are used, we focus on high-order methods like uniform p - and geometric hp -methods. This requires the accurate and efficient evaluation of the boundary integral operators and the assembly of the collocation and Galerkin matrices for high polynomial degrees.

The chapter is organized as follows. In the first section we give a short overview on existing software packages for boundary element methods. Next, we describe the implementation of NURBS-based BEM, where we first discuss general implementational aspects. We then go into detail on the implementation of collocation and Galerkin methods, where the collocation and Galerkin matrices are assembled with the algorithms developed in Chapter 4 by a black box implementation. For both collocation and Galerkin methods, we present numerical results, which show that our implementation works well for high-order NURBS-enhanced methods and low order isogeometric methods.

5.1. Overview on Existing Software Packages

There are many software packages for boundary element methods. In this section, we give an overview on some software packages, which is by no means complete.

5. Implementation and Numerical Results

- **BEMLIB** is a boundary element software library of Fortran 77/90 and MATLAB codes, which is based on the book of Pozrikidis ([Poz02]). It implements isoparametric methods with quadratic and cubic splines for Laplace, Helmholtz, and Stokes problems in two and three dimensions. Furthermore, it supports both collocation and Galerkin methods.
- **BEM++** [ŠBA⁺15] is a C++ software package implementing the Galerkin method for two and three dimensional Laplace, Helmholtz, and Maxwell problems. Piecewise polynomial basis functions up to order 10 and plane triangular grids are supported. The arising singular integrals are evaluated with the quadrature rules of Sauter and Schwab [SaSch97]. Furthermore, \mathcal{H} matrices [BGH03] and ACA [Beb00] are supported by an interface to the library AHMED [Beb08].
- **epsBEM** [BBF13, Ban13] is a software package for two-dimensional *hp*-BEM for Laplace and Lamé problems. The software package provides a stable and efficient implementation of the *hp*-BEM on polygonal boundaries for high polynomial degrees by evaluating the arising integrals analytically with recurrence relations. **epsBEM** is implemented in a combination of MATLAB and C. While the core routines, which are critical with respect to the performance are implemented in C and parallelized with OpenMP, the top layer functions are implemented in MATLAB. This results in an implementation that can be used by students and researchers alike.
- **HILBERT** [AEF⁺14] (**H**ilbert **I**s a **L**ovely **B**oundary **E**lement **R**esearch **T**ool) is a software package for the solution of two dimensional Poisson problems on polygonal domains which is implemented in MATLAB and C. It features functions for the evaluation of the boundary integral operators and the assembly of the Galerkin matrices for lowest order ansatz functions. The arising integrals are evaluated with quadrature rules or semi-analytically. Specifically the inner integral is evaluated exactly, while the outer integral is evaluated with a quadrature rule. Furthermore, **HILBERT** provides the implementation of several *h*-adaptive algorithms using weighted residual, $(h-h/2)$ -type, and two-level error estimators.
- **HyENA** [MMR⁺14] (**H**yperbolic and **E**lliptic **N**umerical **A**nalysis) is a C++ software package for the solution of two and three dimensional Galerkin and collocation boundary element methods, where the use of collocation methods is limited to Symm's integral equation. The collocation and Galerkin matrices can be assembled for linear and quadratic ansatz functions on polygonal and polyhedral boundaries for all partial differential equations which have a fundamental solution of a specific type. This yields a wide field of

application. The singular integrals arising in the assembly of the Galerkin matrices are regularized with the coordinate transformation given in [Duf82].

- **Maiprogs** is a Fortran-based software package for solving Laplace, Lamé, and Helmholtz problems with *hp*-BEM. The multiple precision library ARCPREC [BHL⁺02] is used for the assembly of the Galerkin matrices with quadruple precision. In [Mai12], several numerical results are collected.
- In [Sim12] a MATLAB implementation of an isogeometric collocation BEM for two-dimensional Lamé problems is presented. Particularly, the software package supports the solution of Symm's integral equation. The arising integrals are evaluated with quadrature rules, where the singular and nearly singular integrals are regularized with the Telles transformation [Tel86].

All software packages only feature the solution of specific boundary integral equations, basis functions or boundary approximations. In the following, we present a more general black box implementation for two dimensional NURBS-based boundary element methods supporting general boundary representations. Similar to the software package **HyENA**, we support the solution of all fundamental solutions, which are of the general types (4.3) and (4.26), respectively, with Galerkin and collocation methods. Hence, the implementation can be used for a wide range of BIEs. Furthermore, we provide the use of different sets of basis functions. Besides polynomial ansatz spaces with Legendre and Lobatto bases, for which we present a stable implementation for high orders (we present results for $p \leq 128$), we also implement isogeometric methods with NURBS basis functions.

5.2. Implementation

The goal of our implementation is to provide an efficient implementation for a wide class of NURBS-based BEM, which is easy to use. Therefore, the functions are implemented in a combination of MATLAB and C. While the functions that are critical with respect to performance are implemented in C, the top layer functions are written in MATLAB, which results in an easy to understand, straight-forward code. To illustrate the simple use of our black box implementation, Listing 5.1 shows an example for the solution of Symm's integral equation for the Laplace operator

$$\mathcal{V}\varphi = \frac{1}{12}(3\theta^2 - 6\pi\theta + 2\pi^2) \quad \text{on } \Gamma := \partial\Omega, \quad \Omega := \{x \in \mathbb{R}^2 : \|x\|_2 < 0.25\}$$

with a Galerkin method:

5. Implementation and Numerical Results

Listing 5.1: Solution of Symm's integral equation $\mathcal{V}\varphi_h = f$ for the Laplace problem.

```
1  *** specify operator, geometry, basis, and polynomial degree
2  operator = 'laplace';
3  problem  = 'exSymmCircle';
4  basis    = 'Leg';
5  p        = {[5;2;4;8]};
6
7  *** reset the path
8  restoredefaultpath;
9  *** get home directory of NURBSbem
10 home = '..';
11 libdir = [home,filesep,'lib',filesep];
12 exdir  = [home,filesep,'examples',filesep];
13 *** addpath standard routines
14 addpath([libdir,'general']);
15 addpath([libdir,'general',filesep,'c']);
16 *** addpath routines of operator
17 addpath([libdir,operator,filesep,'mat']);
18 *** add problem and get data
19 addpath([exdir,operator,filesep,problem]);
20
21 *** load and display geometry
22 [curves,splines,options] = loadSplines;
23 figure(1)
24 plotGeometry(splines)
25
26 *** compute solution of Symm's integral equation
27 %   assemble V
28 %   assemble f
29 %   solve V phi_h = f
30 phi_h = solveSymm_f(curves,splines, p, basis, @f, options);
31
32 *** display solution over arc length
33 figure(2)
34 plotArclength(curves, splines, basis, p, x, @phi, options)
35
36 *** display solution in domain
37 figure(3)
38 showSolDom(curves,splines,[], [], [], phi_h, basis, p, ...
39           linspace(-1,1,30), linspace(-1,1,30), 'interior');
```

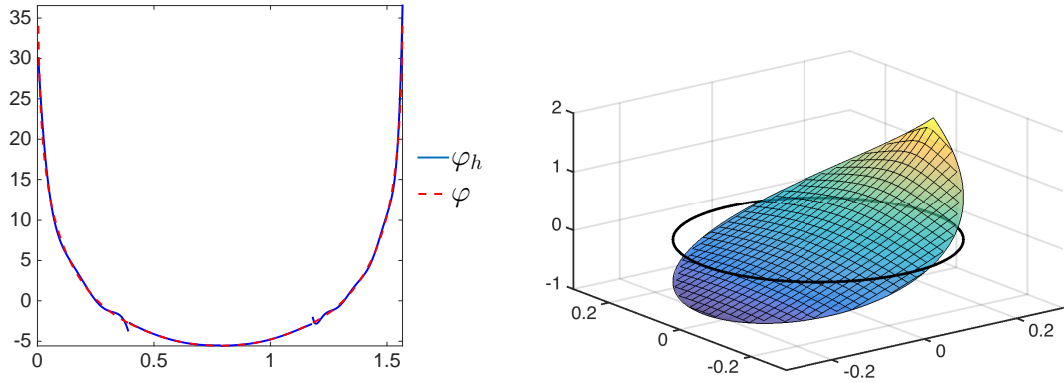


Figure 5.1.: Solution φ_h and exact solution φ plotted over arc length (left) and $\mathcal{V}\varphi_h$ plotted in the domain Ω (right) for the non-symmetric polynomial degree vector $\mathbf{p} = [5, 2, 4, 8]$.

We start the description of our implementation with some general aspects, i.e. the data structures for the boundary representation, the implementation of the basis functions, and the numerical integration, before we go into detail on the implementation of collocation and Galerkin methods.

5.2.1. General Aspects of Implementation

Representation of NURBS curves. With the notation of Definition 3.1.1 we represent NURBS curves by MATLAB structs, that contain the following fields:

Struct representing a NURBS curve	
$\mathbf{Xi} \in \mathbb{R}^{n+q+1}$	open knot vector
$q \in \mathbb{N}$	degree of the NURBS curve
$\mathbf{Qw} \in \mathbb{R}^{3 \times n}$	weighted control points $Q_k^\omega = (q_k^{(1)}\omega_k, q_k^{(2)}\omega_k, \omega_k)$ column by column
$\text{isClosed} \in \{0, 1\}$	1 if NURBS curve is closed, 0 else
$\text{type} \in \{'D', 'N'\}$	character indicating if the NURBS curve belongs to the Dirichlet or Neumann boundary
$\mathbf{h} \in \mathbb{R}^m$	vector containing the arc length h_i of each element T_i
$\mathbf{rho} \in \mathbb{R}^m$	vector containing the semi-axis sum ρ_i of the ellipse \mathcal{E}_{ρ_i} defined in Definition 3.2.9

Apart from the parameters \mathbf{Xi} , q , \mathbf{Qw} , isClosed , and type , which are needed for the definition of the NURBS curve and are specified by the user, we compute and save some additional information on the NURBS curve needed for the implementation in the fields \mathbf{rho} and \mathbf{h} . The

5. Implementation and Numerical Results

semi-axis sums ρ_i , which are used for the computation of the quadrature and interpolation orders of all arising integrals, are computed by the function

$$\text{splines} = \text{getRho}(\text{splines})$$

by solving the root finding problem in Remark 3.2.11 with the MATLAB function `roots`. The arc length

$$h_i = \int_{-1}^1 |\dot{\gamma}_i(t)| dt$$

is computed with a Gauss-Legendre quadrature rule by the function

$$\text{splines} = \text{getArcLength}(\text{splines}).$$

In order to save computational time, the evaluation of the NURBS curves, their derivatives, and the corresponding basis functions is implemented in C and connected to MATLAB with Mex-interfaces.

Representation of the geometry. For the implementation of NURBS-based boundary element methods, we consider general Lipschitz domains that may contain holes and whose boundary Γ is decomposed into a Dirichlet boundary Γ_D and a Neumann boundary Γ_N . Let \mathcal{N}_c denote the number of connected pieces of the boundary and let each connected piece of the boundary in Γ_D and Γ_N be parametrized by one NURBS curve. For the representation of the boundary in MATLAB, we use the data structures `curves` and `splines`. `splines` is a vector of MATLAB structs, where each struct describes one NURBS curve. The NURBS curves are sorted such that all NURBS curves belonging to one connected piece of the boundary are listed subsequently. The topological structure of the boundary is represented by the vector `curves` $\in \mathbb{N}^{\mathcal{N}_c+1}$, which contains the index of the first NURBS curve on each connected piece of boundary. Hence, the expression `(curves(k) : curves(k+1)-1)` gives the indices of the NURBS curves parametrizing the k -th connected piece of the boundary. Figure 5.2 illustrates a simple example.

Integration in NURBS-based BEM. For the implementation of NURBS-based BEM, integrals of the type

$$\int_{-1}^1 f(t) |\dot{\gamma}_i(t)| dt$$

have to be computed for a smooth function f up to a given accuracy `tol`. In particular, integrals of this type arise in the projection of the Dirichlet and Neumann data onto the ansatz spaces, in the assembly of the right-hand sides of the discrete variational formulations for Symm's and the hypersingular integral equations, and in the computation of the arc lengths of the elements. While the integrals can be evaluated with adaptive quadrature rules, we give an estimate for

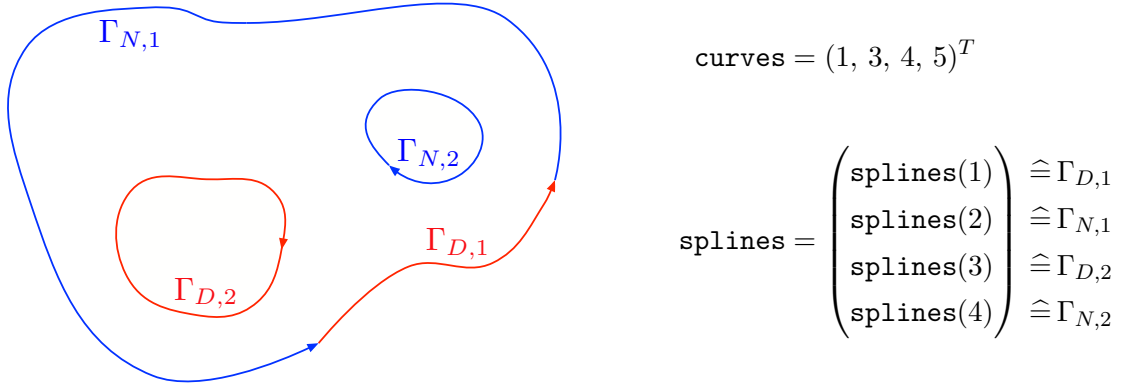


Figure 5.2.: Boundary representation for a Lipschitz domain with two holes.

the a priori computation of the quadrature order, such that the tolerance is met. According the Theorem 2.2.11, the quadrature error is bounded by

$$|R_n| \leq \max_{z \in \partial \mathcal{E}_\rho} |f(z)| |\dot{\gamma}_i(z)| \left| \frac{\ell(\mathcal{E}_\rho)}{\rho^{2n+1}} \right|, \quad 1 < \rho < \rho_i. \quad (5.1)$$

In general, computing the constant $\max_{z \in \partial \mathcal{E}_\rho} |\dot{\gamma}_i(z)|$ explicitly is inefficient. We can apply the worst case estimate

$$\max_{z \in \partial \mathcal{E}_\rho} |\dot{\gamma}_i(z)| \leq \frac{(a_i + a)^{2(q-1)}}{(a_i - a)^{2q}} \frac{(a_i - 1)^{2q}}{(a_i + 1)^{2(q-1)}} \max_{z \in [-1,1]} |\dot{\gamma}_i(z)| =: c(a) h_i, \quad (5.2)$$

which is given in Lemma 3.2.12 in order to obtain an upper bound. Here, a and a_i denote the lengths of the real semi-axis of \mathcal{E}_ρ and \mathcal{E}_{ρ_i} , and q denotes the order of γ_i . This implies that the quadrature order has to be chosen according to

$$n \geq \left\lceil \frac{\log(C) + \log(c(a) h_i) + \log(\pi(\rho + \rho^{-1})) - \log(\text{tol})}{2 \log \rho} + \frac{1}{2} \right\rceil =: c_1(\rho), \quad (5.3)$$

where $C := \max_{z \in \partial \mathcal{E}_\rho} |f(z)|$. Although this estimate for the quadrature order yields reliable results for the approximated integral for all $1 < \rho < \rho_i$, it overestimates the quadrature order needed to meet the tolerance in most practical examples.

For the implementation, we propose to choose the quadrature order according to

$$\begin{aligned} n &\geq \left\lceil \frac{\log(\tilde{C}) + \log(\max_{z \in [-1,1]} |\dot{\gamma}_i(z)|) + \log(\pi(\rho_i + \rho_i^{-1})) - \log(\text{tol})}{2 \log \rho_i} + \frac{1}{2} + q \right\rceil \\ &=: c_2 \end{aligned} \quad (5.4)$$

with $\tilde{C} := \max_{z \in [-1,1]} |f(z)|$. This bound is obtained from (5.3) by choosing $\rho = \rho_i$, but only considering the maximum value of the integrand on $[-1, 1]$ instead of \mathcal{E}_{ρ_i} . The choice $\rho = \rho_i$ implies that the exact asymptotic behavior of the quadrature error is reflected by c_2 . Furthermore,

5. Implementation and Numerical Results

we obtain an upper bound for the quadrature error for $n = 0$, since plugging in $\rho = 1$ in (5.1) yields

$$|R_n| \leq \max_{z \in [-1,1]} |f(z)| |\dot{\gamma}_i(z)| \cdot 2 < \max_{z \in [-1,1]} |f(z)| |\dot{\gamma}_i(z)| \cdot \frac{\ell(\mathcal{E}_\rho)}{\rho}, \quad 1 < \rho < \rho_i.$$

As long as the pre-asymptotic area in the behavior of the quadrature error is small, the tolerance tol is met by choosing the quadrature order according to (5.4) and we obtain reliable results. However, oscillating integrands generally have a large pre-asymptotic area. The asymptotic behavior is not reached until the quadrature order is chosen such that the oscillations are resolved. In order to resolve the possibly occurring oscillations in the boundary parametrization we add the order q to the bound in (5.4). Furthermore, if f is a polynomial of degree p , we obtain

$$|R_n| \leq \max_{z \in \partial \mathcal{E}_\rho} |\dot{\gamma}_i(z)| \cdot \frac{\ell(\mathcal{E}_\rho)}{\rho^{2n-p+1}}, \quad 1 < \rho < \rho_i. \quad (5.5)$$

Thus, we additionally increase the quadrature order by $\lceil p/2 \rceil$.

In the following, we compare the results of both bounds $c_1(\rho)$ and c_2 with the optimal order $c^{(opt)}$, which is needed to meet a given tolerance. For the bounds $c_1(\rho)$, we choose equidistant values of $\rho \in (1, \rho_i)$. Further, we consider the integral

$$\int_{-1}^1 |\dot{\gamma}_i(t)| dt,$$

which corresponds to computing the arc length of the element T_i . The optimal order $c^{(opt)}$ is computed adaptively. For our examples, we choose four different NURBS curves, which are illustrated in Figure 5.3. Specifically a smooth second degree, a non-smooth second degree, an almost closed fifth degree, and an oscillating fifth degree NURBS curve. Figure 5.4 shows the quadrature orders computed by $c_1(\rho)$ and c_2 as well as the adaptively computed order $c^{(opt)}$ plotted against tol^{-1} for all four NURBS curves. The top left subfigure shows that for the smooth curves the order obtained by c_2 corresponds to the order obtained with $c_1(\rho)$ with the optimal value of ρ . However, for the non-smooth and higher-order curves the bound c_2 is significantly smaller than $c_1(\rho)$ for all $1 < \rho < \rho_i$. The last figure shows that for the tolerance 10^{-15} , $c_1(\rho)$ is larger than the optimal order by a factor of six, i.e. $c_1(\rho) \approx 900$ as compared to $c^{(opt)} \approx 150$. On the other hand we obtain $c_2 \approx 200$, which is less than twice the optimal order. The bottom left subfigure shows that the orders are invariant with respect to a scaling of the parametrization. All subfigures indicate that the bound c_2 yields a reliable and sharp estimate for the quadrature order for the examples considered, although it can not be proven that the bound c_2 is reliable for general curves.

Remark 5.2.1. For the computation of the L^2 and H^1 projection, we assume that the Dirichlet and Neumann data are analytic. However, for several benchmark examples the boundary conditions are of the form $f(t) = t^\alpha \tilde{f}(t)$ with $\alpha \in (-1, 1)$ and \tilde{f} analytic. Hence, applying a

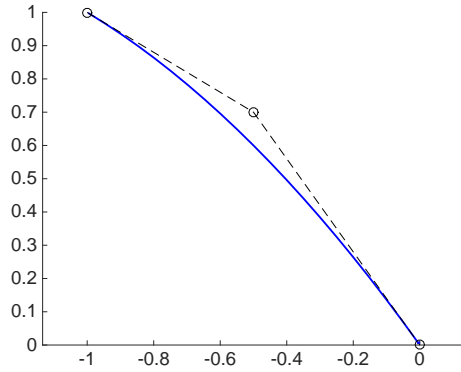
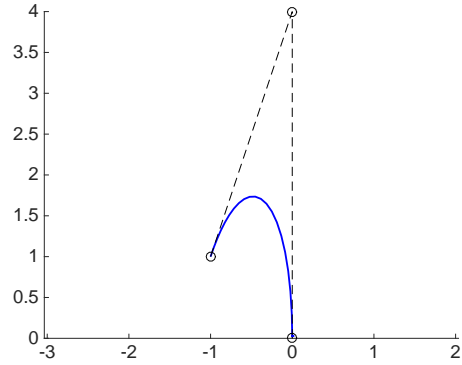
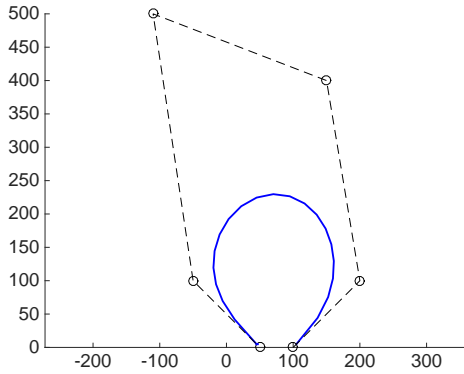
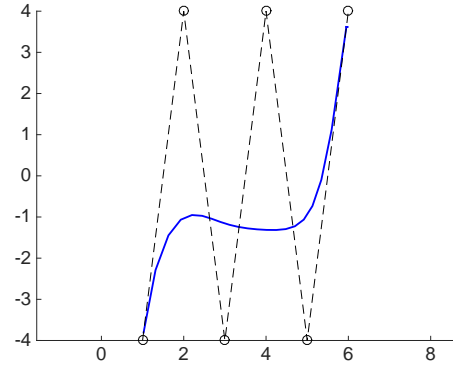
(a) Second degree NURBS curve with $\rho_i = 7.10$.(b) Second degree NURBS curve with $\rho_i = 1.28$.(c) Fifth degree NURBS curve with $\rho_i = 1.46$.(d) Fifth degree NURBS curve with $\rho_i = 1.12$.

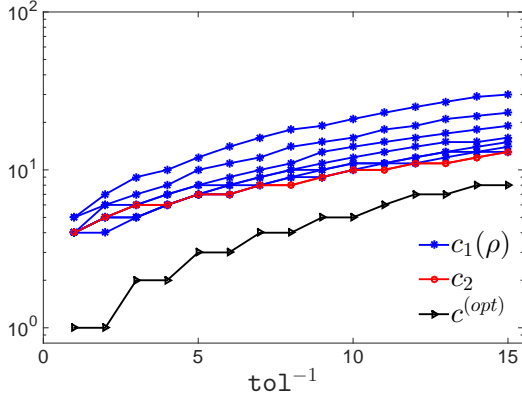
Figure 5.3.: Different smooth and non-smooth NURBS curves with corresponding semi axis sums ρ_i used for benchmarks.

Gauss-Legendre quadrature only yields algebraic convergence. Gauss-Jacobi quadrature rules can be applied for fixed α in order to achieve an exponential decay of the quadrature error. The corresponding nodes and weights can be computed in an efficient and accurate way with the same techniques as presented in Section 2.2.

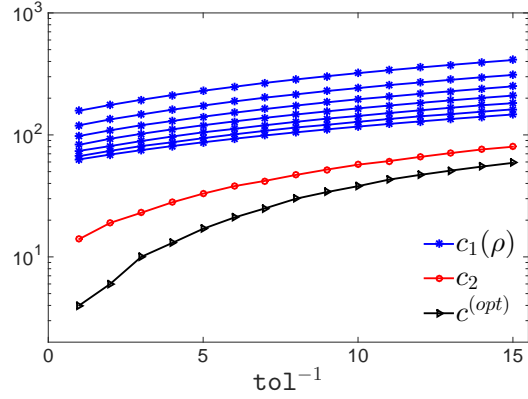
Basis functions. For the implementation, we support four different sets of basis functions, that are specified by the string `basis` $\in \{ \text{'Leg'}, \text{'Lob'}, \text{'NURBS0'}, \text{'NURBS1'} \}$. For the Legendre and Lobatto basis functions, we additionally require a cell array `p` of the same length as the vector `splines`. Each field `p{k}` contains a vector with the local polynomial degrees on all elements of the NURBS curve represented by `splines(k)`.

For isogeometric methods, we feature two different bases, a globally continuous basis `'NURBS1'` and a globally discontinuous basis `'NURBS0'`. The basis functions specified by `'NURBS1'` are the same basis functions used for the boundary parametrization. Since each connected piece

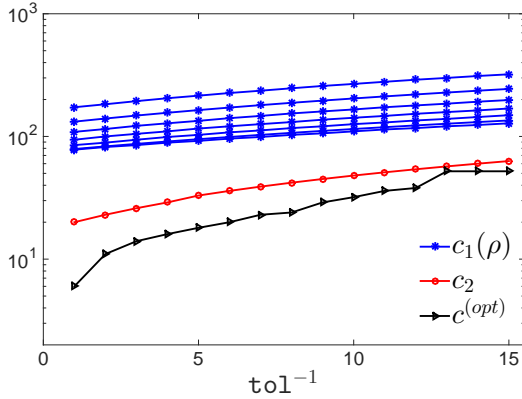
5. Implementation and Numerical Results



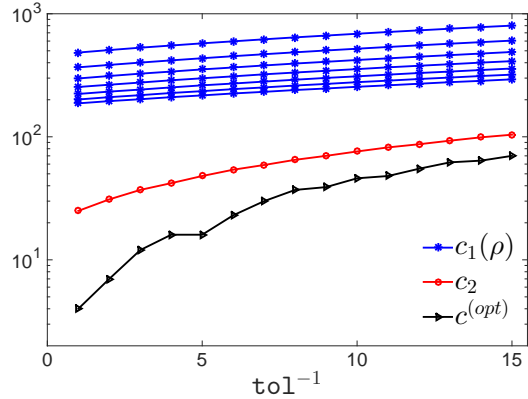
(a) Second degree NURBS curve with $\rho_i = 7.10$.



(b) Second degree NURBS curve with $\rho_i = 1.28$.



(c) Fifth degree NURBS curve with $\rho_i = 1.46$.



(d) Fifth degree NURBS curve with $\rho_i = 1.12$.

Figure 5.4.: Quadrature order computed with $c_1(\rho)$ for equidistant values of $1 < \rho < \rho_i$ and c_2 as well as the adaptively computed order $c^{(opt)}$. Each subfigure corresponds to the NURBS curves depicted in Figure 5.3.

of the boundary can be parametrized by more than one NURBS curve, we have to add up the nodal basis functions at the transitions of the Dirichlet and the Neumann boundary, in order to obtain a globally continuous basis. We remark, that with this boundary representation we do not construct basis functions of higher regularity at the intersections of the Dirichlet and Neumann boundaries. However, since in many practical applications singularities of the solution are expected at these intersections, basis functions with higher regularity at these points do generally not yield better approximations of the solution as compared to functions with less regularity.

The globally discontinuous basis 'NURBS0' is constructed from the knot vector of the NURBS parametrization of the boundary. By deleting the first and the last knot in the open knot vector, which corresponds to the inverse process of k -refinement, the degree and the inter-element regularity of the standard NURBS basis are reduced by one. Since it is not determined which

weights have to be used, we simply delete the first weight. This allows for the construction of globally discontinuous functions even for isogeometric methods, which can be used for the approximation of the Sobolev space $H^{-1/2}(\Gamma)$.

All sets of bases are evaluated with the MATLAB function

```
val=evalBasis(spline,z,p,basis,nodes).
```

The input parameters are the struct `spline` defining the NURBS curve, the m evaluation points $\mathbf{z} \in \mathbb{R}^m$, the local polynomial degree `p`, the string `basis` specifying the basis, and the vector `nodes` containing the nodes of the element, on which the basis has to be evaluated. Optionally, `evalBasis` returns as second argument the derivative of the basis functions, which is needed for the assembly of the Galerkin matrix of the hypersingular integral operator.

The choice of the basis functions significantly affects the condition numbers of the Galerkin matrices. Figure 5.5 shows the condition number for the single layer Galerkin matrix of the Laplace operator on the circle parametrized by the NURBS in Example 3.1.3 for all sets of bases introduced above. We refer to the globally discontinuous and continuous NURBS basis functions by $\mathcal{R}_k^{(0)}$ and $\mathcal{R}_k^{(1)}$, respectively. We consider different refinement strategies, i.e. uniform p -refinement, uniform k -refinement (only for NURBS basis functions), and geometric hp -refinement (only for Legendre and Lobatto basis functions). For all bases, we also investigate the condition number of the Galerkin matrix, which is scaled by its diagonal.

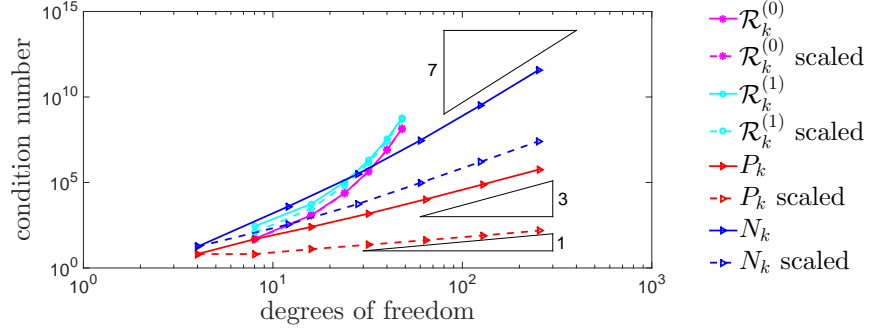
For uniform p -refinements, we see that the condition number grows exponentially for the NURBS basis functions, while we observe an algebraic growth for the Legendre and the Lobatto basis. Specifically, the Galerkin matrix with respect to the Legendre basis behaves like $\mathcal{O}(p^3)$, which coincides with the theoretical result stated in [Heu92, Heu96]. Further, the condition number of the scaled Galerkin matrix with respect to the Legendre basis only grows linearly, which is also observed for the geometric hp -refinement.

- Remark 5.2.2.** (i) The linear growth of the condition numbers with respect to the Legendre and Lobatto basis functions for the uniform p - and geometric hp -refinements indicates that these basis functions are an appropriate choice for high-order NURBS-enhanced methods.
- (ii) Since the condition numbers grow exponentially for the NURBS basis functions for high orders \mathbf{p} and high regularities \mathbf{k} , these basis functions are inappropriate for the use of high-order methods without any suitable preconditioning strategy. In this work, we do not discuss advanced preconditioning methods for these bases, but present new results for uniform p - and k -refinements with moderate polynomial degrees.

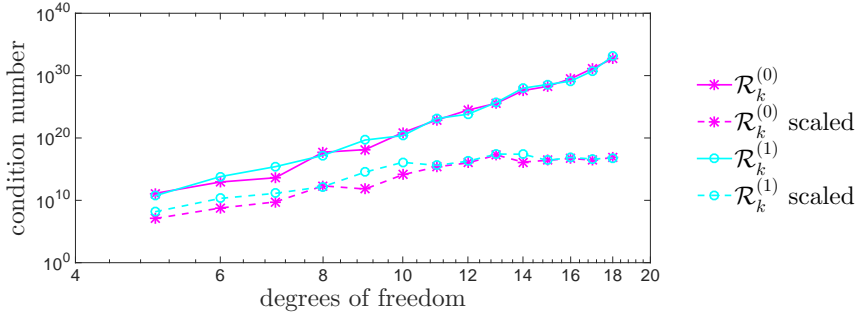
5.2.2. Collocation Methods

For the implementation of collocation methods we discuss two aspects. The first aspect is the evaluation of the integrals according to the algorithms presented in Section 4.2 as black box.

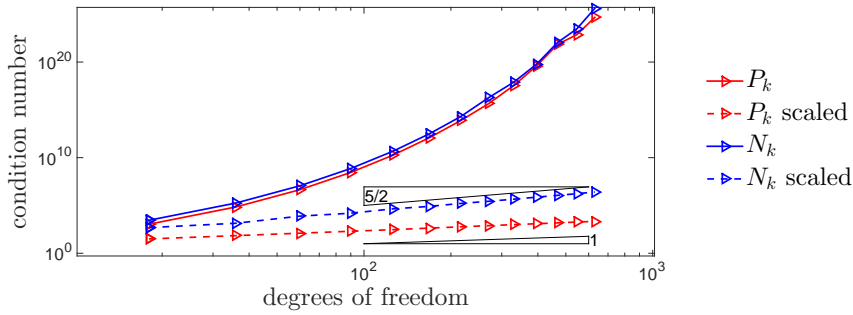
5. Implementation and Numerical Results



(a) Uniform p -refinement with $N_e = 4$ elements.



(b) Uniform k -refinement.



(c) Geometric hp -refinement with $\vartheta = 0.5$ and $\sigma = 1$.

Figure 5.5.: Condition number of the single layer Galerkin matrix for the Laplace equation on the circle parametrized by the NURBS curve defined in Example 3.1.3. Here, "scaled" means that the Galerkin matrices are scaled by their diagonals.

Second, we address the choice of the collocation points, since the location of the collocation points has a large impact on the stability of the collocation methods. In the end of this section, we present benchmark examples, in order to show that our implementation is numerically stable.

Assembly of the Collocation Matrices

The evaluation of the boundary integral operators \mathbf{V} , \mathbf{K} , \mathbf{A} , and \mathbf{W} is implemented in the MATLAB-functions

```
V = potV(splines, basis, p, x, N, options,varargin)
K = potK(splines, basis, p, x, N, options,varargin)
A = potA(splines, basis, p, x, N, options,varargin)
W = potW(splines, basis, p, x, N, options,varargin).
```

The struct `splines` describes the NURBS curve on which the integral operators are evaluated, `basis` and `p` specify the basis functions used for the computations, `x` is a $(\mathcal{N}_p \times 2)$ -matrix containing \mathcal{N}_p evaluation points, and `N` denotes the interpolation order used for the computations. The struct `options` contains parameters belonging to the underlying BIE, e.g. the Lamé coefficients λ and μ , the wave number κ , and σ_Ω indicating if interior or exterior problems are considered. Optionally, all functions get the vector `u` and a tolerance `tol`. The vector `u` contains the coefficients of the solution with respect to the basis functions and is used for the evaluation of the solution in the domain Ω . The tolerance `tol` is used for the near- and far-field classification, see Algorithm 4.1. The functions return a matrix containing the values of the boundary integral operator at all evaluation points for all non-vanishing basis functions on the NURBS curve.

In the sequel we describe the classification of the evaluation points and the evaluation for far-field, near-field and singular integrals in more detail.

For the classification of the evaluation points, the complex zeros z_x as defined in Definition 4.2.14 have to be computed. According to Remark 4.2.5 (i), we compute the roots of the complex polynomial

$$f(z) = \omega_i(z) [(x_1 - \gamma_{i,1}(z)) + i(x_2 - \gamma_{i,2}(z))] \in \mathbb{C}$$

for all evaluation points $(x_1, x_2) \in \mathbb{R}^2$. Listing 5.2 shows an excerpt of the MATLAB code.

Listing 5.2: Excerpt of the function `getZeros.m` for the computation of z_x (Definition 4.2.14).

```
1 %*** get coefficients of numerator and denominator
2 t = cos( ((0:splines.q)+1/2)*pi/(splines.q+1))';
3 tt = (nodes(2)-nodes(1))/2*t+(nodes(2)+nodes(1))/2;
4 [Num,Den] = evalCurve(splines.q,splines.U,splines.Pw,tt);
5 tmp = vander(t)\[Num',Den'];
```

5. Implementation and Numerical Results

```

6  c1 = complex(tmp(:,1),tmp(:,2));
7  c2 = tmp(:,3);
8  %*** compute zeros
9  pts = [];
10 for k=1:size(x,1)
11     pts = [pts;roots(c1-complex(x(k,1),x(k,2))*c2)'];
12 end

```

First, we compute the coefficients of the numerator and the denominator of γ_i with respect to the monomials by interpolation. Therefore, the numerator and denominator of γ_i are evaluated at the zeros of the $(q+1)$ -th Chebyshev polynomial with the Mex-function `evalCurve` and the system of linear equations is solved. In Lines 10-12, we compute the roots of f with the MATLAB function `roots`. We remark that in the case of linear and quadratic NURBS curves we use explicit formulas in order to compute the roots of f for all evaluation points, simultaneously. Due to the efficient realization of vector operations in MATLAB we hence save computational time. The classification of the evaluation points is then implemented according to Algorithm 4.1.

The evaluation of the boundary integral operators is implemented as a black box. Therefore, general kernel functions of the type

$$\tilde{K}(x-y) := g_{-1}(x-y) + g_0(x-y) \log|x-y| + \sum_{\ell=1}^N g_\ell(x-y) |x-y|^{-2\ell} \quad (5.6)$$

are supported. For the use of our implementation, only the non-vanishing coefficient functions g_μ , $\mu = -1, \dots, N$, and K , which are implemented in the functions `gm1`, `g0`, ..., `gN`, and `K`, have to be specified by the user. Hence for the single layer operator of the Laplace problem, we only implement the coefficient function $g_0(x-y) := -\frac{1}{2\pi}$, since all other coefficient functions are not present in Equation (5.6). This allows the easy incorporation of new kernel functions into the software package.

Table 5.1 shows an overview on the present terms in the kernel functions for Laplace, Lamé, and Helmholtz equations, for which our implementation can be used.

For far-field elements, we support both the evaluation of the regular integrals with a Gauss-Legendre quadrature and in the special case of the Legendre basis functions the interpolation method introduced in Section 4.2.1, which is based on the Legendre expansion of the kernel function. Figure 5.6 shows the computational time for both the Gauss-Legendre quadrature and the interpolation method over the polynomial degree p . The single layer operator of the Laplace equation is evaluated at $\mathcal{N}_p = 5083$ far-field points for the Legendre basis functions and the

	V	K	A	W
g_{-1}	x	x	x	x
g_0	x	x	x	x
g_1	x	x	x	x
g_2		x	x	x
g_3				x

Table 5.1.: Overview on the terms used for the evaluation of the integral operators, which arise for Laplace, Lamé, and Helmholtz problems.

quarter circle NURBS curve defined in Example 3.1.3. Both the quadrature and the interpolation order are chosen such that all integrals are evaluated up to an accuracy $\varepsilon = 10^{-14}$.

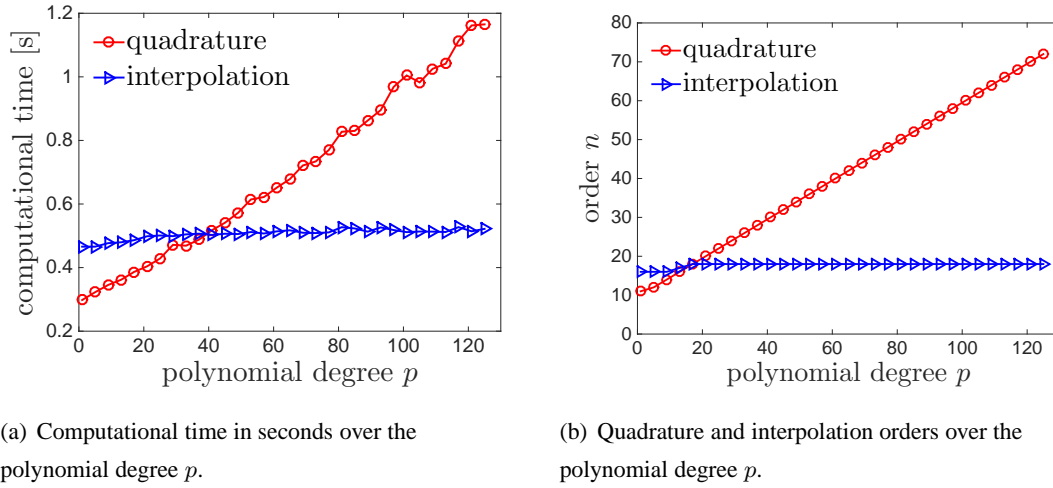


Figure 5.6.: Comparison of Gauss-Legendre quadrature and the interpolation method for the evaluation of the single layer operator of the Laplace problem for $\mathcal{N}_p = 5083$ far-field points. The computations are performed on a desktop computer with an AMD Phenom II X6 processor, 16GB RAM, and the Ubuntu 10.04 operating system.

For small polynomial degrees, we see that the Gauss-Legendre quadrature outperforms the interpolation method. This can be explained by the fact that the absolute error of the Gauss-Legendre quadrature decreases with twice the rate as compared to the interpolation method (cf. Lemmas 4.2.6 and 4.2.9). However, for linearly increasing polynomial degrees both the computational time and the quadrature order increase linearly for the Gauss-Legendre quadrature. Since the interpolation method only interpolates the kernel and exploits the orthogonality of the Legendre polynomials, the order and hence the computational time are independent of the polynomial de-

5. Implementation and Numerical Results

gree p (cf. Remark 4.2.10). For high polynomial degrees $p > 34$ the interpolation method is more efficient as compared to the Gauss-Legendre quadrature.

In order to show the accuracy of our near-field algorithm, we consider the following example.

Example 5.2.3. We consider the evaluation of the double layer operator for the Helmholtz equation ($\kappa = 1$)

$$(\mathcal{K}\tilde{N}_1)(x) = \int_{T_i} \gamma_{1,y}^- G(x-y) \tilde{N}_1(y) ds_y$$

for the Lobatto function \tilde{N}_1 and four evaluation points

$$x = x(D) := \gamma_i(1/3) + D \cdot \nu_i(1/3), \quad D \in \{10^{-1}, 10^{-2}, 10^{-3}, 10^{-4}\}. \quad (5.7)$$

The quarter circle T_i and its NURBS parametrization γ_i are defined in Example 3.1.3 and ν_i denotes the unit normal vector.

We compare our near-field algorithm with the Telles transformation [Tel86], which is proposed in [SBT⁺12, SIS198] for the evaluation of nearly singular integrals. Figure 5.7 shows the absolute error plotted against the order for both approaches.

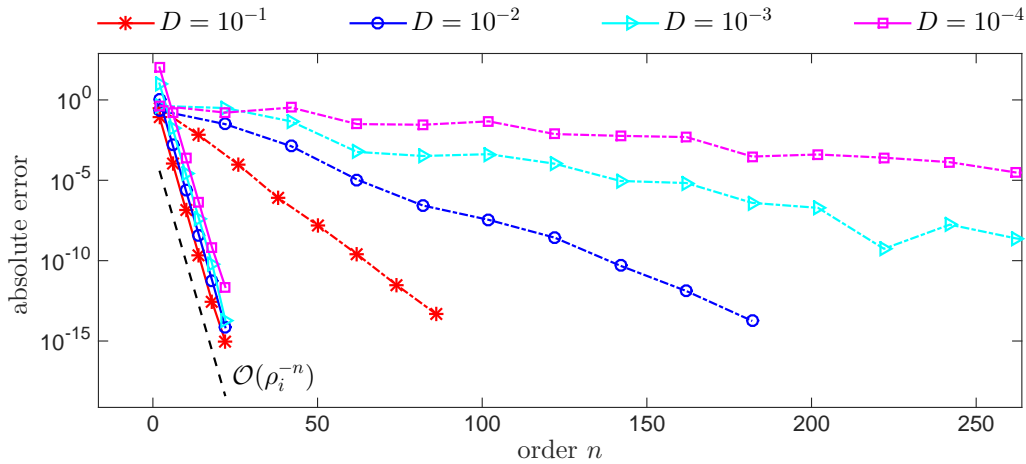


Figure 5.7.: Absolute error over the order n for the Helmholtz problem defined in Example 5.2.3.

Solid lines: Near-field algorithm presented in Section 4.2.2, dashed lines: Telles transformation.

For all distances D , the absolute error for the evaluation according to the algorithms presented in Section 4.2.2 (solid lines) converges exponentially with factor ρ_i , which shows the independency of the convergence rate on the evaluation point x , see Remark 4.2.21. As compared to the Telles transformation (dashed lines), where a very slow exponential convergence can be observed, this yields a significant speed up. Specifically for $D = 10^{-4}$, the error can only be

reduced to approximately 10^{-5} with order $n = 256$ by the Telles transformation, while the error is reduced to 10^{-13} with order $n \approx 20$ by our implementation. Similar results are also obtained for all other coordinate transformations presented in [SlSl98, Tel86, TM74], as the dependency on the evaluation point can generally not be eliminated by coordinate transformations.

Although the absolute error is reduced by almost 16 significant digits for all evaluation points, which shows the stability of the evaluation, the absolute error can not be evaluated up to an accuracy of 10^{-16} . The reason is that the constant $c_\ell(x)$ in the error estimate given in Lemma 4.2.18 still depends on the evaluation point x and hence on the distance D , i.e. $c_\ell(x) = \mathcal{O}(D^{-2\ell+1})$. Hence, we only expect an accuracy of $10^{15-2\ell}$ for the evaluation with double precision, but remark that with multiple precision libraries more accurate result can be obtained.

Figure 5.8 shows surface plots of all four boundary integral operators for Laplace, Lamé, and Helmholtz equations and Legendre, Lobatto and NURBS basis functions. In all plots, the boundary is the quarter circle parametrized by the NURBS curve defined in Example 3.1.3.

Choice of Collocation Points

An important aspect for the implementation of collocation methods is the choice of the collocation points, since they have a large impact on the condition number of the collocation matrices and on the stability of the collocation method. However, there are only few theoretically proven results for the appropriate choice of the collocation points:

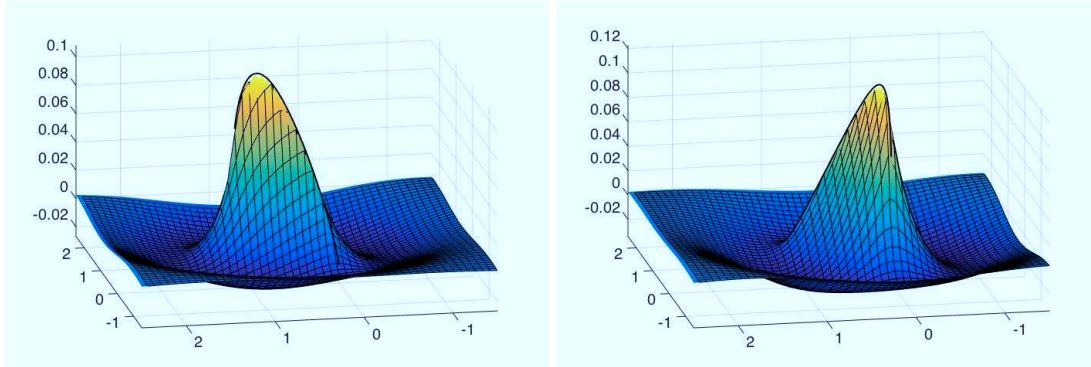
For collocation methods with spline ansatz functions of highest regularity, i.e. the ansatz space $S(\mathcal{T}, \mathbf{h}, \mathbf{p}, \mathbf{p})$, and smooth boundaries Γ , the collocation points are chosen to be the element endpoints for odd degree splines, see [AW83]. For even degree splines the collocation points can be chosen as element midpoints, see [SW85]. In [Dom03], convergence is also proven for collocation points that are shifted by $\varepsilon > 0$ from the endpoint- and midpoints, which is called ε -collocation. For the solution of Symm's and the hypersingular integral equation on an interval with a uniform p -method, convergence is proven in [SlSt92, ES92]. Here, the Chebyshev polynomials of first and second kind are used as basis functions and their zeros are chosen as collocation points, respectively.

For isogeometric methods, the knot averages, called Greville points, and the extrema of the Chebyshev splines, called Demko points [Dem85], are proposed in [SBT⁺12].

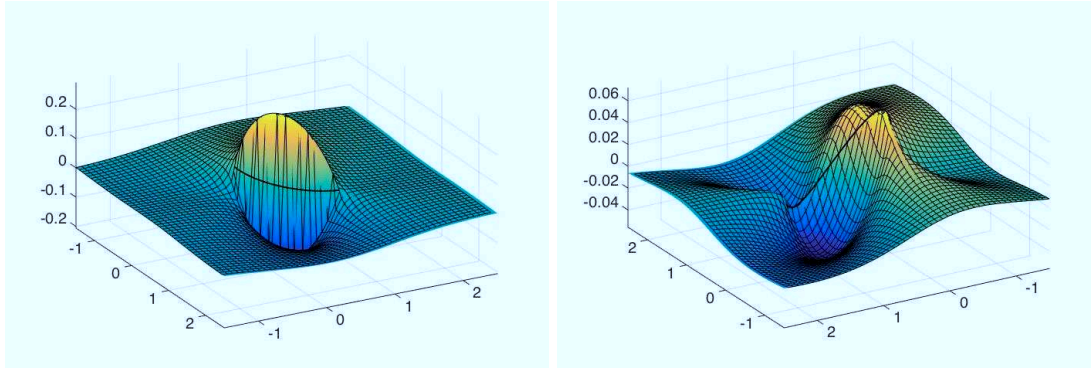
In the sequel, we discuss the choice of the collocation points for NURBS-enhanced and isogeometric methods, separately.

For our implementation of NURBS-enhanced methods with the Legendre polynomials and the Lobatto shape functions, we choose their zeros as collocation points, which coincides with the

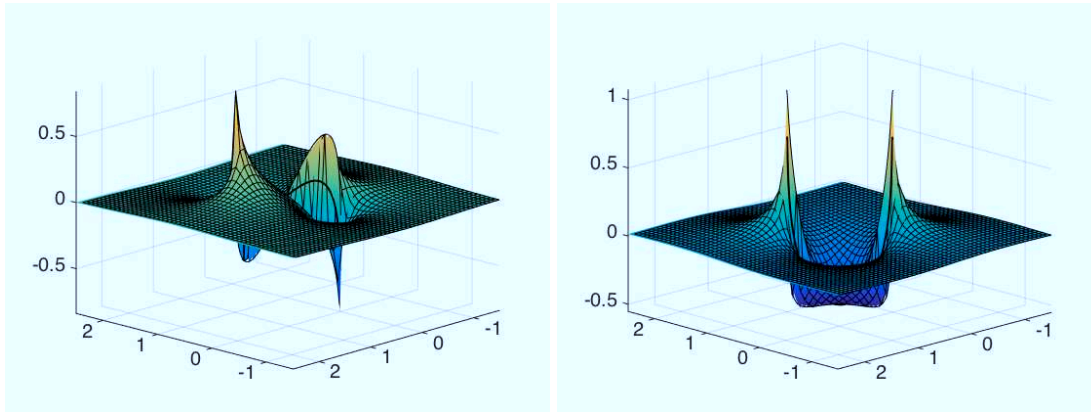
5. Implementation and Numerical Results



(a) Real (left) and imaginary (right) part of the single layer operator $(\mathcal{V}\tilde{\mathcal{R}}_1)(x)$ for Helmholtz problems with $\kappa = 2 + i$.



(b) Both components of the double layer operator $(\mathcal{K}(\tilde{\mathcal{N}}_3, 0)^T)(x)$ for Lamé problems with $\lambda = 600$ and $\mu = 300$.



(c) Adjoint and hypersingular integral operator, $(\mathcal{A}\tilde{\mathcal{P}}_3)(x)$ and $(\mathcal{W}\tilde{\mathcal{N}}_3)(x)$, for the Laplace problem with $\nu_x = (1, -1)^T$.

Figure 5.8.: Surface plots of the boundary integral operators for different sets of basis functions on the quarter circle NURBS curve.

approach proposed in [SlSt92] for the Chebyshev basis. Although we do not prove the convergence or the stability of the resulting collocation method, we numerically investigate the effect of the collocation points on the energy error and the condition number of the collocation matrices. Therefore, we consider two benchmark examples of Symm's and the hypersingular integral equations on the slit.

Example 5.2.4. We consider Symm's integral equation

$$\mathcal{V}\varphi = \frac{x}{2} \quad \text{on } \Gamma := (-1, 1).$$

With the identity

$$\int_{-1}^1 \log|x-t| \frac{T_n(t)}{\sqrt{1-t^2}} dt = \begin{cases} -\pi \log(2), & n = 0 \\ -\frac{\pi}{n} T_n(x), & n > 0, \end{cases}$$

which is proven in [Rea79], the exact solution can be computed by $\varphi(x) = x(1-x^2)^{-1/2}$ and has two singularities at the end points ± 1 .

For this benchmark, we choose the Legendre basis and compare the zeros of the Legendre polynomials $x_j^{(Gauss)}$ with the zeros of the Chebyshev polynomials $x_j^{(Cheb)}$ and optimal collocation points. For the computation of the optimal collocation points, we consider two criterions for the optimality, the minimization of the error and the minimization of the condition number of the single layer collocation matrix \mathbf{V} . Since the energy norm $\|\cdot\|_{\mathcal{V}}^2 := \langle \mathcal{V}\cdot, \cdot \rangle$ is equivalent to the $H^{-1/2}$ -norm, we consider the energy norm of the solution in the numerical examples. The corresponding minimization problems read

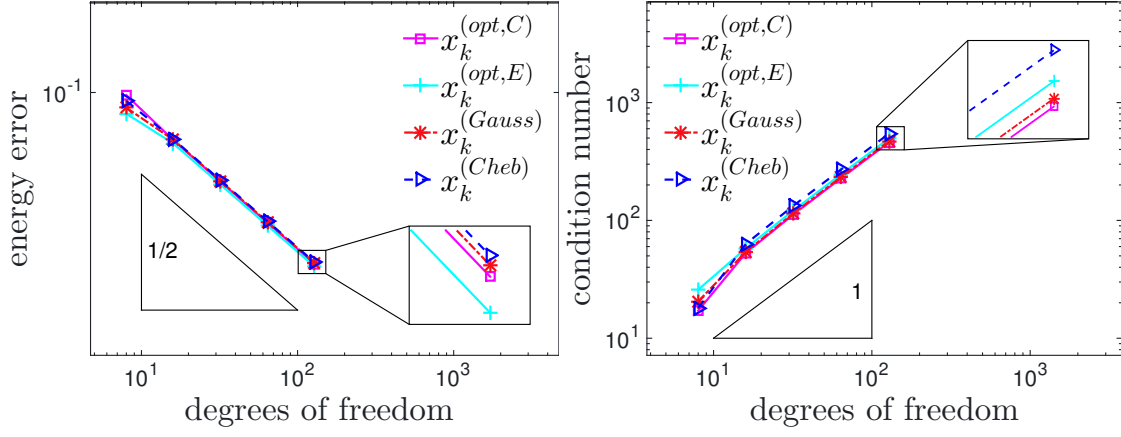
$$\left\{ \begin{array}{l} \text{Find } x_0^{(opt,E)}, \dots, x_p^{(opt,E)} \in (-1, 1), \text{ s.t.} \\ \|\varphi - \varphi_h\|_{\mathcal{V}} \rightarrow \min \\ \mathcal{V}\varphi_h(x_j^{(opt,E)}) = f(x_j^{(opt,E)}), \quad j = 1, \dots, \mathcal{N} \end{array} \right.$$

and

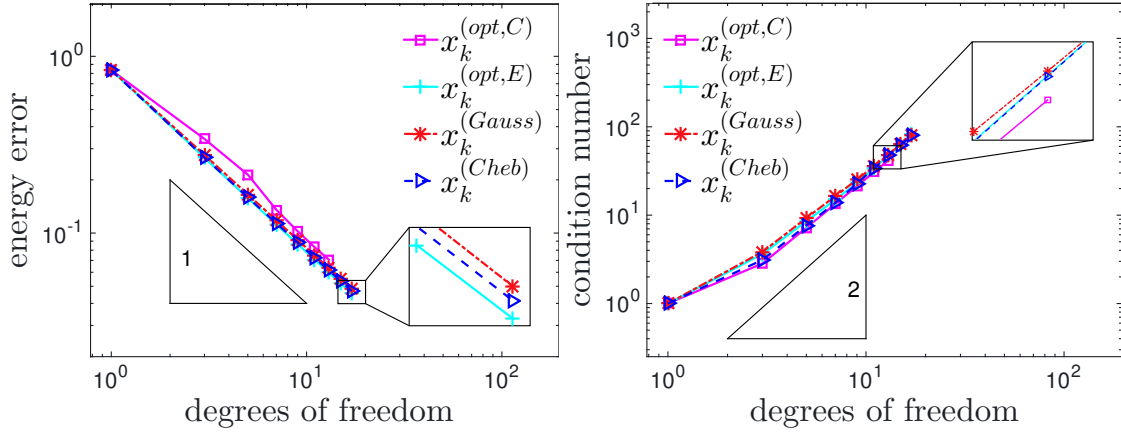
$$\left\{ \begin{array}{l} \text{Find } x_0^{(opt,C)}, \dots, x_p^{(opt,C)} \in (-1, 1), \text{ s.t.} \\ \text{cond}(\mathbf{V}) \rightarrow \min \\ \mathcal{V}\varphi_h(x_j^{(opt,C)}) = f(x_j^{(opt,C)}), \quad j = 1, \dots, \mathcal{N}. \end{array} \right.$$

In order to solve the minimization problems we start with equidistant collocation points and assume that the optimal points are located symmetrically in the interval $(-1, 1)$. The minimization problems are solved with the MATLAB function `fmincon`.

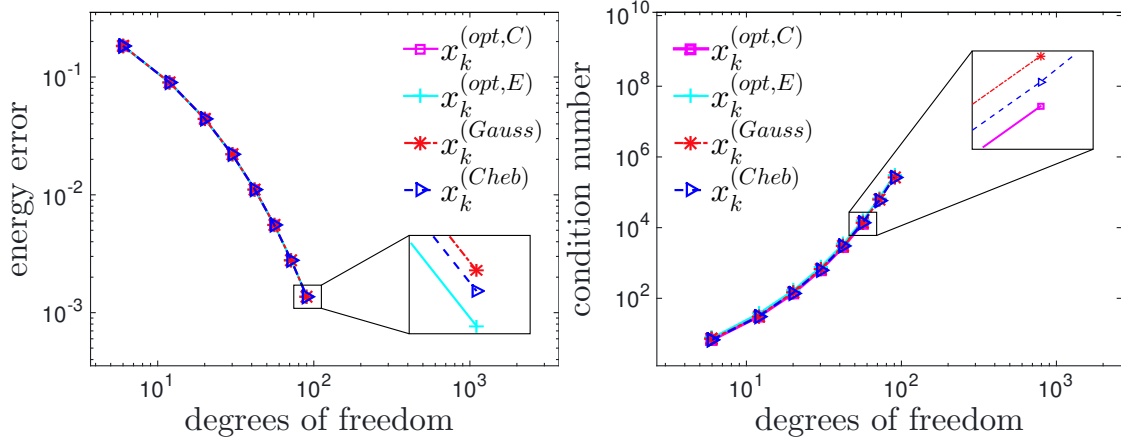
5. Implementation and Numerical Results



(a) Uniform h -refinement with $p = 7$.



(b) Uniform p -refinement.



(c) Geometric hp -refinement with $\vartheta = 0.25$ and $\sigma = 1$.

Figure 5.9.: Energy error (left) and condition number of the single layer operator (right) over the degrees of freedom.

We consider three different types of mesh refinement, specifically a uniform h -refinement with polynomial degree $p = 7$, a uniform p -refinement with $\mathcal{N}_e = 2$ elements, and a geometric hp -refinement, where the mesh is refined towards the singularities of the solution at ± 1 . Figure 5.9 shows the energy error over the degrees of freedom (left) and the condition number of the single layer collocation matrix over the degrees of freedom (right).

For all refinements, the minimal energy error is attained for the optimal collocation points $x_k^{(opt,E)}$ and the minimal condition number of the single layer collocation matrix is attained for the optimal collocation points $x_k^{(opt,C)}$, which indicates that the minimization problems are solved correctly. For uniform h - and p -refinement, the behavior for all four types of points is similar. Particularly, the energy error decays algebraically with order $1/2$ for uniform h -refinement and with order 1 for uniform p -refinement. For the geometric hp refinement, we observe an exponential decay of the error. Both the condition number and the energy error only differ slightly in the constant for all refinement strategies. Overall, both the zeros of the Legendre and the Chebyshev polynomials yield good results for both the condition number and the energy error. Furthermore, the optimal collocation points are located similarly in the interval $(-1, 1)$ as compared to the zeros of the orthogonal polynomials, specifically the collocation points become more frequent at the endpoints ± 1 . Figure 5.10 shows that the Chebyshev zeros are located more closely to the optimal points with respect to the energy error, while the zeros of the Legendre polynomials are located more closely to the optimal points with respect to the condition number.

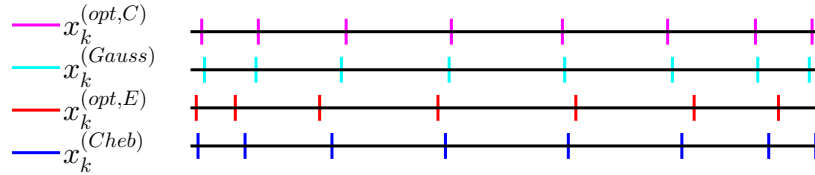


Figure 5.10.: Location of the collocation points for $p = 7$ and $\mathcal{N}_e = 1$ element.

For the Lobatto basis functions, we consider the following benchmark example of the hypersingular integral equation.

Example 5.2.5. We consider the hypersingular integral equation

$$\mathcal{W}u = 1 \quad \text{on } \Gamma := (-1, 1).$$

The exact solution is given by $u(x) = 2(1 - x^2)^{1/2}$.

As the Lobatto shape functions are defined as antiderivatives of the Legendre polynomials, we compare their zeros $x_j^{(Lob)}$ with the extrema of the Chebyshev polynomials $x_j^{(Cheb1)}$ and the op-

5. Implementation and Numerical Results

timal collocation points, with respect to the energy error and the condition number. Specifically, the minimization problems read:

$$\left\{ \begin{array}{l} \text{Find } x_0^{(opt,E)}, \dots, x_p^{(opt,E)} \in [-1, 1], \text{ s.t.} \\ \|u - u_h\|_{\mathcal{W}} \rightarrow \min \\ \mathcal{W}u_h(x_j^{(opt,E)}) = f(x_j^{(opt,E)}), \quad j = 1, \dots, \mathcal{N} \end{array} \right.$$

and

$$\left\{ \begin{array}{l} \text{Find } x_0^{(opt,C)}, \dots, x_p^{(opt,C)} \in [-1, 1], \text{ s.t.} \\ \text{cond}(\mathbf{W}) \rightarrow \min \\ \mathcal{W}\varphi_h(x_j^{(opt,C)}) = f(x_j^{(opt,C)}), \quad j = 1, \dots, \mathcal{N}. \end{array} \right.$$

The minimization problems are again solved by the MATLAB-function `fmincon` with equidistant initial points, whereby the element endpoints are fixed as collocation points. Figure 5.11 shows the energy error and the condition number over the degrees of freedom for a uniform h -refinement with $p = 7$, a uniform p -refinement with $\mathcal{N}_e = 2$ elements and a geometric hp -refinement with the same geometrically graded mesh as used for the previous example.

Again, the minimal energy error is obtained by the collocation points $x_j^{(opt,E)}$ and the minimal condition number is obtained by the points $x_j^{(opt,C)}$, which indicates that the minimization problems are solved correctly. We see that the zeros of the Lobatto shape functions as well as the extrema of the Chebyshev polynomials yield the optimal behavior with almost optimal constant for both the energy error and the condition number for all considered refinements. Furthermore, this benchmark example shows the sensitivity of the energy error with respect to the collocation points. Specifically, we see that the convergence of the energy error breaks for the collocation points $x_j^{(opt,C)}$ for the uniform h - and geometric hp -refinements. Figure 5.12 shows the distribution of the different sets of collocation points for the polynomial degree $p = 7$. It can be seen that the optimal points become more frequent towards the endpoints, which is the same behavior as for the Lobatto points and Chebyshev extrema.

For the implementation of isogeometric methods, we support the Greville and the Demko points, which are also proposed in [ADH⁺10]. For the knot vector $\Xi = \{-1 = \xi_0, \dots, \xi_{n+q+1} = 1\}$ and the degree q , the knot averages are defined by

$$x_k = \frac{\xi_{k+1} + \dots + \xi_{k+q}}{q}, \quad k = 0, \dots, n-1.$$

The Demko points are defined as the extrema of the Chebyshev splines and have no explicit

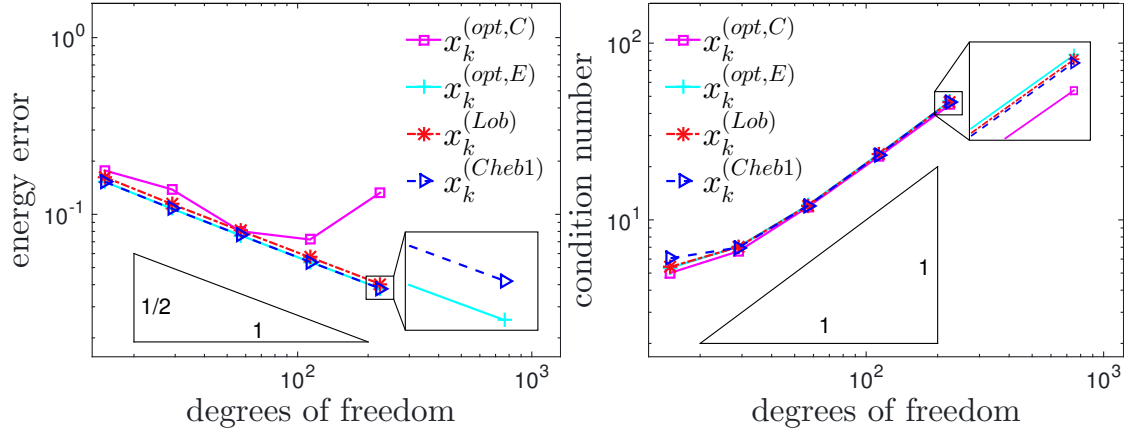
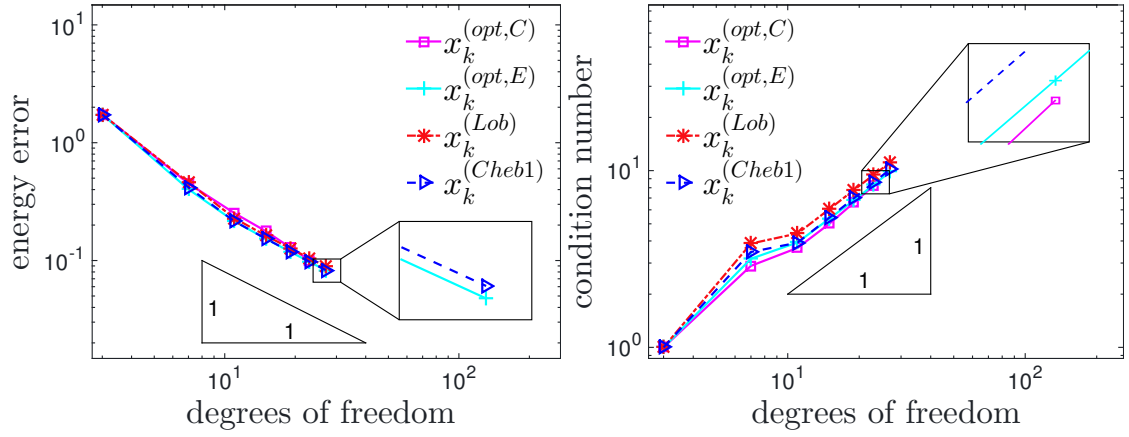
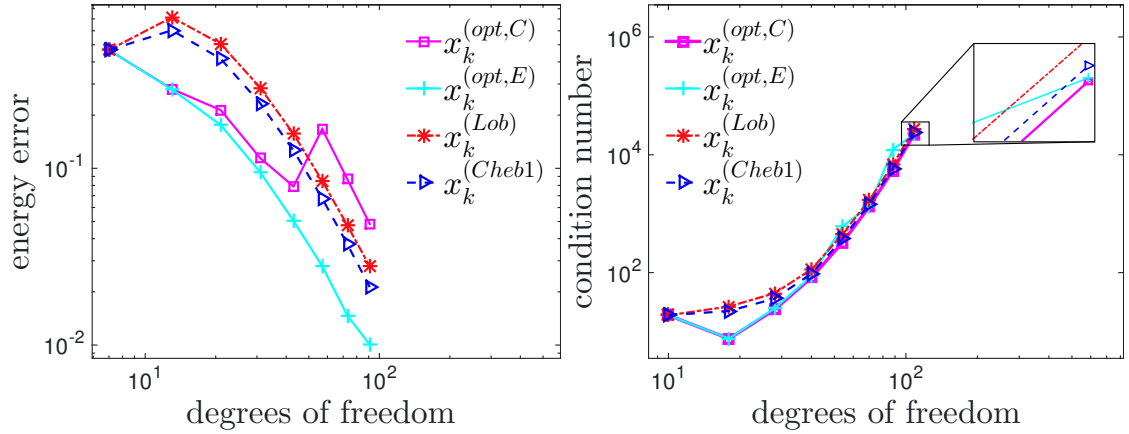
(a) Uniform h -refinement with $p = 7$.(b) Uniform p -refinement.(c) Geometric hp -refinement with $\vartheta = 0.25$ and $\sigma = 1$.

Figure 5.11.: Energy error (left) and condition number of the hypersingular operator (right) over the degrees of freedom.

5. Implementation and Numerical Results

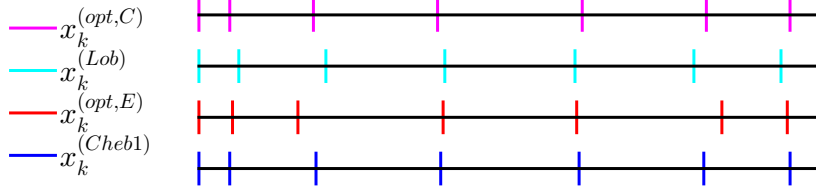


Figure 5.12.: Location of the collocation points for $p = 7$ and $\mathcal{N}_e = 1$ element.

representation, but can be computed approximately with the Matlab-function `chbpnt`. Both Greville and Demko points contain the element endpoints and are hence only appropriate for the continuous NURBS basis functions 'NURBS1'. For our application to the globally discontinuous basis function 'NURBS0', these points cannot directly be used. Therefore, we compute the collocation points with respect to the modified knot vector

$$\hat{\Xi} = \{-1, \Xi, 1\}$$

with degree $q + 1$ and remove the first and the last collocation point such that only interior collocation points are obtained.

Remark 5.2.6. (i) For NURBS-enhanced methods, the zeros of the Legendre polynomials and the Lobatto shape functions are an appropriate choice for the collocation points, as they yield an almost optimal behavior of the energy error and the condition number of the single layer and the hypersingular collocation matrix.

(ii) For isogeometric methods, we choose the Greville points and the modified Greville points as collocation points, as they can be computed in an efficient and accurate way. The numerical experiments in the subsequent section will show, that these points yield good results for low-order isogeometric BEM.

Numerical Experiments

We perform numerical experiments in order to show that the choice of the collocation points and the evaluation of the boundary integral operators yield accurate results for collocation methods. Since we do not provide a consistency analysis for collocation methods within the scope of this work, we choose the interpolation order for the evaluation of the boundary integral operators uniformly, i.e. $n = 2 \max\{\mathbf{p}\} + 1$. Although this choice is not optimal, it is sufficient for the numerical examples presented in this section. The linear system of equations is solved with the MATLAB-backslash operator. Since the energy norms $\|\cdot\|_{\mathcal{V}} := \langle \mathcal{V}\cdot, \cdot \rangle^{1/2}$ and $\|\cdot\|_{\mathcal{W}} := \langle \mathcal{W}\cdot, \cdot \rangle^{1/2}$, which are induced by the single layer and the hypersingular integral operators, are equivalent to the $H^{-1/2}$ and $H^{1/2}$ norms, respectively, we consider the error in these

norms. For Helmholtz problems, the energy norms with respect to the Laplace problem are chosen. We perform three benchmark examples on the circle, the smoothened L-shaped domain, and the slit.

Example 5.2.7. We consider Symm's integral equation for the Laplace problem

$$\mathcal{V}\varphi = f \quad \text{on } \Gamma := \{x \in \mathbb{R}^2 : \|x\|_2 = 0.25\},$$

where the right-hand side is given in polar coordinates by $f(r, \theta) = \frac{1}{12}(3\theta^2 - 6\pi\theta + 2\pi^2)$. With the identities proven in [BS87, Section 4.4.1.2, Equations (24), (26)] and the mapping properties of \mathcal{V} the exact solution can be computed by $\varphi(r, \theta) = -8 \log(2 \sin(\frac{\theta}{2}))$, which contains a logarithmic singularity for $\theta = 0$. The boundary is parametrized by the NURBS curve as defined in Example 3.1.3.

We run different refinement algorithms for the Legendre basis, a uniform h -refinement with polynomial degree $p = 0$, a uniform p -refinement with $\mathcal{N}_e = 16$ elements, a geometric hp -refinement, where the hp -mesh is created with the parameters $\vartheta = 0.25$ and $\vartheta = 0.5$ (cf. Section 1.4), respectively. For the NURBS basis functions, we run uniform h -methods with $q = 2$ for Greville and Chebyshev collocation points.

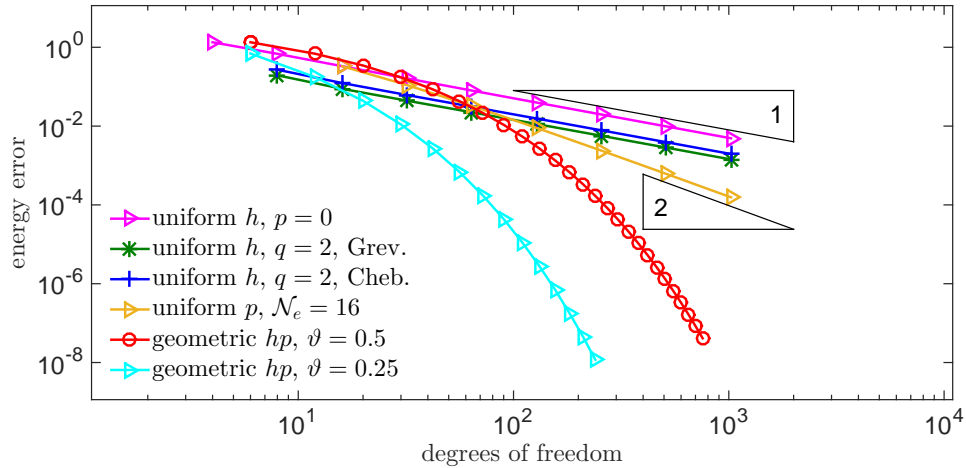


Figure 5.13.: Energy error $\|\varphi_h - \varphi\|$ over the degrees of freedom \mathcal{N} for the Laplace problem given in Example 5.2.7.

Figure 5.13 shows the energy error over the degrees of freedom. We see that the error converges algebraically with order 1 for all uniform h -methods. For uniform p -methods we obtain twice the convergence rate, which is a similar behavior as expected for Galerkin methods, although no

5. Implementation and Numerical Results

corresponding theoretical results for uniform p -refinements are available for collocation methods on closed boundaries. For both geometric hp -meshes, we observe an exponential convergence of the energy error with respect to the degrees of freedom \mathcal{N} , where the convergence for $\vartheta = 0.25$ is faster as compared to the mesh created with $\vartheta = 0.5$. We stress that with both geometric hp -methods the error could be reduced by almost 8 digits.

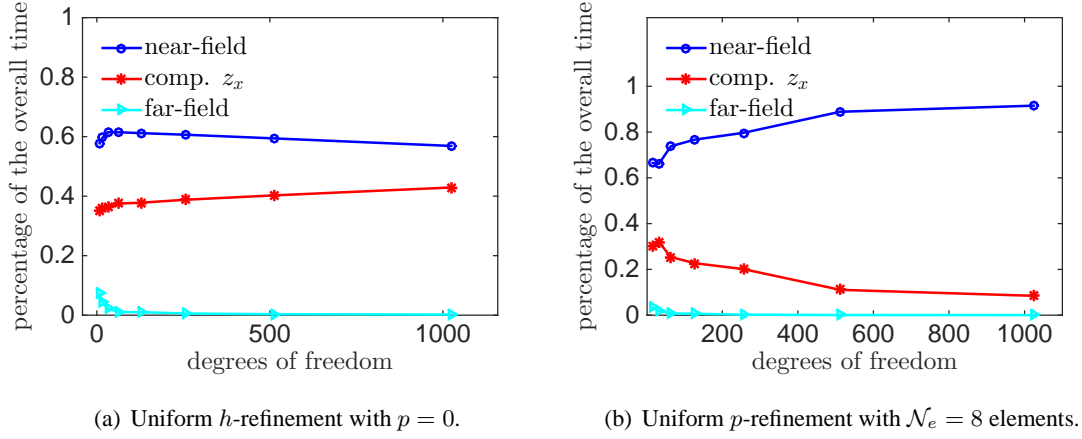


Figure 5.14.: Percentage of the computational time of the near- and far-field integrals and the computation of the zero z_x for the classification according to Remark 4.2.5.

Figure 5.14 shows the percentage of the overall time for the evaluation of the near- and far-field integrals and the computation of the zeros z_x for the classification according to Remark 4.2.5 for the uniform h - and p -methods with the Legendre basis. For both uniform h - and uniform p -refinements, we see that the computational time is dominated by the evaluation of the near-field integrals, while the time for the computation of the far-field integrals is negligible. In particular, for uniform p -refinement the time for the evaluation of the far-field integrals grows linearly in p , since the orthogonality of the Legendre polynomials is exploited. For the evaluation of the near-field integrals for uniform p -refinements, the computational time is proportional to p^2 , since the Legendre expansion of order $n = 2\max\{\mathbf{p}\} + 1$ has to be computed for all $(p + 1)$ basis functions. Furthermore, it can be observed that the time for the computation of z_x is smaller than the time needed for the evaluation of the near-field integrals for both refinements. For the uniform p -refinement, the percentage of the computation of z_x is even smaller, since the zeros z_x are computed for all evaluation points x with the efficient vector operations in MATLAB.

The second benchmark example is the following Helmholtz example on the smoothened L-shaped domain.

Example 5.2.8. We consider Symm's integral equation for the Helmholtz equation

$$\mathcal{V}\varphi = (\mathcal{K} + 1/2)u \quad \text{on } \Gamma,$$

where Γ is the boundary of the smoothened L-shaped domain:

$$q = 2, \quad \Xi = \left\{ -1, -1, -1, -\frac{3}{5}, -\frac{3}{5}, -\frac{1}{5}, -\frac{1}{5}, \frac{1}{5}, \frac{1}{5}, \frac{3}{5}, \frac{3}{5}, 1, 1, 1 \right\},$$

$$\{Q_k, k = 0, \dots, 9\} = \left\{ \begin{pmatrix} 0 \\ 0 \end{pmatrix}, \begin{pmatrix} -\frac{\sqrt{2}}{8} \\ -\frac{\sqrt{2}}{8} \end{pmatrix}, \begin{pmatrix} 0 \\ -\frac{\sqrt{2}}{4} \end{pmatrix}, \begin{pmatrix} \frac{\sqrt{2}}{4} \\ -\frac{\sqrt{2}}{2} \end{pmatrix}, \begin{pmatrix} \frac{\sqrt{2}}{2} \\ -\frac{\sqrt{2}}{4} \end{pmatrix}, \begin{pmatrix} \frac{3\sqrt{2}}{4} \\ 0 \end{pmatrix}, \right.$$

$$\left. \begin{pmatrix} \frac{\sqrt{2}}{2} \\ \frac{\sqrt{2}}{4} \end{pmatrix}, \begin{pmatrix} \frac{\sqrt{2}}{4} \\ \frac{\sqrt{2}}{2} \end{pmatrix}, \begin{pmatrix} 0 \\ \frac{\sqrt{2}}{4} \end{pmatrix}, \begin{pmatrix} -\frac{\sqrt{2}}{8} \\ \frac{\sqrt{2}}{8} \end{pmatrix} \right\}$$

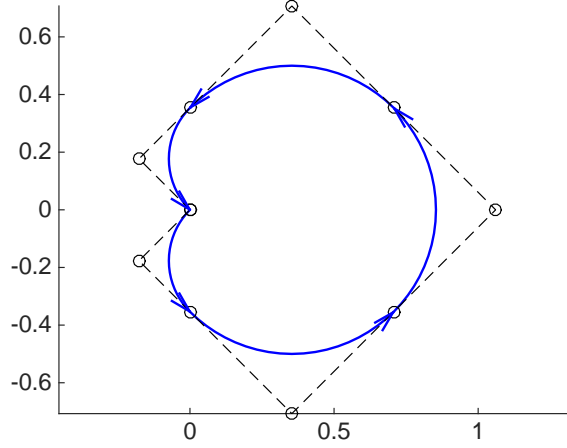


Figure 5.15.: NURBS parametrization for the smoothened L-shaped domain with control polygon (dashed).

The function u is given in polar coordinates by

$$u(r, \theta) = \Gamma(2/3 + 1) J_{2/3}(\kappa r) \sin\left(\frac{2}{3}(\theta + 4\pi/3)\right),$$

where we choose the wave number $\kappa = 2$. The Bessel function of the first kind J_ν is defined in Appendix A. By setting $u_D = u|_\Gamma$ we obtain a benchmark example for Symm's integral equation, where the exact solution has a singularity of order $r^{-1/3}$ at the origin.

For NURBS-enhanced methods, we run a uniform h -refinement with polynomial degree $p = 0$, a uniform p -refinement with $\mathcal{N}_e = 20$ elements, and geometric hp -refinements with the parameters $\vartheta = 0.25$ and $\vartheta = 0.5$ (cf. Section 1.4), respectively. For the NURBS basis functions, we run a uniform h -method with Greville collocation points and $q = 2$.

5. Implementation and Numerical Results

For all refinements, the energy error over the degrees of freedom is depicted in Figure 5.16. It can be seen that the uniform refinements yield an algebraic convergence of the energy error, whereby the error decays with twice the rate for uniform p -refinement as compared to uniform h -refinement. Both geometric hp -refinements yield an exponential decay of the energy error, where the convergence is faster for $\vartheta = 0.25$. In particular, the energy error is reduced by almost 8 digits for $\vartheta = 0.25$.

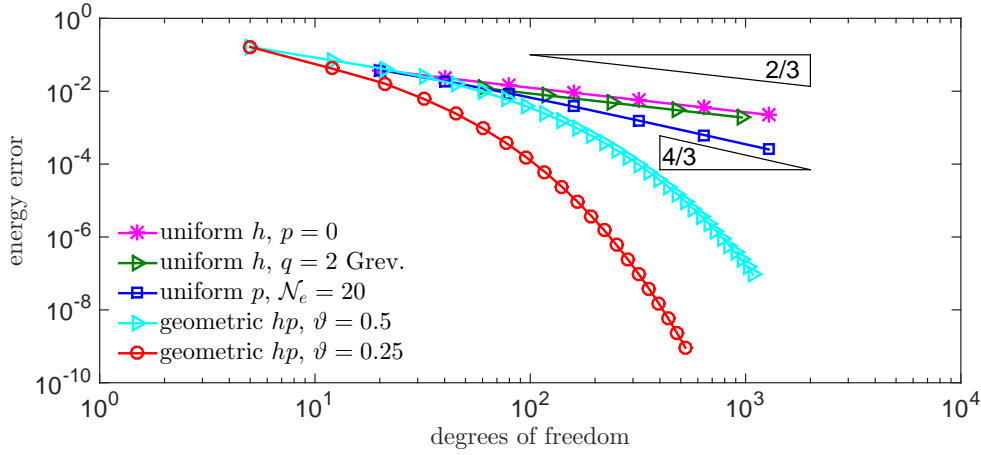


Figure 5.16.: Energy error $\|\varphi_h - \varphi\|$ over the degrees of freedom \mathcal{N} for the Helmholtz problem given in Example 5.2.8.

As third example we consider the hypersingular integral equation. We first present results for the benchmark Example 5.2.5 on the slit domain, where an exact solution is known, before we show that our implementation also works on curved arcs.

For the Lobatto basis, we run a uniform h -method with polynomial degree $p = 1$, a uniform p method with $\mathcal{N}_e = 2$ elements, and a geometric hp -method with $\vartheta = 0.5$. Furthermore, we run a uniform h -method with $q = 4$ for the globally continuous NURBS basis with Greville collocation points.

Figure 5.17 shows the energy error plotted against the degrees of freedom. All uniform methods yield an algebraic convergence, where the uniform p -methods has twice the convergence rate as compared to both uniform h -methods. For the geometric hp -method, we observe an exponential decay of the energy error. However, the convergence breaks at the level of 10^{-3} , which is caused by the exponential growth of the condition number of the hypersingular collocation matrix. Particularly in the last step we get $\text{cond}(\mathbf{W}) = 1.9 \cdot 10^8$. Using double arithmetics, only 7 significant digits of the solution of the system of linear equations are certainly correct (see [Sch88, page 34]). Since the square root is taken for the computation of the energy error,

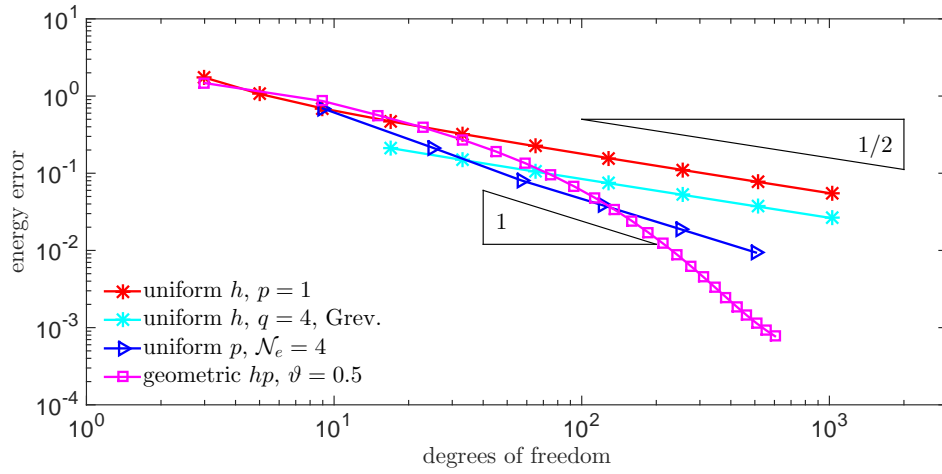


Figure 5.17.: Energy error $\|u_h - u\|$ over the degrees of freedom \mathcal{N} for the Laplace problem on the slit domain given in Example 5.2.5.

the energy error is only computed accurately up to an accuracy of 10^{-3} .

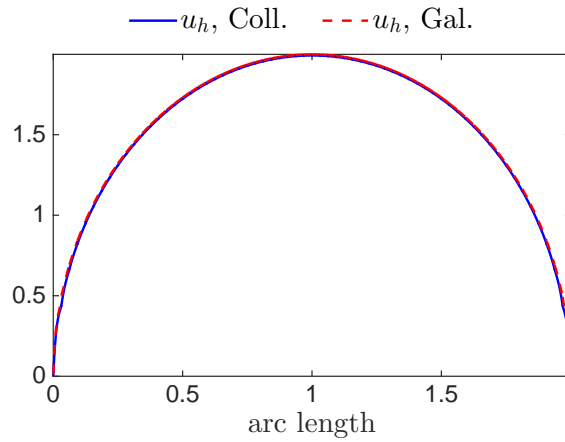


Figure 5.18.: Solution of the hypersingular integral equation $\mathcal{W}u = 1$ on the quarter circle NURBS curve defined in Example 3.1.3 computed with the collocation and the Galerkin method by a uniform h -refinement with polynomial degree $p = 3$.

We consider the hypersingular integral equation $\mathcal{W}u = 1$ on the quarter circle NURBS curve defined in Example 3.1.3. The solution is computed with a uniform h -refinement with polynomial degree $p = 3$. Since we do not know an exact solution, the discrete solution computed with the collocation method is compared with the one computed with the Galerkin method, see Figure 5.18.

Lastly, we consider a practical example of the scattering of a plane wave, which corresponds to

5. Implementation and Numerical Results

the solution of the following exterior Helmholtz problem.

Example 5.2.9. We consider Symm's integral equation for the exterior Helmholtz problem

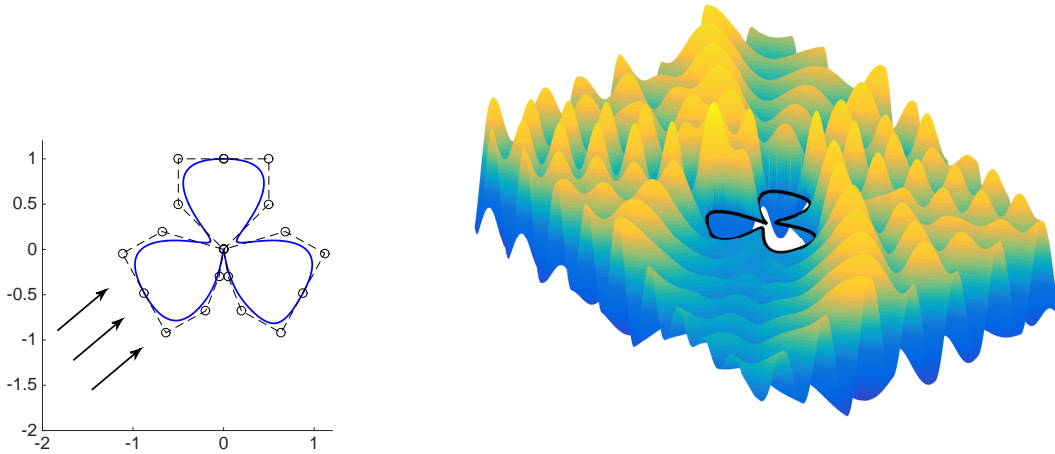
$$-\mathcal{V}\varphi = (-\mathcal{K} + 1/2)u_i \quad \text{on } \Gamma,$$

where Γ is the boundary of the scattering obstacle illustrated in Figure 5.19 (a). The incoming acoustic plane wave is defined by

$$u_i(x) = -\exp(i\kappa(\cos(\alpha)x_1 + \sin(\alpha)x_2)),$$

where we choose $\kappa = 10$ and $\alpha = \frac{5}{4}\pi$.

The solution is computed with a uniform p -method with $\mathcal{N}_e = 12$ elements. Figure 5.19 (b) shows the total acoustic wave u comprised of the incoming and scattered wave around the obstacle.



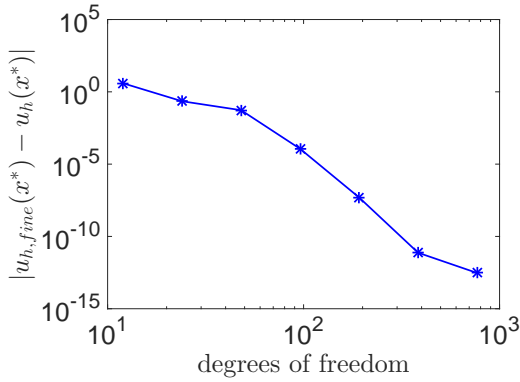
(a) Boundary of the obstacle with control polygon and direction of the incoming acoustic plane wave u_i .

(b) Total acoustic wave around the obstacle.

Figure 5.19.: Scattering of the acoustic plane wave given in Example 5.2.9.

Figure 5.20 (a) shows the point-wise error $|u_{h,fine}(x^*) - u_h(x^*)|$ for $x^* = (-0.05, -0.1)$ close to the corner of the boundary over the degrees of freedom. The fine solution $u_{h,fine}$ is computed with $\mathcal{N}_e = 12$ elements and polynomial degree $p = 128$.

Remark 5.2.10. (i) The numerical experiments show that our implementation of NURBS-enhanced and isogeometric collocation methods, specifically the evaluation of the boundary integral operators and the choice of the collocation points, yields accurate results even



(a) Point-wise error $|u_{h,fine}(x^*) - u_h(x^*)|$. The fine solution is computed with $p = 128$.

\mathcal{N}	p	absolute value $ u_h(x^*) $
96	8	$9.73702474 \cdot 10^{-5}$
192	16	$1.80172142 \cdot 10^{-5}$
384	32	$1.79677630 \cdot 10^{-5}$
768	64	$1.79677696 \cdot 10^{-5}$
1536	128	$1.79677695 \cdot 10^{-5}$

(b) Absolute value $|u_h(x^*)|$ for different degrees of freedom \mathcal{N} .

Figure 5.20.: Solution $u_h(x^*)$ evaluated at the point $x^* = (-0.05, -0.1)$ near the corner with a uniform p -method.

for high polynomial degrees $p \leq 64$ for all academic benchmark examples in the case of NURBS-enhanced methods. In the last example we present stable results even for polynomials degree $p \leq 128$.

- (ii) In contrast to the software packages HyENA [MMR⁺14] and [Sim12] we also implement the collocation method for the hypersingular integral equation, which requires the accurate evaluation of Hadamard finite part integrals.
- (iii) Due to the exponential convergence obtained for the geometrical hp -meshes, we are able to reduce the energy error by almost 8 digits for Symm's integral equation. This is close to double machine precision, since the square root is taken for the computation of the energy error. As all computations are performed in double arithmetics, this is optimal.
- (iv) Concerning the computational times we see that the overall time is dominated by the evaluation of the near-field integrals. The percentage of the time needed for the evaluation of the near-field integrals can be reduced by exploiting the knowledge on the fundamental solution and the used basis functions. Particularly, for the Laplace problem with the Legendre basis, the Legendre polynomials have to be evaluated only once for all elements. Furthermore, the Chebyshev expansion only has to be computed once for all evaluation points, as the coefficient function $g_0(x - y) = -\frac{1}{2\pi}$ in (4.3) is independent of the evaluation point x .

5.2.3. Galerkin Methods

For the implementation of Galerkin methods, we go into detail on the assembly of the Galerkin matrices \mathbf{V} , \mathbf{K} , and \mathbf{W} with the quadrature rules introduced in Section 4.3 and the a priori

5. Implementation and Numerical Results

computation of the quadrature orders.

Assembly of the Galerkin Matrices

The assembly of the Galerkin matrices is implemented in the MATLAB functions

```
V = buildV(curves,splines,p,basis,options)
K = buildK(curves,splines,p1,p2,basis1,basis2,options)
W = buildW(curves,splines,p,basis,options).
```

The input parameters `curves` and `splines` describe the geometry of the problem, `p` and `basis` specify the basis which is used for the computation, and the struct `options` contains parameters belonging to the underlying BIE, e.g. the Lamé coefficients λ and μ or the wave number κ and the flag σ_Ω specifying if interior or exterior problems are considered. All three functions allow the use of all different sets of basis functions. Hence, also modified integral equations like the Brackhage Werner formulation [BW65], where globally continuous ansatz functions are used for the Galerkin matrix of the single layer operator \mathbf{V} , can be solved with both NURBS-enhanced and isogeometric methods. Furthermore, the symmetry of the Galerkin matrices \mathbf{V} and \mathbf{W} is exploited in order to save computational time.

For the assembly of the Galerkin matrix \mathbf{W} of the hypersingular integral equation, we use the relationship to the single layer operator \mathbf{V} , which is given in Theorems 1.3.1 (iii), 1.3.2 (iii), and 1.3.5 (v) for the Laplace, Lamé, and Helmholtz equations. Since the basis functions Ψ_k and their arc length derivatives $\frac{\partial}{\partial s}\Psi_k$ have to be evaluated, we support a general linear combination

$$a \Psi_k + b \frac{\partial}{\partial s} \Psi_k, \quad a, b \in \mathbb{C}$$

for the assembly of the Galerkin matrix \mathbf{W} , which is specified for each partial differential operator in the function `basisW`.

The Galerkin matrices are assembled element-by-element, where we distinguish far-field, neighboring and identical elements. For the non-local basis functions, the local contributions are added up.

The assembly of the Galerkin matrices is implemented as black box. Since after the regularization with the coordinate transformations (4.32) and (4.48) for neighboring and identical elements only the logarithmic term has to be evaluated with a special Gauss-Log quadrature, we consider kernel functions of the general type

$$\tilde{K}(x - y) = g_1(x - y) \log |x - y| + g_2(x - y). \quad (5.8)$$

Hence, for the assembly of the Galerkin matrices only the functions g_1 , g_2 , and K have to be implemented by the user in the MATLAB functions `g1`, `g2`, and `K`, which allows the easy incorporation of new kernel functions into the software package. We remark that although the whole

kernel function K can be evaluated by the functions g_1 and g_2 with representation (5.8), the user has to implement the function K separately in order to save computational time.

If only one of the two functions g_1 and g_2 is present in (5.8), only this function has to be implemented by the user. In this case only the integrals corresponding to the non-vanishing function are evaluated, which saves computational time.

For neighboring and identical elements we proceed as follows. After having applied the coordinates transformations we split the logarithm in (5.8) according to Equations (4.34) and (4.49). In the case of identical elements, we hence obtain for the transformed kernel

$$\begin{aligned} K(\gamma_i(\theta_1(u, v)), \gamma_i(\theta_2(u, v))) \\ &= g_1(\gamma_i(\theta_1(u, v)) - \gamma_i(\theta_2(u, v))) \log\left(\frac{v+1}{2}\right) \\ &+ g_1(\gamma_i(\theta_1(u, v)) - \gamma_i(\theta_2(u, v))) \log\left(\frac{|\gamma_i(\theta_1(u, v)) - \gamma_i(\theta_2(u, v))|}{v+1}\right) \\ &+ g_2(\gamma_i(\theta_1(u, v)) - \gamma_i(\theta_2(u, v))). \end{aligned}$$

While the first term is evaluated with a combination of Gauss-Log quadrature in v and Gauss-Legendre quadrature in u , the second and third terms are evaluated with a tensor Gauss-Legendre quadrature.

A Priori Computation of the Quadrature Order

The quadrature orders are computed according to the estimates given in Tables 4.1-4.3, such that the consistency error arising in the assembly of the Galerkin matrices does not affect the convergence rates of the Galerkin method. Since the asymptotic behavior of the quadrature error is described by the maximum ellipses contained in the domain of analyticity of the kernel (with respect to both integration variables), the semi-axis sums ρ_1 and ρ_2 of these ellipses have to be computed explicitly in order to obtain sharp and reliable bounds.

For identical elements, we have proven the analyticity of the kernel on \mathcal{E}_{ρ_i} (cf. Lemma 4.3.22 and Corollary 4.3.23). Since the semi-axis sum ρ_i is already precomputed and stored in the field `splines.rho`, we obtain a sharp estimate for the needed quadrature order in this case.

For far-field and neighboring elements, the optimal values of ρ_1 and ρ_2 can also be computed explicitly. The domain of analyticity is limited by the zeros of

$$\gamma_i(s) - \gamma_i(t)$$

for far-field and the zeros of

$$\frac{\gamma_i\left(\frac{(1+u)(1-v)}{2} - 1\right) - \gamma_j(v)}{1-v}$$

5. Implementation and Numerical Results

for neighboring elements. Therefore, the optimal values of ρ_1 are obtained by computing the zeros with respect to s and u for fixed $t, v \in [-1, 1]$, respectively. Similarly, the optimal values of ρ_2 are obtained by computing the zeros with respect to t and v for fixed $s, u \in [-1, 1]$, respectively. The values ρ_1 and ρ_2 are then the semi-axis sums of the largest ellipses not containing any zero. However, in both cases the computation is very time-consuming and most of the overall computational time would be spent in the computation of the quadrature order, but not in the quadrature itself. Hence, we use the worst case estimates given in Lemmas 4.3.2 and 4.3.12 for the computation of ρ_1 and ρ_2 , which yield larger estimates for the quadrature orders, but can be computed very efficiently. In the following, we only describe the computation of the semi-axis sum ρ_1 , the computation of ρ_2 is alike. For far-field and neighboring elements, the semi-axis sum ρ_1 is of the type

$$\begin{aligned} \rho_1 &= \min\{a + \sqrt{a^2 - 1}, \rho_i\}, \\ a &= 1 + \frac{D}{c(a) \max_{t \in [-1, 1]} |\dot{\gamma}_i(t)|} =: 1 + c(a)^{-1} \tilde{C}. \end{aligned} \quad (5.9)$$

Here, the constant $c(a)$ is given by

$$c(a) = \frac{(a_i + a)^{2(q-1)}}{(a_i - a)^{2q}} \frac{(a_i - 1)^{2q}}{(a_i + 1)^{2(q-1)}}, \quad (5.10)$$

where a_i denotes the length of the real semi-axis of \mathcal{E}_{ρ_i} and q denotes the order of the boundary parametrization (cf. Lemma 3.2.12). For far-field elements, the constant D is the distance of both elements and for neighboring elements D depends on the shape, the angle, and the ratio of the arc lengths of both elements. Since both sides of (5.9) depend on a we obtain the maximum value of a by solving

$$\max_{1 < a < a_i} \min \left\{ a, 1 + c(a)^{-1} \tilde{C} \right\}, \quad (5.11)$$

which is equivalent to solving the equation

$$f(a) := 1 + c(a)^{-1} \tilde{C} - a = 0. \quad (5.12)$$

An example is illustrated in Figure 5.21.

In order to obtain an approximate solution of (5.12) we apply one step of Newton's method with initial value $a = 1$. With

$$f'(a) = -\tilde{C} \frac{(a_i + 1)^{2(q-1)}}{(a_i - 1)^{2q}} \left(2q \frac{(a_i - a)^{2q-1}}{(a_i + a)^{2(q-1)}} + 2(q-1) \frac{(a_i - a)^{2q}}{(a_i + a)^{2q-1}} \right) - 1$$

we obtain as approximate solution

$$a = 1 - \frac{f(1)}{f'(1)} = 1 + \frac{\tilde{C}}{\tilde{C} [2q(a_i - 1)^{-1} + 2(q-1)(a_i + 1)^{-1}] - 1}.$$

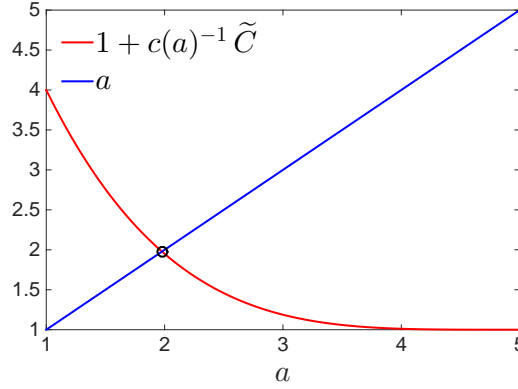


Figure 5.21.: Problem (5.11) for $a_i = 5$ and $\tilde{C} = 3$. The optimal parameter a is depicted as a black dot.

In order to investigate how accurate the approximation is, we compare the optimal semi-axis sums $\rho^{(opt)}$ with the semi-axis sums $\rho^{(WC)}$ obtained by the worst case estimates of Lemmas 4.3.2 and 4.3.12 for far-field and neighboring elements. Besides simple geometries occurring in most academic examples, we also consider element combinations that are known to be critical for the evaluation of the arising integrals with a Gauss-Legendre quadrature, see [AG10].

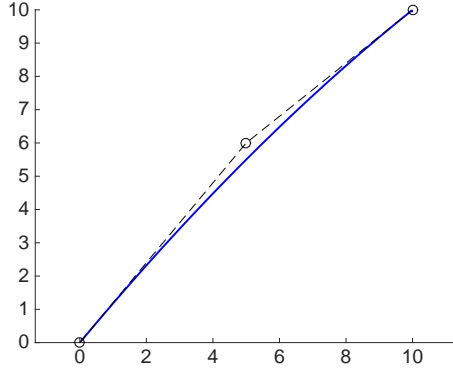
For far-field elements, we consider four benchmark examples: a quadratic smooth, the standard quadratic quarter circle, a quadratic non-smooth, and an oscillating fifth degree NURBS curve. All curves are illustrated in Figure 5.22.

In order to compare $\rho^{(opt)}$ and $\rho^{(WC)}$, we proceed as follows. First, we refine each spline until we obtain $n \in \mathbb{N}$ elements. Then, we compute for each far-field element combination (T_1, T_j) , $j = 3, \dots, n$, the semi-axis sums $\rho_j^{(opt)}$ and $\rho_j^{(WC)}$.

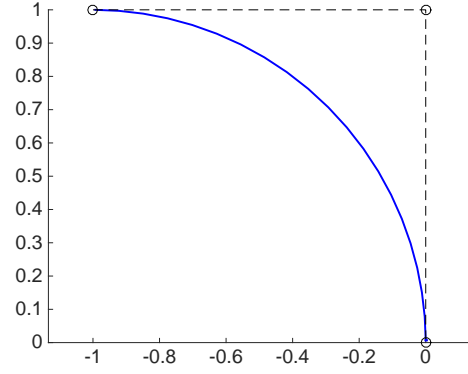
Figure 5.23 shows $\log(\rho_j^{(opt)})$ and $\log(\rho_j^{(WC)})$ plotted against the element index j . In all examples we see the dependency of both semi-axis sums on the distance D , particularly the decreasing domain of analyticity for a decreasing distance D . Hence, we only obtain a very slow exponential convergence of the quadrature error for small distances D . Furthermore, both bottom subfigures show that the value $\log(\rho_j^{(opt)})$ is spoiled by the small domain of analyticity \mathcal{E}_{ρ_i} of the parametrization, which explains the cut off in both red plots. Overall, we see that $\rho_j^{(WC)}$ is a reliable lower bound for all $j = 1, \dots, n$, which imitates the behavior of the optimal value $\rho_j^{(opt)}$.

Next, we investigate the factor, by which the optimal quadrature order computed with $\rho_j^{(opt)}$ is overestimated by the order computed with our worst case approximation $\rho_j^{(WC)}$. Figure 5.24

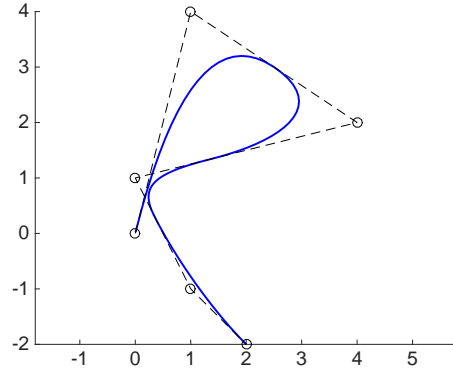
5. Implementation and Numerical Results



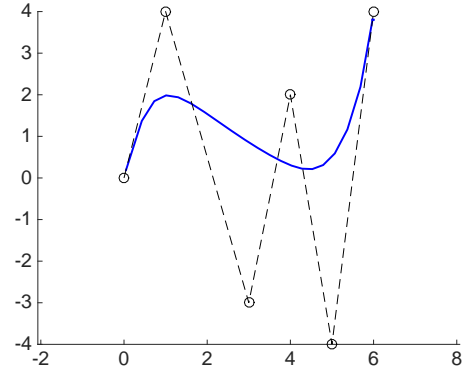
(a) Second degree NURBS curve with $\rho_i = 14.1$.



(b) Second degree NURBS curve with $\rho_i = 5.02$.



(c) Second degree NURBS curve with four elements and $\rho_i = (1.80, 1.57, 1.82, 4.6)$.



(d) Fifth degree NURBS curve with $\rho_i = 1.21$.

Figure 5.22.: NURBS curves for the benchmarks in the case of far-field elements.

shows the quotients

$$r_{\min} = \min_{j=3,\dots,n} \frac{\log(\rho_j^{(opt)})}{\log(\rho_j^{(WC)})} \quad \text{and} \quad r_{\max} = \max_{j=3,\dots,n} \frac{\log(\rho_j^{(opt)})}{\log(\rho_j^{(WC)})} \quad (5.13)$$

of each refinement step plotted against the number of refinements of the NURBS curves. In all subfigures the minimal quotient decreases with respect to the number of refinements and is smaller than 2 for all examples after 10 refinements. The maximum quotient r_{\max} is bounded for all four curves. Asymptotically, the quadrature order is overestimated by a factor of at most 3.5 for the bottom right example, while we obtain less than a factor of 2 for both top subfigures. For all examples, the maximum value r_{\max} is attained for the element combination (T_1, T_3) , which corresponds to almost neighboring elements. Here, there holds $\frac{D}{h_1} \approx 1$ and hence the constant $c(a)$ has a big impact on the worst case estimate $\rho_3^{(WC)}$ in Equation (5.9). This implies that we overestimate the quadrature error by a larger factor in this case. The effect is strengthened for

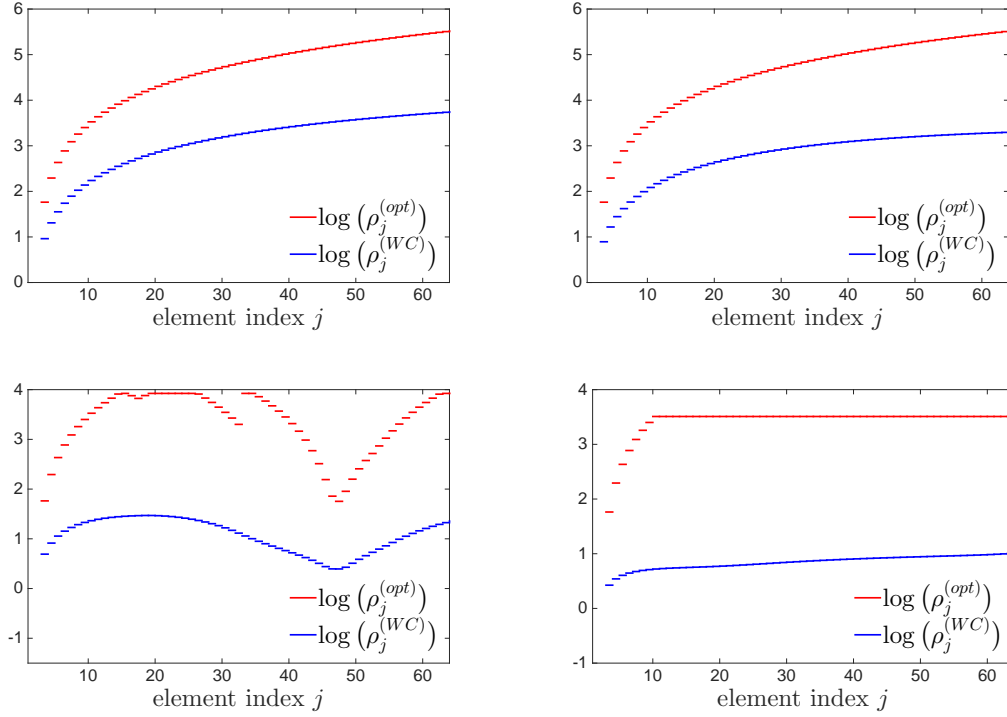


Figure 5.23.: Optimal value $\log(\rho_j^{(opt)})$ and approximated value $\log(\rho_j^{(WC)})$ plotted over j for $n = 64$ elements. All subfigures correspond to the NURBS curves illustrated in the respective subfigures in Figure 5.22.

high-order and non-smooth NURBS curves. For large distances D , the impact of $c(a)$ on $\rho_3^{(WC)}$ is small, which yields good results for the quadrature orders in most cases.

For neighboring elements, we investigate the effect of the angle between both elements on the optimal and the approximated semi-axis sums $\rho^{(opt)}$ and $\rho^{(WC)}$, where we consider three benchmark curves: linear elements, the standard quarter circles with mesh-width ratio 2, and a second order non-smooth NURBS curve, see Figure 5.25. For all curves we start with angle $\beta \approx 0$ and increase the angle linearly by rotating the control points belonging to the second element until both elements intersect.

Figure 5.26 shows $\log(\rho^{(opt)})$ and $\log(\rho^{(WC)})$ (left) and the quotient $\frac{\log(\rho^{(opt)})}{\log(\rho^{(WC)})}$ (right) plotted against the angle β . All left subfigures show that both semi-axis-sums $\rho^{(WC)}$ and $\rho^{(opt)}$ tend to 1, as the angle between both elements vanishes. Hence, for elements with small angles $\beta > 0$, we have a slow exponential, nearly algebraic convergence of the quadrature error, which implies that high quadrature orders are needed.

5. Implementation and Numerical Results

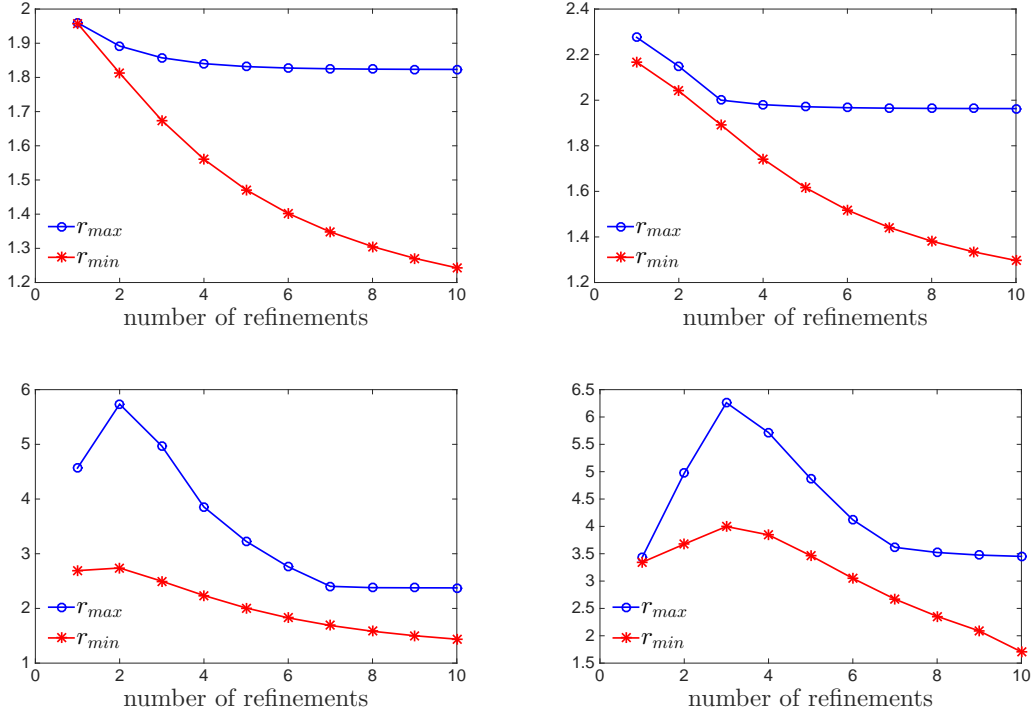
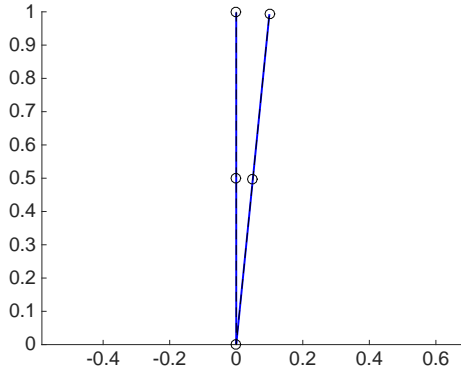


Figure 5.24.: Quotient r_{\max} and r_{\min} as defined in Equation (5.13) plotted over the number of refinements. All subfigures correspond to the NURBS curves illustrated in the respective subfigures in Figure 5.22.

The middle and bottom figures on the left-hand side of Figure 5.26 show that the optimal values $\log(\rho^{(opt)})$ are cut off for all angles $\approx \pi$, which is due to the small domain of analyticity of the NURBS curve itself. Similarly to the far-field case, the approximations $\rho^{(WC)}$ provide a lower bound for all angles and all curves. However, $\rho^{(WC)}$ is a coarse approximation of $\rho^{(opt)}$ for most angles and the needed quadrature order is overestimated, which is illustrated in the right-hand side plots. While for the standard quarter circle with mesh-width ratio 2 the quadrature order is overestimated by a factor of 4, the factor is much smaller for the non-smooth NURBS curve for angles $\beta \in (0.6\pi, \pi)$. This is due to the small domain of analyticity of the NURBS parametrization itself. For linear elements, $\log(\rho^{(WC)})$ is by a factor of 2-2.6 smaller than $\log(\rho^{(opt)})$. For the uniform h -refinement, we hence expect that the quadrature order is asymptotically overestimated by factors between 2 and 3, since all NURBS curves converge to linear elements.

In order to investigate the effect of large mesh-width ratios $\sigma(\mathbf{h})$ on the domain of analyticity of the kernel function for neighboring elements, we consider the linear elements depicted in Figure 5.25 (a) with angle $\beta = \pi/2$ for different mesh-width ratios. Figure 5.27 (left) shows



(a) Linear elements with mesh-width ratio 1.

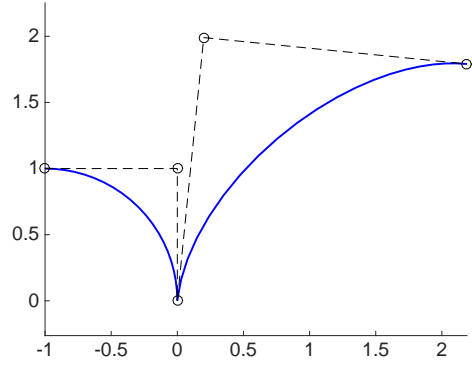
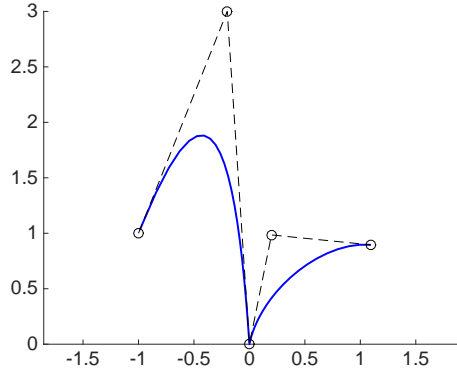
(b) Second degree NURBS curve with $\rho_i = (5.02, 5.02)$ and mesh-width ratio 2.(c) Second degree NURBS curve with four elements and $\rho_i = (1.24, 2.6)$ and mesh-width ratio 2.1.

Figure 5.25.: NURBS curves used for the benchmarks in the case of neighboring elements.

the optimal semi-axis sum $\log(\rho^{(opt)})$ and the approximation $\log(\rho^{(WC)})$ over the mesh-width ratio $\sigma(\mathbf{h})$. Both semi-axis sums decrease as the mesh-width ratio increases, which shows the sensitivity of the quadrature rules on high mesh-width ratios. In addition, the approximation behaves like the optimal value $\log(\rho^{(opt)})$, whereby the optimal value is approximated better for larger mesh-width ratios (see Figure 5.27 (right)).

Finally, we show the quadrature orders used for the assembly of the single layer Galerkin matrix on the circle, which are computed with the a priori estimates given in Table 4.1. Figure 5.28 shows the number of Gauss points $\log(n_1 \cdot n_2)$ for a uniform mesh with $\mathcal{N}_e = 32$ elements and uniform polynomial degree $\mathbf{p} = 2$ and a geometrically graded mesh with $\vartheta = 0.25$ and $\sigma = 1$ ($\mathcal{N}_e = 25$). The first and last element correspond to the smallest elements with polynomial degrees $p_1 = p_{25} = 0$.

5. Implementation and Numerical Results

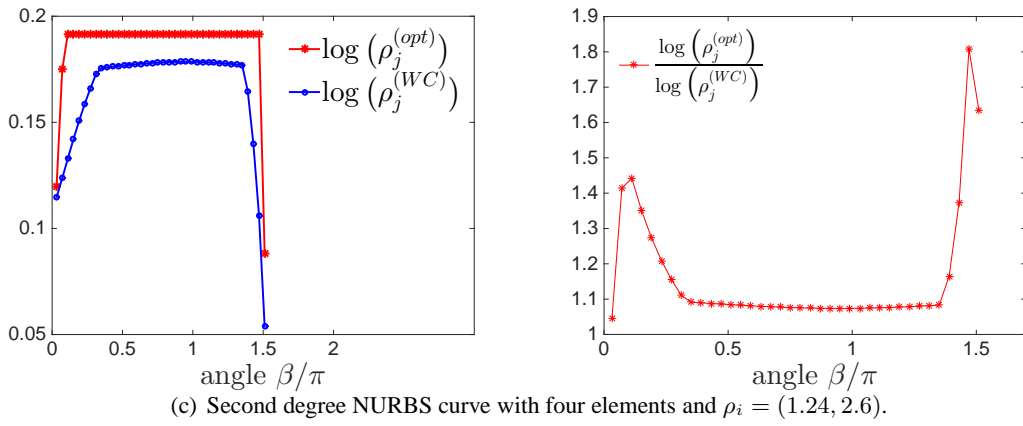
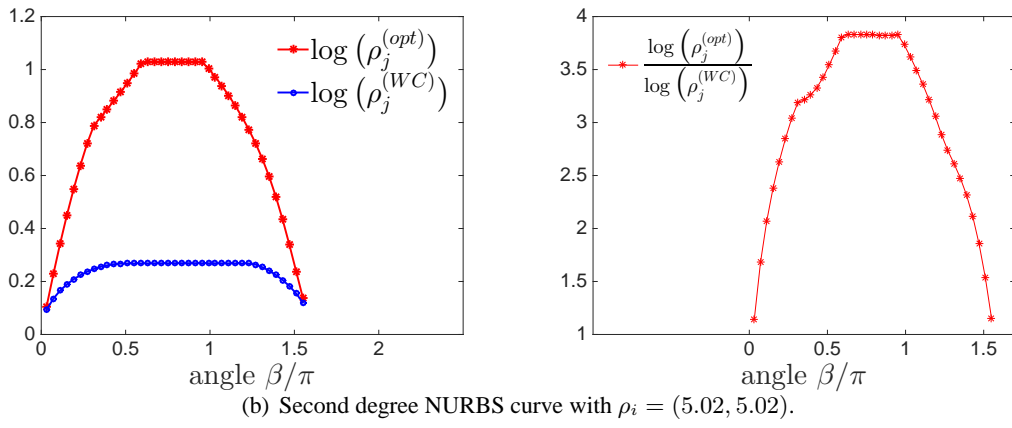
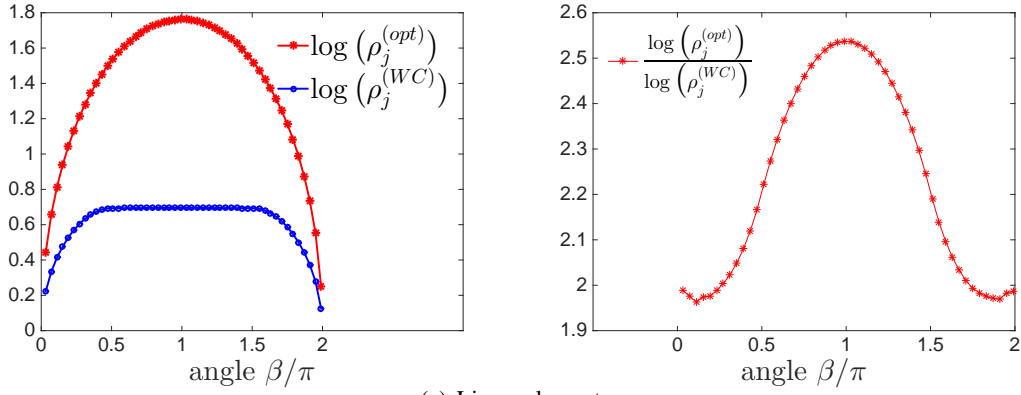


Figure 5.26.: $\log(\rho^{(WC)})$ and $\log(\rho^{(opt)})$ plotted against the angle between both elements (left) and the corresponding ratio $r = \log(\rho^{(opt)})/\log(\rho^{(WC)})$ (right). The three subfigures on the left- and right-hand side correspond to the NURBS curves illustrated in the respective subfigures in Figure 5.25.

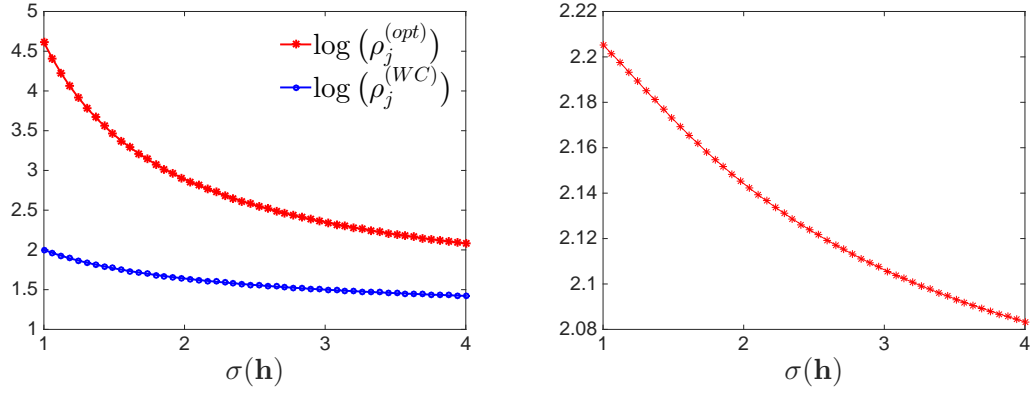
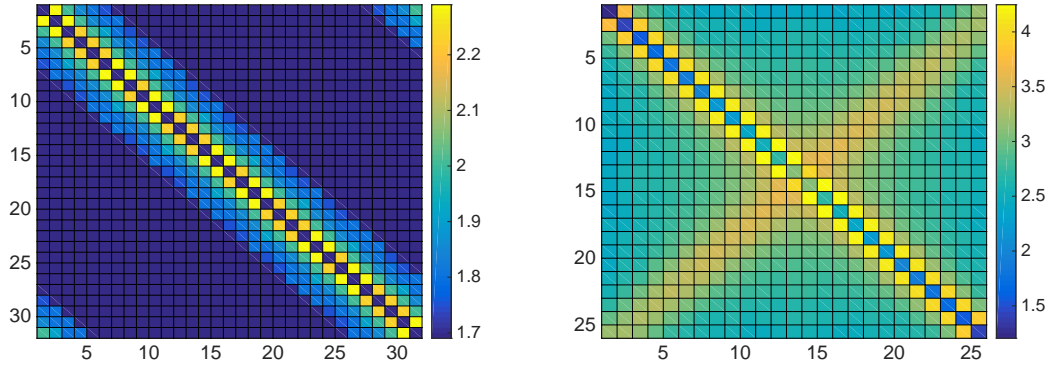


Figure 5.27.: The values of $\log(\rho^{(WC)})$ and $\log(\rho^{(opt)})$ (left) and corresponding ratio $r := \log(\rho^{(opt)}) / \log(\rho^{(WC)})$ (right) plotted against the mesh-width ratio $\sigma(\mathbf{h})$.

Both subfigures show that the quadrature orders are symmetric with respect to both diagonals,



(a) Uniform mesh with $\mathcal{N}_e = 32$ elements and polynomial degree $\mathbf{p} = 2$.

(b) Geometrically graded mesh with $\vartheta = 0.25$ and $\sigma = 1$ and $\mathcal{N}_e = 25$ elements.

Figure 5.28.: The number of Gauss points $\log(n_1 \cdot n_2)$ computed with the a priori estimates given in Table 4.1 for the single layer operator on the circle. The geometrically graded mesh is refined towards the first element.

which is what we expected as the uniform and the geometrically graded meshes are symmetric. In the case of the uniform mesh (subfigure (a)) the number of Gauss points for far-field elements increases as the distance between both elements decreases, which coincides with the behavior of $\rho^{(WC)}$ illustrated in Figure 5.23. In particular, $n_1 \cdot n_2 = 49$ Gauss points are chosen for elements with large distances, while for almost neighboring elements the quadrature order increases to $n_1 \cdot n_2 = 100$. The highest quadrature orders are chosen for neighboring elements,

5. Implementation and Numerical Results

i.e. $n_1 \cdot n_2 = 168$, whereas for identical elements, $n_1 \cdot n_2 = 49$ Gauss points suffice.

For the geometrically graded hp -mesh (subfigure (b)), we obtain similar results, where we can additionally observe the linear dependency of the quadrature order on the polynomial degree. In particular, we see that the quadrature order increases linearly towards the diagonal pointing from the bottom left to the top right, which corresponds to the elements with the largest polynomial degrees.

Numerical Experiments

We present several benchmark examples for isogeometric and NURBS-enhanced Galerkin methods in order to show that our implementation produces accurate results. For the solution of the system of linear equations the MATLAB backslash operator is used. For NURBS-enhanced methods, the Galerkin matrix is preconditioned by a diagonal scaling. All computations are performed on a desktop computer with an AMD Phenom II X6 processor (6 cores), 16GB RAM, and the Ubuntu 10.04 operating system.

The first benchmark example is Symm's integral equation for the Laplace operator, which is introduced in Example 5.2.7. For NURBS-enhanced methods, we run a uniform h -method with polynomial degree $p = 5$, a uniform p -method with $\mathcal{N}_e = 16$ elements and geometric hp -methods with $\vartheta = 0.25$ and $\vartheta = 0.5$, respectively. Figure 5.29 shows the energy error and the computational time for the assembly of the linear system of equations over the degrees of freedom. The uniform h -method converges algebraically with order 1, while we observe twice the order for the uniform p -method, which is the expected behavior, see Theorem 1.6.5 and Remark 1.6.6. The geometric hp -methods converge exponentially with respect to the degrees of freedom. For $\vartheta = 0.25$, we are able to reduce the energy error by almost 8 digits, which is close to double machine precision.

The computational times, which are the times for the assembly of the Galerkin matrix and the right-hand side, are illustrated in the bottom picture of Figure 5.29. It can be seen that for the uniform h -refinement the computational time is proportional to \mathcal{N}^2 and the computational time asymptotically grows with order 4 for uniform p -refinement.

For isogeometric methods, we run uniform h -, p -, and k -refinements. In order to guarantee that the NURBS parametrization is $C^\infty(-1, 1)$ regular, the boundary is parametrized by the following NURBS-curve:

$$q = 5, \quad \Xi = \{-1, -1, -1, -1, -1, -1, 1, 1, 1, 1, 1, 1\},$$

$$\{Q_k, k = 0, \dots, 4\} = \left\{ \begin{pmatrix} 0.5 \\ 0 \end{pmatrix}, \begin{pmatrix} 0.5 \\ 2 \end{pmatrix}, \begin{pmatrix} -1.5 \\ 1 \end{pmatrix}, \begin{pmatrix} -1.5 \\ -1 \end{pmatrix}, \begin{pmatrix} 0.5 \\ -2 \end{pmatrix} \right\}.$$

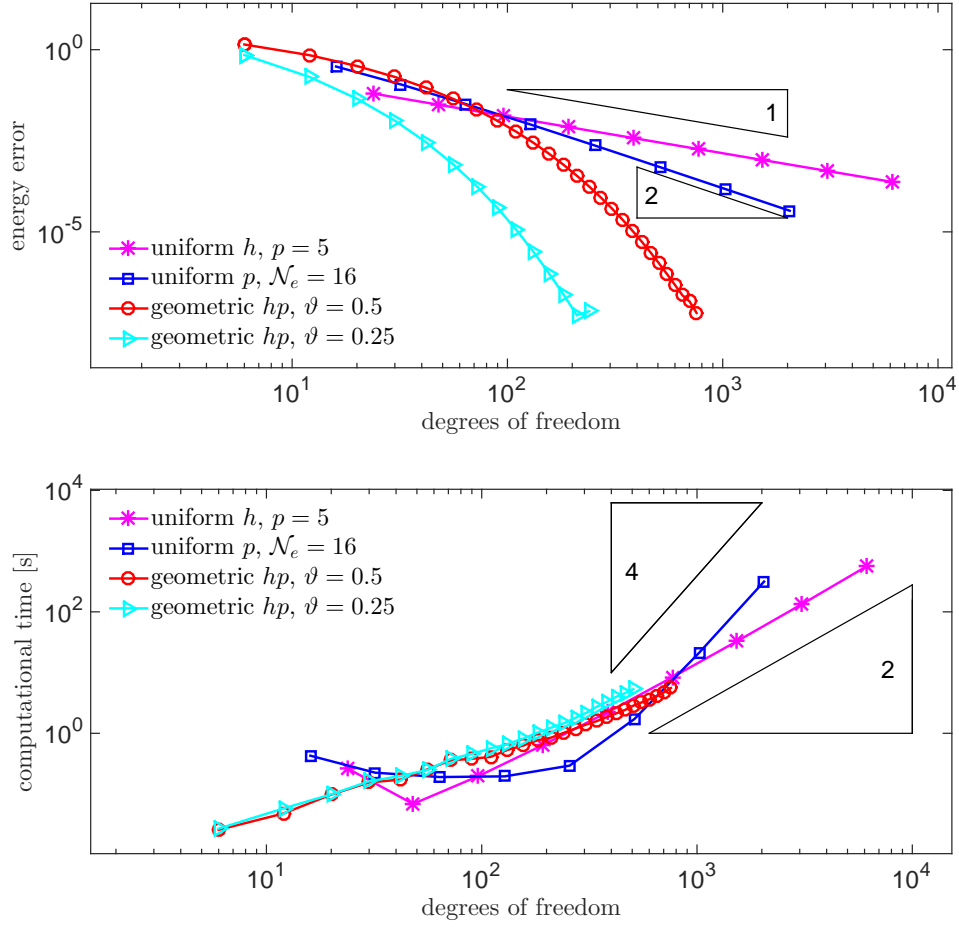


Figure 5.29.: Energy error $\|\varphi - \varphi_h\|$ (top) and computational time (assembly of the Galerkin matrix and right-hand side) in seconds (bottom) over the degrees of freedom \mathcal{N} for the Laplace Example 5.2.7.

For the computations, the NURBS curve is two times pre-refined.

Figure 5.30 shows the energy error over the degrees of freedom. We see that both uniform h -refinements yield an algebraic convergence with order 1, while we obtain twice the convergence rates for the uniform p - and k -refinements. Due to the exponential growth of the condition number of the single layer Galerkin matrix for the uniform p - and k -refinements, which is observed in Figure 5.5, the convergence breaks for $p = 25$ and $p = 27$, respectively.

The second benchmark is the Helmholtz problem on the smoothened L-shaped domain defined in Example 5.2.8. Again, we compute the energy error with respect to the single layer operator of the Laplace equation, which is equivalent to the $H^{-1/2}$ norm. For NURBS-enhanced meth-

5. Implementation and Numerical Results

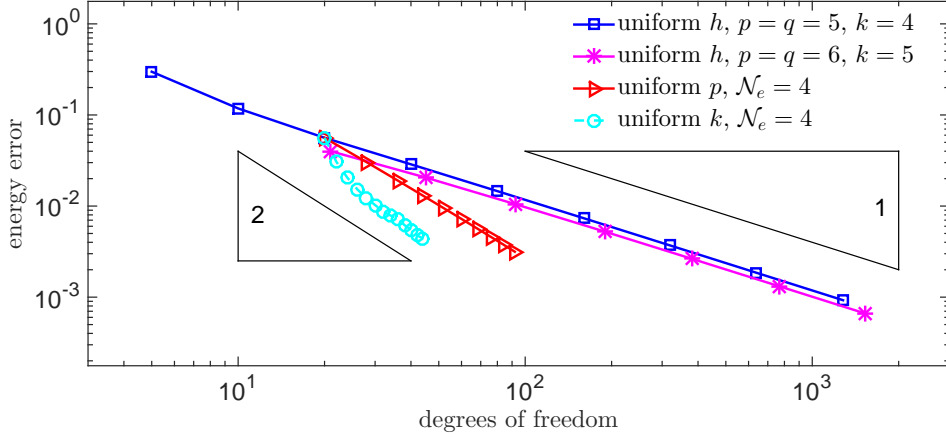


Figure 5.30.: Energy error $\|\varphi - \varphi_h\|$ over the degrees of freedom \mathcal{N} for the Laplace Example 5.2.7.

ods, we run a uniform h -method with polynomial degree $p = 0$, a uniform p -refinement with $\mathcal{N}_e = 20$ elements, and geometric hp -methods with $\vartheta = 0.25$ and $\vartheta = 0.5$, respectively. For the NURBS basis functions, we run a uniform h -method with $q = 2$. Figure 5.31 shows the energy error and the computational times (for the assembly of the single layer operator and the right-hand side) over the degrees of freedom.

The top picture shows that all uniform methods yield an algebraic decay of the energy error, the uniform p -method having twice the convergence rate of the uniform h -methods. Both geometric hp -refinements yield an exponential convergence, where the energy error could be reduced to 10^{-9} with less than 600 degrees of freedom using $\theta = 0.25$. Looking at the computational times we see that the times are proportional to \mathcal{N}^2 for the uniform h -methods and \mathcal{N}^4 for the uniform- p method. Since the overall time is dominated by the evaluation of the Hankel and Bessel functions, the computational time for the uniform p -method is smaller as compared to both uniform h -methods. Further, the computational times for both geometric hp -refinements are proportional to \mathcal{N}^2 .

As third benchmark example, we investigate the following Lamé problem on the smoothened L-shaped domain:

Example 5.2.11. We consider the hypersingular integral equation for the Lamé problem

$$\mathcal{W}u = (1/2 - \mathcal{K}')\varphi \quad \text{on } \Gamma,$$

where Γ is the boundary of the smoothened L-shaped domain defined in Example 5.2.8. We

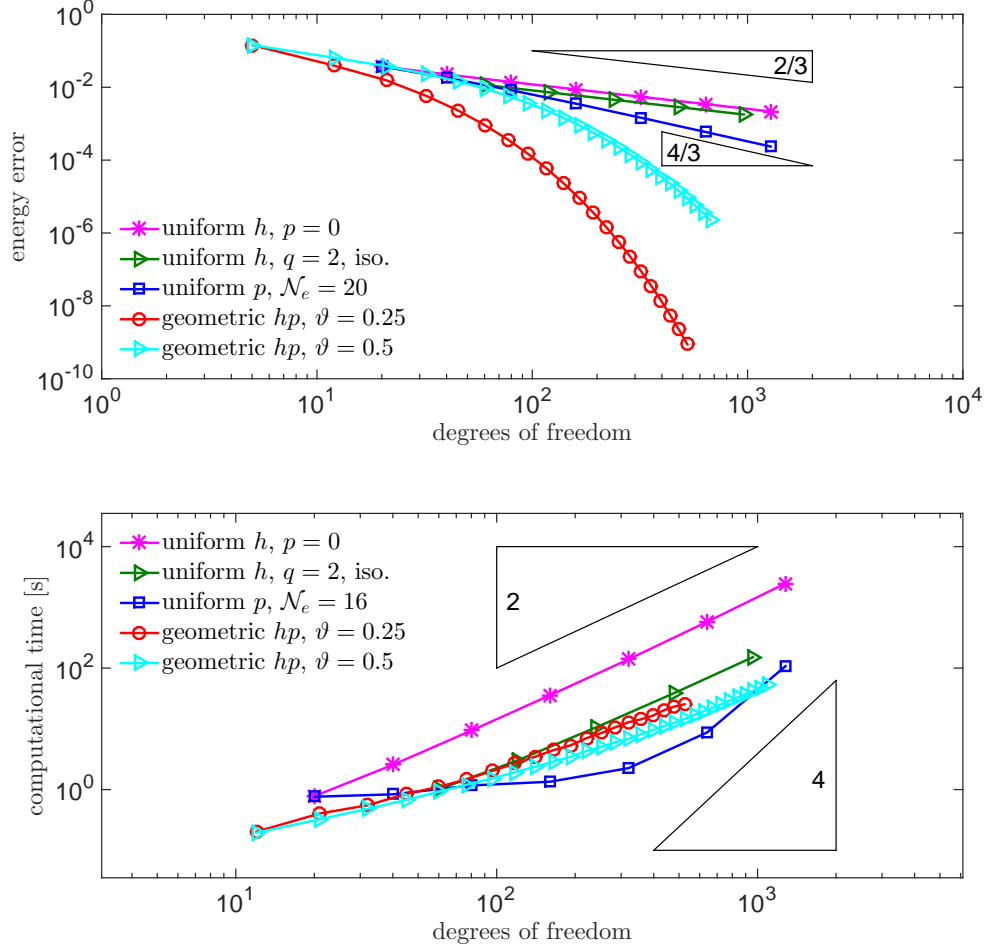


Figure 5.31.: Energy error $\|\varphi - \varphi_h\|$ (top) and computational time (assembly of \mathbf{V} and the right-hand side $(\mathbf{K} + 1/2\mathbf{M})\mathbf{u}$) in seconds (bottom) over the degrees of freedom \mathcal{N} for the Helmholtz Example 5.2.8.

define the function u in polar coordinates by

$$u(r, \theta) := \frac{r^\alpha}{2\mu} \begin{pmatrix} \{-(\alpha+1) \cos[(\alpha+1)\theta] + [C_2 - (\alpha+1)] C_1 \cos[(\alpha-1)\theta]\} \\ \{(\alpha+1) \sin[(\alpha+1)\theta] + [C_2 + \alpha - 1] C_1 \sin[(\alpha-1)\theta]\} \end{pmatrix}$$

with $\alpha := 0.544483736782464$, $C_1 := -\frac{\cos((\alpha+1)\omega)}{\cos((\alpha-1)\omega)}$, $C_2 := \frac{\lambda+2\mu}{\lambda+\mu}$, and $\omega = \frac{3\pi}{4}$. By setting $\varphi := \gamma_1^- u|_\Gamma$ to be the interior co-normal derivative of u , we obtain a benchmark example.

We run uniform h -methods with polynomial degrees $q = 2$ for the isogeometric basis and $p = 7$ for the Lobatto basis, a uniform p -method with $\mathcal{N}_e = 20$ elements, and geometric hp -methods with $\vartheta = 0.5$ and $\vartheta = 0.25$, respectively.

Figure 5.32 shows the energy error and the computational times for the assembly of \mathbf{W} and

5. Implementation and Numerical Results

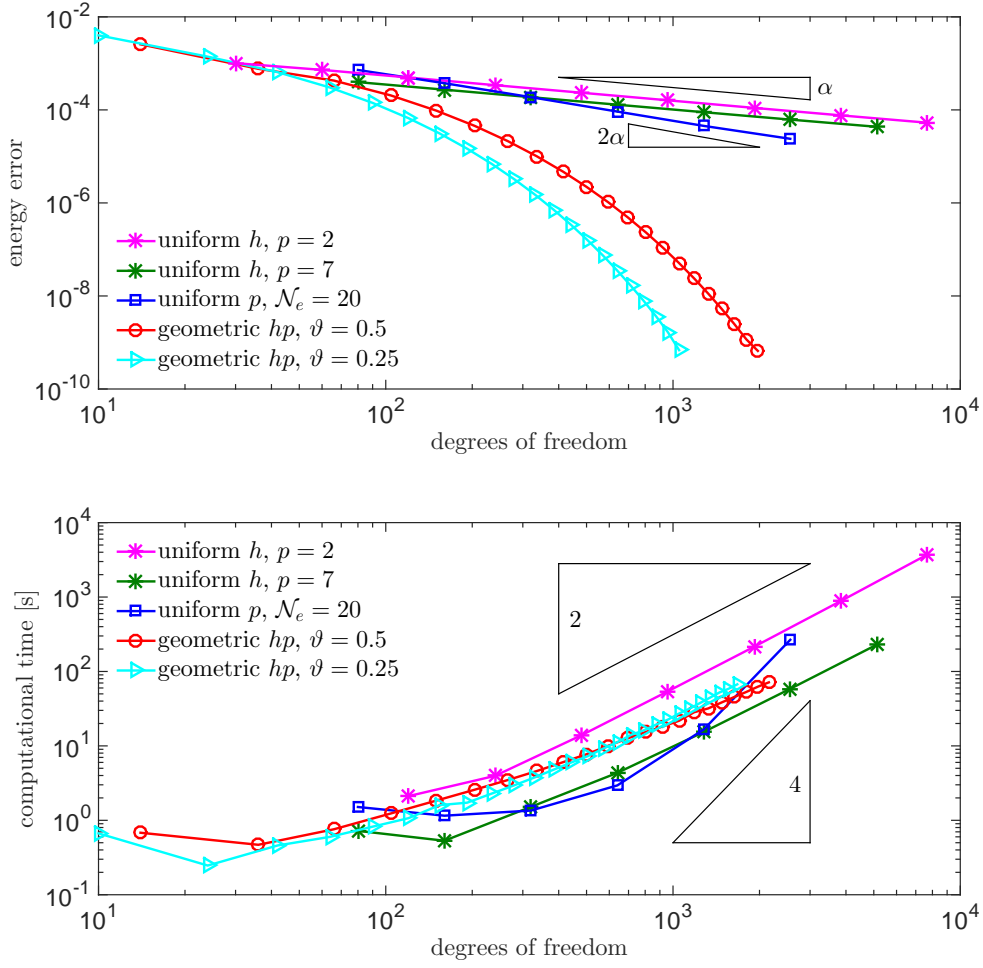


Figure 5.32.: Energy error $\|u - u_h\|$ (top) and computational time for the assembly of \mathbf{W} and the right-hand side in seconds (bottom) over the degrees of freedom \mathcal{N} for the Lamé Example 5.2.11.

the right-hand side over the degrees of freedom. For all uniform methods, we observe an algebraic decay of the energy error with rate α for the uniform h - and 2α for the uniform p -refinement, which is the expected rate for this Lamé example. The geometric hp -refinements yield an exponential convergence, whereby the energy error can be reduced by 7 significant digits for $\vartheta = 0.25$. In the bottom picture showing the computational times we see a quadratic growth for the assembly of the system of linear equations for both uniform h - and geometric hp -methods. For the uniform p -refinement, we observe an algebraic growth with order 4 for large polynomial degrees p .

Lastly, we consider a practical problem in linear elasticity, specifically the mixed traction and

displacement problem.

Example 5.2.12. We consider the mixed Lamé problem

$$\begin{aligned} -\operatorname{div} \sigma(u) &= 0, & \text{in } \Omega \\ u &= 0, & \text{on } \Gamma_D \\ \sigma(u)\nu &= (-1, 0), & \text{on } \Gamma_{N,1} \\ \sigma(u)\nu &= (0, 0), & \text{on } \Gamma_{N,2}. \end{aligned}$$

Particularly, the workpiece is fixed at the bottom side Γ_D and a traction is applied to $\Gamma_{N,1}$. The Lamé coefficients $\lambda = 57692$ and $\mu = 38462$ correspond to plexiglass. The geometry, its NURBS parametrization, and the splitting into the Dirichlet and Neumann boundaries are illustrated in Figure 5.33 (a).

The solution is computed with a uniform p -method with $\mathcal{N}_e = 21$ elements. Figure 5.33 (b) shows the displaced workpiece, where the displacement is scaled by a factor of 500. The colors denote the elastic shear energy density of the solution [ACF⁺02], which is defined by

$$\left(\frac{\mu^2}{24(\lambda + \mu)^2} + \frac{1}{8} \right) (\sigma_{11} + \sigma_{22})^2 - \frac{\sigma_{12}^2 - \sigma_{11}\sigma_{22}}{2\mu}. \quad (5.14)$$

Figure 5.34 (a) shows the point-wise error $|u_{h,fine}(x^*) - u_h(x^*)|$ for $x^* = (-0.8, -10)$ close to the top left edge of the boundary over the degrees of freedom. The fine solution $u_{h,fine}$ is computed with $\mathcal{N}_e = 21$ elements and polynomial degree $p = 64$.

Remark 5.2.13. (i) The numerical results show that our implementation of Galerkin methods is stable for all sets of basis functions and BIEs considered in this work. In the case of NURBS-enhanced methods, our implementation is stable even for high-order methods, i.e. accurate result can be produced for polynomial degrees $p \leq 128$. Further, the energy error is reduced by 7 digits with the geometric hp -meshes, which is close to double machine precision and hence optimal, since no multiple precision libraries are used for the implementation.

(ii) For isogeometric methods, accurate results for uniform h -methods are presented. Furthermore, the potential of high-order isogeometric methods is shown. With our implementation accurate results for uniform p - and k -refinements are obtained for polynomial degrees up to $q = 25$. Hereby, the effect of the increasing global regularity on the energy error can be observed. In particular, we obtain twice the convergence rate as for the uniform

5. Implementation and Numerical Results

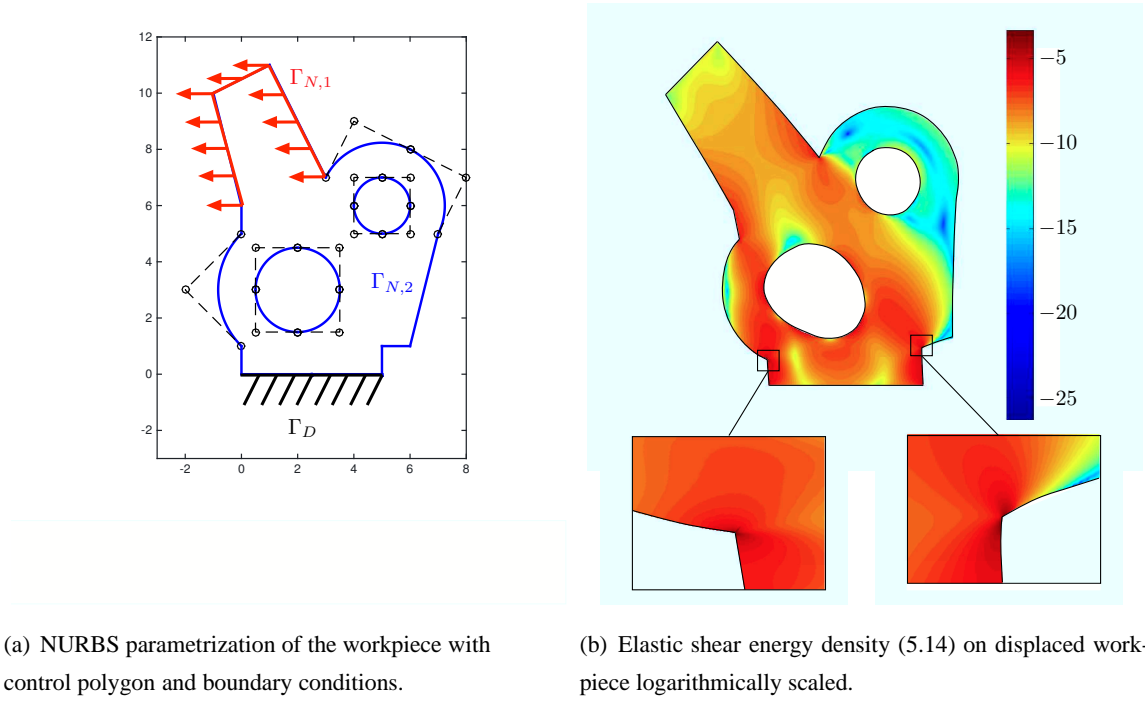


Figure 5.33.: Mixed traction and displacement problem of a workpiece.

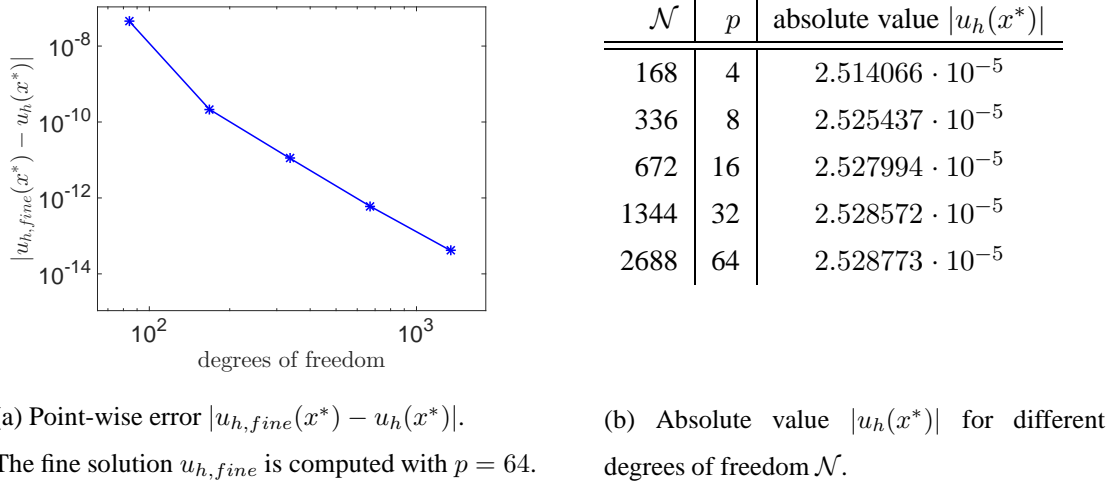


Figure 5.34.: Solution $u_h(x^*)$ evaluated at the point $x^* = (-0.8, 10)$ near the top left edge with a uniform p -method.

h -refinement and the same behavior with a better constant as compared to the uniform p -refinement. The reason for the limitation of the computations is the exponential growth of the condition number with respect to the degrees of freedom.

- (iii) The computational times for the assembly of the Galerkin matrices show a behavior, which is almost proportional to \mathcal{N}^2 for uniform h -methods. Since \mathcal{N}^2 entries have to be com-

puted, the assembly of the Galerkin matrix is almost independent of \mathbf{h} , which is a nearly optimal behavior. For uniform p -methods, the time for the assembly is proportional to \mathcal{N}^4 . This is caused by the assembly of the neighboring and identical matrix blocks. Due to the coordinate transformations and the fact that the quadrature order is linearly dependent on the polynomial degree p , each basis function has to be evaluated at p^2 points. We remark that the time for the evaluation of the far-field blocks with the Gauss-Legendre quadrature is proportional to \mathcal{N}^3 and hence the overall time for the assembly of the Galerkin matrix is dominated by the time for neighboring and identical elements.

- (iv) Table 5.2 shows a comparison of the computational times for the assembly of the single layer collocation and Galerkin matrices for the circular boundary (Example 5.2.7). For the uniform h -refinement, the time for the assembly of the collocation and Galerkin matrix show the same behavior, specifically both times are proportional to \mathcal{N}^2 . Here, the assembly of the collocation matrix is faster by a factor of $\approx \frac{2}{3}$. For the uniform p -refinement, we see that for small polynomial degrees the assembly of the Galerkin matrix is faster, while for large polynomial degrees the assembly of the collocation matrix is faster. This can be explained by the algebraic growth of the computational time of order 4 for the Galerkin matrix.

\mathcal{N}	uniform $h, p = 0$		uniform $p, \mathcal{N}_e = 8$	
	Galerkin	Collocation	Galerkin	Collocation
128	7.42	4.92	0.14	0.61
256	29.64	19.73	0.87	1.82
512	120.65	80.45	10.86	10.00
1024	512.96	337.03	197.35	59.87

Table 5.2.: Computational times for the assembly of the collocation and Galerkin matrices for Example 5.2.7

Conclusions

Through the course of this dissertation we have developed the implementation of NURBS-based boundary element methods for the Laplace, Lamé, and Helmholtz equations in two dimensions. Using an exact NURBS parametrization of the boundary, no geometric error is induced. Thus, there is no deterioration of the convergence rates of high-order collocation or Galerkin methods. This allows the computation of highly accurate solutions on complicated domains with few degrees of freedoms. Besides isogeometric methods, which had previously been introduced for finite element methods, we presented NURBS-enhanced methods, which combine the advantages of standard high-order boundary element methods with the concept of isogeometric analysis. By choosing the Legendre polynomials and their antiderivatives, called the Lobatto shape functions, as basis functions of the polynomials ansatz spaces, we were able to stably and efficiently implement high-order NURBS-enhanced methods. In particular, we observed a linear relationship between the condition number of the Galerkin matrices and the polynomial degree p . By exploiting the L^2 orthogonality of the Legendre polynomials efficient algorithms for the evaluation of the arising integrals were developed for high-order collocation and Galerkin methods.

Three aspects of NURBS-based boundary element methods were explored in detail. First, we examined the computation of Gauss quadrature rules and the derivation of error bounds for the absolute quadrature error. We then discussed the derivation of algorithms for the efficient and accurate evaluation of all integrals arising in NURBS-based collocation and Galerkin methods. Lastly, we presented a black box implementation of NURBS-based BEM, which has a wide field of application and a natural extension to other BIEs.

The foundation for the implementation of NURBS-based boundary element methods is the efficient and accurate numerical integration using Gauss quadrature rules. As most fundamental solutions of elliptic partial differential operators in two dimensions contain a logarithmic singularity, we discussed the computation of Gauss-Log quadrature rules. The key for the efficient and stable computation of their nodes and weights for high orders with the algorithm of Golub and Welsh [GW69] was the use of the modified Chebyshev algorithm presented in [Gau10] and the explicit representation of the modified moments with respect to the Jacobi polynomials [BF14]. These modified moments can also be used for the computation of quadrature rules for some

Conclusions

modified logarithmic as well as Jacobi weight functions.

Based on numerical experiments, we then derived a new error bound for the Gauss-Log quadrature rule, which served as the foundation for the consistency error analysis for Galerkin methods. Our results indicated that the bound was reliable for integrands, which are analytically extendable on ellipses \mathcal{E}_ρ with $\rho > 1.01$, and all orders $n \leq 2048$. This includes most practical applications.

Further research should be conducted on this topic. A theoretically proven error bound for Gauss-Log quadrature rules is desired. Therefore, estimates for the maximum of the kernel $K_n(z) = \frac{\pi_n(z)}{\rho_n(z)}$ on confocal ellipses \mathcal{E}_ρ would need to be derived. Up to now, corresponding results are only proven for some special weights, like Jacobi and Chebyshev weights, for which closed formulas for $K_n(z)$ are available [GV83]. For the kernel with respect to the Gauss-Log weight function, closed formulas and asymptotic estimates with respect to n are not yet known.

We also examined the efficient and stable evaluation of the integrals arising in NURBS-based BEM. For both collocation and Galerkin methods, we considered kernel functions of a general type, which provides a wide field of application in two-dimensional BEM.

For the integrals arising in collocation methods, we developed new algorithms for the evaluation of far-field, near-field, and singular integrals including error estimates for the absolute error. The far-field integrals with respect to the Legendre basis functions were evaluated with an algorithm based on the Legendre expansion of the kernel and the orthogonality of the Legendre polynomials. We showed that the complexity and the decay of the absolute error are independent of the order p , thus improving the evaluation with a Gauss-Legendre quadrature rule for high polynomial degrees.

For the near-field integrals, which are numerically most challenging, we presented an algorithm yielding the maximum convergence rate of the absolute error independent of the evaluation point. This approach was based on the efficient and stable evaluation of basic integrals presented in [Ban13] and the exact knowledge of the zero z_x decreasing the domain of analyticity of the kernel. As compared to existing approaches based on the regularization with coordinate transformations, we accelerated the decay of the absolute error significantly. Furthermore, this approach could also be generalized to the case of singular integrals, thus allowing for the stable implementation for singular integrals as well.

For the evaluation of the double integrals arising in Galerkin methods, we introduced coordinate transformations in order to regularize the singular integrals arising for neighboring and identical element combinations. The remaining singular integrals containing a logarithmic type singularity were evaluated efficiently with a combination of Gauss-Log and Gauss-Legendre quadratures. We proved there is an exponential decay of the quadrature error for all integrals. With the estimates of the absolute quadrature error we could provide a complete consistency

error analysis including computable a priori estimates for the quadrature order. This opens the door for the efficient implementation of Galerkin methods.

Whereas Galerkin methods are well-understood from the theoretical point of view, there are several open questions for collocation methods. Specifically, a priori estimates for ansatz functions others than smoothest splines as well as consistency estimates, which can be used for the a priori computation of the quadrature orders, have yet to be derived. If estimates for the effect of the absolute error in the collocation matrix on the consistency error were available, we could derive a priori estimates for the quadrature and interpolation orders, improving the efficiency of the collocation method.

Lastly, we described the black box implementation of NURBS-based boundary element methods. The focus was on an implementation that has a wide field of application and can be readily extended to other kernel functions. Both NURBS-enhanced and isogeometric methods could be used for solving Symm's integral equation as well as the hypersingular and mixed boundary integral equations with Galerkin and collocation methods. The implementation was used to investigate the appropriate choice of the collocation points for NURBS-enhanced methods, where optimal points were computed by solving minimization problems. Furthermore, we examined the effect of the high global regularity of the isogeometric basis functions on the energy error in numerical examples.

Our implementation serves as a basis to explore the full potential of isogeometric BEM. With appropriate pre-conditioning strategies, high-order isogeometric methods can be advanced. Combinations of the classical h - and p -refinement with the new k -refinement as well as adaptive refinement strategies, which have been investigated for low-order methods in [FGP15], are desired.

Using the Legendre polynomials and their antiderivatives was the key for the stable implementation of high-order NURBS-enhanced methods. Our final numerical examples showed that our implementation produces accurate results for high polynomial degree $p \leq 128$. Furthermore, we were able to reduce the energy error up to machine precision for both collocation and Galerkin methods on geometrically graded hp -meshes. Overall, our implementation can be used for the computation of highly accurate solutions of practice-relevant problems in two dimensional potential theory, linear elasticity, and acoustic scattering. By using NURBS parametrizations of the boundary we are able to compute the solution of the boundary integral equations on complicated domains with few degrees of freedom.

A. Explicit Representation of the Integral Operators

In this section we give an overview on the kernel functions and their co-normal derivatives of the Laplace, Lamé, and Helmholtz equations.

Laplace equation. For the Laplace operator, the kernel functions of the single layer, the double layer, the adjoint, and hypersingular operators are given in the following lemma.

Lemma A.1. *The fundamental solution of the Laplace equation is given by $G(x - y) = -\frac{1}{2\pi} \log |x - y|$. The co-normal derivatives with respect to x and y are given by*

$$\gamma_{1,x}G(x - y) = -\frac{1}{2\pi} \frac{(x - y)^T \nu_x}{|x - y|^2}$$

and

$$\gamma_{1,y}G(x - y) = \frac{1}{2\pi} \frac{(x - y)^T \nu_y}{|x - y|^2}.$$

The second order co-normal derivative is given by

$$\gamma_{1,x}(\gamma_{1,y}G(x - y)) = \frac{1}{\pi} \frac{\nu_x^T(x - y)(x - y)^T \nu_y}{|x - y|^4} - \frac{1}{2\pi} \frac{\nu_x^T \nu_y}{|x - y|^2}.$$

Proof. The representation of the fundamental solution is e.g. proven in [McL00]. For $n \in \mathbb{R}^2$ we obtain

$$(\nabla_x \log |x - y|)^T n = \frac{(x - y)^T n}{|x - y|^2} = -(\nabla_y \log |x - y|)^T n.$$

Since the co-normal derivative coincides with the normal derivative for the Laplace operator, we obtain with $n := \nu_x$

$$\gamma_{1,x}G(x - y) = -\frac{1}{2\pi} \frac{(x - y)^T \nu_x}{|x - y|^2}$$

and with $n := \nu_y$

$$\gamma_{1,y}G(x - y) = \frac{1}{2\pi} \frac{(x - y)^T \nu_y}{|x - y|^2}.$$

A. Explicit Representation of the Integral Operators

With the identity

$$\frac{\partial}{\partial \nu_x} \frac{(x-y)^T \nu_y}{|x-y|^2} = 2 \frac{\nu_x^T (x-y)(x-y)^T \nu_y}{|x-y|^4} - \frac{\nu_x^T \nu_y}{|x-y|^2}$$

we directly obtain the last statement and we conclude the proof. □

An overview on the coefficient functions in the general representation (4.3), which are directly defined by the previous lemma, is given for the Laplace equation in Table 1.1.

	V	K	A	W
g_{-1}				
g_0	x			
g_1		x	x	x
g_2				x
g_3				

Table 1.1.: Overview on the terms g_μ in representation (4.3) for the Laplace equation.

Lamé equation. Let $\lambda, \mu \in \mathbb{R}$ with $\mu > 0$ and $\lambda + 2\mu > 0$ denote the Lamé coefficients. The fundamental solution and its co-normal derivatives are given in the subsequent lemma.

Lemma A.2. A fundamental solution of the Lamé equation is given by

$$G(x - y) = \frac{1}{4\pi\mu(\lambda + 2\mu)} \left(-(3\mu + \lambda) \log |x - y| \mathbf{I} + (\lambda + \mu) \frac{(x - y)(x - y)^T}{|x - y|^2} \right)$$

Let $\mathbf{I} \times \mathbf{I} := \begin{pmatrix} 0 & 1 \\ -1 & 0 \end{pmatrix}$. For the co-normal derivatives of G the following identities hold

$$\begin{aligned} \gamma_{1,x} G(x - y) &= -\frac{\mu}{2\pi(\lambda + 2\mu)} \left(\frac{(x - y)^T \nu_x}{|x - y|^2} \mathbf{I} + \frac{(x - y)^T \tau_x}{|x - y|^2} \mathbf{I} \times \mathbf{I} \right) \\ &\quad + \frac{\lambda + \mu}{\pi(\lambda + 2\mu)} \frac{(x - y)^T \nu_x}{|x - y|^4} (x - y)(x - y)^T \\ &= -\gamma_{1,y} G(x - y) \end{aligned} \tag{A.1}$$

as well as

$$\begin{aligned} &\gamma_{1,x}(\gamma_{1,y} G(x - y)) \\ &= \frac{\lambda\mu}{\pi(\lambda + 2\mu)} \frac{(x - y)^T \nu_x (x - y)^T \nu_y}{|x - y|^4} \mathbf{I} - \frac{\mu^2}{\pi(\lambda + 2\mu)} \frac{(x - y)^T \tau_x (x - y)^T \tau_y}{|x - y|^4} \mathbf{I} \\ &\quad + \frac{\mu^2}{\pi(\lambda + 2\mu)} \frac{(x - y)^T \tau_x (x - y)^T \nu_y - (x - y)^T \nu_x (x - y)^T \tau_y}{|x - y|^4} \mathbf{I} \times \mathbf{I} \\ &\quad + \frac{\mu^2}{\pi(\lambda + 2\mu)} \frac{\nu_x^T \nu_y \mathbf{I} + \tau_x^T \tau_y \mathbf{I} \times \mathbf{I}}{|x - y|^2} \\ &\quad + \frac{\mu(\lambda + \mu)}{\pi(\lambda + 2\mu)} \left(\frac{\nu_x^T \nu_y}{|x - y|^4} - 8 \frac{(x - y)^T \nu_x (x - y)^T \nu_y}{|x - y|^6} \right) (x - y)(x - y)^T \\ &\quad + \frac{\mu(\lambda + \mu)}{\pi(\lambda + 2\mu)} \frac{(x - y)^T \nu_y (\nu_x (x - y)^T + (x - y) \nu_x^T)}{|x - y|^4} \\ &\quad - \frac{\mu(\lambda + \mu)}{\pi(\lambda + 2\mu)} \frac{(x - y)^T \tau_y [\mathbf{I} \times \mathbf{I} \tau_x (x - y)^T \mathbf{I} \times \mathbf{I}] + (x - y)^T \nu_x \nu_y (x - y)^T}{|x - y|^4}. \end{aligned} \tag{A.2}$$

Proof. The representation of the fundamental solution is e.g. proven in [McL00]. For the co-normal derivatives of the fundamental solution we use the identity

$$\gamma_1 u = \sigma(u) \nu = \mu(\nabla u + \nabla u^T) + \lambda \operatorname{div}(u) \mathbf{I}.$$

In order to apply the co-normal derivative to the columns of the fundamental solution G , we denote the columns of G by G_i , $i = 1, 2$. For simplicity, we abbreviate $z := x - y$. We get

$$\nabla \begin{pmatrix} \log |x - y| \\ 0 \end{pmatrix} = \frac{1}{|z|^2} \begin{pmatrix} z_1 & z_2 \\ 0 & 0 \end{pmatrix} \quad \text{and} \quad \nabla \begin{pmatrix} \frac{z_1^2}{|z|^2} \\ \frac{z_1 z_2}{|z|^2} \end{pmatrix} = \begin{pmatrix} 2 \frac{z_1}{|z|^2} - 2 \frac{z_1^3}{|z|^4} & -2 \frac{z_1^2 z_2}{|z|^4} \\ \frac{z_2}{|z|^2} - 2 \frac{z_1^2 z_2}{|z|^4} & \frac{z_1}{|z|^2} - 2 \frac{z_1 z_2^2}{|z|^4} \end{pmatrix}.$$

A. Explicit Representation of the Integral Operators

Hence, the first column of the co-normal derivative is given by

$$\begin{aligned}
\sigma(G_1(z))n_x &= \mu(\nabla G_1(z) + \nabla G_1(z)^T) + \lambda \operatorname{div}(G_1(z)) \mathbf{I} \\
&= -\frac{3\mu + \lambda}{4\pi(\lambda + 2\mu)} \begin{pmatrix} 2\frac{z_1}{|z|^2} & \frac{z_2}{|z|^2} \\ \frac{z_2}{|z|^2} & 0 \end{pmatrix} \nu_x + \frac{\lambda + \mu}{4\pi(\lambda + 2\mu)} \begin{pmatrix} 4\frac{z_1}{|z|^2} - 4\frac{z_1^3}{|z|^4} & \frac{z_2}{|z|^2} - 4\frac{z_1^2 z_2}{|z|^4} \\ \frac{z_2}{|z|^2} - 4\frac{z_1^2 z_2}{|z|^4} & 2\frac{z_1}{|z|^2} - 4\frac{z_1^3}{|z|^4} \end{pmatrix} \nu_x \\
&\quad - \frac{\lambda(3\mu + \lambda)}{4\pi\mu(\lambda + 2\mu)} \begin{pmatrix} 2\frac{z_1}{|z|^2} & 0 \\ 0 & 2\frac{z_1}{|z|^2} \end{pmatrix} \nu_x + \frac{\lambda(\lambda + \mu)}{4\pi\mu(\lambda + 2\mu)} \begin{pmatrix} 2\frac{z_1}{|z|^2} & 0 \\ 0 & 2\frac{z_1}{|z|^2} \end{pmatrix} \nu_x \\
&= -\frac{\mu}{2\pi(\lambda + 2\mu)} \frac{z^T \nu_x}{|z|^2} \begin{pmatrix} 1 \\ 0 \end{pmatrix} - \frac{\lambda + \mu}{\pi(\lambda + 2\mu)} \frac{z^T \nu_x}{|z|^4} \begin{pmatrix} z_1^2 \\ z_1 z_2 \end{pmatrix} - \frac{\mu}{2\pi(\lambda + 2\mu)} \frac{z^T \tau_x}{|z|^2} \begin{pmatrix} 0 \\ -1 \end{pmatrix}
\end{aligned}$$

For the second column, we get with

$$\nabla \begin{pmatrix} 0 \\ \log|x - y| \end{pmatrix} = \frac{1}{|z|^2} \begin{pmatrix} 0 & 0 \\ z_1 & z_2 \end{pmatrix} \quad \text{and} \quad \nabla \begin{pmatrix} \frac{z_1 z_2}{|z|^2} \\ \frac{z_2^2}{|z|^2} \end{pmatrix} = \begin{pmatrix} \frac{z_2}{|z|^2} - 2\frac{z_1^2 z_2}{|z|^4} & \frac{z_1}{|z|^2} - 2\frac{z_1 z_2^2}{|z|^4} \\ -2\frac{z_1 z_2^2}{|z|^4} & 2\frac{z_2}{|z|^2} - 2\frac{z_2^3}{|z|^4} \end{pmatrix}.$$

the following representation

$$\begin{aligned}
\sigma(G_2(z))n_x &= \mu(\nabla G_2(z) + \nabla G_2(z)^T) + \lambda \operatorname{div}(G_2(z)) \mathbf{I} \\
&= -\frac{3\mu + \lambda}{4\pi(\lambda + 2\mu)} \begin{pmatrix} 0 & \frac{z_1}{|z|^2} \\ \frac{z_1}{|z|^2} & 2\frac{z_2}{|z|^2} \end{pmatrix} \nu_x + \frac{\lambda + \mu}{4\pi(\lambda + 2\mu)} \begin{pmatrix} 2\frac{z_2}{|z|^2} - 4\frac{z_1^2 z_2}{|z|^4} & \frac{z_1}{|z|^2} - 4\frac{z_1 z_2^2}{|z|^4} \\ \frac{z_1}{|z|^2} - 4\frac{z_1 z_2^2}{|z|^4} & 4\frac{z_2}{|z|^2} - 4\frac{z_2^3}{|z|^4} \end{pmatrix} \nu_x \\
&\quad - \frac{\lambda(3\mu + \lambda)}{4\pi\mu(\lambda + 2\mu)} \begin{pmatrix} 2\frac{z_2}{|z|^2} & 0 \\ 0 & 2\frac{z_2}{|z|^2} \end{pmatrix} \nu_x + \frac{\lambda(\lambda + \mu)}{4\pi\mu(\lambda + 2\mu)} \begin{pmatrix} 2\frac{z_2}{|z|^2} & 0 \\ 0 & 2\frac{z_2}{|z|^2} \end{pmatrix} \nu_x \\
&= -\frac{\mu}{2\pi(\lambda + 2\mu)} \frac{z^T \nu_x}{|z|^2} \begin{pmatrix} 0 \\ 1 \end{pmatrix} - \frac{\lambda + \mu}{\pi(\lambda + 2\mu)} \frac{z^T \nu_x}{|z|^4} \begin{pmatrix} z_1 z_2 \\ z_2^2 \end{pmatrix} - \frac{\mu}{2\pi(\lambda + 2\mu)} \frac{z^T \tau_x}{|z|^2} \begin{pmatrix} 1 \\ 0 \end{pmatrix}.
\end{aligned}$$

The representations of both columns yield

$$\begin{aligned}
\gamma_{1,x}G(x - y) &= -\frac{\mu}{2\pi(\lambda + 2\mu)} \left(\frac{(x - y)^T \nu_x}{|x - y|^2} \mathbf{I} + \frac{(x - y)^T \tau_x}{|x - y|^2} \mathbf{I} \times \mathbf{I} \right) \\
&\quad + \frac{\lambda + \mu}{\pi(\lambda + 2\mu)} \frac{(x - y)^T \nu_x}{|x - y|^4} (x - y)(x - y)^T \\
&= -\gamma_{1,y}G(x - y).
\end{aligned}$$

For the kernel $\gamma_{1,x}(\gamma_{1,y}G(x - y))$ of the hypersingular operator we introduce the notation $\nu_y := (m_1, m_2)^T$ and $T(x - y) := \gamma_{1,y}G(x - y)$, where we denote the columns of T by T_i , $i = 1, 2$.

There holds

$$\nabla \begin{pmatrix} \frac{z^T \nu_y}{|z|^2} \\ -\frac{z^T T_y}{|z|^2} \end{pmatrix} = \begin{pmatrix} \frac{m_1}{|z|^2} - 2\frac{z_1 z^T \nu_y}{|z|^4} & \frac{m_2}{|z|^2} - 2\frac{z_2 z^T \nu_y}{|z|^4} \\ -\frac{m_2}{|z|^2} + 2\frac{z_1 z^T T_y}{|z|^4} & \frac{m_1}{|z|^2} + 2\frac{z_2 z^T T_y}{|z|^4} \end{pmatrix}$$

and

$$\nabla \begin{pmatrix} \frac{z_1^2 z^T \nu_y}{z^4} \\ \frac{z_1 z_2 z^T \nu_y}{z^4} \end{pmatrix} = \begin{pmatrix} \frac{z_1^2 m_1 + 2z_1 z^T n_y}{|z|^4} - 4 \frac{z_1^3 z^T n_y}{|z|^6} & \frac{z_1^2 m_2}{|z|^4} - 4 \frac{z_1^2 z_2 z^T n_y}{|z|^6} \\ \frac{z_1 z_2 m_1}{|z|^4} + \frac{z_2 z^T n_y}{|z|^4} - \frac{4z_1^2 z_2 z^T n_y}{|z|^6} & \frac{z_1 z_2 m_2}{|z|^4} + \frac{z_1 z^T n_y}{|z|^4} - 4 \frac{z_1 z_2^2 z^T n_y}{|z|^6} \end{pmatrix}.$$

Plugging in the gradients, we get

$$\begin{aligned} \sigma(T_1(z))n_x &= \mu(\nabla T_1(z) + \nabla T_1(z)^T) + \lambda \operatorname{div}(T_1(z)) \text{ I} \\ &= -\frac{\mu^2}{2\pi(\lambda + 2\mu)} \begin{pmatrix} 2\frac{m_1}{|z|^2} - 4\frac{z_1 z^T \nu_y}{|z|^4} & 2\frac{(z_1 - z_2) z^T \nu_y}{|z|^4} \\ 2\frac{(z_1 - z_2) z^T \tau_y}{|z|^4} & 2\frac{m_1}{|z|^2} + 4\frac{z_2 z^T \tau_y}{|z|^4} \end{pmatrix} \nu_x \\ &\quad + \frac{\mu(\lambda + \mu)}{\pi(\lambda + 2\mu)} \begin{pmatrix} \frac{2z_1^2 m_1 + 4z_1 z^T n_y}{|z|^4} - 8\frac{z_1^3 z^T n_y}{|z|^6} & \frac{(z_1^2 m_2 + z_1 z_2 m_1)}{|z|^4} + \frac{z_2 z^T n_y}{|z|^4} - 8\frac{z_1^2 z_2 z^T n_y}{|z|^6} \\ \frac{(z_1^2 m_2 + z_1 z_2 m_1)}{|z|^4} + \frac{z_2 z^T n_y}{|z|^4} - 8\frac{z_1^2 z_2 z^T n_y}{|z|^6} & 2\frac{z_1 z_2 m_2}{|z|^4} + 2\frac{z_1 z^T n_y}{|z|^4} - 8\frac{z_1 z_2^2 z^T n_y}{|z|^6} \end{pmatrix} \nu_x \\ &\quad - \frac{\mu\lambda}{2\pi(\lambda + 2\mu)} \begin{pmatrix} 2\frac{m_1}{|z|^2} - 2\frac{(z_1 - z_2) z^T \nu_y}{|z|^4} & 0 \\ 0 & 2\frac{m_1}{|z|^2} - 2\frac{(z_1 - z_2) z^T \nu_y}{|z|^4} \end{pmatrix} \nu_x, \end{aligned}$$

where we used that

$$\operatorname{div} \begin{pmatrix} \frac{z_1^2 z^T \nu_y}{z^4} \\ \frac{z_1 z_2 z^T \nu_y}{z^4} \end{pmatrix} = 0.$$

Simplifying the terms we obtain

$$\begin{aligned} \sigma(T_1(z))n_x &= \mu(\nabla T_1(z) + \nabla T_1(z)^T) + \lambda \operatorname{div}(T_1(z)) \text{ I} \\ &= \begin{pmatrix} \frac{\lambda\mu}{\pi(\lambda + 2\mu)} \frac{z^T \nu_x z^T \nu_y}{|z|^4} - \frac{\mu^2}{\pi(\lambda + 2\mu)} \frac{z^T \tau_x z^T \tau_y}{|z|^4} \end{pmatrix} \begin{pmatrix} 1 \\ 0 \end{pmatrix} \\ &\quad + \frac{\mu^2}{\pi(\lambda + 2\mu)} \frac{z^T \tau_x z^T \nu_y - z^T \nu_x z^T \tau_y}{|z|^4} \begin{pmatrix} 0 \\ -1 \end{pmatrix} \\ &\quad + \frac{\mu^2}{\pi(\lambda + 2\mu)} \left(\frac{\nu_x^T \nu_y}{|z|^2} \begin{pmatrix} 1 \\ 0 \end{pmatrix} + \frac{\nu_x^T \tau_y}{|z|^2} \begin{pmatrix} 0 \\ -1 \end{pmatrix} \right) + \frac{\mu(\lambda + \mu)}{\pi(\lambda + 2\mu)} \left(\frac{\nu_x^T \nu_y}{|z|^4} - 8\frac{z^T \nu_x z^T \nu_y}{|z|^6} \right) \begin{pmatrix} z_1^2 \\ z_1 z_2 \end{pmatrix} \\ &\quad + \frac{\mu(\lambda + \mu)}{\pi(\lambda + 2\mu)} \frac{z^T \nu_y}{|z|^4} (z_1 \nu_x + m_1 z) - \frac{\mu(\lambda + \mu)}{\pi(\lambda + 2\mu)} \frac{z^T \tau_y + \tau_x z^T}{|z|^4} \begin{pmatrix} 0 \\ -1 \end{pmatrix} + \frac{z_1 z^T \nu_x}{|z|^4} \nu_y. \end{aligned}$$

For the second column, we get by analogy for the gradients of both terms

$$\nabla \begin{pmatrix} \frac{z^T \tau_y}{|z|^2} \\ \frac{z^T \nu_y}{|z|^2} \end{pmatrix} = \begin{pmatrix} \frac{m_2}{|z|^2} - 2\frac{z_1 z^T \nu_y}{|z|^4} & -\frac{m_1}{|z|^2} - 2\frac{z_2 z^T \nu_y}{|z|^4} \\ \frac{m_1}{|z|^2} - 2\frac{z_1 z^T \nu_y}{|z|^4} & \frac{m_2}{|z|^2} - 2\frac{z_2 z^T \nu_y}{|z|^4} \end{pmatrix}$$

and

$$\nabla \begin{pmatrix} \frac{z_1 z_2 z^T \nu_y}{z^4} \frac{z_2^2 z^T \nu_y}{z^4} \end{pmatrix} = \begin{pmatrix} \frac{z_1 z_2 m_1}{|z|^4} + \frac{z_2 z^T n_y}{|z|^4} - \frac{4z_1^2 z_2 z^T n_y}{|z|^6} & \frac{z_1 z_2 m_2}{|z|^4} + \frac{z_1 z^T n_y}{|z|^4} - 4\frac{z_1 z_2^2 z^T n_y}{|z|^6} \\ \frac{z_2^2 m_1}{|z|^4} - 4\frac{z_1 z_2^2 z^T n_y}{|z|^6} & \frac{z_2^2 m_2 + 2z_2 z^T n_y}{|z|^4} - 4\frac{z_2^3 z^T n_y}{|z|^6} \end{pmatrix}.$$

A. Explicit Representation of the Integral Operators

Plugging in the gradients we obtain

$$\begin{aligned}
\sigma(T_2(z))n_x &= \mu(\nabla T_2(z) + \nabla T_2(z)^T) + \lambda \operatorname{div}(T_2(z)) \text{ I} \\
&= -\frac{\mu^2}{2\pi(\lambda + 2\mu)} \begin{pmatrix} 2\frac{m_2}{|z|^2} - 4\frac{z_1 z^T \nu_y}{|z|^4} & -2\frac{(z_1+z_2) z^T \nu_y}{|z|^4} \\ -2\frac{(z_1+z_2) z^T \tau_y}{|z|^4} & 2\frac{m_2}{|z|^2} - 4\frac{z_2 z^T \tau_y}{|z|^4} \end{pmatrix} \nu_x \\
&+ \frac{\mu(\lambda + \mu)}{\pi(\lambda + 2\mu)} \begin{pmatrix} 2\frac{z_1 z_2 m_1}{|z|^4} + 2\frac{z_2 z^T n_y}{|z|^4} - 8\frac{z_1^2 z_2 z^T n_y}{|z|^6} & \frac{z_1 z_2 m_2 + z_2^2 m_1}{|z|^4} + \frac{z_1 z^T n_y}{|z|^4} - 8\frac{z_1 z_2^2 z^T n_y}{|z|^6} \\ \frac{z_1 z_2 m_2 + z_2^2 m_1}{|z|^4} + \frac{z_1 z^T n_y}{|z|^4} - 8\frac{z_1 z_2^2 z^T n_y}{|z|^6} & 2\frac{z_2^2 m_2 + 2z_2 z^T n_y}{|z|^4} - 8\frac{z_2^3 z^T n_y}{|z|^6} \end{pmatrix} \nu_x \\
&- \frac{\mu\lambda}{2\pi(\lambda + 2\mu)} \begin{pmatrix} 2\frac{m_2}{|z|^2} - 2\frac{(z_1+z_2) z^T \nu_y}{|z|^4} & 0 \\ 0 & 2\frac{m_2}{|z|^2} - 2\frac{(z_1+z_2) z^T \nu_y}{|z|^4} \end{pmatrix} \nu_x
\end{aligned}$$

Rearranging the terms yields

$$\begin{aligned}
\sigma(T_2(z))n_x &= \mu(\nabla T_2(z) + \nabla T_2(z)^T) + \lambda \operatorname{div}(T_2(z)) \text{ I} \\
&\left(\frac{\lambda\mu}{\pi(\lambda + 2\mu)} \frac{z^T \nu_x z^T \nu_y}{|z|^4} - \frac{\mu^2}{\pi(\lambda + 2\mu)} \frac{z^T \tau_x z^T \tau_y}{|z|^4} \right) \begin{pmatrix} 0 \\ 1 \end{pmatrix} \\
&+ \frac{\mu^2}{\pi(\lambda + 2\mu)} \frac{z^T \tau_x z^T \nu_y - z^T \nu_x z^T \tau_y}{|z|^4} \begin{pmatrix} 1 \\ 0 \end{pmatrix} \\
&+ \frac{\mu^2}{\pi(\lambda + 2\mu)} \left(\frac{\nu_x^T \nu_y}{|z|^2} \begin{pmatrix} 0 \\ 1 \end{pmatrix} + \frac{\nu_x^T \tau_y}{|z|^2} \begin{pmatrix} 1 \\ 0 \end{pmatrix} \right) + \frac{\mu(\lambda + \mu)}{\pi(\lambda + 2\mu)} \left(\frac{\nu_x^T \nu_y}{|z|^4} - 8\frac{z^T \nu_x z^T \nu_y}{|z|^6} \right) \begin{pmatrix} z_1 z_2 \\ z_2^2 \end{pmatrix} \\
&+ \frac{\mu(\lambda + \mu)}{\pi(\lambda + 2\mu)} \frac{z^T \nu_y}{|z|^4} (z_2 \nu_x + m_2 z) - \frac{\mu(\lambda + \mu)}{\pi(\lambda + 2\mu)} \frac{z^T \tau_y + \tau_x z^T}{|z|^4} \begin{pmatrix} 1 \\ 0 \end{pmatrix} + \frac{z_2 z^T \nu_x \nu_y}{|z|^4}.
\end{aligned}$$

Finally, we obtain with the representations of both columns of $\sigma(T(x - y))\nu_x$ the identity

$$\begin{aligned}
&\gamma_{1,x}(\gamma_{1,y}G(x - y)) \\
&= \frac{\lambda\mu}{\pi(\lambda + 2\mu)} \frac{(x - y)^T \nu_x (x - y)^T \nu_y}{|x - y|^4} \text{ I} - \frac{\mu^2}{\pi(\lambda + 2\mu)} \frac{(x - y)^T \tau_x (x - y)^T \tau_y}{|x - y|^4} \text{ I} \\
&+ \frac{\mu^2}{\pi(\lambda + 2\mu)} \frac{(x - y)^T \tau_x (x - y)^T \nu_y - (x - y)^T \nu_x (x - y)^T \tau_y}{|x - y|^4} \text{ I} \times \text{ I} \\
&+ \frac{\mu^2}{\pi(\lambda + 2\mu)} \frac{\nu_x^T \nu_y \text{ I} + \nu_x^T \tau_y \text{ I} \times \text{ I}}{|x - y|^2} \\
&+ \frac{\mu(\lambda + \mu)}{\pi(\lambda + 2\mu)} \left(\frac{\nu_x^T \nu_y}{|x - y|^4} - 8\frac{(x - y)^T \nu_x (x - y)^T \nu_y}{|x - y|^6} \right) (x - y)(x - y)^T \\
&+ \frac{\mu(\lambda + \mu)}{\pi(\lambda + 2\mu)} \frac{(x - y)^T \nu_y (\nu_x (x - y)^T + (x - y)\nu_x^T)}{|x - y|^4} \\
&- \frac{\mu(\lambda + \mu)}{\pi(\lambda + 2\mu)} \frac{(x - y)^T \tau_y [\text{I} \times \text{I} \tau_x (x - y)^T \text{I} \times \text{I}] + (x - y)^T \nu_x \nu_y (x - y)^T}{|x - y|^4}.
\end{aligned}$$

□

An overview on the coefficient functions in the general representation (4.3), which are directly defined by the previous lemma, is given for the Lamé equation in Table 1.2.

	V	K	A	W
g_{-1}				
g_0	x			
g_1	x	x	x	x
g_2		x	x	x
g_3				x

Table 1.2.: Overview on the terms g_μ in representation (4.3) for the Lamé equation.

A. Explicit Representation of the Integral Operators

Helmholtz equation. Before we give an explicit representation of a fundamental solution and its co-normal derivatives for the Helmholtz equation, we introduce the Bessel and Hankel functions and summarize some important properties.

Lemma A.3 ([BOL⁺10]). *The Bessel function of first kind is defined by*

$$J_\nu(z) = \left(\frac{z}{2}\right)^\nu \sum_{k=0}^{\infty} (-1)^k \frac{\left(\frac{1}{2}z^2\right)^k}{k! \Gamma(\nu + k + 1)}$$

and the Bessel function of second kind is given by

$$Y_\nu(z) = \frac{J_\nu(z) \cos(\nu\pi) - J_{-\nu}(z)}{\sin(\nu\pi)}.$$

The Hankel function is defined as linear combination of both Bessel functions, i.e.

$$H_\nu^{(1)}(z) = J_\nu(z) + iY_\nu(z).$$

The following properties hold.

(i) $J_\nu(z)$ is an analytic function for all integer ν .

(ii) For $\nu \in \mathbb{N}$ the derivatives of the Bessel and Hankel functions are given by

$$\begin{aligned} J'_0(z) &= -J'_1(z) & J'_\nu(z) &= \frac{1}{2} (J_{\nu+1}(z) + J_{\nu-1}(z)) \\ Y'_0(z) &= -Y'_1(z) & Y'_\nu(z) &= \frac{1}{2} (Y_{\nu+1}(z) + Y_{\nu-1}(z)) \\ (H_0^{(1)})'(z) &= -H_1^{(1)}(z) & (H_\nu^{(1)})'(z) &= \frac{1}{2} (H_{\nu+1}^{(1)}(z) + H_{\nu-1}^{(1)}(z)) \end{aligned}$$

(iii) For $\nu \in \mathbb{N}$, the Bessel function of second kind has the following power series representation

$$\begin{aligned} Y_\nu(z) &= \frac{1}{\pi} \left(2 \log\left(\frac{z}{2}\right) J_\nu(z) - \left(\frac{2}{z}\right)^\nu \sum_{k=0}^{\nu-1} \frac{(\nu-k-1)!}{4^k k!} z^{2k} \right. \\ &\quad \left. - \left(\frac{z}{2}\right)^\nu \sum_{k=0}^{\infty} [\psi(k+1) + \psi(k+1+\nu)] \frac{(-1)^k}{4^k k! (k+\nu)!} z^{2k} \right), \end{aligned}$$

where $\psi(1) = \gamma$ and $\psi(n+1) = \sum_{k=1}^n \frac{1}{k} - \gamma$. Here, γ denotes the Euler constant.

Lemma A.4. For $\kappa \in \mathbb{C} \setminus \{0\}$, a fundamental solution of the Helmholtz equation is given by

$$G(x-y) = \frac{i}{4} H_0^{(1)}(\kappa|x-y|) = \frac{i}{4} (J_0(\kappa|x-y|) + iY_0(\kappa|x-y|)).$$

The co-normal derivatives with respect to x and y are given by

$$\gamma_{1,x} G(x-y) = -\frac{i\kappa}{4} H_1^{(1)}(\kappa|x-y|) \frac{(x-y)^T \nu_x}{|x-y|}$$

and

$$\gamma_{1,y}G(x-y) = \frac{i\kappa}{4}H_1^{(1)}(\kappa|x-y|)\frac{(x-y)^T\nu_y}{|x-y|}.$$

The second order co-normal derivative is given by

$$\begin{aligned} & \gamma_{1,x}(\gamma_{1,y}G(x-y)) \\ &= \frac{i\kappa}{4} \left(\kappa \frac{H_2^{(1)}(\kappa|x-y|) + H_0^{(1)}(\kappa|x-y|)}{2} \frac{\nu_x^T(x-y)(x-y)^T\nu_y}{|x-y|^2} \right. \\ & \quad \left. - H_1^{(1)}(\kappa|x-y|)\frac{\nu_x^T(x-y)(x-y)^T\nu_y}{|x-y|^3} + H_1^{(1)}(\kappa|x-y|)\frac{\nu_x^T\nu_y}{|x-y|} \right) \end{aligned}$$

Proof. The representation of the fundamental solution is e.g. proven in [McL00]. For the co-normal derivatives of the fundamental solution, which coincide with the normal derivatives, we get with Lemma A.3 (ii)

$$\gamma_{1,x}G(x-y) = \frac{\partial}{\partial\nu_x}G(x-y) = -\frac{i\kappa}{4}H_1^{(1)}(\kappa|x-y|)\frac{(x-y)^T\nu_x}{|x-y|}$$

and

$$\gamma_{1,y}G(x-y) = \frac{\partial}{\partial\nu_y}G(x-y) = \frac{i\kappa}{4}H_1^{(1)}(\kappa|x-y|)\frac{(x-y)^T\nu_y}{|x-y|}.$$

For the second order co-normal derivative we get with

$$\frac{\partial}{\partial\nu_x}\frac{(x-y)^T\nu_y}{|x-y|} = \frac{\nu_x^T\nu_y}{|x-y|} - \frac{\nu_x^T(x-y)(x-y)^T\nu_y}{|x-y|^3}$$

and Lemma A.3 (ii) the following representation

$$\begin{aligned} & \gamma_{1,x}(\gamma_{1,y}G(x-y)) \\ &= \frac{i\kappa}{4} \left(\kappa \frac{H_2^{(1)}(\kappa|x-y|) + H_0^{(1)}(\kappa|x-y|)}{2} \frac{\nu_x^T(x-y)(x-y)^T\nu_y}{|x-y|^2} \right. \\ & \quad \left. - H_1^{(1)}(\kappa|x-y|)\frac{\nu_x^T(x-y)(x-y)^T\nu_y}{|x-y|^3} + H_1^{(1)}(\kappa|x-y|)\frac{\nu_x^T\nu_y}{|x-y|} \right). \end{aligned}$$

□

In order to derive a representation according to (4.3) we use the series representation of Y_ν stated in Lemma A.3 (ii).

Lemma A.5. *The kernel functions can be split according to (4.3) as follows:*

(i) *single layer operator*

$$\begin{aligned} G(x-y) &= \underbrace{G(x-y) + \frac{1}{2\pi}J_0(\kappa|x-y|)\log|x-y|}_{=:g_{-1}(x-y)} - \underbrace{\frac{1}{2\pi}J_0(\kappa|x-y|)\log|x-y|}_{=:g_0(x-y)} \\ &= g_{-1}(x-y) + g_0(x-y)\log|x-y| \end{aligned}$$

A. Explicit Representation of the Integral Operators

(ii) double layer operator

$$\begin{aligned}
\gamma_{1,y}G(x-y) &= \underbrace{\gamma_{1,y}G(x-y) + \frac{\kappa}{2\pi}J_1(\kappa|x-y|)\frac{(x-y)^T\nu_y}{|x-y|}\log|x-y| - \frac{1}{2\pi}\frac{(x-y)^T\nu_y}{|x-y|^2}}_{=:g_{-1}(x-y)} \\
&\quad - \underbrace{\frac{\kappa}{2\pi}J_1(\kappa|x-y|)\frac{(x-y)^T\nu_y}{|x-y|}\log|x-y|}_{=:g_0(x-y)} + \underbrace{\frac{(x-y)^T\nu_y}{2\pi}}_{=:g_1(x-y)}\frac{1}{|x-y|^2} \\
&= g_{-1}(x-y) + g_0(x-y)\log|x-y| + g_1(x-y)\frac{1}{|x-y|^2}
\end{aligned}$$

(iii) adjoint operator

$$\begin{aligned}
\gamma_{1,x}G(x-y) &= \underbrace{\gamma_{1,x}G(x-y) - \frac{\kappa}{2\pi}J_1(\kappa|x-y|)\frac{(x-y)^T\nu_x}{|x-y|}\log|x-y| + \frac{1}{2\pi}\frac{(x-y)^T\nu_y}{|x-y|^2}}_{=:g_{-1}(x-y)} \\
&\quad + \underbrace{\frac{\kappa}{2\pi}J_1(\kappa|x-y|)\frac{(x-y)^T\nu_x}{|x-y|}\log|x-y|}_{=:g_0(x-y)} - \underbrace{\frac{(x-y)^T\nu_y}{2\pi}}_{=:g_1(x-y)}\frac{1}{|x-y|^2} \\
&= g_{-1}(x-y) + g_0(x-y)\log|x-y| + g_1(x-y)\frac{1}{|x-y|^2}
\end{aligned}$$

(iv) hypersingular integral operator

$$\begin{aligned}
&\gamma_{1,x}(\gamma_{1,y}G(x-y)) \\
&= \left[\gamma_{1,x}(\gamma_{1,y}G(x-y)) \right. \\
&\quad + \left\{ \frac{\kappa^2}{4\pi}(J_2(\kappa|x-y|) + J_0(\kappa|x-y|))\frac{\nu_x^T(x-y)(x-y)^T\nu_y}{|x-y|^2} \right. \\
&\quad + \frac{\kappa}{2\pi}\frac{J_1(\kappa|x-y|)}{|x-y|}\left(\frac{\nu_x^T(x-y)(x-y)^T\nu_y}{|x-y|^2} - \nu_x^T\nu_y\right) \left. \right\} \log|x-y| \\
&\quad + \left. \frac{1}{2\pi}\frac{\nu_x^T\nu_y}{|x-y|^2} - \frac{1}{\pi}\frac{\nu_x^T(x-y)(x-y)^T\nu_y}{|x-y|^4} \right] \\
&\quad - \left\{ \frac{\kappa^2}{4\pi}(J_2(\kappa|x-y|) + J_0(\kappa|x-y|))\frac{\nu_x^T(x-y)(x-y)^T\nu_y}{|x-y|^2} \right. \\
&\quad - \frac{\kappa}{2\pi}\frac{J_1(\kappa|x-y|)}{|x-y|}\left(\frac{\nu_x^T(x-y)(x-y)^T\nu_y}{|x-y|^2} - \nu_x^T\nu_y\right) \left. \right\} \log|x-y| \\
&\quad - \frac{1}{2\pi}\frac{\nu_x^T\nu_y}{|x-y|^2} + \frac{1}{\pi}\frac{\nu_x^T(x-y)(x-y)^T\nu_y}{|x-y|^4} \\
&=: g_{-1}(x-y) + g_0(x-y)\log|x-y| + g_1(x-y)\frac{1}{|x-y|^2} + g_2(x-y)\frac{1}{|x-y|^4}.
\end{aligned}$$

Here, the function g_{-1} is defined by the terms in the box brackets, the function g_0 is defined by the terms in curved brackets, and we set $g_1(x, y) := -\frac{1}{2\pi}\nu_x^T\nu_y$ and $g_2(x-y) := \frac{1}{\pi}\nu_x^T(x-y)(x-y)^T\nu_y$.

Proof. In order to proof the representations, we have to proof the analyticity of the coefficient functions g_μ , $\mu = -1, \dots, 2$. Therefore, we consider the series expansion given in Lemma A.3 (iii). Since the functions g_{-1} are obtained by subtracting the logarithmic and algebraic singularities in the series representation of the Bessel functions Y_ν and since the term $|x - y|$ only arises in even powers, g_{-1} is analytic for all boundary integral operators.

(i) Since the Bessel function J_0 is analytic and $|x - y|$ only appears in even powers in the series representation the coefficient functions g_0 is analytic.

(ii),(iii) With the series representation of J_1 we get

$$\frac{\kappa}{2\pi} (x - y)^T \nu_y \frac{J_1(\kappa|x - y|)}{|x - y|} = \frac{\kappa}{2\pi} (x - y)^T \nu_y \frac{\kappa}{2} \sum_{k=0}^{\infty} (-1)^k \frac{(\frac{1}{2}z^2)^k}{k! \Gamma(k + 2)},$$

which proofs the analyticity of g_0 . The analyticity of g_1 is obvious.

(iv) The series representation of J_ν in Lemma A.3 (iii) shows that $J_0(\kappa|x - y|)$, $J_2(\kappa|x - y|)$, and $\frac{J_1(\kappa|x - y|)}{|x - y|}$ are analytic. Furthermore, the terms $\frac{\nu_x^T (x - y)(x - y)^T \nu_y}{|x - y|^2}$ and $\nu_x^T \nu_y$ are analytic and hence the function g_0 is analytic. The analyticity of g_1 and g_2 is obvious.

□

An overview on the coefficient functions in the general representation (4.3) is given for the Helmholtz equation in Table 1.3.

	V	K	A	W
g_{-1}	x	x	x	x
g_0	x	x	x	x
g_1		x	x	x
g_2				x
g_3				

Table 1.3.: Overview on the terms g_μ in representation (4.3) for the Helmholtz equation.

Remark A.0.14. The representation of the kernel functions according to (4.26), which is used for the assembly of the Galerkin matrix for the single and double layer operator can directly be obtained by the representation given in Lemma A.5 (i) and (ii).

Bibliography

- [AG10] M. Abbaspour and M. Ghodsi. Gauss integration limits in nearly singular integrals of BEM for geometrically linear elements. *Transaction B: Mechanical Engineering*, 17:285–300, 2010.
- [AF03] R.A. Adams and J.J.F. Fournier. *Sobolev Spaces*. Academic Press, 2003.
- [ACF⁺02] J. Albery, C. Carstensen, S. Funken, and R. Klose. Matlab implementation of the finite element method in elasticity. *Computing*, 69:239–263, 2002.
- [AR91] B. Alpert and V. Rokhlin. A fast algorithm for the evaluation of Legendre expansions. *SIAM J. Sci. Stat. Comput.*, 12:158–179, 1991.
- [AW83] D.N. Arnold and W.L. Wendland. On the asymptotic convergence of collocation methods. *Math. Comput.*, 41:349–381, 1983.
- [AEF⁺14] M. Aurada, M. Ebner, M. Feischl, S. Ferraz-Leite, T. Führer, P. Goldenits, M. Karkulik, M. Mayr, and D. Praetorius. HILBERT - A Matlab implementation of adaptive 2d-BEM. *Numer. Algorithms*, 67:1–32, 2014.
- [ADH⁺10] F. Auricchio, L.B. Da Veiga, T.J.R. Hughes, A. Reali, and G. Sangalli. Isogeometric collocation methods. *Math. Mod. Meth. Appl. S.*, 20(11):2075–2107, 2010.
- [ACH⁺12] F. Auricchio, F. Calabró, T.J.R. Hughes, A. Reali, and G. Sangalli. A simple algorithm for obtaining nearly optimal quadrature rules for NURBS-based isogeometric analysis. *Comput. Meth. Appl. Mech. Engrg.*, 249-252:15–27, 2012.
- [BS91] I. Babuska and B. Szabó. *Finite element analysis*. John Wiley & Sons, Inc., 1991.
- [BHL⁺02] D.H. Bailey, Y. Hida, X.S. Li, and B. Thompson. ARPREC: An arbitrary precision computation package. Lbnl-53651, Lawrence Berkeley National Laboratory, 2002.
- [BBF13] A. Bantle, M. Bantle, and S. Funken. epsBEM, efficient p -stable Matlab implementation of 2d BEM for Laplace and Lamé problems. Technical report, University of Ulm, Germany, 2013.

Bibliography

- [BF14] A. Bantle and S. Funken. On some logarithmic modified weight functions - Modified moments, Gauss quadrature, and error bounds. (work in progress), 2014.
- [Ban13] M. Bantle. *On hp-boundary element methods for the Laplace operator in two dimensions - Implementation, hp-adaptive algorithms, and data compression*. PhD thesis, University of Ulm, Germany, 2013.
- [BCZ⁺06] Y. Bazilevs, V.M. Calo, Y. Zhang, and T.J.R. Hughes. Isogeometric fluidstructure interaction analysis with applications to arterial blood flow. *Comput. Mech.*, 38:310-322, 2006.
- [BH08] Y. Bazilevs and T.J.R. Hughes. NURBS-based isogeometric analysis for the computation of flows about rotating components. *Comput. Mech.*, 43:143-150, 2008.
- [Beb00] M. Bebendorf. Approximation of boundary element matrices. *Numer. Math.*, 86:565-589, 2000.
- [Beb08] M. Bebendorf. *Hierarchical matrices: A means to efficiently solve elliptic boundary value problems*. Springer Berlin Heidelberg, 2008.
- [BBH⁺10] D.J. Benson, Y. Bazilevs, M.C. Hsu, and T.J.R. Hughes. Isogeometric shell analysis: The Reissner-Mindlin shell. *Comput. Meth. Appl. Mech. Engrg.*, 199:276-289, 2010.
- [BGH03] S. Boerm, L. Grasedyck, and W. Hackbusch. Hierarchical matrices. *Lecture Notes*, 21, 2003.
- [BOL⁺10] R.F. Boisvert, F.W.J. Olver, D.W. Lozier, and C.W. Clark. *NIST: Handbook of mathematical functions*. Cambridge University Press, 2010.
- [BW65] H. Brakhage and P. Werner. Über das Dirichletsche Außenproblem für die Helmholtzsche Schwingungsgleichung. *Arch. Math.*, 16:325-329, 1965.
- [BS08] S.C. Brenner and L.R. Scott. *The mathematical theory of finite element methods*. Springer Science & Business Media, 2008.
- [BS87] I.N. Bronstein and K.A. Semendjajew. *Taschenbuch der Mathematik*. B.G. Teubner, 1987.
- [BM71] A.J. Burton and G.F. Miller. The application of integral equation methods to the numerical solution of some exterior boundary value problems. *Proc. Royal Society*, 323:201-210, 1971.

- [Che59] P.L. Chebyshev. Sur l'interpolation par la méthode des moindres carrés. *Saint-Pétersbourg: Eggers*, 1:1–24, 1859.
- [CZS⁺07] X.D. Chen, Y. Zhou, Z. Shu, H. Su, and J.C. Paul. Improved algebraic algorithm on point projection for Bezier curves. *Proceedings of the Second International Multi-Symposiums on Computer and Computational Sciences*, 158–163, 2007.
- [CK83] D. Colton and R. Kress. *Integral equation methods in scattering theory*. John Wiley & Sons, Inc., 1983.
- [CS85a] M. Costabel and E.P. Stephan. On the asymptotic convergence of collocation methods for boundary integral equations on polygons. *Math. Comput.*, 49:461–478, 1985.
- [CS85b] M. Costabel and E.P. Stephan. A direct boundary integral equation method for transmission problems. *J. Math. Anal. Appl.*, 106:367–413, 1985.
- [CRB⁺06] J.A. Cottrell, A. Reali, Y. Bazilevs, and T.J.R. Hughes. Isogeometric analysis of structural vibrations. *Comput. Meth. Appl. Mech. Engrg.*, 195:5257–5296, 2006.
- [CHR07] J.A. Cottrell, T.J.R. Hughes, and A. Reali. Studies of refinement and continuity in isogeometric structural analysis. *Comput. Meth. Appl. Mech. Engrg.*, 196:4160–4183, 2007.
- [CHB09] J.A. Cottrell, T.J.R. Hughes, and Y. Bazilevs. *Isogeometric Analysis: Toward integration of CAD and FEA*. John Wiley & Sons, Inc., 2009.
- [DR75] P.J. Davis and P. Rabinowitz. *Methods of numerical integration*. Academic Press, 1975.
- [Dem85] S. Demko. On the existence of interpolating projections onto spline spaces. *J. Approx. Theory*, 43:151–156, 1985.
- [Dij08] W. Dijkstra. Condition numbers in the boundary element method: Shape and solvability. PhD thesis, Eindhoven University of Technology, 2008.
- [Dom03] V. Dominguez. High-order collocation and quadrature methods for some logarithmic kernel integral equations on open arcs. *J. Comput. Math.*, 161:145–159, 2003.
- [Duf82] M.G. Duffy. Quadrature over a pyramid or cube of integrands with a singularity at a vertex. *SIAM J. Numer. Anal.*, 19:1260–1262, 1982.

Bibliography

- [Ehr54] L. Ehrenpreis. Solution of some problems of division. Part I: Division by a polynomial of derivation. *Am. J. Math.*, 76:883–903, 1954.
- [ES92] V.J. Ervin and E.P. Stephan. Collocation with Chebyshev polynomials for a hypersingular integral equation on an interval. *J. Comput. Appl. Math.*, 43:221–229, 1992.
- [Far99] G.E. Farin. *NURBS - From projective geometry to practical use*. A K Peters, Ltd., 1999.
- [FGP15] M. Feischl, G. Gantner, and D. Praetorius. Reliable and efficient a posteriori error estimation for adaptive IGA boundary element methods for weakly-singular integral equations. *Comput. Meth. Appl. Mech. Engrg.*, 44:153–176, 2015.
- [FB06] E. Freitag und R. Busam. *Funktionentheorie 1*. Springer Berlin Heidelberg, 2006.
- [Gau81] W. Gautschi. Minimal solutions of three-term recurrence relations and orthogonal polynomials. *Math. Comput.*, 36(154):1–8, 1981.
- [GV83] W. Gautschi and R.S. Varga. Error bounds for Gaussian quadrature of analytic functions. *SIAM J. Numer. Anal.*, 20(6):1170–1186, 1983.
- [Gau92] W. Gautschi. Remainder estimates for analytic functions. *Numerical Integration*, 357:133–145, 1992.
- [Gau06] W. Gautschi. *Orthogonal polynomials, quadrature, and approximation: Computational methods and software (in Matlab)*. Springer Berlin Heidelberg, 2006.
- [Gau10] W. Gautschi. *Orthogonal polynomials: Computation and approximation*. Oxford University Press, 2010.
- [Geo07] E.H. Georgoulis. Inverse-type estimates on *hp*-finite elements spaces and applications. *Math. Comput.*, 77(261):201–219, 2007.
- [GW69] G.H. Golub and J.H. Welsch. Calculation of Gauss quadrature rules. *Math. Comput.*, 23(106):221–230, 1969.
- [GC87] M. Guiggiani and P. Casalani. Direct computation of Cauchy principle value integrals in advanced boundary element methods. *Int. J. Numer. Meth. Eng.*, 24:1711–1720, 1987.
- [GG90] M. Guiggiani and A. Gigante. A general algorithm for multidimensional Cauchy principle value integrals in the BEM. *J. Appl. Mech.*, 57(4):906–915, 1990.

- [GKR⁺92] M. Guiggiani, G. Krishnasamy, T.J. Rudolphi, and F.T. Rizzo. A general algorithm for the solution of hypersingular BEM. *J. Appl. Mech.*, 59(3):604–614, 1992.
- [GH06] B. Guo and N. Heuer. The optimal convergence of the *hp* version of the boundary element method with quasiuniform meshes for elliptic problems on polygonal domains. *Adv. Comput. Math.*, 24(822):353–374, 2006.
- [GS93] J. Gwinner and E.P. Stephan. A boundary element procedure for contact problems in plane linear elastostatics. *Modélisation Mathématique et Analyse Numérique*, 27(4):457–480, 1993.
- [HS93] W. Hackbusch and S.A. Sauter. On the efficient use of the Galerkin-method to solve Fredholm integral equations. *Appl. Math.*, 38:301–322, 1993.
- [Heu92] N. Heuer. *hp-Versionen der Randelementmethode*. PhD thesis, University of Hannover, Germany, 1992.
- [Heu96] N. Heuer. Efficient algorithms for the *p*-version of the boundary element method. *Journal of Integral Equations and Applications*, 8(3):1–24, 1996.
- [HS96] N. Heuer and E.P. Stephan. The *hp*-version of the boundary element method on polygons. *J. Integral Equations Applications*, 8(2):173–212, 1996.
- [HK12] R. Hiptmair and L. Kielhorn. BETL - A generic boundary element template library. Technical report, ETH Zürich, Switzerland, 2012.
- [HSW85] G.C. Hsiao, E.P. Stephan, and W.L. Wendland. An integral equation formulation for a boundary value problem of elasticity in the domain exterior to an arc. *Lecture Notes in Mathematics*, 1121:153–165, 1985.
- [HCB05] T.J.R. Hughes, J.A. Cottrell, and Y. Bazilevs. Isogeometric analysis: CAD, finite elements, NURBS, exact geometry and mesh refinement. *Comput. Meth. Appl. Mech. Engrg.*, 194:4135–4195, 2005.
- [Jae99] K. Jänich. *Funktionentheorie*. Springer Berlin Heidelberg, 1999.
- [Lei65] R. Leis. Zur Dirichletschen Randwertaufgabe des Außenraums der Schwingungsgleichung. *Math. Z.*, 90:205–211, 1965.
- [LR84] D.S. Lubinsky and P. Rabinowitz. Rates of convergence of Gaussian quadrature for singular integrands. *Math. Comput.*, 43:219–242, 1984.
- [MRW96] J. Ma, V. Rocklin, and S. Wandzura. Generalized Gaussian quadrature rules for systems of arbitrary functions. *SIAM J. Numer. Anal.*, 33:971–996, 1996.

Bibliography

- [Mac67] T.M. MacRobert. *Spherical harmonics. An elementary treatise on harmonic functions with applications*. Pergamon Press, 1967.
- [Mai96] M. Maischak. *hp-Methoden für Randintegralgleichungen bei 3D-Problemen, Theorie und Implementierung*. PhD thesis, University of Hannover, Germany, 1996.
- [Mai97] M. Maischak. The analytical evaluation of the Galerkin elements for the Laplace, Lamé, and Helmholtz equation in 2d BEM. Technical report, University of Hannover, Germany, 1997.
- [Mai12] M. Maischak. B.O.N.E. Book of numerical experiments. Technical report, University of Hannover, Germany, 2012.
- [McL00] W. McLean. *Strongly elliptic systems and boundary integral equations*. Cambridge University Press, 2000.
- [MMR⁺14] M. Messner, M. Messner, F. Rammerstorfer, and P. Urthaler. HyENA - Hyperbolic and elliptic numerical analysis. Preprint TU Graz, Austria, 2014.
- [NWW⁺05] Z. Niu, W.L. Wendland, X. Wang, and H. Zhou. A semi-analytic algorithm for the evaluation of nearly singular integrals in three-dimensional boundary element methods. *Comput. Methods Appl. Mech. Engrg.*, 194:1057–1074, 2005.
- [Pan65] O.I. Panich. On the question of the solvability of the exterior boundary problem for the wave equation and Maxwell’s equation. *Uspeki Mat. Nauk*, 20:221–226, 1965.
- [PT97] L. Piegl and W. Tiller. *The NURBS Book*. Springer Berlin Heidelberg, 1997.
- [PA92] A. Portela and M.H. Aliabadi. On the question of the solvability of the exterior boundary problem for the wave equation and Maxwell’s equation. *Int. J. Numer. Meth. Eng.*, 33:1269–1287, 1992.
- [Poz02] C. Pozrikidis. *A practical guide to boundary element methods with the software library BEMLIB*. Chapman&Hall/CRC, 2002.
- [PK94] H. Prautzsch and L. Kobbelt. Derivatives of rational Bezier curves. *Adv. Comput. Math.*, 2:143–154, 1994.
- [RY90] K.R. Rao and P. Yip. *Discrete cosine transform: Algorithms, advantages, applications*. Academic Press, 1990.
- [Rea79] J.B. Reade. Asymptotic behaviour of eigenvalues of certain integral equations. *Proc. Edinburgh Math. Soc.*, 22:137–144, 1979.

- [Riv90] T.J Rivlin. *Chebyshev polynomials - From approximation theory to algebra and number theory*. John Wiley & Sons, Inc., 1990.
- [RS07] S. Rjasanow and O. Steinbach. *The fast solution of boundary integral equations*. Springer US, 2007.
- [SW85] J. Saranen and W.L. Wendland. On the asymptotic convergence of collocation methods with spline functions of even degree. *Math. Comput.*, 45:91–108, 1985.
- [Sau92] S.A. Sauter. *Über die effiziente Verwendung des Galerkinverfahrens zur Lösung Fredholmscher Integralgleichungen*. PhD thesis, University of Kiel, Germany, 1992.
- [SaSch97] S.A. Sauter and C. Schwab. Quadrature for *hp*-Galerkin BEM in \mathbb{R}^3 . *Numer. Math.*, 78:211–258, 1997.
- [SaSch04] S. Sauter and C. Schwab. *Randelementmethoden*. Vieweg+Teubner, 2004.
- [Sch97] T. Schira. The remainder term for analytic functions of symmetric Gaussian quadratures. *Math. Comput.*, 66:297–310, 1997.
- [Sch86] G. Schmidt. On ε -collocation for pseudodifferential equations on a closed curve. *Math. Nachr.*, 126:183–196, 1986.
- [Sch94] C. Schwab. Variable order composite quadrature of singular and nearly singular integrals. *Computing*, 53:173–194, 1994.
- [Sch98] C. Schwab. *p- and hp- finite element methods. Theory and applications in solid and fluid mechanics*. Oxford University Press, 1998.
- [Sch88] H.R. Schwarz. *Numerische Mathematik*. B.G. Teubner, 1988.
- [SSE⁺13] M.A. Scott, R.N. Simpson, J.A. Evans, S. Lipton, S.P.A. Bordas, T.J.R. Hughes, and T.W. Sederberg. Isogeometric boundary element analysis using unstructured T-splines. *Comput. Meth. Appl. Mech. Engrg.*, 254:197–221, 2013.
- [SFH08] R. Sevilla, S. Fernández-Méndez, and A. Huerta. NURBS-enhanced finite element method (NEFEM). *Int. J. Numer. Meth. Eng.*, 76:56–83, 2008.
- [SFH11] R. Sevilla, S. Fernández-Méndez, and A. Huerta. NURBS-enhanced finite element method (NEFEM). A seamless bridge between CAD and FEM. *Arch. Comput. Method E.*, 18:441–484, 2011.
- [Sim12] R.N. Simpson. *Matlab code for isogeometric boundary element analysis*, <https://github.com/bobbiesimpson/Isogeometric-BEM>, 2012.

Bibliography

- [SBT⁺12] R.N. Simpson, S.P.A. Bordas, J. Trevelyan, and T. Rabczuk. A two-dimensional isogeometric boundary element method for elastostatic analysis. *Comput. Meth. Appl. Mech. Engrg.*, 209-212:87–100, 2012.
- [ST99] K.M. Singh and M. Tanaka. Analytical integration of weakly singular integrals in boundary element analysis of Helmholtz and advection-diffusion equations. *Comput. Meth. Appl. Mech. Engrg.*, 189:625–640, 1999.
- [SIS198] J. Sladek and V. Sladek. *Singular integrals in boundary element methods*. Computational Mechanics Publications Southhampton, 1998.
- [SISp88] I.H. Sloan and A. Spence. The Galerkin method for integral equations of the first kind with logarithmic kernel: Theory. *IMA J. Numer. Anal.*, 8:105–122, 1988.
- [SIS92] I.H. Sloan and E.P. Stephan. Collocation with Chebyshev polynomials for Symm’s integral equation on an interval. *J. Austral. Math. Soc. Ser. B*, 34:199–211, 1992.
- [ŚBA⁺15] W. Śmigaj, T. Betcke, S. Arridge, J. Phillips, and M. Schweiger. Solving boundary integral problems with BEM++. *ACM Trans. Math. Software*, 41(2):1–40, 2015.
- [Ste03] O. Steinbach. *Numerische Näherungsverfahren für elliptische Randwertprobleme. Finite Elemente und Randelemente*. B.G. Teubner, 2003.
- [SW84] E.P. Stephan and W.L. Wendland. An augmented Galerkin procedure for the boundary integral method applied to two-dimensional screen and crack problems. *Appl. Anal.*, 18:183–219, 1984.
- [StSu89] E.P. Stephan and M. Suri. On the convergence of the p -version of the boundary element Galerkin method. *Math. Comput.*, 52(185):31–48, 1989.
- [StSu91] E.P. Stephan and M. Suri. The h - p version of the boundary element method on polygonal domains with quasiuniform meshes. *ESAIM: Mathematical Modeling and Numerical Analysis - Modélisation Mathématique et Analyse Numérique*, 25(6):783–807, 1991.
- [TM74] H. Takahasi and M. Mori. Double exponential formulas for numerical integration. *Publ. RIMS*, 9:721–741, 1974.
- [Tel86] J.C.F. Telles. A self-adaptive co-ordinate transformation for efficient evaluation of general boundary element integrals. *Int. J. Numer. Meth. Eng.*, 24:959–973, 1986.
- [WFC08] W.A. Wall, M.A. Frenzel, and C. Cyron. Isogeometric structural shape optimization. *Comput. Meth. Appl. Mech. Engrg.*, 197:2976–2988, 2008.

- [Zie71] O.C. Zienkiewicz. *The finite element method in engineering science*. McGraw-Hill, 1971.

List of Symbols

The numbers in the end of each row indicate the page number.

General Notation

$ \cdot $	absolute value or cardinality of a set
$\partial/\partial s$	arc length derivative
$\mathcal{O}(f)$	Landau symbol, f is an asymptotic upper bound
\lesssim, \gtrsim	smaller than or equal to and greater than or equal to up to constant
$\operatorname{Re}(z), \operatorname{Im}(z)$	real and imaginary part of a complex number
$\operatorname{span}(X)$	space that contains all linear combinations of elements in the set X
$\operatorname{dist}\{\cdot, \cdot\}$	Euclidean distance
χ	indicator function
$\delta_{k,\ell}$	Kronecker symbol
$p.v., f.p.$	Cauchy principle value and Hadamard finite part

Function Spaces, Scalar Products, and Norms

$\Omega^-, \Omega^+ \subset \mathbb{R}^2$	bounded and unbounded Lipschitz domain, 1
$C^k(\Omega)^m$	space of k times continuously differentiable functions with values in \mathbb{C}^m , 2
$C_0^k(\Omega)^m$	space of functions in $C^k(\Omega)^m$ with compact support in Ω , 2
$C^\infty(\Omega)^m$	space of infinitely times differentiable functions with values in \mathbb{C}^m , 2
$C_0^\infty(\Omega)^m$	space of functions in $C^\infty(\Omega)^m$ with compact support in Ω , 2
$L^2(\Omega)^m$	Lebesgue space of square integrable functions with values in \mathbb{C}^m , 2
$L_{loc}^2(\Omega)^m$	Lebesgue space of locally square integrable functions with values in \mathbb{C}^m , 2
$L^\infty(\Omega)^m$	space of essentially bounded functions with values in \mathbb{C}^m , 2
$H^k(\Omega)^m$	Sobolev space of order k on Ω ($k \geq 0$) with values in \mathbb{C}^m , 3
$H_{loc}^k(\Omega)^m$	space of local $H^k(\Omega)$ functions with values in \mathbb{C}^m , 3
$\tilde{H}^{-k}(\Omega)^m$	dual space of $H^k(\Omega)$ ($k \geq 0$), 4

$(\cdot, \cdot)_{L^2(\Omega)^m}$	scalar product in $L^2(\Omega)^m$, 2
$\langle \cdot, \cdot \rangle_{X \times Y}$	extended L^2 scalar product, 4
$(\cdot, \cdot)_{H^k(\Omega)^m}$	scalar product in $H^k(\Omega)^m$, 3
$\ \cdot\ _{L^2(\Omega)^m}$	norm induced by the scalar product in $L^2(\Omega)^m$, 2
$\ \cdot\ _{H^k(\Omega)^m}, \ \cdot\ _{H^k(\Gamma)^m}$	norm on $H^k(\Omega)^m$ and $H^k(\Omega)^m$, 3
$ \cdot _{H^\sigma(\Omega)}$	Sobolev-Slobodeckij semi norm ($\sigma \in (0, 1)$), 3
$\gamma_0^-, \gamma_0^+, \gamma_0$	trace operators, 5
$\gamma_1^-, \gamma_1^+, \gamma_1$	co-normal derivatives, 5
σ_Ω	1 if Ω is bounded, 0 if Ω is unbounded, 5

The index m is omitted if the range of the function is clear.

Special Functions

$J_\nu(\cdot), Y_\nu(\cdot),$	Bessel functions of first and second kind, respectively, 186
$H_\nu^{(1)}(\cdot)$	Hankel function, 14, 186
$\Gamma(\cdot), \psi(\cdot)$	Gamma function and digamma function, respectively, 37
$\gamma,$	Euler constant, 186
$P_n^{(\alpha, \beta)}(\cdot)$	Jacobi polynomials, 37

Boundary Integral Equations

L	elliptic, linear, second-order, self-adjoint partial differential operator, 5
$G(x - y)$	fundamental solution of the partial differential operator L , 5
λ, μ	Lamé coefficients, 12
κ	wave number for Helmholtz problems, 13
$\tilde{\mathcal{V}}, \mathcal{V}$	single layer potential and operator, 6, 8
$\tilde{\mathcal{K}}, \mathcal{K}$	double layer potential and operator, 6, 8
\mathcal{K}'	adjoint double layer operator, 6, 8
\mathcal{W}	hypersingular operator, 6, 7
$\mathbf{V}, \mathbf{K}, \mathbf{W}$	Collocation or Galerkin matrix for single layer, double layer, and hypersingular operator, 19, 20, 23, 24
\mathbf{M}	mass matrix, 20, 24

Orthogonal Polynomial and Quadrature Rules

\mathcal{E}_ρ, ρ	complex ellipse with semi-axis sum ρ and foci ± 1 , 30
$\omega(x)$	weight function, 31
$(\pi_n)_{n \in \mathbb{N}_0}, (\rho_n)_{n \in \mathbb{N}_0}$	sequence of monic orthogonal polynomials and associated functions, 31
μ_k, m_k	moments and modified moment, 31, 37
P_k, N_k	Legendre polynomials and Lobatto shape functions, 32, 33
$R_n(f), K_n(f)$	remainder and its kernel of the quadrature formula of order n , 40

Non-Uniform-Rational B-Splines (NURBS)

q	degree of NURBS curve, 51
Ξ, ξ_j	open knot vector and knot, 51
$\tilde{\Xi}, \zeta_j, r_j$	unique knot vector, node, and corresponding multiplicity, 51
ω_k, ω	weights and weight functions, 51
$\mathcal{B}_{k,q}, \mathcal{R}_{k,q}$	b-spline and NURBS basis functions, 51
Q_k, Q_k^ω	control points and weighted control points, respectively, 51, 53
γ, γ^ω	NURBS curve mapping from $[-1, 1]$ and projection in \mathbb{R}^3 , 51, 53

Boundary Mesh and Ansatz Spaces

\mathcal{T}	boundary mesh on Γ , 16
\mathcal{P}	patch of elements, 82
$\mathcal{N}_e, \mathcal{N}_v$	number of elements and nodes in \mathcal{T} , 17
T_i	element of \mathcal{T} , 16
ϑ, σ	mesh parameter for geometric meshes, 17
$\mathbf{h}, \sigma(\mathbf{h}), h_i$	mesh-width function, ratio, and mesh width of T_i , 17, 56
\mathbf{p}, p_i	polynomial degree function and polynomial degree on T_i , 17, 56
\mathbf{k}	regularity function, 17, 56
γ, γ_i	NURBS parametrization of the boundary Γ and T_i , respectively, 56
X_ℓ, Y_ℓ	sequence of general discrete spaces, 19, 23
Φ_k, Ψ_k	basis functions of the discrete spaces X_ℓ, Y_ℓ , 19, 23
$\tilde{P}_k^{(i)}$	Legendre polynomial on T_i , 57
$\tilde{N}_k^{(i)}$	Lobatto shape function on T_i , 57
$\tilde{\mathcal{R}}_k$	NURBS basis functions, 56

$S(\mathcal{T}, \mathbf{h}, \mathbf{p}, \mathbf{k})$	space of piecewise polynomial functions with global regularity \mathbf{k} w.r.t. the mesh \mathcal{T} , 17, 57
$\mathcal{R}(\mathcal{T}, \mathbf{h}, \mathbf{p}, \mathbf{k})$	space of rational functions with global regularity \mathbf{k} spanned by NURBS basis functions, 17, 56
\mathcal{N}, \mathcal{M}	dimension of discrete space if the spaces involved are clear, 17, 111

Collocation Methods

x	point for the evaluation of the boundary integral operators, 74
z_x	complex zero of $ \gamma_i(t) - x $ lying in the ellipse \mathcal{E}_ρ , 75, 84
M_f, M_n, M_s	set of far-field, near-field, and singular evaluation points, 76
$A_k^{(i)}(x)$	matrix block of the Collocation matrix, 74
$\tilde{K}(x), K(t)$	kernel function in global and local coordinates, respectively, 74
\tilde{Q}_k^m	associated Legendre functions, 83

Galerkin Methods

$A_{k,\ell}^{(i,j)}(x)$	matrix block of the Galerkin matrix, 91
$\tilde{K}(x, y), K(s, t)$	kernel function in global and local coordinates, respectively, 91
$a(\cdot, \cdot), \tilde{a}(\cdot, \cdot)$	sesquilinear form and perturbed sesquilinear form, 111
f, \tilde{f}	right-hand side and perturbed right-hand side of integral equation, respectively, 111
$\tilde{\mathbf{V}}, \tilde{\mathbf{K}}, \tilde{\mathbf{W}}$	perturbed Galerkin matrices, 115, 117, 118

Curriculum Vitae

Personal Data

NAME	Andreas Bantle
DATE OF BIRTH	October 12, 1986
PLACE OF BIRTH	Laupheim, Germany
NATIONALITY	German

Education

SINCE OCT 2012	Doctoral studies, Institute for Numerical Mathematics, University of Ulm, Germany
OCT 2010 - SEP 2012	Graduate Studies in Mathematics & Computer Science University of Ulm, Germany Master of Science
OCT 2007 - SEP 2010	Undergraduate Studies in Mathematics & Computer Science University of Ulm, Germany Bachelor of Science
SEP 1997 - JUL 2006	Albert-Einstein Gymnasium, Ulm, Germany Abitur

Awards and Scholarships

NOV 2010	Scholarship of Stiftung WiMa Ulm
OCT 2007	Scholarship of University of Ulm

Work Experience

SINCE OCT 2012	Research Associate, Institute for Numerical Mathematics, University of Ulm, Ulm, Germany
OCT 2010 - AUG 2012	Graduate Teaching Assistant, University of Ulm, Ulm, Germany
OCT 2008 - AUG 2010	Undergraduate Teaching Assistant, University of Ulm, Ulm, Germany

Publications

A. Bantle, M. Bantle, and S. Funken.

epsBEM, Efficient P-Stable Matlab Implementation of 2D BEM for Laplace and Lamé Problems.
Technical Report, University of Ulm, Germany, 2013.

A. Bantle.

Efficient Implementation of the hp Boundary Element Method for the Navier-Lamé Equation.
Master Thesis, University of Ulm, Germany, 2012.

A. Bantle.

Efficient Implementation of the Collocation Method for the Navier-Lamé Equation.
Bachelor Thesis, University of Ulm, Germany, 2010.

Selected Talks

A. Bantle and S. Funken.

Implementation of Isogeometric/NURBS-Enhanced Galerkin Boundary Element Method in 2D.
World Congress of Computational Mechanics XI, Barcelona, Spain, July. 20 - 25, 2014.

A. Bantle, S. Funken.

NURBS-Enhanced Boundary Element Methods.

11. Workshop on Fast Boundary Element Methods in Industrial Applications, Oberstdorf, Germany, Sept. 26 - 29, 2013.

Erklärung

Ich, Andreas Bantle, versichere hiermit, dass ich die vorliegende Arbeit selbständig angefertigt habe und keine anderen als die angegebenen Quellen und Hilfsmittel benutzt sowie die wörtlich oder inhaltlich übernommenen Stellen als solche kenntlich gemacht habe. Ich erkläre außerdem, dass die von mir vorgelegte Dissertation bisher nicht im In- oder Ausland in dieser oder ähnlicher Form in einem anderen Promotionsverfahren vorgelegt wurde. Ich versichere ferner die Richtigkeit der im Lebenslauf gemachten Angaben.

Ulm, den 03.07.2015

(Unterschrift)